



**DEVELOPMENT OF GROUNDWATER FLOW MODEL FOR
WATER RESOURCES MANAGEMENT IN THE DEVELOPMENT
AREAS OF THE WESTERN DESERT,
EGYPT**

Dissertation

submitted to the faculty of Natural Sciences III

of the

Martin Luther University Halle-Wittenberg

in partial fulfillment of the requirements for the award of the
degree of Doctor of Natural Sciences

BY

AHMED M. SEFELNASR

MSc. in Hydrogeology

Born on: 4.11.1974

Born in: Elwady Elgadid, Egypt

Referee:

1. Prof. Dr. Peter Wycisk
2. Prof. Dr. Maria-Theresia Schafmeister

Halle (Saale), 22.10.2007

urn:nbn:de:gbv:3-000012520

[<http://nbn-resolving.de/urn/resolver.pl?urn=nbn%3Ade%3Agbv%3A3-000012520>]

Knowing is not enough; we must apply!

Goethe

To...

my parents,

my wife,

and my kids

Acknowledgement of Statement

First and foremost, I express my honest gratitude to almighty God, who granted me believe and patience to carry this research out.

This work is a result of considerable amount of sustainable support, advice, assistance, guidance, and encouragement, without which it would not have seen the light of the day. I would like to extend my authentic gratefulness to the following individuals and institutions for their help with this project.

A great deep impassioned thank goes to *Prof. Dr. Peter Wycisk* for his supervision, support, enthusiasm, guidance, and reviewing this work. The institutional trust and freedom he gave me throughout the course of the research created comfortable and fruitful atmosphere for the work. Beside the regular discussions he held with me. His door was always open even when he had piles of work. We worked together with ease and enjoyment. Especially appreciated is the extra effort he put in to ensure work was progressing even during personal crises for both of us.

I wish to express my sincere gratitude to *Dr. habil. Wolfgang Gossel* for his invaluable guidance, encouragement, constructive criticism, great discussions, and careful review of the draft of this thesis. That are some of the many contributions that he has made during the course of this research even on the personal scale, he was always so close. His dedication to education is unsurpassed. I owe him a lot of my knowledge and experience.

I would also like to extend my gratitude to *Prof. Dr. A.M. Ebraheem* for his suggestions and discussions in the early stages of this research. He was the first who thought me about groundwater modeling.

This research was also benefited from discussions with fellow students within the workgroup of hydrogeology and environmental geology at the Martin Luther University Halle-Wittenberg, they offered very pleasant work environment with high professional discussions; are to mention Mr. Christian Neumann, Mr. Ronny Lähne, Mr. Dirk Schlesier, Mr. Tobias Hubert, Mr. Philip Stankiewicz, Mrs. Andrea Hanf, and Mr. Raafat Wassef.

I would passionately like to show appreciation to the German Academic Exchange Service (*DAAD*) for the generous funding that made this research possible.

Finally, I would also like to express my genuine thanks to my wife for her moral support. She believed in me and stood always behind me encouraging and pushing forward to bring this work in its final form. A cordial, warm, and passionate thank goes to my children, who accepted my long working hours and absence with remarkable patience.

Abstract

Many studies concerned with investigating the groundwater resources of the Nubian Sandstone Aquifer System (NSAS). However, these studies focused either only on the regional groundwater hydrodynamics of the aquifer, or on local-scale case studies without taking into account the regional boundary conditions of the whole system. This work was an attempt to develop a three-dimensional transient groundwater flow model for the NSAS that is based on GIS-Database integration. This approach was proposed to 1) define and calibrate the regional boundary conditions of the NSAS, 2) to simulate the groundwater management options for the different stressed areas within the aquifer, and 3) to predict the environmental impact of the present and future groundwater extraction schemes on the different exploitation sites. The calibration was carried out under the transient conditions using the trial and error method for the period 1960-2005 based on the availability and temporal distribution of the data. The calibrated regional model was used afterward for the development and integration of local-scale (refined) models for the Dakhla oasis, Lake Nasser, and the Tushka area, to consider local detailed data inputs and to give a deeper view on the local hydrodynamic changes. Based on the actual and full capacity planned extraction rates of the NSAS, five extraction scenarios were suggested in an attempt to investigate the most feasible groundwater management option in terms of the economic lifting depth in a prediction simulation until 2100. The results of simulating the present extraction rates of the NSAS showed that the free flowing phenomenon will disappear all over the modeled area and the average depth to groundwater will range from 5 m in the Bahariya oasis to 36 m (bgl) in the Kharga oasis at the end of the simulation. At this simulation time, a groundwater volume of 354 km³ will be extracted from the aquifer storage. The application of scenario 3 was found to be the optimal groundwater management option that meets the development ambitions and the proposed economic lifting depth, while scenario 5 resulted in a depth to groundwater values sink faraway beyond the 100-m (bgl) limit of the economic lifting depth in the Kufra oasis and the East Oweinat area. In the Dakhla oasis the simulation of scenario 1 showed that the depth to groundwater in all the cultivable areas will be less than 75 m (bgl) by 2100 and the annual change in the hydraulic head would be 0.57 m/y. On the other hand, it was concluded that scenario 3 is the allowable groundwater development option in the Dakhla oasis, while scenario 5 led to successive increase of the depth to groundwater to have values greatly exceeding 100 m and cover most of the oasis. Lake Nasser raised the groundwater level with an average of 25 m within a 25 km strip and recharged the NSAS with a volume of 281.5 km³ until 1998. The cumulative recharge from Lake Nasser and the Tushka lakes until 2005 was calculated to be about 9.66×10^{11} m³.

Table of Contents

Acknowledgement of Statement	I
Abstract	II
Table of Contents	III
List of Figures	VI
List of Tables	XII
List of Abbreviations	XIII
1 Introduction	1
1.1 Background and motivation	1
1.2 Purpose and scope	2
1.3 Previous work	3
1.4 Structure of the thesis	5
2 Geographical Setting	7
2.1 Outlines and location	7
2.2 Geomorphology	9
2.3 Climate	14
3 Geological Setting	15
3.1 Stratigraphy	17
3.1.1 Precambrian	17
3.1.2 Cambrian and Ordovician	19
3.1.3 Silurian	19
3.1.4 Devonian	19
3.1.5 Carboniferous	20
3.1.6 Triassic and Lower Jurassic	20
3.1.7 Upper Jurassic and Lower Cretaceous	20
3.1.8 Upper Cretaceous and Tertiary	23
3.1.9 Quaternary	23
3.2 Major structural framework	24
4 Hydrogeological setting	26
4.1 Nubian Sandstone Aquifer System	26
4.1.1 Extension and boundaries	26
4.1.2 Subunits of the aquifer system	27
4.1.3 Basins of the NSAS	30
4.1.3.1 The Northern Basin	30
4.1.3.2 The Dakhla Basin	30
4.1.3.3 The Upper Nile Platform	31
4.1.3.4 The Northern Sudan Platform	32
4.1.3.5 The Kufra Basin	32
4.2 Aquifer systems in Egypt	32
4.2.1 The Coastal Aquifer	32

4.2.2	The Nile Aquifer	33
4.2.3	The Moghra Aquifer	33
4.2.4	The fissured Carbonate Aquifer	33
4.2.5	The Nubian Sandstone Aquifer	33
4.3	NSAS as a Transboundary Aquifer	34
4.4	Environmental situation	36
4.4.1	Groundwater residence time	37
4.5	Origin of groundwater in the NSAS	38
4.5.1	Origin theory	38
4.5.2	Recharge	39
4.5.2.1	Nile water seepage	39
4.5.2.2	Recharge from the South	39
4.5.2.3	Local infiltration in the past	39
4.6	Natural discharge	40
4.7	Aquifer parameters	41
5	Methodology	44
5.1	Introduction	44
5.2	Governing equations	45
5.3	Conceptualization	48
5.4	Interpolation	50
5.4.1	Kriging	51
5.4.2	Variograms	51
5.5	Boundary conditions	51
5.6	Initial conditions	55
5.7	Discretization	55
5.8	Calibration	58
5.8.1	Trial and error	59
5.8.2	Automated methods	59
5.9	Data requirements	61
6	Regional Model	62
6.1	Data acquisition	62
6.2	Model development and design	63
6.2.1	Digital encoding and translation	65
6.2.2	Conceptual model	66
6.2.3	GIS-Database	67
6.2.4	Interpolation and layer generation	68
6.2.4.1	Generation of layers and slices	70
6.2.4.2	Aquifer parameters	71
6.2.5	Boundary conditions	73
6.2.5.1	1 st type, Dirichlet boundary condition	73
6.2.5.2	2 nd type, Neuman boundary condition	73
6.2.5.3	4 th type, Well boundary condition	75
6.2.6	Initial conditions	77
6.2.7	Recharge	77
6.2.8	Evapotranspiration	78
6.2.9	Discretization	78
6.3	Calibration	78

6.4	Linkage with modeling systems.....	82
6.5	Regional model output	82
6.5.1	Hydraulic head.....	82
6.5.2	Drawdown.....	83
6.5.3	Depth to groundwater	86
6.5.4	Groundwater balance	91
7	Local Model-Dakhla Oasis	94
7.1	Introduction	94
7.2	Locality	96
7.3	Geomorphological background.....	96
7.4	Geological background.....	97
7.5	Water quality	99
7.6	Model input and structure.....	100
7.7	Model output.....	100
7.7.1	Scenario 1	102
7.7.2	Scenario 2	107
7.7.3	Scenario 3	107
7.7.4	Scenario 4	111
7.7.5	Scenario 5	113
7.8	Socio-economic feasible use.....	116
8	Local Model-Lake Nasser-Tushka	117
8.1	Introduction	117
8.2	Site description.....	118
8.3	Model input and boundaries	120
8.4	Model output.....	122
8.5	Recharge from the lakes	126
9	Summary and conclusions	128
	Bibliography	133
	Appendices	150
	Appendix A	150
	Appendix B	159

List of Figures

Figure 1.1 An illustration showing the structure of the thesis5

Figure 2.1 The upper image is a satellite image of North Africa including the Sahara. The lower one is an image from the DEM of the Eastern Sahara including the study area of the Nubian Sandstone Aquifer System. Sources: NASA (2005, 2006), and USGS (2004).....8

Figure 2.2 The background is a satellite image of the Eastern Sahara showing the main highlands and depressions within the NSAS. The foreground illustrates the main physiographic features of the Eastern Sahara. (Satellite image obtained from NASA (2006). The physiographic features compiled from Neumann (1989), Mainguet (1995), and Nicoll (2001).....10

Figure 3.1 Localities, famous features, and names mentioned in this chapter.....16

Figure 3.2 Lithostratigraphic sections along the domain area of the NSAS. The corresponding locations are shown in the overview map, compiled from Hissene (1986), Kheir (1986), and Hesse et al. (1987).....18

Figure 3.3 Schematic geological map of the NSAS. Digitized from maps of CONOCO (1987) and USGS (2004)21

Figure 3.4 Simplified sections for different locations within the NSAS. Adapted from Thorweihe and Heintz (2002)22

Figure 3.5 General structural framework of the NSAS. Adapted from Klitzsch (1984) and Klitzsch and Wycisk (1989)25

Figure 4.1 Regional hydrogeological overview of the Nubian Sandstone Aquifer System. Compiled from: CEDARE (2002), Salem and Pallas (2004), and Bakhbakhi (2006).....28

Figure 4.2 Locality map showing the thickness, major uplifts and the structural units of the NSAS. Locations of uplifts adapted from thickness after Klitzsch (1983), Hissene (1986), Hesse et al. (1987), and Thorweihe (1996).....31

Figure 4.3 The aquifer systems of Egypt. Modified after RIGW (1998).....34

Figure 4.4	Diagram of the transboundary Nubian Sandstone Aquifer System. Adapted from Salem and Pallas (2004) and Bakhbakhi (2006)	35
Figure 4.5	The concept of the non-renewability of the Nubian Sandstone Aquifer System. Typically, recharge area, transmission area, and discharge area. Modified after Margat et al. (2006).....	36
Figure 4.6	Histogram representing a North-South profile for the historical climatic changes of the Eastern Sahara deduced from detailed radiometric Playa and lake sediments. Adapted from Pachur (1999).....	41
Figure 4.7	Overview of the hydraulic conductivities of some locations of the NSAS. The interpretation of the hydraulic conductivities based on the simplified sections of Thorweihe and Heintl (2002) and the cross sections of Hesse et al. (1987)	43
Figure 5.1	Schematic illustration showing the Procedure of translating the geologic framework of the real world to digital form	50
Figure 5.2	(a) Diagram showing the spatial distribution of the independent random variables and the separating lag distance between them; (b) diagram represents the variogram components and a typical and experimental curve. Compiled from Surfer® 8 User’s Guide (2002) and Bohling (2005)	52
Figure 5.3	Diagram of regional groundwater flow system representing the physical and hydraulic boundary conditions. Modified after Anderson and Woessner (1992)	53
Figure 5.4	The concept of the effect of the size of the time steps on the simulation of the decay of the groundwater hydraulic head. Solid line represents the analytical solutions and the points represent the numerical solutions (modified after Townley and Wilson 1980).....	58
Figure 5.5	(a) Graph illustrating the instability of time oscillations; (b) Maximum and minimum Courant Number criteria for one dimensional simulations (modified after Fabritz 1995)	58
Figure 6.1	Schematic illustration of the procedure of developing a regional groundwater flow model for the NSAS	63
Figure 6.2	Schematic drawing shows the location, extent, development areas, and boundary conditions of the NSAS	64

Figure 6.3	Block representation of a flowchart for the typical steps for the development of the 3D conceptual model	66
Figure 6.4	Schematic example configures the conceptualization idea and the location of some regional cross sections in plan view	69
Figure 6.5	Digital Elevation Model and basement relief of the NSAS, as well as a corresponding Gaussian variogram for the basement relief	72
Figure 6.6	The distribution of the hydraulic conductivities as obtained from the appropriate statistical procedures. A matching spherical variogram is shown at the top of the figure	74
Figure 6.7	The distribution of the initial potentiometric head in the NSAS and the schemes of the extraction rates. Initial heads adapted from Ball (1927) and Sandford (1935)	76
Figure 6.8	Cluster chart represents the total extraction rates of the Dakhla oasis in time since 1960. Source MPWWR (1999) and personal contact (2005).....	77
Figure 6.9	The result of model calibration under transient conditions and the spatial distribution of the field observations.....	79
Figure 6.10	Scatter diagram showing simulated vs. measured heads at calibration targets. The histogram represents the frequency range of the residuals	81
Figure 6.11	Hydrograph of history matching, a comparison between observed and computed heads with time (time scale represents the calibration period from 1960 until 2005).....	81
Figure 6.12	The distribution of the simulated hydraulic head of the NSAS by 2005 in comparison to the initial heads of year 1960	85
Figure 6.13	The decline of the groundwater head (drawdown) within the depressions of the NSAS by 2005	86
Figure 6.14	Simulated hydraulic head for the lower aquifer of the NSAS by 2050. The extraction rates of scenario 1 are proposed to be constant until 2100	87
Figure 6.15	Simulated hydraulic head for the lower aquifer of the NSAS by 2100. The extraction rates of scenario 1 are proposed to be constant until 2100	87
Figure 6.16	Simulated hydraulic head for the lower aquifer of the NSAS by 2050. The extraction rates of scenario 5 are proposed to be constant until 2100. Contour interval 25 m.....	88

Figure 6.17	Simulated hydraulic head for the lower aquifer of the NSAS by 2100. The extraction rates of scenario 5 are proposed to be constant until 2100. Contour interval 25 m.....	88
Figure 6.18	Resulting drawdown by 2050 in the NSAS, suggesting the extraction rates of scenario 1 are constant until 2100.....	89
Figure 6.19	Resulting drawdown by 2100 in the NSAS, suggesting the extraction rates of scenario 1 are constant until 2100.....	89
Figure 6.20	Resulting drawdown by 2050 in the NSAS, suggesting the extraction rates of scenario 5 are constant until 2100.....	90
Figure 6.21	Resulting drawdown by 2100 in the NSAS, suggesting the extraction rates of scenario 5 are constant until 2100.....	90
Figure 6.22	Groundwater balance for the NSAS for the period 1960-2100, scenario 1	92
Figure 6.23	Groundwater balance for the NSAS for the period 1960-2100, scenario 5	92
Figure 6.24	Cumulative decrease in groundwater storage of the NSAS for the period 1960-2100, scenario 1.....	93
Figure 6.25	Cumulative decrease in groundwater storage of the NSAS for the period 1960-2100, scenario 5.....	93
Figure 7.1	Location map of the Dakhla oasis showing the depression, settlements, and topography. The topography is obtained from the DEM of the SRTM-03 (USGS 2004; NASA 2005)	95
Figure 7.2	Geological map of the Dakhla oasis. Digitized from Conoco (1989), lithostratigraphic units adapted from El Khawaga et al. (2005).....	98
Figure 7.3	Location map of the Dakhla oasis showing the distribution of pumping-well fields and locations of wells of the simplified cross sections.....	101
Figure 7.4	Simplified cross sections of selected locations in the east, middle, and west of the Dakhla oasis based on the well logs (modified after Sefelnasr 2002)	101
Figure 7.5	Simulated hydraulic head m (amsl) for the NSAS in the Dakhla oasis by 2005	103
Figure 7.6	Simulated hydraulic head m (amsl) for the NSAS in the Dakhla oasis by 2050, scenario 1	103

Figure 7.7	Simulated hydraulic head m (amsl) for the NSAS in the Dakhla oasis by 2100, scenario 1	104
Figure 7.8	Simulated decline in potentiometric surface for the NSAS in the Dakhla oasis by 2005	104
Figure 7.9	Simulated decline in potentiometric surface for the NSAS in the Dakhla oasis by 2050, scenario 1.....	105
Figure 7.10	Simulated decline in potentiometric surface for the NSAS in the Dakhla oasis by 2100, scenario 1.....	105
Figure 7.11	Calculated depth to groundwater for the NSAS in the Dakhla oasis by 2005	106
Figure 7.12	Calculated depth to groundwater for the NSAS in the Dakhla oasis by 2100, scenario 1	106
Figure 7.13	Simulated hydraulic head m (amsl) for the NSAS in the Dakhla oasis by 2100, scenario 2	108
Figure 7.14	Simulated decline in potentiometric surface for the NSAS in the Dakhla oasis by year 2100, scenario 2.....	108
Figure 7.15	Simulated hydraulic head m (amsl) for the NSAS in the Dakhla oasis by 2050, scenario 3	109
Figure 7.16	Simulated hydraulic head m (amsl) for the NSAS in the Dakhla oasis by 2100, scenario 3	109
Figure 7.17	Simulated decline in potentiometric surface for the NSAS in the Dakhla oasis by 2050, scenario 3.....	110
Figure 7.18	Simulated decline in potentiometric surface for the NSAS in the Dakhla oasis by 2100, scenario 3.....	110
Figure 7.19	Calculated depth to groundwater for the NSAS in the Dakhla oasis by 2100, scenario 3	111
Figure 7.20	Simulated hydraulic head m (amsl) for the NSAS in the Dakhla oasis by 2100, scenario 4	112
Figure 7.21	Simulated decline in potentiometric surface for the NSAS in the Dakhla oasis by 2100, scenario 4.....	112
Figure 7.22	Simulated hydraulic head m (amsl) for the NSAS in the Dakhla oasis by 2050, scenario 5	113
Figure 7.23	Simulated hydraulic head m (amsl) for the NSAS in the Dakhla oasis by 2100, scenario 5	114

Figure 7.24	Simulated decline in potentiometric surface for the NSAS in the Dakhla oasis by 2050, scenario 5.....	114
Figure 7.25	Simulated decline in potentiometric surface for the NSAS in the Dakhla oasis by 2100, scenario 5.....	115
Figure 7.26	Calculated depth to groundwater for the NSAS in the Dakhla oasis by 2100, scenario 5	115
Figure 8.1	Location map showing (a) the study area, (b) schematic cross section, and (c) geologic map of the area with the location of cross section. (Geological map after Conoco (1987), the cross section after Kim and Sultan (2002))	119
Figure 8.2	Fluctuations of Lake Nasser-water level from 1964-2005. Sources: GALND (1997), RIGW (1998), and personal contact (2003) and (2006).....	121
Figure 8.3	Location image of Lake Nasser, the Tushka lakes, and the surrounding areas showing the location of the available observation wells. Satellite image from NASA (2005)	121
Figure 8.4	Hydrograph illustrating the changes in hydraulic head at selected observation wells west of Lake Nasser and how they reproduce the fluctuations of the lake levels	122
Figure 8.5	Contour map shows the distribution of the initial hydraulic head around Lake Nasser and the Tushka area before the construction of the Aswan High Dam.....	123
Figure 8.6	Contour map represents the distribution of the hydraulic head around Lake Nasser and the Tushka area in 1998 just before the development of Tushka lakes	124
Figure 8.7	Contour map represents the distribution of the hydraulic head around Lake Nasser and the Tushka area in 2000	125
Figure 8.8	Contour map represents the distribution of the hydraulic head around Lake Nasser and the Tushka area by 2005	126
Figure 8.9	The cumulative recharge from Lake Nasser and the Tushka lakes to the NSAS for the period 1964-2005.	127

List of Tables

Table 4.1	Area, fresh storage, and present extraction rates of the Nubian Sandstone Aquifer System.....	29
Table 4.2	Average aquifer thickness, transmissivity, and hydraulic conductivity of the oases and development areas of the Nubian Sandstone Aquifer System.....	42
Table 6.1	The different extraction scenarios (Mill m ³ /y) for the different stress areas within the NSAS	75
Table 6.2	Calibration statistics for simulated hydraulic heads of the NSAS.....	80
Table 6.3	Average Changes in hydraulic head, drawdown, and depth to groundwater for the stressed areas of the NSAS	84

List of Abbreviations

AHD	Aswan High Dam, Egypt
AHDA	Aswan High Dam Authority, Egypt
amsl	above mean sea level
ASCII	American Standard Code for Information Interchange
bgl	below ground level
BGR	Federal Institute for Geosciences and Natural Resources
CEDARE	Centre for Environment & Development for the Arab Region and Europe
CGMW	Commission for the Geological Map of the World
DEM	Digital Elevation Model
DMA-TM	Defense Mapping Agency-Technical Manual
DMA-TR	Defense Mapping Agency-Technical Report
EC	Electrical Conductivity
EIA	Environmental Impact Assessment
ERWR	External Renewable Water Resources
ESRI	Environmental Systems Research Institute
FAO	Food and Agriculture Organization of the United Nations
GALND	General Authority for Lake Nasser Development
GARPAD	General Authority for Rehabilitation Projects and Agricultural Development, Egypt
GEODE	Geological Data Explorer
GIS	Geographic Information System
GMMRA	Great Man-Made River Authority, Libya
GPS	Global Positioning System
GRLND	General Authority for Lake Nasser Development, Egypt
GWA	General Water Authority, Libya
IAEA	International Atomic Energy Agency
IAH	International Association of Hydrogeologists
IFAD	International Fund for Agricultural Development
IGRAC	International Groundwater Resources Assessment Center
IHP	International Hydrogeological Program (UNESCO)
IISD	International Institute for Sustainable Development
IRWR	Internal Renewable Water Resources
ISARM	Internationally Shared (Transboundary) Aquifer Resource Management
KADCO	Kingdom Agriculture Development Company, Cairo
MALR	Ministry of Agriculture and Land Reclamation, Egypt
MCM	Million Cubic Meter

MPWWR	Ministry of Public Works and Water Resources, Egypt
NAS	Nubian Aquifer System
NASA	National Aeronautics and Space Administration
NIMA	National Imagery and Mapping Agency
NSAS	Nubian Sandstone Aquifer System
PNAS	Post Nubian Aquifer System
REGWA	General Company for REsearch and GRound Water, Cairo
RIGW	Research Institute for Ground Water, Egypt
SAR	Sodium Adsorption Ratio
SRTM	Shuttle Radar Topography Mission
TARM	Transboundary Aquifer Resources Management
TDS	Total Dissolved Solids
TIFF	Tagged Image File Format
TIN	Triangular Irregular Network
UN	United Nations
UNDP	United Nations Development Programme
UNESCO	United Nations Educational, Scientific and Cultural Organization
USGS	United States Geological Survey
UTM	Universal Transverse Mercator
WGS84	World Geodetic System 1984
WHO	World Health Organization
WRC	Water Research Centre, Egypt
WWAP	World Water Assessment Program
WYMAP	Worldwide Hydrogeological Mapping and Assessment Program



Introduction

1.1 Background and motivation

The Nubian Sandstone Aquifer System (NSAS) is a transboundary groundwater aquifer in the Eastern Sahara of Africa. The water of this international aquifer is non-renewable and shared among Egypt, Libya, Sudan, and Chad. The area occupied by the aquifer system is about 2.35 million km². It is of significant importance because it is the only water resource for this arid area. The increasing demographic growth and the lack of renewable fresh water resources in this arid region have resulted in an increasing attention to the groundwater potential represented by the NSAS.

During the past three decades, Egypt, Libya, and Sudan have made separate attempts to develop and utilize the NSAS and the overlying desert lands. Each country thus has its specific experiences, motivations, and success in that field.

Under the scarce conditions of water in the study area, which is an essential constraint to development, and in light of the non-renewability of the NSAS, which poses more complexity in its management (in terms of aridity, non-renewability, and water demand), there is still considerable room for utilization of this resource provided its exploitation is governed by principles of rationality and wisdom.

In Egypt, to overcome the problem of overpopulation around the Nile valley and Delta areas, where the balance between the land and man is distorted, the government has decided to extend or move the land reclamation activities into the vast, isolated desert areas, based on the utilization of the available groundwater resources.

Most of the present water extracted from the NSAS is used for agriculture, either for large development projects in Libya or for farms located in old traditional oases in Egypt (New Valley). However, an important project (the Great Man-Made River) designed for transporting water to the coast from the NSAS is under development in Libya and is already supplying about 70 million m³/a of water to Benghazi and to the major coastal cities northwest of Libya.

Over 40 billion m³ of water was extracted in the past 40 years, leading to a continuous drop of the water level and to the disappearance of most of the naturally flowing wells and springs.

Based on the highlights mentioned above, an integrated management of the limited groundwater resources is most critical for the development of the NSAS. The most sophisticated method that helps investigate such complex systems is the numerical groundwater modeling, and that is what this thesis stands for.

1.2 Purpose and scope

In the scope of sustainable groundwater management for the NSAS, the focus of this work could be divided into two points. The first point concerns fundamental analysis, which has the objective to understand the physical processes of the NSAS. The second task is problem oriented and carefully directed to the management decisions to be made. Close to the above points of interest are the following specific objectives, which make up the major parts of this work:

- Using the available data for the NSAS, a GIS-database is to be created. It comprises the geological and hydrogeological information from previous studies, the newly drilled water wells in Egypt and Libya up to year 2005.
- The GIS-Database is used and incorporated to establish a conceptual framework to model the real hydrogeologic system, which is an essential step before the development of a numerical groundwater flow model. This includes different assumptions which lead to the estimation or quantification of the different components of the aquifer system, including hydraulic conductivities, storativities, etc.
- Development of a 3D-regional groundwater flow model for the NSAS to serve as a base model for the local interests.
- Calibration of the regional groundwater flow model against predefined criteria using numerical simulation techniques.
- Estimation of the available groundwater as a basic aspect of groundwater management. Mathematical modeling is one of the methods that can be effectively used to obtain such estimates. These prognostic calculations were elaborated not regarding ongoing theoretical discussions about the admissibility of prognostic calculations.
- Integrating a local model for the Dakhla oasis by refining the mesh (grid cells) of the calibrated regional model of the NSAS to involve the local details. Inputs of the regional model serve as boundary conditions for these local approaches. This allows precise input of the pumping schemes and more accurate analysis of the resulting decline of the hydraulic head (drawdown) as well as taking into account the groundwater extraction from the other stressed areas within the NSAS.

- The calibrated model is further used to determine the impact of the present and planned extraction rates on the aquifer behavior by making the necessary prediction-simulations to accomplish a good management scheme for the NSAS.
- Investigating the groundwater-lake interaction between Lake Nasser and the NSAS to study whether the water body of Lake Nasser noticeably recharges the aquifer.

1.3 Previous work

The NSAS has been subject to a lot of studies since the beginning of the twentieth century. All the studies until the beginning of the 1980s (e.g., Ball 1927; Sandford 1935; Hellstroem 1939; Himida 1960; Ezzat 1974; Amer et al. 1981) have concluded that the NSAS has been under steady state conditions before 1960 and that groundwater flow is driven from areas with precipitation which is sufficient for groundwater recharge. However, recent studies indicate that this aquifer had been in transient conditions for thousands of years before 1960, and the climate changes including wet periods supplied plenty of precipitation to suffice for local groundwater formation. Brief notes on the historical development of the most well known of the research works are given below:

- **Hume (1925) and Ball (1927)** discussed the origin of the groundwater of the Western Desert, as it was derived from the rainfalls on the western Sudan. Ball (1927) drew a contour map for static water levels on the assumption that all wells and springs in the Western Desert of Egypt were fed from a continuous stream of groundwater, which made it evident that this water does not come from the Nile.
- **Sandford (1935)** extended Ball's groundwater static head contour map over the northwestern Sudan.
- **Attia (1954)** stated that the Nubian Sandstone receives its water on account of the heavy rainfall on the aquifer surface in the central Sudan, which infiltrates downward into the formation and fills it. Partial groundwater recharge of the Nubian sandstone formations comes from the Nile.
- **Murray (1952)** considered the artesian water beneath Egypt as fossil water, which was formed on account of the rain which fell on the hills of western Sudan many thousands of years ago.
- **Shata et al. (1962)** stated that the artesian water of the Western Desert is of pluvial origin, based on data obtained by ^{14}C dating method.
- **Diab (1972)** studied the hydrogeological and hydrogeochemical aspects. He noted that the artesian Nubian Aquifer is composed mainly of two water-bearing complexes. The first and most important one is the water-bearing complex contained in the Nubian facies series. The second one is the water-bearing complex contained in the Post Nubian rocks.
- **Brinkmann and Heintz (1985)** presented a numerical groundwater flow model for the whole Nubian Aquifer System. They concluded that the groundwater flows mainly from local centers of recharge and discharge.

- **Sonntag (1985)** estimated the hydraulic conductivity of the Nubian sandstone layers in the range of 10^{-6} m/s to 10^{-4} m/s with an average value of 10^{-5} . He believed that the potentiometric surface (hydraulic head) roughly follows the gentle slope of the ground surface from south to north at the average depth of about 60 m below ground. Therefore, in the depression areas groundwater levels are close to the surface, where the hydraulic heads are often above ground level.
- **Thorweihe (1985)** concluded that the groundwater reservoir in the Nubian Aquifer System was formed during frequent wet periods in the past and that recent groundwater formation is not detectable.
- **Brinkmann et al. (1987)** presented a prospective simulation of groundwater flow in the Nubian Aquifer System and summarized that groundwater was recharged over large areas in the whole system. No large-scale flow occurs during the recharge periods. Infiltration stopped roughly 8,000 years ago but continued on a small scale in different areas.
- **Hesse et al. (1987)** declared that the groundwater of the Nubian Aquifer System was formed mainly autochthonically during wet periods in the past, and recent groundwater formation by admixture of Nile water is qualitatively verified. He considered that the groundwater influx from rain regions at the south is hydraulically traceable.
- **Sonntag and Christmann (1987)** estimated the natural groundwater discharge of the Nubian Aquifer System by evapotranspiration in East-Saharan depressions to have a mean value of 10 mm/year.
- **Thorweihe (1990)** concluded that the groundwater influx from southern regions is one order of magnitude lower than the artificial groundwater use in the New Valley and that a major discharge of influx amount by evaporation in the Gebel Oweinat–Aswan uplift area is likely. The groundwater yield differs regionally and vertically.
- **Heinl and Thorweihe (1993)** developed a regional groundwater flow model for the Nubian Aquifer System to simulate the groundwater flow system under climatic changes for the last 8,000 years.
- **CEDARE (2002)** has developed a regional groundwater flow model for the NSAS setting the northern model boundaries to the shoreline of the Mediterranean Sea.
- **Ebraheem et al. (2002)** concluded from a numerical groundwater flow model that the steady state solution could not be obtained under the present arid conditions within the NSAS. He also studied the impact of the groundwater extractions on the aquifer behavior.
- **Gossel et al. (2004)** have developed a large scale groundwater flow model for the NSAS and studied the response of the aquifer to the climatic changes that occurred during the last 25,000 years.

1.4 Structure of the thesis

This work is composed of nine chapters including this one. As stated earlier, this chapter is a general introduction. It introduces a general background on the problem, an overview on the well known previous work, the objectives, and the idea behind this research.

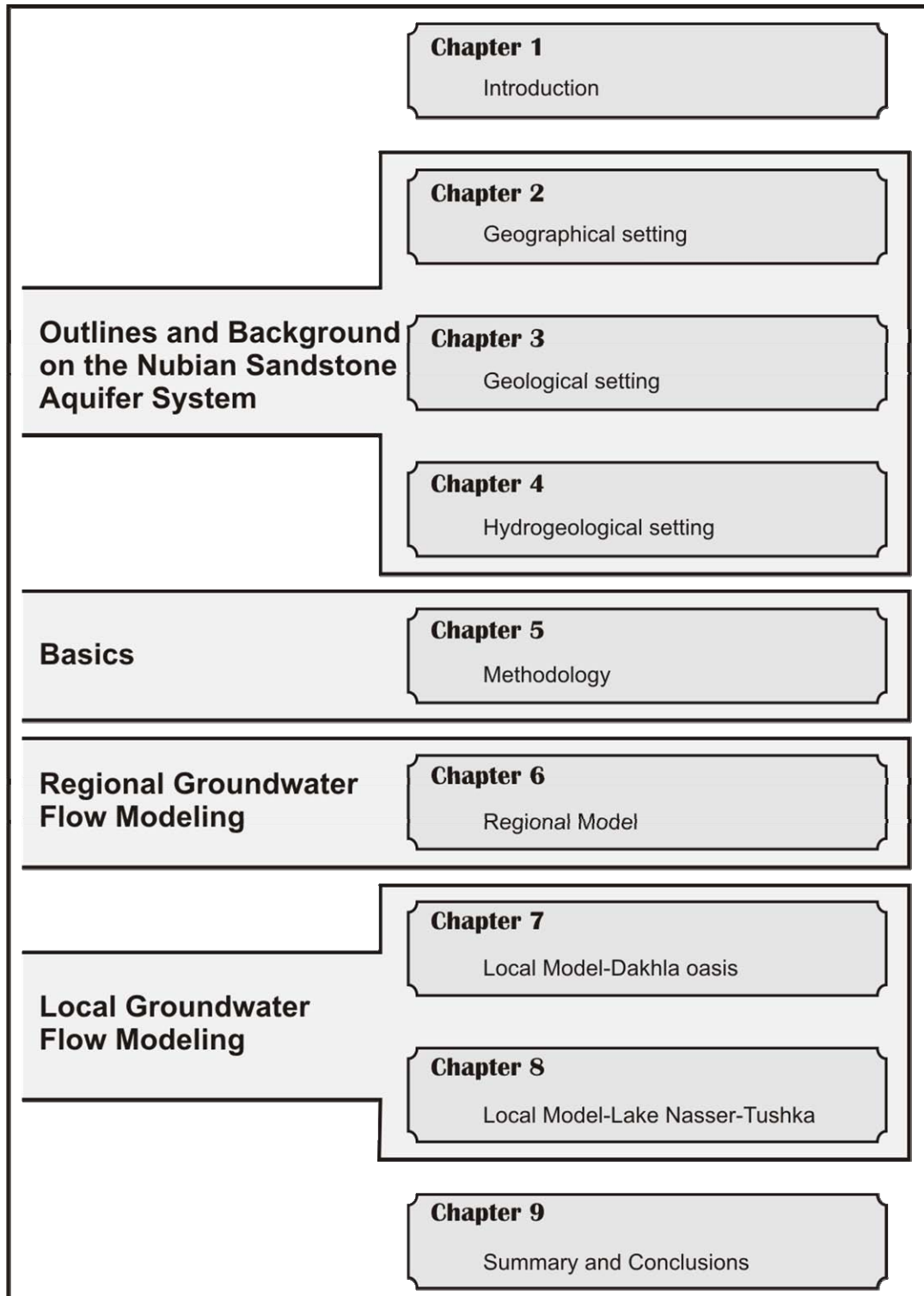


Figure 1.1. An illustration showing the structure of the thesis.

Chapter Two sets the scene within the study area by describing the outlines, location and important regional physical setting controlling the area of interest in terms of the geomorphological features and climate.

Chapter Three produces the geological settings of the study area and discusses the lithological as well as the stratigraphic units composing the NSAS, as this discussion helps greatly in the further formulation and development of the conceptual framework. The major structural framework is also presented.

Chapter Four describes the hydrogeology of the NSAS. The purpose is to characterize the structural and dynamic properties of the system, to provide a coherent hydrogeologic framework, and develop a conceptual model. It delineates the extension, boundaries, subunits, and basins of the NSAS and discusses the issue of the NSAS as a transboundary aquifer system. In addition, Chapter Four presents the aquifer systems in Egypt. The environmental situation, origin of groundwater in the aquifer, natural discharge, and the hydraulic parameters are discussed as well.

Chapter Five highlights and debates the concept and proposed computation methodology of groundwater flow modeling.

Chapter Six figures the procedure of creating a GIS-database and the development of a coherent, reliable conceptual model for the NSAS. The boundary conditions, initial conditions, as well as the calibration of the regional groundwater flow model of the NSAS are characterized and delineated. In addition, the results of the regional groundwater flow modeling in terms of the decline of the hydraulic head and depth to groundwater are examined, interpreted, and introduced in this chapter.

Chapter Seven presents the local groundwater flow modeling within the Dakhla oasis (an oasis in the Western Desert of Egypt). In this context the groundwater management options are investigated and discussed in terms of studying the impact of applying the different groundwater extraction schemes on the aquifer behavior and setting different broadcasting simulations for this purpose.

Chapter Eight examines and debates the groundwater-lake interaction between the NSAS and Lake Nasser. The purpose of this investigation is to determine whether the water body of Lake Nasser affects the groundwater recharge of the NSAS.

Chapter Nine integrates the information from the preceding chapters into a final discussion and presents conclusions regarding the main problems addressed in the thesis.

2

Geographical Setting

2.1 Outlines and location

The study area of the Nubian Sandstone Aquifer System covers the majority of the Eastern Sahara area and extends from $14^{\circ} - 30^{\circ}$ N, and $19^{\circ} - 34^{\circ}$ E, about 1,670 km length and 1,600 km wide at its longest and widest parts, respectively (Figure 2.1).

The Sahara is the largest desert in the world, encircling almost all of northern Africa (Figure 2.1). Covering an area of about 9,065,000 km², that forms about one tenth of Africa's area (White 1983). The Sahara is diagonally split into a western and an eastern part by a series of highlands. The Eastern Sahara is usually further divided into three regions (Williams and Faure 1980): the Libyan Desert, which extends west from the Nile valley through eastern Egypt and northern Sudan, and eastern Libya; the Arabian Desert, or Eastern Desert, which lies between the Nile valley and the Red Sea in Egypt; and the Nubian Desert, which lies in northeastern Sudan (Figure 2.2). The Eastern Sahara has an area that roughly exceeds 2 million km².

The whole area described above is composed of one huge, unbroken tract of true desert area which is characterized by extreme aridity. The only slight exceptions are the narrow littoral zone extending along the Mediterranean Sea and the most southern margins of the area that receive scanty amounts of rainfall, seasonal irregular runoff, and poor, scattered plant cover. The only islands of life in the interior of this desert are represented by the oases regions, which are located in a series of depressions in the desert plateau and owe their existence exclusively to the groundwater resources. More than two thirds of the inhabitants of the Eastern Sahara are concentrated in oases where it is possible to find water (Cloudsley-Thompson 1984).

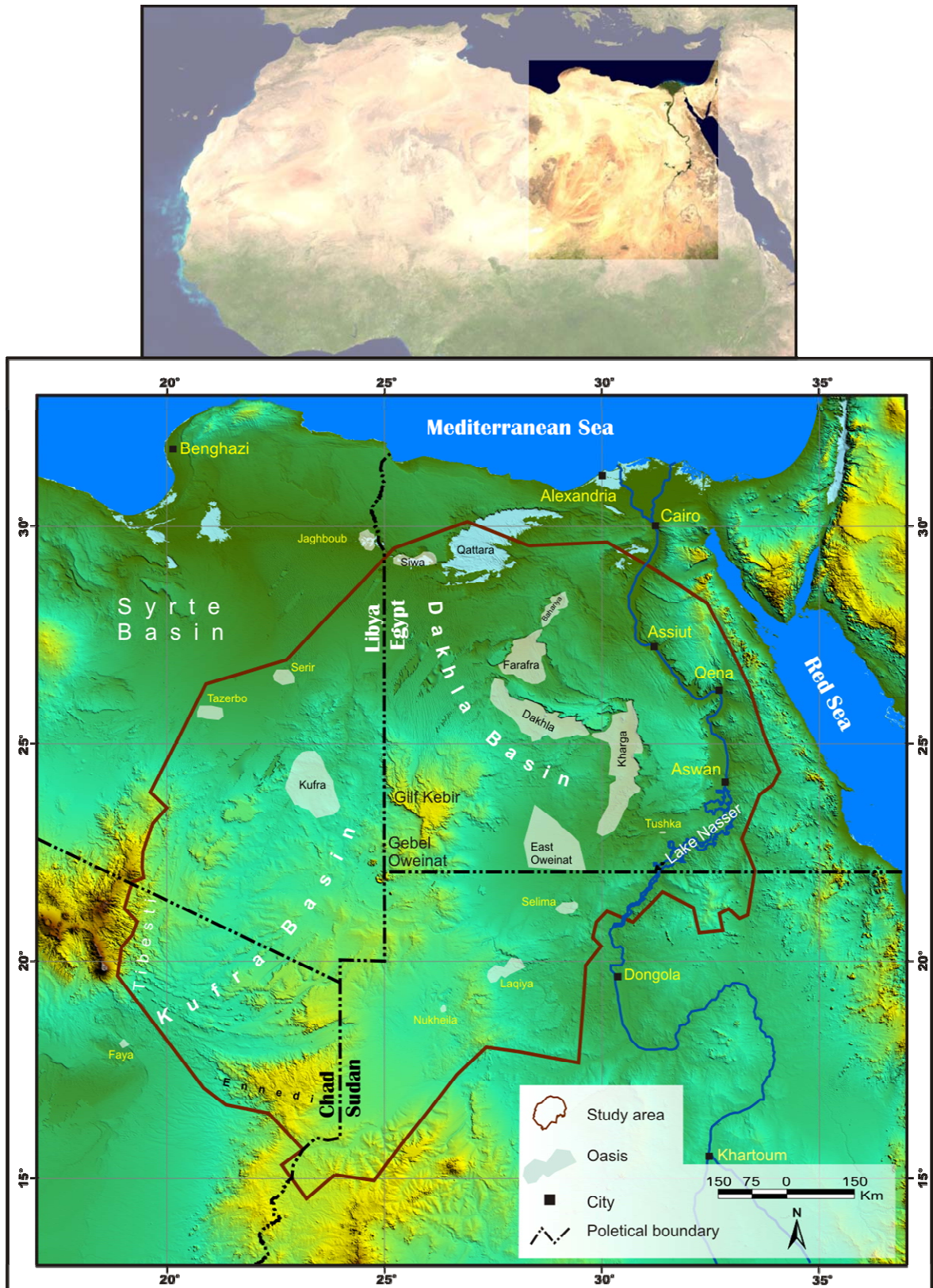


Figure 2.1. The upper image is a satellite image of North Africa including the Sahara. The lower one is an image from the DEM of the Eastern Sahara including the study area of the Nubian Sandstone Aquifer System. Sources: NASA (2005, 2006) and USGS (2004).

2.2 Geomorphology

Principal topographic features include large oasis depressions, extensive stony plains, rock-strewn plateaus, abrupt mountains, sand sheets and dunes, and sand seas. Huge areas of it are empty, but scattered clusters of inhabitants survive in fragile ecological balance wherever water sources occur. Sedentary living is restricted to oasis areas. The Eastern Sahara area is characterized generally by extreme aridity, absence of relatively recent drainage lines, and uniformity. It is characterized by bare rocky plateaus and sandy plains. Ridges and deep depressions (basins) exist in several parts of the desert, and no rivers or streams drain into or out of the area, except for the Nile, which fed from the mountainous areas outside of the region (Cloudsley-Thompson 1984).

The tilted rock strata are eroded as the land rises southward, resulting in a series of scarps that run parallel to the sea, and form cliffs that sometimes reach several hundred meters high (Figure 2.2). At some points at the base of the scarps, the wind has excavated depressions which reach into the groundwater lying under the whole of the Libyan Desert (Tawadros 2001). Precambrian rocks are exposed in a few places across the Eastern Sahara. During the Mesozoic most of North Africa was under water, and marine deposits were deposited. The area was uplifted in the Middle Tertiary and has been eroding ever since. The surface of the desert ranges from large areas of sand dunes (which are called Erg), to stone plateaus (Hamadas), gravel plains (Regs), dry valleys (Wadis), and salt flats. The northern and southern margins of the area still also receive more rainfall and have greater vegetation than central ones do (El-Sayed 1995; Zahoran and Willis 1992).

Despite the apparent homogeneity of the Eastern Sahara, closer examination of the desert surface permits the recognition of several physiographic regions, each of which exhibits a particular landscape (Said 1960; Neumann 1989). These can be seen in Figure 2.2 and are briefly described as follows:

- **Mediterranean Coastal Plain**

This is a relatively narrow plain running in an east-west direction parallel to the coastline. It is bounded at its southern side by a low escarpment rising about 100 m above sea level (Himida 1970). This plain is characterized by a series of elongated ridges taking the same direction of the plain itself and alternating with shallow depression areas. Such ridges are composed of oolitic limestone.

- **Plateaus (Hamadas)**

Hamada is an Arabic word describing plateaus (dead, lifeless). It is a type of desert landscape consisting of largely barren, hard, rocky plateaus with very little loose material.



Figure 2.2. The background is a satellite image of the Eastern Sahara showing the main highlands and depressions within the NSAS. The foreground illustrates the main physiographic features of the Eastern Sahara. Satellite image obtained from NASA (2006); the physiographic features compiled from Neumann (1989), Mainguet (1995), and Nicoll (2001).

Hamadas are tabular, rocky trays restricted by cliffs. They are of sedimentary origin, frequently calcareous. The best known plateaus are the following: *The Marmarican Homoclinal Plateau* forms the extreme northern area of the Eastern Desert. It extends from the Nile Delta westward to Cyrenaica in northeastern Libya and forms the North Mediterranean Coastal Plain southward to the Qattara Depression. It is an almost flat plateau sloping regionally both to north and west and rising 300-400 m from sea level. *The Limestone Plateau* covers an extensive area west of the Nile valley and has an elongated shape, mainly north-south parallel to the Nile valley. It is composed mainly of compact limestone and extends southward until it ends with an escarpment about 300 m high overlooking the sandstone plateau. *The Sandstone Plateau* covers more than half the area of the Eastern Sahara and forms an extensive plateau extending from the Nile valley to the east until the Tibesti and Ennedi highlands to the west and from Kordofan region to the south until the limestone plateau to the north (Kehl and Bornkamm 1993).

▪ **The Ergs (Sand Seas)**

An erg (an Arabic word expressing the vein-like features) is a large, relatively flat area of desert covered with huge volume of parallel sand dunes excavated by the aeolian activities and having little to no vegetation cover (Maxwell 1982; Waltham 2001). These are normally hundreds of kilometers in length and occasionally reach heights of a hundred meters. There are three Great Sand Seas within the Eastern Sahara: the Egyptian Great Sand Sea, the Calanascio Sand Sea, and the Rebiana Sand Sea. The three sand seas contain dunes up to 110 meters in height and cover approximately one quarter of the region (Neumann 1989).

This Egyptian Great Sand Sea occupies most of the northeastern part of the Libyan Desert south of Siwa and to the west of Bahariya and Farafra, giving way to gravel plains, mudpans, and the perfectly flat and featureless Selima Sand Sheet plains in northern Sudan further south, roughly along latitude 23 North (Nicoll 2001). A tongue of the Great Sand Sea turns west and continues across the flat plains in Libya, where it is called the Calanascio Sand Sea. After losing height and tapering off, the dunes gain strength once more and form the Rebiana Sand Sea, which occupies the western edge of the Eastern Sahara (El-Baz and Mainguet 1981; El-Baz 1992; Waltham 2001).

▪ **Depressions**

Depressions are natural excavations in the desert. According to most of the recent authors, these depressions owe their origin to tectonic factors at the first stage of their development (Knetsch and Yallouze 1955; Said 1960; Hermina 1990). These tectonic factors were supplemented afterwards by weathering and erosion action along lines of weakness. There are several important depressions in the Eastern Sahara. All of them are located at the foot of scarps and are considered oases; the exception is Qattara Depression, which contains the

Sahara's lowest point, just to the south of the northernmost scarp, with Siwa oasis at its western extremity largely below sea level (its lowest point is 134 meters below sea level). It is covered by badlands, salt marshes, and salt lakes (Hughes and Hughes 1992).

The other major oases form a topographic chain of basins extending from Al-Fayoum Depression which lies sixty kilometers southwest of Cairo along with Siwa and Jaghboub in Libya, south to the Bahariya, Farafra, and Dakhla oases before reaching the Kharga oasis (Klitzsch and Squyres 1990). These depressions are occasionally covered with plains of sandstone that belong to the sandstone series. The average ground levels within these depressions differ according to the location and get deeper northward. For instance, it is about 115 m above sea level in the Dakhla oasis and more or less near the sea level or a few meters deeper in the Siwa oasis.

There are a few scattered, seldom inhabited or completely uninhabited small oases, usually linked to the major depressions, where water can be found by digging to a few meters in depth. In the west, in Libya, there is a widely dispersed group of oases in unconnected shallow depressions named the Kufra group. It comprises Tazerbo, Rebiana, Sarra, Bishara, and Kufra, the Mourdi Depression in Chad, and the Selima and Nukheila in northern Sudan (Cloudsley-Thompson 1984). Among all physiographic regions of the Eastern Sahara, the depression areas are especially interesting, as they include the oases regions and the areas liable to be reclaimed.

▪ Regs

Regs are also known as gravel desert. They are extensive, nearly level, low desert plains from which fine sand has been removed by wind, leaving a sheet of coarse, smoothly angular, wind-polished gravel, and small stones lying on an alluvial soil (Cloudsley-Thompson 1984) strongly cemented by mineralized solutions to form a broad desert pavement. It is called locally in Egypt "Battikh Wadis" or melon valleys due to the appearance they show.

▪ Sabkhas

This is a smooth, flat plain usually high in salt; after a rain the plain may become a marsh or a shallow lake until the water evaporates. These occur usually at the depressions of the domain, where water exists on the ground surface: i.e., north and south of Wadi Howar and in the ancient Lake Ptolemy in Sudan, within the Egyptian depressions, east of Tibesti Mountains and within the Kufra oasis (White 1983; Pachur 1999).

▪ Guelta

A Guelta is a peculiar type of wetland such as a marsh or swamp. It is formed when underground water in lowland depressions spills to the surface and creates permanent pools and reservoirs without visible flow. It can be pools in the beds of Wadis (White 1983).

▪ Wadis

Wadis are dry riverbeds that contain water only during times of heavy rain; they are watercourses with temporary visible flow, such as Wadi Howar and Wadi El Milek in Sudan and Wadi Qena in Egypt (Williams and Faure 1980; Kroepelin 1990; Zahoran and Willis 1992; Robinson et al. 2006).

▪ White Deserts

The white desert owes its name to the presence of limestone and chalk which reflect white color where they are exposed. Examples of such features can be found stretching east of the Nile valley in the Eastern Desert of Egypt and over the Reg plain of Farafra oasis (Said 1990; Brook et al. 2002; Halliday 2003).

▪ Mountains and Highlands

Aside from the scarps, the general flatness is only interrupted by a series of plateaus and massifs.

These are represented by the following:

The mountains of the Nubian Arabian Shield (Red Sea Mountains) extend along the western coast of the Red Sea. *The Gilf Kebir Plateau*, is located about 150 kilometers north of Gebel Oweinat, it rises about 300 meters above the general plain and about 2,000 m above sea level and lies entirely in Egypt. Dozens of Wadis extend into the desert around its perimeter (Klitzsch 1979; Alaily et al. 1987; Kehl and Bornkamm 1993; Robinson et al. 2006). These Wadis were formed by water erosion in a wetter phase millions of years ago in the late Tertiary age. Then it was a great divide, draining water in all directions, north, south, east, and west. Slightly further to the south, near the centre of the Libyan Desert, around the convergence of the Egyptian-Sudanese-Libyan borders, the massifs of *Arkenu*, *Oweinat*, and *Kissu* occur. These granite mountains are very ancient and were formed a long time before the sandstones surrounding them. *Arkenu* and *Western Oweinat* are ring complexes (Jas et al. 1988). *Gebel Kamel* is a raised sandstone plateau adjacent to the granite part further west. The plain to the north of Oweinat is dotted with eroded volcanic features. Gebel Oweinat includes peaks reaching elevations just under 2,000 m (Klitzsch and Wycisk 1984, 1999; Kehl and Bornkamm 1993).

The *Tibesti Mountains* area is found in the northern portion of Chad and extends marginally a short distance into southern Libya. The Tibesti Mountains consist of seven inactive volcanoes. The mountains are the largest and highest range in the Sahara, with the highest peak of *Emi Koussi*, which reaches 3,415 m above sea level. *Emi Koussi* lies at the south end of the Tibesti Mountains in northern Chad (Gourgaud and Vincent 2004). It rises about 2.3 km above the surrounding sandstone plains and is about 65 km wide. Other important highlands are the Ennedi, Erdis, and Kordofan.

2.3 Climate

The climate of the Sahara has undergone noticeable variations between wet and dry over the last few tens of thousand years. The last wet period occurred 4,000 to 8,000 years BP (this issue will be further discussed in Chapter 4).

The Eastern Sahara has one of the hottest and harshest climates in the world. In the hottest months temperatures can rise to over 50 °C, and temperatures can fall below the freezing point (0 °C) in the winter. It is also extremely windy. Hot, dust-filled winds create dust devils, which can make the temperatures seem even hotter. Daytime temperatures are extremely high; Azizia, in western Libya, recorded the world's highest official temperature in the shade at 58 °C in September 1922. Heat loss is rapid at night, as a single daily variation of -0.5 °C to 37.5 °C has been recorded. Average annual temperatures exceeding 30 °C are common. Freezing temperatures are not uncommon at night from December to February (Mildrexler et al. 2006). The Eastern Sahara is located in the trade winds belt. The region is subjected to winds that are frequently strong and that blow constantly from the northeast and it changes its pattern from southward in the northern part of the Eastern Sahara to westward in the southern part (El-Baz 1998). The dust winds are registered north and south of the desert, where they are variously known as Khamasin. The region's low relative humidity rarely exceeds 30% and is often in the 4% to 5% range. The solar radiation is capable of evaporating over 200 times the amount of rainfall. The maximum average of annual sunshine duration is recorded also in the Eastern Sahara (eastern Libya); it receives about 4,300 hours (97% of the possible astronomic value). Rainfall is extremely variable and unpredictable (El-Baz 1998), as it rains in the center of the desert only once in 20 to 50 years.

3

Geological Setting

The region of the Nubian Sandstone Aquifer System as a major constituent of the Eastern Sahara was subjected to intensive geological studies on all scales. These permanent long studies presented the modern knowledge about the geology of the Eastern Sahara. Examples of these studies are given in Sandford (1935), Shata (1953), Knetsch and Yallouze (1955), Ibrahim (1956), Sigaev (1959), Elgezeery (1960), Said (1962), Hume (1965), Ambroggi (1966), Ezzat (1974), Amer et al. (1981), Klitzsch and Wycisk (1987, 1999), Klitzsch et al. (1987), Schandelmeier et al. (1987a), Wycisk (1987a, 1990, 1993, 1994), El Gaby and Greiling (1988), Gras (1988), Klitzsch (1989, 1994) Hermina (1990), Klitzsch and Squyres (1990), Salem and Belaid (1991), Klitzsch and Semtner (1993), Mansour et al. (1993), and Thorweihe and Schandelmeier (1993).

The region of the Eastern Sahara is known also as the Libyan Desert, which is distinguished from the Western Sahara by the western boundaries of the Eastern Sahara. These boundaries are located along the series of highlands running northwest of El-Fashir in Sudan and include the Ennedi, Erdis, and Tibesti Mountains as well as the Hamada desert area of Fezzan in Libya (Himida 1970). The eastern side of this desert is limited to the Nile Valley. The southern margins are distinguished by the Darfur and Kordofan mountainous areas in Sudan, while the desert extends to the north until it reaches the Mediterranean shoreline (Figures 2.2, 3.1 and 3.2).

The sediments body of the Eastern Sahara forms huge morphologic depression structure in the areas of Chad and Libya, as the sediments outcrop at all margins of the basin and the older sediments are generally overlain by the younger ones in the direction of the depression center. In the eastern part of the area (North Sudan and Egypt) a vast monoclinical structure occurs where the older formations outcrop at the southern localities, whereas they generally dip, increase in thickness, and disappear under the younger formations northward (Himida 1970).

Along the coastal zone of the Red Sea, western margins, and in the most southern regions of the domain, there are outcrops of rocks belonging to the crystalline basement complex,

which are composed of granites, granodiorites, diorites, gneisses, schists, and basalts. The ages of these rocks in most localities are assigned to the Precambrian period. However, in many localities intrusive rocks of younger ages are recorded (Klitzsch 1989, 1994).



Figure 3.1. Localities, famous features, and names mentioned in this chapter.

Moving from the southern localities of the area northward, the rocks of the basement complex are gradually overlain by a series of mostly unfossiliferous formations composed of sands, sandstones, clays, and shales which are commonly termed the Nubian Sandstone Series. The Nubian Sandstone Series varies in thickness from some few tens of meters in the northern regions of Sudan to about 250 m in the southern localities of the Kharga oasis, 900 m in the northern localities of the same oasis, and about 1,800 m in the Bahariya oasis, while it attains a thickness of more than 3,500 m in the northern localities of the Dakhla

Basin and over 4,500 in the northwestern part (Hermina 1990; Klitzsch and Wycisk 1999) of the Kufra Basin of the Libyan Desert (Figure 3.2).

Regionally, the Nubian Sandstone Series changes gradually from mainly continental sandy facies in the southern regions of the aquifer domain, to intercalations of sandstones and clays of alternating continental and shallow marine facies in the central regions of the area, to mainly marine facies in the northern regions, where it consists of thick beds of clays intercalated by beds of limestones, dolomites, and sandstones. Generally, it may be concluded that the Nubian Series, by its stratigraphical position, ranges from Cambrian to Upper Cretaceous (Thorweihe and Schandelmeier 1993).

3.1 Stratigraphy

Descriptions of the different lithostratigraphic units forming the body of the Nubian Sandstone Aquifer System in the Eastern Sahara are hereafter given from older to younger. Figure 3.3 is a schematic surface geological map of the NSAS area showing the distribution of the stratigraphic units in correspondence to their ages. The stratigraphic type sections in different localities within the domain of the Nubian Sandstone Aquifer System are represented in Figure 3.4.

3.1.1 Precambrian

As mentioned above, the Precambrian is represented by the basement complex overlain by the sediment pile of the aquifer system and outcropping at the marginal areas (Himida 1970; Bellini and Massa 1980). The crystalline basement is exposed extensively in the mountains of the Eastern Desert of Egypt, the Nubian Desert of Sudan, at Gebel Oweinat and at Kordofan, Darfur, and Tibesti massifs in Sudan, Chad, and Libya, respectively. Smaller isolated exposures also occur at different locations between Bir Safsaf and Nasser Lake in southern Egypt and northwestern Sudan (Figure 3.1 and 3.3). The basement complexes of the Eastern Desert of Egypt and the Nubian Desert of North Sudan (the Nubian-Arabian Shield) are composed mainly of high grade metamorphic rocks interrupted by granite intrusions (Elgaby 1985; El Ramly and Hussein 1985; Khudeir 1983; El Gaby et al. 1990). The basement massif of Gebel Oweinat occupies an area of about 40,000 km² and is composed mainly of alkaline, ring structured granites and metamorphic rocks, however with some volcanic interruptions of younger age (Klitzsch and Wycisk 1987; Meneisy 1990; Schandelmeier and Richter 1990). Kordofan and Darfur massifs are also composed of meta-gneisses and granites with some younger volcanic activities. Tibesti highlands are characterized by successive volcanic eruptions (Figure 3.3) forming the highest highland in the Sahara which is Emi Koussi (Bellini et al. 1991).

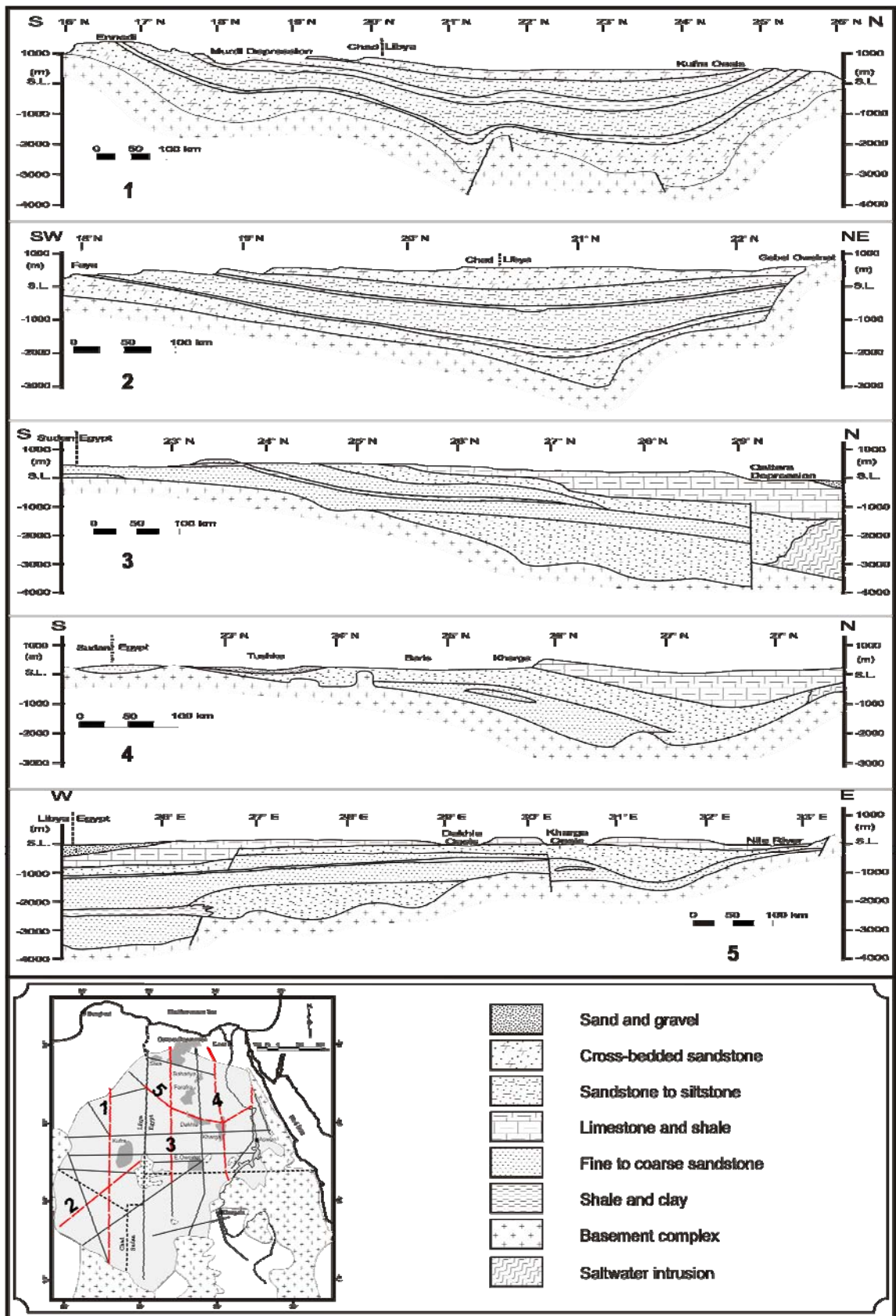


Figure 3.2. Lithostratigraphic sections along the domain area of the NSAS. The corresponding locations are shown in the overview map, compiled from Hissene (1986), Kheir (1986), and Hesse et al. (1987).

3.1.2 Cambrian and Ordovician

The strata of Cambrian and Ordovician are well known from the southern edge of the Ennedi Mountains in northeastern Chad, the Tibesti Mountains in Libya, and also from north of Kufra oasis in Libya (Figure 3.3). These strata are dipping towards the Kufra Basin where the basement rocks are unconformably overlain by over 1,000 m of sandstone in some regions (Hissene 1986) to the north of Libya. The aspect of the Cambro-Ordovician rocks is quite characteristic and uniform over large zones with the rough morphology of its outcrops. The strata consist mainly of well cross bedded sandstone of fluvial origin and intercalations of deltaic and near shore marine sandstone only in the Ordovician part of the section (Bellini and Massa 1980; Hissene 1986; Klitzsch 1987). These sediments are also detected in northern Wadi Qena in the Eastern Desert of Egypt. From the subsurface investigations in the northern part of the whole area of the aquifer system, strata that were similar but up to 1,000 m in thickness were found (Figure 3.2).

3.1.3 Silurian

The layers of this age were recorded in the same places in Libya and Chad as outcrops of small thickness but sufficiently noticeable, where they overly the Cambro-Ordovician sandstones and dip also to the center of the basin (Figure 3.3). The same strata were found also in the northwestern part of Sudan in small thickness that becomes remarkably thicker towards the west. They are composed of greenish and gray shale and clay of shallow marine origin and intercalated with siltstone (Wycisk 1987a, 1991, 1993; Klitzsch and Squyres 1990). In general, the Silurian section reaches several hundred meters of thickness near the Sudanese border with northeastern Chad and has a maximum thickness of about 500 m in the middle part of Kufra Basin.

3.1.4 Devonian

The Devonian strata outcrop in the mountainous areas of Tibesti, Ennedi, and Gebel Oweinat (Figure 3.3). The sediments of the Devonian age are completely fluvial. They are formed dominantly of continental sandstone with some minor, local shale and marine sandstone intercalations in the Libyan and Chadian areas (Klitzsch 1984, 1989). In Libya it grades to near shore marine sandstone of middle Devonian age. In northwestern Sudan as well as in southwest Egypt, this sandstone above the partly marine Silurian beds is also present, but it was nowhere observed to be grading into marine deposits. The sandstones are generally very thickly bedded and with cross bedding overturned to cross laminations and slumping. These strata seem to wedge out towards the southwest of the Kufra Basin and they cannot be distinguished beyond this. In general, this section represents the beginning of a new sedimentary cycle. In the Libyan parts these strata range from a few meters to more than 1,000 meter in thickness (Bellini et al. 1991).

3.1.5 Carboniferous

The Carboniferous beds overly the Devonian sediments and outcrop typically where the Devonian sediments outcrop (Figure 3.3). At the north of Kufra oasis, this layer also outcrops and overlies a sandstone layer of Upper Devonian-Lower Carboniferous age (Hissene 1986). The Carboniferous sediments are formed generally of cross bedded sandstones, mainly medium, fine grained, and sometimes even coarse grained in the lower third part of the bed as well as mostly well bedded. The upper part of the bed is generally formed of intercalations of silt to sandstone with limestone and shale of marine origin. In some parts this layer unconformably overlies the Devonian sandstone strata. It is normally several 10 meters thick and gets thicker towards the west (Klitzsch and Wycisk 1987, 1999). North of the Ennedi range, Carboniferous strata are made of 100-200 m of shale, siltstone, and sandstone intercalations. It is partly fluvio-continental and partly shallow marine and wedging out westward.

3.1.6 Triassic and Lower Jurassic

The strata assigned to this age are outcropping to the top at the northwestern Sudan, west of Gebel Oweinat, the northern margins of Ennedi Mountains, and the eastern margins of Tibesti Mountains (Figure 3.3). These are sandstones of totally continental origin and interbedded with paleosoils. The upper section of these strata contains flora of probably early Jurassic. These strata are of relatively big thickness in the Libyan areas and overlain by Holocene sand dunes and sandstones of Cretaceous age. These strata are more than 200 m thick in the central and northern parts of the study area (Wycisk 1987, 1993; Klitzsch 1989).

3.1.7 Upper Jurassic and Lower Cretaceous

These layers cover aquifer domain surface in most of the Chadian, Libyan and Egyptian areas as well as the northwestern part of Sudan. They are forming the top of most of the huge basin structure, which is known with the Kufra Basin (Figure 3.3). These layers form a sediment pile reaching 1,500 m at the southern Egyptian oases and increase successively northward to reach a thickness more than 3,500 m in the most northern parts of the domain (Bellini and Massa 1980). In the south these sediments are formed of sandstone and some silt of continental origin. Nevertheless, by moving northward, this situation changes to sediments of dominant marine origin. In addition, the uppermost part of these sediments is intercalated with shale deposits of marine origin with a few tens of meters thickness (Wycisk 1994). To the north of the Dakhla and Kharga oases, these sediments are overlain by rock series of proper marine facies consisting of phosphate beds, chalky limestone, and shales of Upper Cretaceous and Paleocene ages.

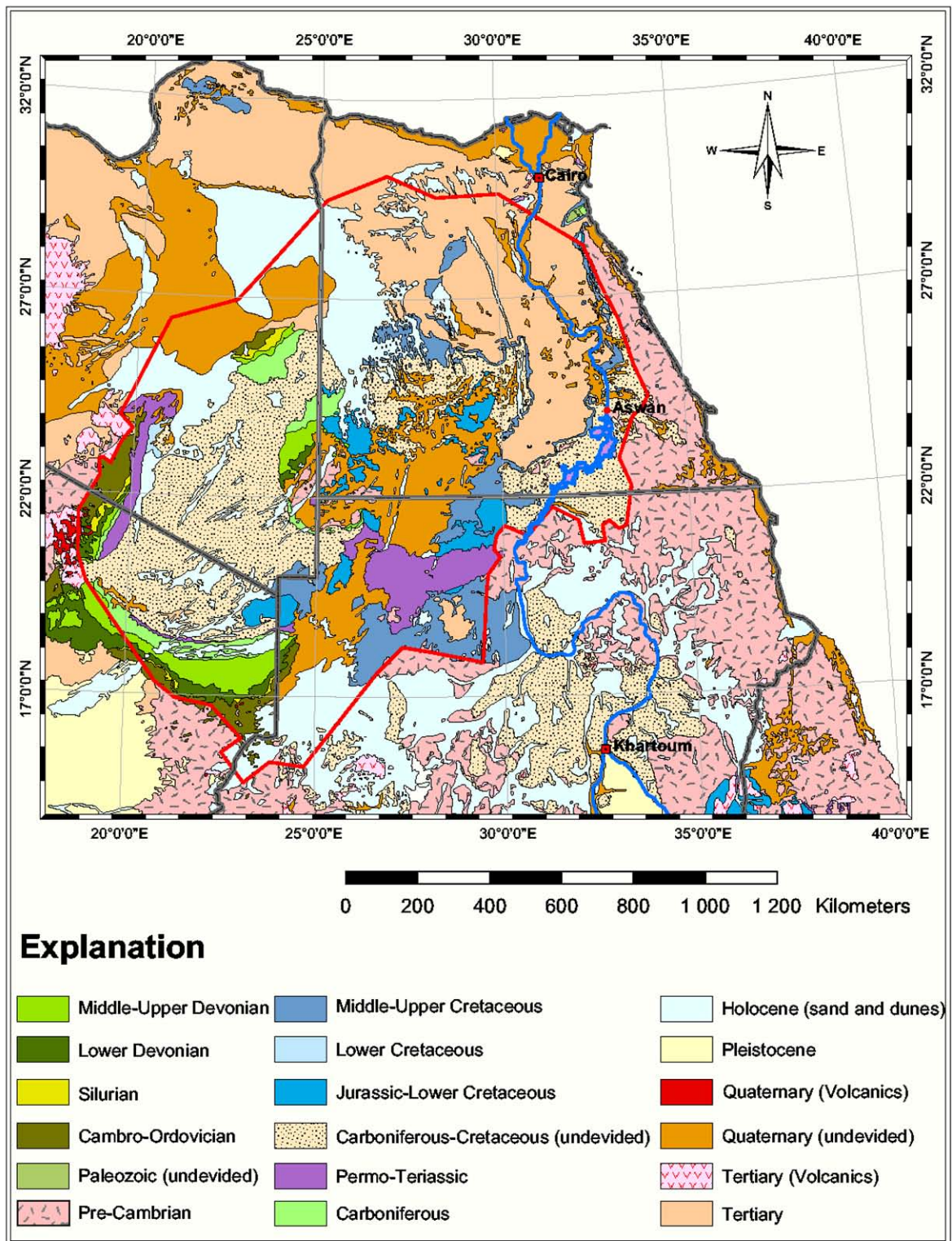


Figure 3.3. Schematic geological map of the NSAS. Digitized from maps of CONOCO (1987) and USGS (2004).

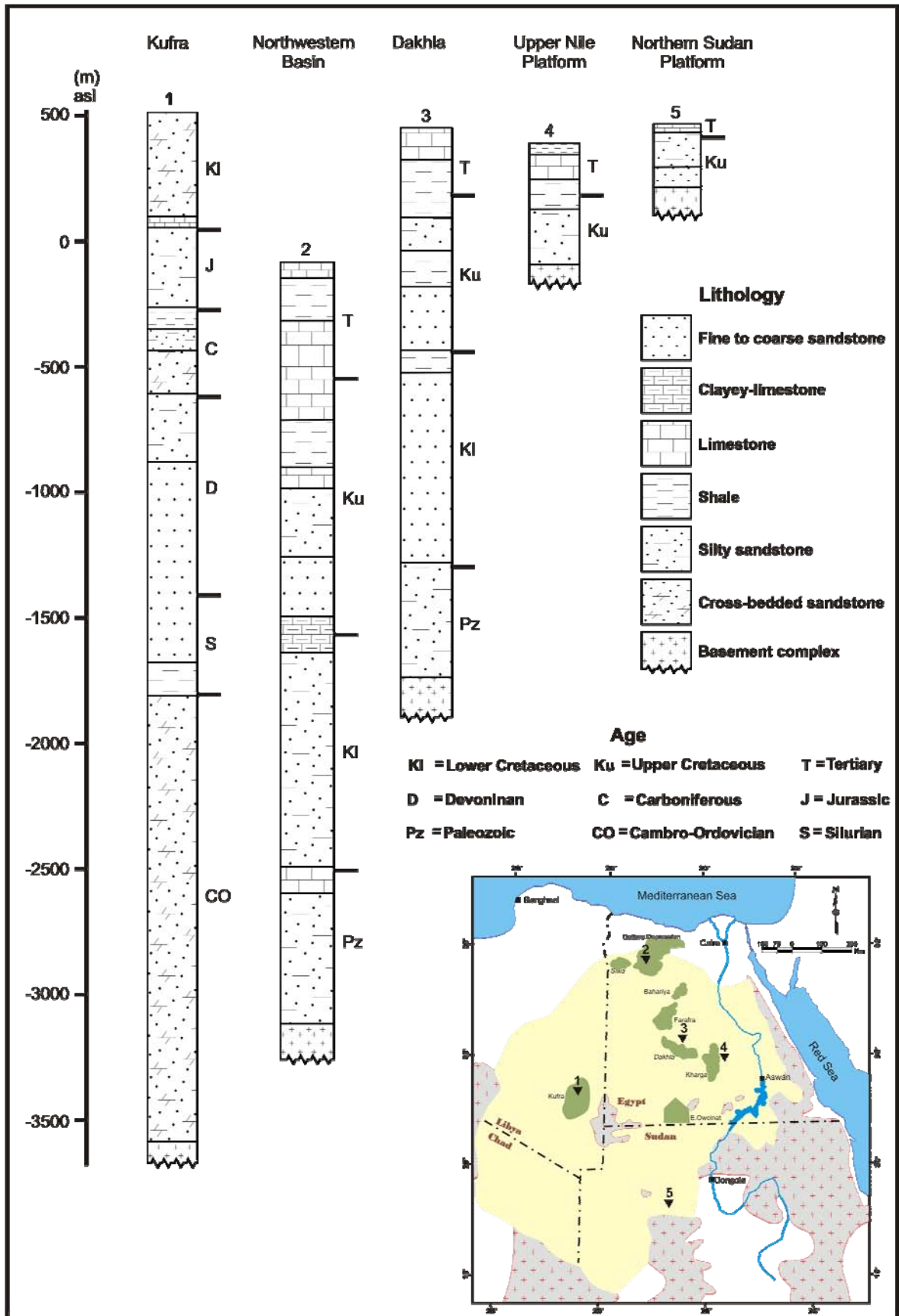


Figure 3.4. Simplified sections for different locations within the NSAS. Adapted from Thorweihe and Heinl (2002).

3.1.8 Upper Cretaceous and Tertiary

The Upper Cretaceous sediments are mainly fluvial sandstone and could be found at the surface in northern Sudan, southern Egypt between East Oweinat and Tushka, Wadi Qena, the eastern borders of the Kharga oasis, the northern borders of the Dakhla oasis, and south of the Farafra oasis. Continental, freshwater, and marine deposits of Oligocene age consisted of coarse-grained sandstones, conglomerates, and shales occupying only a very limited area of the northern region of the Libyan Desert (Tawadros 2001). In the southern localities of the Siwa Oasis region, Paleogene formations gradually disappear underneath the Miocene formations (Klitzsch 1989; Wycisk 1994). Shales, limestones, chalky limestones, and argillaceous limestones of Paleogene age cover a relatively extensive territory of the Egyptian Western Desert. In the southern regions Paleogene formations generally conformably overlie the Upper Cretaceous formations. Pliocene deposits are recorded in some regions in the most northern part of the Egyptian Western Desert and the Nile Valley (Hermina 1990). Some volcanic activities have taken place in Tertiary age (Figure 3.3), developing volcanic interruptions in many localities as mentioned in section 3.1.1. These are mostly basaltic outcrops of average round shape, occupying relatively large areas and forming plateaus of very flat and smooth surfaces (Bellini and Massa 1980).

3.1.9 Quaternary

Pleistocene and Recent deposits are represented by fluvial deposits in the Nile Valley and Delta, gravel terraces bordering the Nile valley, lacustrine deposits covering the ground surface in some of the depressions, and Wadi fillings at the edges of the desert plateau and in the Eastern Desert. Consolidated dunes of Holocene age are found along the coastal zone of the Mediterranean, and the widespread free-moving sand deposits in the form of sand dunes and sand sheets are found on the top of a great part of the study area (Said 1990). Lake sediments and Sabkhas are major constituents of the surface of most of the depressions and oases, as they occur in thickness reaching 60 m in Sudan and the Kufra depression and about 40 m in the Kharga oasis (Kroepelin 1999).

3.2 Major structural framework

Since early Paleozoic time vertical movements in this area have been very slow and are epeirogenesis in nature, and since they take the form of either uplift or subsidence, it is a chiefly vertical form of movement and plays little role in either plate tectonics or mountain building. Local interruptions with some faults and small deformation movements with minor displacements are, however, present. Faulting is much diffused in the Paleozoic outcrops, and many of the faults are intruded and therefore show up as dikes. This characteristic is also present in the continental Mesozoic outcrops (Schandelmeier et al. 1987). The general structural framework of the Eastern Sahara area is demonstrated in Figure 3.5.

The epeirogenetic vertical movements led to the formation of the large basins of the area, which are now filled up with sediments over 4,500 m thick and bordered or separated by zones of minor subsidence or uplift. Within the central Sahara, the structural development follows fairly regular patterns, with an older NNW-striking pattern and a younger one with an approximately NE orientation. Over large distances the Precambrian basement is at the surface or covered by only thin sediments (Klitzsch 1983, Wycisk et al. 1990).

An old, early Paleozoic NNW-striking uplift called Howar-Oweinat Uplift extends from the eastern part of Wadi Howar in Sudan northward across Gebel Oweinat in southwestern Egypt. This uplift separates the area of southwestern Egypt that is known as the Dakhla Basin and the Kufra Basin. The sediments east of Howar-Oweinat Uplift seem to be shallow. Around Bir Misaha in the south of Egypt and Gebel Abiad north of Sudan, relatively small basins of minor importance were developed parallel to the Howar-Oweinat Uplift (Meshref 1990).

To the west and southwest of Aswan in Egypt, there are several east-west faults with vertical displacement of Mesozoic and Tertiary strata of up to a few hundred meters. The major uplift among them is the Safsaf-Aswan Uplift. It extends further westward until the basement of Bir Misaha. Another one crosses the East Oweinat area until Gebel Oweinat. It is well known as the Oweinat-Safsaf Uplift (Wycisk 1987b, Morgan 1990, Klitzsch and Wycisk 1999).

A great Paleozoic tectonic event was responsible for the formation of the Ennedi-Oweinat Uplift that has a tectonic trend direction of NE-SW.

During Tertiary, a large area between the Oweinat region and the Bahariya oasis was affected by volcanic activity, resulting mainly in ring structures, but also locally in pipes, small volcanoes, or basalt blankets (Figure 3.3). The Oweinat area itself is characterized not only by volcanic activities but also by large acid to intermediate intrusions of Tertiary (Klitzsch 1989). In Kufra Basin, the dip of the continental Paleozoic and Mesozoic sediments follows the outline of the basin edges (Bellini and Massa 1980).

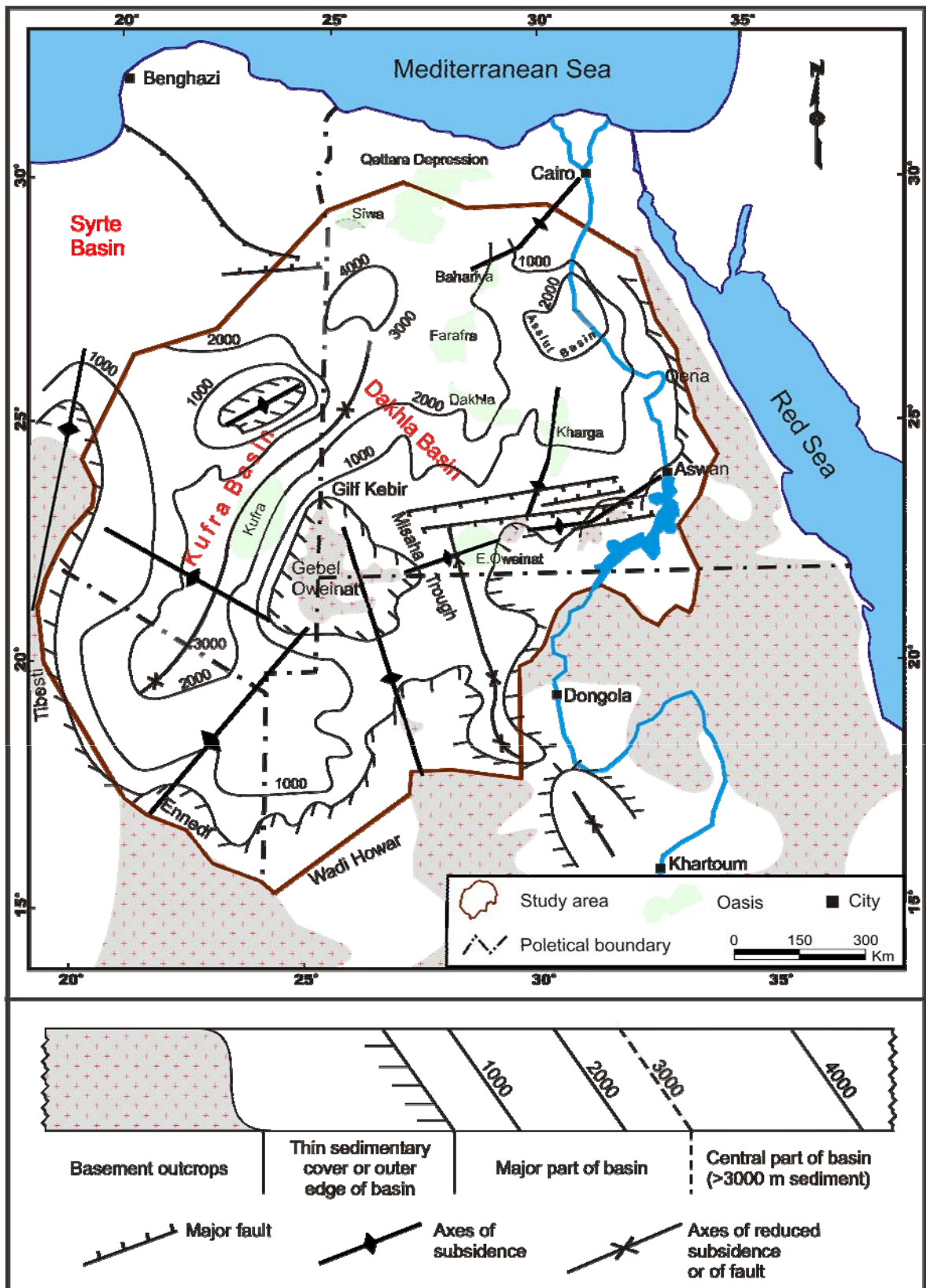


Figure 3.5. General structural framework of the NSAS, adapted from Klitzsch (1984), Klitzsch and Wycisk (1989).

4

Hydrogeological setting

4.1 Nubian Sandstone Aquifer System

4.1.1 Extension and boundaries

The Nubian Sandstone Aquifer System (NSAS) is considered to be one of the most significant and potable groundwater basins in the world, as it is the only water resource for most of the areas sharing its valuable reserve. It extends over a vast area in Egypt, Libya, Sudan, and Chad (Figure 4.1).

In spite of its vast area, it is considered as a broadly closed system, as it has natural boundaries to the east and southeast formed by the mountain ranges of the Nubian Shield and is bounded to the south and west by the mountainous outcrops of Kordofan Block, Ennedi, and Tibesti. To the southwestern part of the basin, the aquifer is bounded by the groundwater divide located between Ennedi and Tibesti Mountains. The natural northern boundary of the Nubian Sandstone Aquifer System is set to the so-called Saline-Freshwater Interface, whose location is considered spatially stable, although slight movement is believable (Thorweihe 1987; Thorweihe and Heintl, 1996, 1999, 2000).

The NSAS has a complex structure, which precludes adequate identification of the hydraulic continuity between the various sub-basins. The hydraulic interconnection is emphasized between sub-basins within individual countries sharing the system as well as between the different basins forming the system at the regional level (Wycisk 1993, 1994; Klitzsch and Wycisk 1999).

The NSAS consists of a thick sequence of coarse (refer to Chapter 2 for detailed geological outlines), clastic sediments of sandstone along with siltstone interbedded with impermeable shale and clay beds. The more claylike impermeable beds restrict the vertical movement of water. These beds of lower permeability, however, are lenticular and discontinuous at some locations (Idris and Nour 1990; Thorweihe and Heintl 2002).

4.1.2 Subunits of the aquifer system

The area of the Nubian Sandstone Aquifer System is composed of different water bearing strata (CEDARE 2002; Foster and Loucks 2006) laterally and/or vertically interconnected. It can be differentiated into two major reservoirs (Figure 4.1). The oldest and the most extended reservoir is the Nubian Aquifer System (NAS). It is largely prevailing unconfined conditions and includes a number of basins that are hydraulically connected. The unconfined part of the Nubian aquifers includes the most important groundwater potential of the whole basin (Bakbakhi 2006).

The other reservoir includes parts of Libya and Egypt. It is referred to as the Post Nubian Aquifer System (PNAS). The NAS underlies almost all the area of Egypt, Eastern Libya, Northern Sudan, and Northern Chad. The NAS comprises the Paleozoic and the Mesozoic deposits and overlies the Pre-Cambrian basement complex. The PNAS occurs generally to the north of the 25th latitude overlying the NAS in the north of the Western Desert of Egypt and Northeastern Libya (Bakbakhi 2006).

The PNAS comprises the Tertiary continental deposits in Libya and Egypt and the Tertiary (Upper Cretaceous-Eocene) shale and carbonate complex that confine the system at the topographic depressions in Egypt. A low permeability layer belonging to the Upper Cretaceous and the lower Tertiary sediments separates the two reservoir systems (CEDARE 2002; Bakbakhi 2006).

Groundwater mining of the reserves of the Nubian Sandstone Aquifer System is presently taking place and increasing yearly. In the past 40 years over 40 billion cubic meters ($40 \times 10^9 \text{ m}^3$) of groundwater has been exploited from the system in Egypt and Libya (Margat et al. 2006). This has provoked the groundwater level to decline progressively. Consequently, over 35% of the free-flowing wells and springs in many locations had to be deepened or substituted with deeper wells. The area of the Nubian Sandstone Aquifer System of the Eastern Sahara is about 2.35 km². A great part of this area lies on the Egyptian side, as it possesses about 880,000 km² distributed nearly all over the country (CEDARE 2001). The remaining area is contributed by the other sharing countries as shown in Table 4.1.

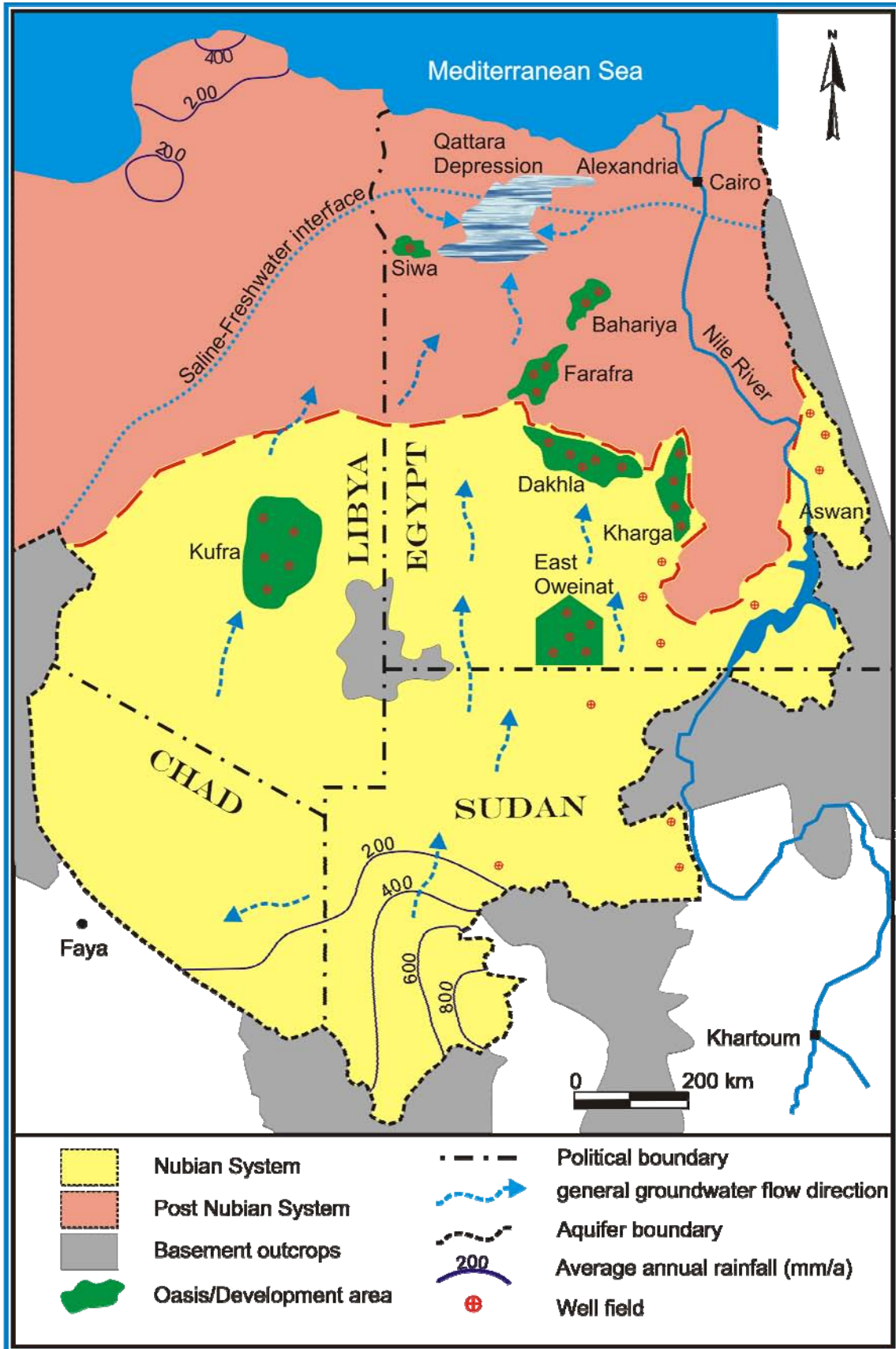


Figure 4.1: Regional hydrogeological overview of the Nubian Sandstone Aquifer System. Compiled from: CEDARE (2002), Salem and Pallas (2004), Bakhbaki (2006).

Groundwater storage of the NSAS in the Eastern Sahara is huge and represents the largest fresh groundwater reserve in the Arab world or maybe in the whole world (CEDARE 2001, 2002). This issue has been published frequently. The most known studies are from Ambroggi (1966), who estimated the total groundwater volume of the Sahara at 15,000 km³, and from Gischler (1976), who considered it to be at least 60,000 km³. Thorweihe and Heintl (1996) estimated the groundwater volume of the Nubian Sandstone Aquifer System 150,000 km³, with a very large amount of water largely exceeding the previous estimates. CEDARE/IFAD (2002) in a program for the development of a regional strategy for the utilization of the Nubian Sandstone Aquifer System has estimated the fresh groundwater volume within the system at 372,950 km³ (Table 4.1).

Based on the most updated database and the GIS technique, the groundwater resources of the Nubian Sandstone Aquifer System were calculated by the author using the modeled saturated volume and the calibrated hydraulic parameters of the system (refer to Chapter 6). Since it is economically unreasonable and infrastructurally impossible to obtain groundwater from great depths over broad areas of the aquifer system, the total volume of the groundwater resources is to some extent of academic interest. For the interpretation of groundwater ages based on radiocarbon analyses, however, it is very important to have an idea of the groundwater's mean residence time, which is dependent on water volume and discharge rate (Figure 4.5).

Table 4.1. Area, freshwater storage, and present extraction rates of the Nubian Sandstone Aquifer System.

Country	Area (1000 km ²)			Freshwater storage ¹ (km ³)			Present extraction (km ³ /year)		
	PNAS	NAS	Total	PNAS	NAS	Total	PNAS	NAS	Total
Egypt	569	311	880	102,417	52,299	154,716	0.306	0.2	0.506
Libya	350	300	650	11,240	125,309	136,549	0.264	0.567	0.831
Sudan	-	750	750	-	47,807	47,807	-	0.84	0.84
Chad	-	70	70	-	33,878	33,878	-	0.0	0.0
Total	919	1430	2,350	113,657	259,293	372,950	0.57	1.607	2.177

¹ Assuming a storativity of 10⁻⁴ of the confined part of the aquifer and 7% effective porosity of the unconfined part.

Source: CEDARE/IFAD (2002). Programme for the Development of a Regional Strategy for the Utilization of the Nubian Sandstone Aquifer System.

4.1.3 Basins of the NSAS

Regional faults and uplifts divide the entire Nubian Sandstone Aquifer System into four basins (Ezzat 1974; RIGW 1988, 1993, 1999; FAO 1997; Attia 1998; MPWWR 1999; Thorweihe and Heintz 2002). Two of them are major basins and of high significance, and these are the Kufra Basin of eastern Libya, northeastern Chad, the most northwestern strip of Sudan, and the Dakhla Basin of the Western Desert of Egypt. The other two subunits are the Upper Nile platform and northern Sudan Platform; they are of minor importance in relation to the Kufra and Dakhla basins, as the thickness of their sediments ranges from little wedges to a few hundred meters (Klitzsch 1994; Klitzsch and Wycisk 1999).

The Kufra and Dakhla basins are filled by fluvial Paleozoic and Mesozoic sandstone forming an enormous groundwater-bearing formation with a thickness reaching 3,500 m in the northern part of the system in Egypt and about 4,500 m in the northern (Klitzsch and Squyres 1990) part of the Kufra Basin in Libya (Figure 4.2). On the other hand, continental sediments of a few hundred meters' thickness predominately cover the Upper Nile and northern Sudan platforms (Heintz and Brinkmann 1989). These basins are discussed briefly as follows (Attia 1998; RIGW 1999):

4.1.3.1 The Northwestern Basin

It lies northwest of the Cairo-Bahariya Uplift that separates it from the Dakhla Basin to the south of it (Figure 4.2). Only the southernmost strip of that unit stretches to the south of the Saline-Freshwater Interface that outlines the northern boundary of the Nubian Sandstone Aquifer System. It is composed of marine shale and limestone that have thickness ranges from 3,000-5,000 m, and in its central part these marine sediments are overlain by Miocene continental sandstone, forming a phreatic aquifer with very good hydraulic conductivity (Hantar 1990).

4.1.3.2 The Dakhla Basin

It is the largest and most important unit in Egypt. It consists of fine to coarse grained continental sandstone of Lower Cretaceous with good permeability and thickness reaching 3,500 m. Two beds of the Silurian, low permeable sediments, which are of marine origin, occur mainly as marine shale and intercalate the sandstone sequence (Hermina 1990, Wycisk 1993). These two beds are of a few tens of meters in thickness and thicken to the north. The aquifer system is unconfined to the south of the basin, where the sandstone outcrops, while to the north, where the sandstone is overlain by the impermeable marine shale and clay, the aquifer reveals confined conditions (Hermina 1990; Klitzsch and Schandelmeier 1990; Klitzsch and Wycisk 1999). Actually, all the Egyptian oases and almost all the newly constructed development areas lie in this basin.

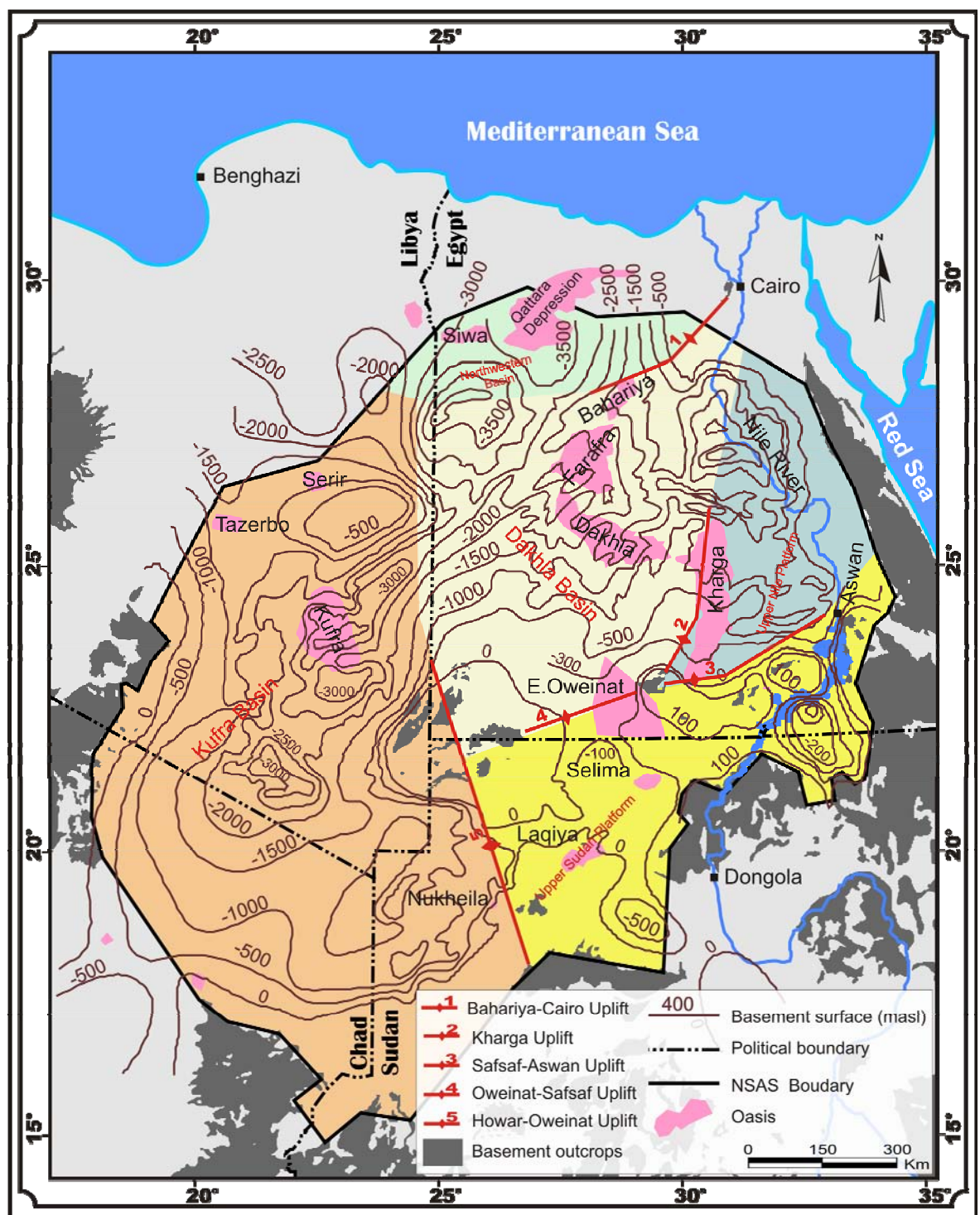


Figure 4.2: Locality map showing the thickness, major uplifts, and the structural units of the NSAS. Locations of uplifts adapted from thickness after Klitzsch (1983), Hissene (1986), Hesse et al. (1987), and Thorweihe (1996).

4.1.3.3 The Upper Nile Platform

The Kharga Uplift separates the Upper Nile Platform from the Dakhla Basin that is located west of it. On the other hand, the Oweinat-Safsaf Uplift and the Safsaf-Aswan Uplift

separate both the Dakhla Basin and the Upper Nile Platform from the Upper Sudan Platform that lies to the south of them (Figure 4.2). The sediments of this basin are of Cretaceous age but have a relatively much higher rate of shale intercalations than those of Dakhla Basin; hence, the sediments of the Upper Nile Platform have much lower permeability than their equivalent in the Dakhla Basin (Thorweihe 1996).

4.1.3.4 The Northern Sudan Platform

It forms an area where only thin sediments of less than 300 m thickness occur. This unit is bounded to the east and south by the basement outcrops and to the west by Howar-Oweinat Uplift, which separates it from the Kufra Basin. The basin is formed mainly of continental sandstone and very a few tens of meters thick bed of marly limestone that cover the plateaus of the basin (Hermina 1990; Wycisk 1993).

4.1.3.5 The Kufra Basin

It extends over the southeast of Libya, northeast of Chad, and northeast of Sudan. Continental sandstones of Cambro-Ordovician to Lower Cretaceous generally form the basin with minor intercalations of marine deposits of Lower Silurian and Carboniferous. One hundred fifty to 200 m of shale and clay are intercalating the aquifer and increasing in thickness toward the south and southwest of the basin. The greatest thickness of the Nubian Sandstone Aquifer System is recorded within this basin (Hissene 1986; Salem and Pallas 2004), as the thickness of the sediments reaches 4,500 to the north of it (Figure 4.2).

4.2 Aquifer systems in Egypt

Groundwater in Egypt is not extracted only from the Nubian Sandstone Aquifer System but could also be withdrawn from some different bearing formations that can provide fresh groundwater to satisfactory limits quantitatively and qualitatively as well. According to the accessibility and locality of the aquifer that plays a big role in the quality of water, the significance of the aquifer comes up for discussion. Hydrogeologically, the framework of Egypt can be characterized into five major aquifer systems (RIGW 1988, 1993; Attia 2001; Allam et al. 2002; Dawoud 2004). They differ in general individualities, including extension, hydraulic conductivity, transmissivity, storage, recharge, etc. (Figure 4.3).

4.2.1 The Coastal aquifer

In the coastal aquifer systems, both along the Mediterranean as well as along the Red Sea coast, the aquifer system is assigned to the Quaternary and Late Tertiary mainly sandstone sediments in the form of scattered pockets. Groundwater is mainly brackish in most areas, and its salinity is affected by the seawater intrusion and is in excess of 2,000 ppm. Groundwater recharge occurs generally from rainfall (Allam et al. 2002).

4.2.2 The Nile Aquifer

This is situated in both the Nile flood plain and the Nile Delta. It consists of Quaternary alluvium of a thick layer of graded sand and gravel covered by clay to silty clay. The aquifer thickness reaches 1,000 m along the Mediterranean coast. The salinity exceeds 1,500 ppm in many parts of the aquifer, especially to the north. This aquifer system is renewable and the main recharge source is the seepage from the Nile and the infiltration from the drainage system of the agriculture activities. The transmissivity is estimated to be about 10,000 m²/d (Attia 1985, 1998).

4.2.3 The Moghra Aquifer

It is dominated by fluvio-marine sands of Lower Miocene and occupies a wide area to the west of the Nile Delta up to the Qattara Depression. The water-bearing strata belong to an ancient delta of a river dating back to early Miocene times. The thickness of the aquifer varies from a few tens of meters on the eastern side to almost 1,000 m on the western side. The water in this aquifer is brackish and changes from saline to hyper-saline further to the west of the aquifer. Recharge is achieved mainly from deep percolation from the Nile alluvium. The transmissivity ranges from 500-5,000 m²/d (RIGW 1992; Laeven 1991; Diab et al. 1995).

4.2.4 The fissured Carbonate aquifer

This aquifer occupies an area of about 500,000 km², or 50% of the surface area of the country, and dominates basically in the north and middle parts of the Western Deserts. In spite of its vast area, it is considered the poorest aquifer in the country. Its sediments are of Eocene to Upper Cretaceous origin and overlie the Nubian Sandstone. The aquifer is formed of limestone, dolomite, chalk, and marl and may locally include phosphate and shale intercalations. Its thickness varies from 200-1,000 m, and brackish water is found in various locations (Dams and Moore 1985; RIGW 1993).

4.2.5 The Nubian Sandstone Aquifer

The NSAS in Egypt is assigned to the Paleozoic-Mesozoic (Wycisk et al. 1990; Klitzsch and Wycisk 1999). It occupies a large area in the Western Desert and parts of the Eastern Desert and Sinai. Groundwater can be found at very shallow depths, where the water bearing formation (horizon) is exposed or at very large depths (up to 1,500 m), where the aquifer is (semi)confined. The deepest water bearing horizons are generally encountered in the north, for example in the Siwa oasis, while the shallowest are encountered in the southern portion in Kharga and the East Oweinat area. The aquifer transmissivity is generally medium to low, varying from 1,000 to 4,000 m²/day. Groundwater quality is generally good in the major part, except near the coastal regions and Sinai (Thorweihe 1990; Thorweihe and Heintl 2002).

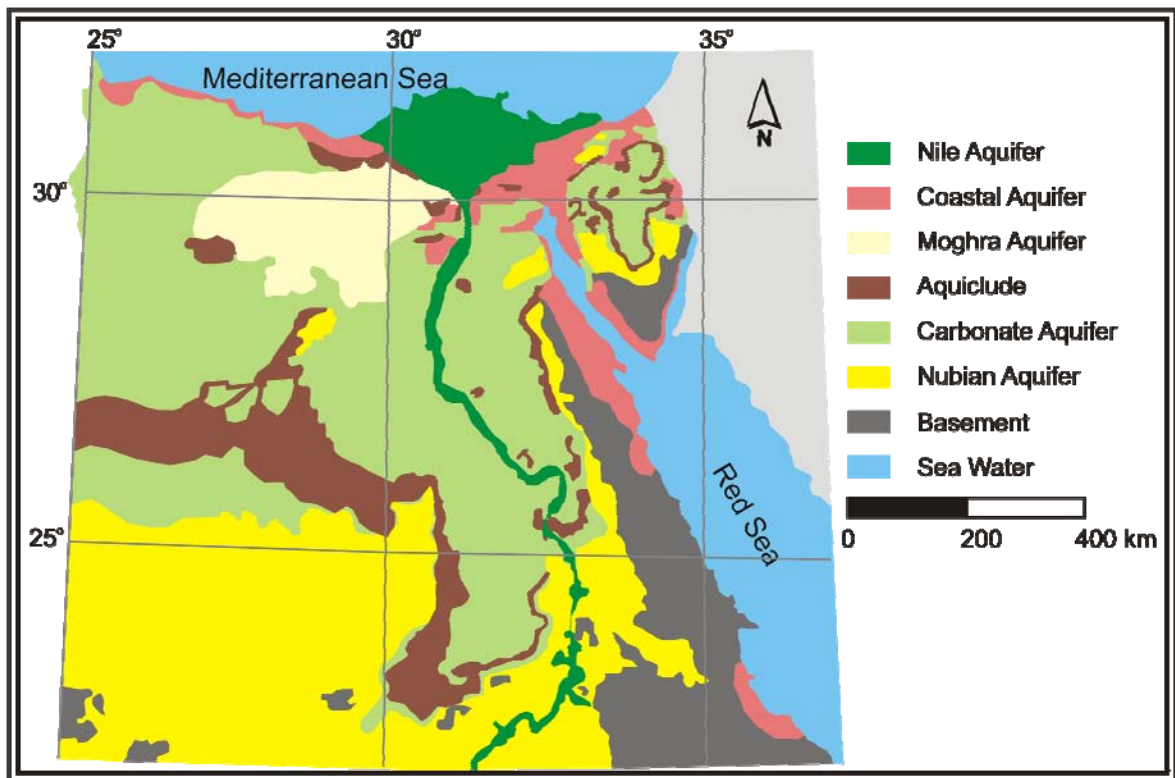


Figure 4.3. The aquifer systems of Egypt. Modified after RIGW (1998).

4.3 NSAS as a Transboundary Aquifer

The term “Transboundary Aquifer” refers exclusively to the aquifers that traverse a political boundary between two or more sovereign states (an example from the Nubian Sandstone Aquifer System is illustrated in Figure 4.4), so it is necessary to view the entire aquifer system, including all aquifers that are hydraulically interconnected, directly by lateral or indirectly through vertical contact or through fractures and low permeability formations (aquitards). Groundwater is usually a part of a greater hydrologic system, sometimes with the surface water and/or groundwater of a neighboring country (Eckstein et al. 2005).

Four case models to characterize the transboundary and international provinces associated with groundwater resources were suggested by Barberis (1986):

- A confined aquifer that is intersected by an international boundary and hydraulically is not connected to other ground water or surface water. It alone forms the shared natural resource.
- An aquifer that lies completely within the province of one country but is hydraulically adjoined to an international river.
- An aquifer that is located entirely within the territory of a single state and is associated hydraulically with a further aquifer in a neighboring state.

- An aquifer that is located entirely within the province of a certain state but has its recharge zone in another state.

These case models serve as common patterns for the application of international water law.

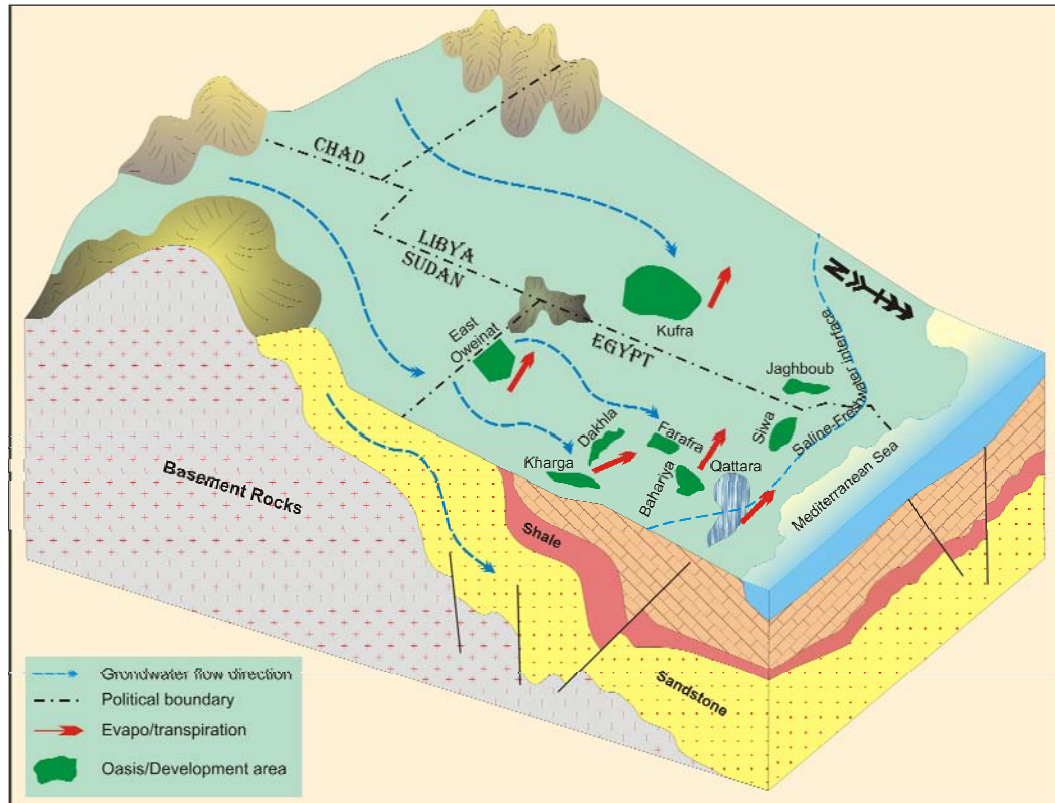


Figure 4.4: Diagram of the transboundary Nubian Sandstone Aquifer System. Adapted from Salem and Pallas (2004), Bakhbakhi (2006).

Although Transboundary Aquifers are as important as Transboundary Rivers, their importance has received insufficient and only secondary consideration, especially in environmental and human development and among legislatures and decision makers. More than one half of the world’s population is depending on groundwater for its essential needs (UN 2003). Neither groundwater nor surface water is confined to political boundaries, but they occur over and/or beyond them in many cases all over the world.

As discussions of the issue concerning the management of transboundary river basins have been taking place for many years (Bourne 1992; Van Dam and Wessel 1993), the same cannot be quite completely stated about transboundary aquifers, as they were hardly at the front of the scientific and political debates.

Lately, some individuals and international associations have started focusing on the issue of the Internationally Shared (Transboundary) Aquifer Resource Management (ISARM) or the Transboundary Aquifer Resources Management (TARM): i.e., the International Association of Hydrogeologists (IAH 2003) and the Federal Institute for Geosciences and

Natural Resources (BGR 2006-Bundesanstalt für Geowissenschaften und Rohstoffe) in the frame of the WHYMAP-project (Worldwide Hydrogeological Mapping and Assessment Program), and (UNESCO-IHP) the UNESCO’s International Hydrogeological Program (Puri et al. 2001).

4.4 Environmental situation

Non-renewability is never strictly expressing groundwater resources, but in many cases, especially in the arid regions, the time span required for aquifer replenishment is normally too long in relation to the normal time frame of human activities in general and of water resources planning in particular. In cases where groundwater is available for extraction from the reserves of an aquifer which has a very low current rate of average annual recharge but a large storage capacity, this groundwater resource can thus be termed “non-renewable”. The NSAS (Figure 4.5) is typically one of these cases, as the development of its reserves involves the mining of its “fossil groundwater”. Fossil groundwater is the water that infiltrated usually 10,000 years ago and often under climatic conditions different from the present and that has been stored underground since that time (Margat et al. 2006).

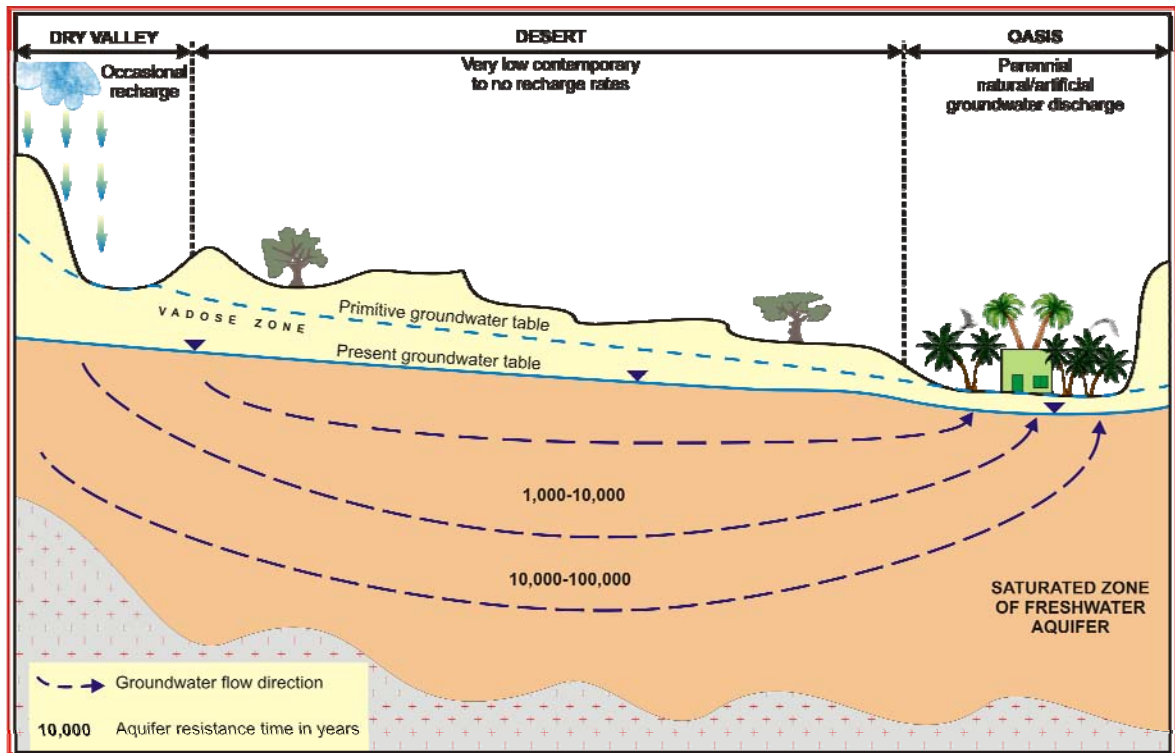


Figure 4.5: The concept of the non-renewability of the Nubian Sandstone Aquifer System. Typically, recharge area, transmission area and discharge area. Modified after Margat et al. (2006).

As an immediate consequence of the groundwater mining of the Nubian Sandstone Aquifer System, a lot of environmental impacts are expected as an outcome (Puri et al. 2001):

- The change of the groundwater flow direction and the hydraulic gradient as is the present case in most of the Egyptian oases.
- The groundwater withdrawal builds cones of depression around the well or well field, which in turn means lowering of the groundwater level or increase of the depth to groundwater. With the successive increase of the depth to groundwater, the water pumping becomes uneconomic or impossible, which sequentially initiates severe environmental hazards and may lead in some cases to the migration of inhabitants.
- Successive lowering of the groundwater level directly affects the hydraulic parameters of the aquifer like the transmissivity.
- Through abrupt groundwater circulation and steepness of the hydraulic gradient, the groundwater quality suffers noticeable changes.
- The groundwater velocity increases as a result of the steepness of the hydraulic gradient.
- In such cases of groundwater overexploitation, the soil will not have better situation, as it gets saltified and turned slowly to become Sabkhas, as the case in Siwa oasis in the north of Egypt.

Under the conditions of water scarcity in the area of the Eastern Sahara, which is overwhelmingly an imperative restriction to development, besides the non-renewability of the NSAS, which imposes more complexity on its management, the utilization of this resource provided by groundwater exploitation must be governed by principles of rationality, wisdom, and sustainable development to avoid the mining of the aquifer storage reserves rather than uneconomic lifting of the groundwater. Groundwater mining refers in this context to the extraction of groundwater from an aquifer that has mainly non-renewable resources with depletion of its reserves. As such development of groundwater resources has special social, economic, and political sensitivity compared to other water resource development.

4.4.1 Groundwater residence time

An approximation of the average residence time of water in an aquifer can be estimated by assuming that steady-state flow conditions exist on an inter-annual basis, and recharge rates and other aquifer properties are constant. In this way, residence time is proportional to the volume of void space in the aquifer. It is used only in situations where the aquifer volume is at least several times as high as the annual groundwater flux. The residence time can then be defined as (Focazio et al. 1998) the ratio of the volume of aquifer void space to the volumetric rate of water moved through the aquifer:

$$t = \frac{n * b}{r} \quad [\text{Eq 4.1}]$$

where t is the residence time [T], b is the aquifer thickness [L], n is the porosity [dimensionless], and r is the annual recharge rate [L/T].

In this way, water in an aquifer having a small void volume [small porosity and (or) thickness] and a high recharge rate will have to move through the aquifer faster (have a shorter residence time) than an aquifer with larger void volume and smaller recharge rates. Therefore, with other aquifer characteristics constant, a higher porosity, a larger thickness, and smaller recharge rate are all independently associated with longer residence time, which is the identical situation within the Nubian Sandstone Aquifer System.

4.5 Origin of groundwater in the NSAS

4.5.1 Origin theory

It is important to understand the origin and movement of the groundwater in the whole aquifer system before a responsible utilization can be made. The origin of groundwater in the NSAS has been intensively discussed by several authors since the 1920s. Two complementary concepts have presented the origin of groundwater in the NSAS as follows (Thorweihe and Heintz 2002):

- The allochthonous concept. It is the oldest theory that postulated flow of groundwater from precipitation in the most southern mountainous parts of the system to provinces of discharge in the aquifer. This concept was justified from the regional piezometric map and flow direction of the aquifer, which illustrates a general flow direction from the southwest to the northeast of the aquifer. According to this theory, the groundwater is renewable, and the basin is receiving some recharge at intake areas estimated to be about 1.6 km³/year. This concept was adapted mainly by Ball (1927) and confirmed by Sandford (1935). This concept has still been valid until now, though rejecting the steady state idea.
- The autochthonous concept. This theory is based mainly on the interpretation of the groundwater isotopes. The concept concluded that no age gradient along hypothetical stream lines has been detected; on the other hand, no flow direction could be seen. This theory concluded that the bulk of the groundwater mass within the basin was formed in situ in the area surrounding the present discharge areas during the humid pluvial periods of the Holocene (Sonntag 1986, Pachur 1999). The further sophisticated studies claimed that the obvious matching among the slope of the groundwater level, the gradient of the precipitation in the southern parts, and the general flow direction to the northeast misled to a conclusion that the

aquifer is renewable and gets continuous recharge from the more humid regions in the south (Brinkmann et al. 1987; Kröpelin 2001). Nevertheless, the groundwater velocity, aquifer resistance time, and climatic changes have to be considered (Figure 4.6).

4.5.2 Recharge

The transient theory of the groundwater origin did not deny completely the possibility of the recharge from the south but disbelieved the quantity or significance of the kind of recharge for the Nubian Sandstone Aquifer System (Sonntag et al. 1987; Thorweihe and Heintz 2002). However, three possible ways of groundwater recharge for the aquifer system are claimed as follow:

- Seepage of Nile water.
- Regional groundwater influx from areas with modern groundwater recharge.
- Local infiltration through precipitation during wet periods in the past.

4.5.2.1 Nile water seepage

According to the geologic components and the relationship between the groundwater level and the level of the surface water of the Nile, the leakage of water from the Nile into the NSAS can only occur along Lake Nasser in Egypt until Wadi Halfa north of the Sudan, where the Nile River starts to cross the basement outcrops. Another possible seepage zone occurs in the area between Dongola in northern Sudan to Khartoum. In Egypt, north to the 25th Meridian the Nile runs across impermeable sediments of Upper Cretaceous to Tertiary. However, the groundwater-surface water interaction in this zone takes place in both directions (effluent and influent) but on very local scales (Heintz and Thorweihe 1993; Ebraheem et al. 2002; Gossel et al. 2004).

4.5.2.2 Recharge from the South

Some parts of the most southern region of the aquifer system are more humid than in the middle or northern parts and get episodic precipitation. Some of this amount in turn infiltrates and adds up to the groundwater recharge (Figure 4.1).

In spite of the presence of this kind of recharge, it is still considered negligibly small in comparison to the evapotranspiration from the discharge depressions of the system (Sonntag 1984, 1986).

4.5.2.3 Local infiltration in the past

The isotopic findings provide strong arguments that the fossil water of the basin was infiltrated during humid periods in the Late Pleistocene and Holocene time (Edmunds and Wright 1979, 2003; Sonntag et al. 1979; Pachur et al. 1987, 1999; Kröpelin 1993b, 1999, 2001; Ebraheem et al. 2002; Gossel et al. 2004). These studies concluded that the groundwater in the aquifer was recharged in the humid periods 20,000 and 5,000 B.P.

Figure 4.6 represents a histogram of the different climatic situations that occurred during the last 30,000 years in different localities within the Eastern Sahara (Pachur 1999). These humid periods ended in the northern Sahara 8,000 years ago and in the southern Sahara 4,000 years ago. Since that time the aquifer underwent semi-arid to arid climatic conditions that caused an unbalanced groundwater situation and successive decline in the groundwater level within the aquifer.

4.6 Natural discharge

In the oases and depressions within the Nubian Sandstone Aquifer System, the groundwater level occurs immediately close to the ground surface or even above, as an artesian groundwater condition, and therefore flows naturally as springs in some locations. Because of the aridity, the natural groundwater discharge occurs either by evaporation from springs, capillary rise from the groundwater table, or by the ascending of confined or artesian groundwater through leaky, confining beds followed by water vapor diffusion through top layers of dry soils and by transpiration of wild vegetation. The estimation of the natural discharge of the NSAS by evapotranspiration in the depressions corresponds to a mean rate of 10-15 mm/a (Ahmad 1983; Sonntag 1986; Brinkmann et al. 1987; Sonntag et al. 1987). This unbalanced loss from fossil groundwater storage induces an exponential decay of hydraulic head around the depressions, which is equivalent to a mean regional decline rate of the groundwater level of 0.5 cm/y. The average groundwater loss from storage was estimated to be some 109 m³/year.

However, an approximation of the evapotranspiration can be given by the Thornthwaite method that can be expressed in the following equation (Zhou et al. 2003):

$$E_t = 1.6 \left(\frac{10 T}{I} \right)^a \tag{Eq 4.2}$$

where E_t is the possible evapotranspiration [cm/month], T is the monthly average temperature [Co], I is calculated as:

$$I = \sum_{i=1}^{12} \left(\frac{T_i}{5} \right)^{1.514} \tag{Eq 4.3}$$

and a is calculated as:

$$a = (492390 + 17920 * I - 77.1 * I^2 + 0.675 * I^3) * 10^{-6} \tag{Eq 4.4}$$

When the monthly average temperature is known for a point, the evapotranspiration can be calculated by the above equations (Zhou et al. 2003).

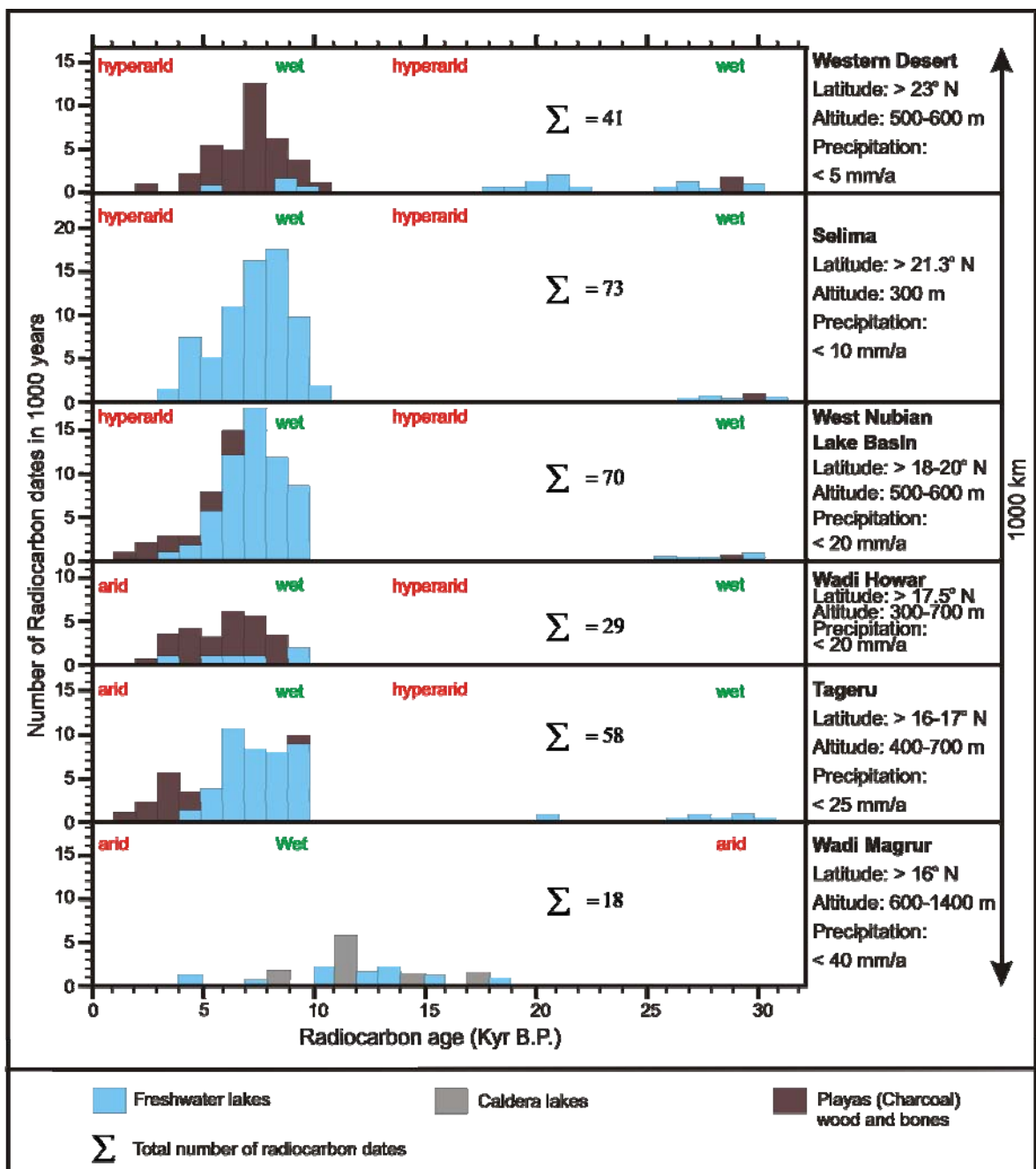


Figure 4.6. Histogram representing a North-South profile for the historical climatic changes of the Eastern Sahara deduced from detailed radiometric Playa and lake sediments. Adapted from Pachur (1999).

4.7 Aquifer parameters

As mentioned before, the NSAS is formed of a pile of mainly continental sandstone of good storage and transmissivity parameters, which makes this aquifer of promising groundwater potential. The aquifer parameters vary vertically due to the transition between aquifers and aquitards. On the other hand, they vary slightly in the horizontal extent,

especially within local considerations. A general overview of the hydraulic parameters of the Nubian Sandstone Aquifer System can be briefly introduced as in Table 4.2 (for localities within the table refer to Figure 4.1).

Table 4.2. Average aquifer thickness, transmissivity, and hydraulic conductivity of the oases and development areas of the Nubian Sandstone Aquifer System.

Area	Average aquifer thickness (m)	Average transmissivity (m ² /s)	Average hydraulic conductivity (m/s)
Kharga	1,250	3.2x10 ⁻²	2.5x10 ⁻⁵
Dakhla	1,750	7.5x10 ⁻²	4.8x10 ⁻⁵
Farafra	2,600	1.2x10 ⁻²	4.2x10 ⁻⁵
Bahariya	1,880	8.8x10 ⁻³	4.5x10 ⁻⁵
East Oweinat	430	1.3x10 ⁻²	2.3x10 ⁻⁵
Kufra	2,850	1.1x10 ⁻²	5.9x10 ⁻⁵
Selima	260	2.6x10 ⁻²	1.3x10 ⁻⁵
Adapted from Hesse et al. (1987) and Sefelnasr (2002).			

The hydraulic conductivities of the NSAS can also be introduced according to the lithologic components of every basin of the aquifer as in Figure 4.7. The accuracy of these parameters depends on the locality and number of aquifer tests held; for instance, the Paleozoic layers are hardly penetrated by a well, so their parameters are always given as an average in correlation to the values calculated for the same layers in different localities, where they are partially or fully penetrated.

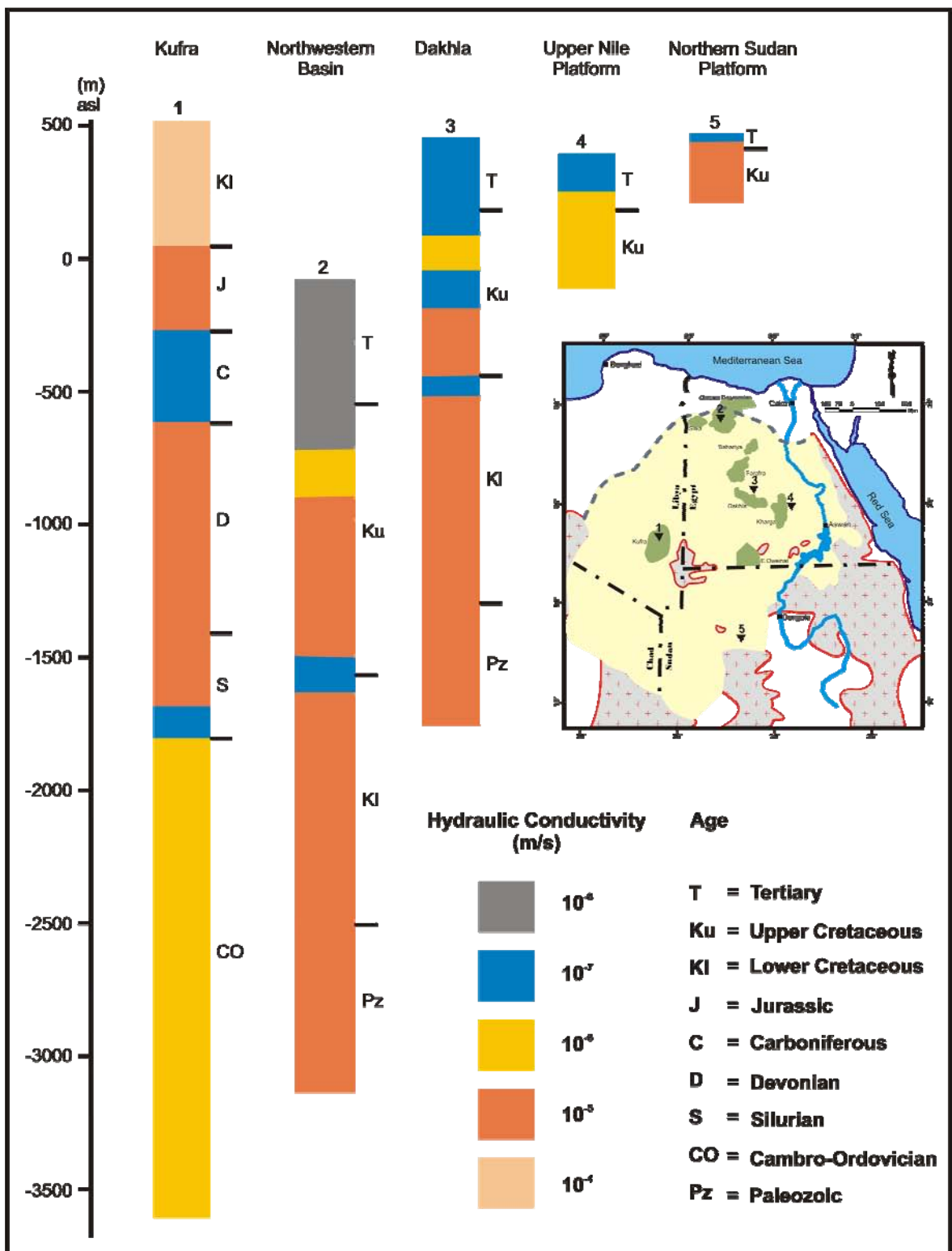


Figure 4.7. Overview of the hydraulic conductivities of some locations of the NSAS. The interpretation of the hydraulic conductivities based on the simplified sections of Thorweihe and Heini (2002) and the cross sections of Hesse et al. (1987).

5

Methodology

5.1 Introduction

Groundwater models could be divided into two categories: *groundwater flow models*, which solve for the distribution of head in a domain. *Solute transport models*, which solve for the concentration of solute as affected by advection, dispersion, and chemical reactions. The flow and transport of groundwater in an aquifer can be simulated by the way of the process of numerical (Poeter and Hill 1997) models that involves:

- a. Defining the problem
- b. Defining the boundary conditions
- c. Development of initial model of the site of interest
- d. Choosing the governing equations (or code) describing the physical problem
- e. Calibration of the numerical model
- f. Validation of the numerical model
- g. Application of the numerical model

Step d has been already well documented, with many codes written to solve the governing equations for the different spatial, geological, and hydrogeological conditions, such as PLASM (Prickett and Lonquist 1971), MODFLOW (McDonald and Harbaugh 1988), FEFLOW (Diersch 1998), and many more. The code (computer program) is a set of commands or algebraic equations generated by approximating the partial differential equations used to solve a mathematical model. Approximating techniques such as the finite difference and finite element methods operate on the mathematical model and change it into a form that can be solved by a computer. Mathematical models have significantly expanded scientists' ability to understand and manage their water system, perform complex analyses, and make informed predictions.

A groundwater model is a physical or numerical representation that represents an approximation, by means of governing equations, of a hydrogeological system of a real world. The model includes a set of boundary and initial conditions, a site-specific nodal grid, site-specific parameter values, and hydraulic stresses (Anderson and Woessner,

1992). Groundwater modeling applications may be of three different types: (a) predictive, used as a framework for prediction of future conditions, (b) interpretative, used for studying system dynamics or organizing data, and (c) generic, used to analyze the hypothetical hydrogeologic systems (Anderson and Woessner 1992).

In spite of the significance of modeling for any of the above mentioned purposes, it is only one component of a hydrogeological investigation requiring sound reasoning database and needs good hydrogeologists to stand behind them. Selecting an appropriate model is critical for the success of the model application. Two criteria are used to classify groundwater models; the first criterion refers to the aquifer characteristics. Aquifers are divided into simple and complex types based on the spatial variation of the hydraulic conductivity and aquifer thickness.

If the two parameters do not vary spatially within a study area, the area is considered to have a simple aquifer condition; otherwise, the aquifer condition is complex. As mentioned, one of the targets of the groundwater flow modeling is the prediction of the hydraulic head behavior of the aquifer under the given stresses with time. The response of the aquifer depends significantly on the spatial and temporal variation of the aquifer parameters, boundary conditions, and stresses on that aquifer. Therefore, the more accurate the aquifer parameters, the more efficient are the models.

5.2 Governing equations

In almost every field of science the techniques of analysis are based on understanding the physical processes, and in most cases it is possible to describe these processes mathematically, and groundwater systems are not exception.

Theory of water flow through porous media is well established. Further readings on basic principals of groundwater flow through porous media are fruitfully presented, such as Theis (1935), Cooper and Jacob (1946), Freeze and Witherspoon (1967), Bear (1972), Freeze and Cherry (1979), Langguth and Voigt (1980), Todd (1980), Verruijt (1982), Heath (1983), Dagan (1989), Fetter (1994), Zekai (1995), Domenico and Schwartz (1998) and Lee (1999).

Mathematical equations describing groundwater flow through a porous medium are based mainly on Darcy's law (Darcy 1958) [Eq 5.1] and the continuity equation [Eq 5.5]. According to Darcy's law, the average flow velocity is proportional to the hydraulic gradient (Freeze and Cherry 1979) and the effective porosity. The proportionality factor is determined as the hydraulic conductivity of the rock.

$$V_x = -\frac{K}{n} \frac{dh}{dx} \quad [\text{Eq 5.1}]$$

where x is the distance in x-direction [L], V_x is the average flow velocity in the x-direction [L/T], n is the porosity, K is the hydraulic conductivity [L/T], h is the hydraulic head [L], and the component dh/dx is the hydraulic gradient in the x-direction [L/L].

The mass balance principle requires that the rate of change in mass storage of an elemental volume with time be equal to the mass inflow rate minus the mass outflow rate.

There is no change in head with time in steady state conditions, so time is not one of the independent variables, and steady state flow can be described by the following three-dimensional partial differential equation:

$$\frac{\partial}{\partial x}\left(K_x \frac{\partial h}{\partial x}\right) + \frac{\partial}{\partial y}\left(K_y \frac{\partial h}{\partial y}\right) + \frac{\partial}{\partial z}\left(K_z \frac{\partial h}{\partial z}\right) = 0 \quad [\text{Eq 5.2}]$$

where x , y , and z are the Cartesian coordinates [L], K_x , K_y , and K_z are the hydraulic conductivity components, and h represents the hydraulic head with the unit of [L].

If the medium is homogeneous and isotropic, equation [5.2] can be expressed by Laplace's equation as follows:

$$\frac{\partial^2 h}{\partial x^2} + \frac{\partial^2 h}{\partial y^2} + \frac{\partial^2 h}{\partial z^2} = 0 \quad [\text{Eq 5.3}]$$

In transient conditions, the law of conservation of mass and the storage parameters of the porous medium are to be taken into account. The flow equation for a transient flow through a saturated anisotropic porous medium is given as:

$$\frac{\partial}{\partial x}\left(K_x \frac{\partial h}{\partial x}\right) + \frac{\partial}{\partial y}\left(K_y \frac{\partial h}{\partial y}\right) + \frac{\partial}{\partial z}\left(K_z \frac{\partial h}{\partial z}\right) = S_s \frac{\partial h}{\partial t} \quad [\text{Eq 5.4}]$$

where S_s represents the specific storage [L^{-1}] and t is the time [T].

The continuity equation for the groundwater system is developed to solve the values of the hydraulic head when the other aquifer parameters are known.

$$\frac{\partial}{\partial x}\left(K_x \frac{\partial h}{\partial x}\right) + \frac{\partial}{\partial y}\left(K_y \frac{\partial h}{\partial y}\right) + \frac{\partial}{\partial z}\left(K_z \frac{\partial h}{\partial z}\right) = S_s \frac{\partial h}{\partial t} + W \quad [\text{Eq 5.5}]$$

where W represents the source/sink term given in [L^3/T].

The solution $h(x, y, z, t)$ describes the value of the hydraulic head at any point of the system at any time. This equation in combination with the initial and boundary conditions describes the transient three dimensional groundwater flow in a heterogeneous and anisotropic porous medium, provided that the principal axes of the hydraulic conductivity are aligned with the coordinate directions.

Within a process of groundwater flow modeling, the three-dimensional aquifer is conceptualized into aquifer layers, which are further discretized into model nodes (Anderson and Woessner, 1992). Flow between these nodes is defined by two hydraulic parameters that describe the aquifer’s ability to store and transmit water. These terms are referred to as storativity and transmissivity, respectively. Transmissivity (T) is defined as the integral hydraulic conductivity (K) of the aquifer material over the saturated thickness of that aquifer (b), such that:

$$T = K * b \quad \text{[Eq 5.6]}$$

Consequently, the governing equation for groundwater flow in the aquifer layer can be expressed by:

$$\frac{\partial}{\partial x} \left(T_x \frac{\partial h}{\partial x} \right) + \frac{\partial}{\partial y} \left(T_y \frac{\partial h}{\partial y} \right) = S \frac{\partial h}{\partial t} + W \quad \text{[Eq 5.7]}$$

The “z” dimension is not considered within the layer approach, and the storage term is stated as the storage coefficient ($S = S_s * b$). When the aquifer layer is modeled as confined, the saturated thickness remains constant, and thus the transmissivity also remains constant. In unconfined conditions the saturated thickness can vary in time. The elevation of the bottom of the aquifer and the hydraulic head in the aquifer are required to calculate the saturated thickness (h). The governing equation in the unconfined layer approach can be expressed as:

$$\frac{\partial}{\partial x} \left(K_x h \frac{\partial h}{\partial x} \right) + \frac{\partial}{\partial y} \left(K_y h \frac{\partial h}{\partial y} \right) = S_y \frac{\partial h}{\partial t} + W \quad \text{[Eq 5.8]}$$

where the storage term is now known as the specific yield (S_y) that represents the unconfined equivalent of the hydrogeologic system. Using the following equations:

$$2h \frac{\partial h}{\partial x} = \frac{\partial h^2}{\partial x} \quad \& \quad 2h \frac{\partial h}{\partial y} = \frac{\partial h^2}{\partial y} \quad \text{[Eq 5.9]}$$

Equation [5.9] can then be written in the following form:

$$\frac{\partial}{\partial x} \left(K_x h^2 \frac{\partial h}{\partial x} \right) + \frac{\partial}{\partial y} \left(K_y h^2 \frac{\partial h}{\partial y} \right) = 2S_y \frac{\partial h}{\partial t} + 2W \quad [\text{Eq 5.10}]$$

In order to compute groundwater flow, a set of initial, boundary, and constraint conditions is required to achieve the solution of the governing equations introduced above. Due to the fact that the non-linear continuity equation cannot be solved analytically in most cases, numerical methods have to be applied in these cases. The numerical solution of nonlinear problems includes a process of iterations where head values are changed such that they satisfy both the head-dependent boundary conditions and the unconfined head and resulting flow in the aquifer. Numerical solutions provide more flexibility in the equation being solved. Numerical solutions require discretization of the model domain into locations (nodes) where the equation is to be solved.

The common techniques for solving the continuity equation are the methods of finite elements (FE) and finite differences (FD). Both methods require a grid of the flow domain, for which the water flow is needed. Additionally, initial conditions for each grid node and boundary conditions along the complete boundary of the flow domain have to be defined (Yeh 1981; Delleur 1999).

5.3 Conceptualization

After defining the problem and problem domain, a connection tool is needed to translate the real world groundwater flow system (including the problem) into numerical ones, taking into account that the geometry, natural components, and characteristics should be translated as precisely as possible. This tool is the conceptual model. A conceptual model is a pictorial interpretation of the groundwater flow system incorporating all available geological, hydrogeological, and hydrological data into a simplified block diagram or cross section (Anderson and Woessner 1992).

The nature of the conceptual model will determine the dimensions and spatial distribution of the numerical model. The significance of building a conceptual model is to simplify the problem of the real world and to organize the associated field data so that the system can be analyzed more readily. The first step in constructing a conceptual model is defining the geological framework of the study area, including number of layers, the thickness of each layer, lithology, and structure of any aquifers and confining units (Figure 5.1).

Many sources contribute to building the geological framework. This data is classically obtained from the geologic information including geologic maps, well logs and borings, cross sections, geophysics, and additional field mapping. Construction of the geological framework then allows the hydrological framework to be defined involving the following: (a) identifying the *boundaries* of the hydrological system, (b) defining *hydrostratigraphic units*, (c) preparing a *water budget*, and (d) defining the *flow system* (Figure 5.1).

- a- Boundaries can be either natural hydrogeological boundaries including the surface of the water table, groundwater divides, and impermeable contacts between different geological units, or they may need to be unnatural. However, for accuracy and simplicity, natural boundaries should be used whenever possible. The boundaries of a model must be identified first so that all the next steps can proceed within their framework.
- b- The geologic information in combination with the information on the hydrogeologic properties supports defining the hydrostratigraphic units (Maxey 1964; Seaber 1988) of the conceptual model. Hydrostratigraphic units comprise geologic units of similar hydrogeologic properties, as several geologic formations may be combined into a single hydrostratigraphic unit or a geologic unit may be distinguished into several aquifers and aquitards. Characterizing hydrostratigraphic units is essential in determining the number of layers controlling groundwater flow within the system. Calculation of hydraulic conductivity and storativity from pump tests are often used to identify and distinguish different hydrostratigraphic units. The concept of a hydrostratigraphic unit is most useful for simulating a geological system on a regional scale.
- c- Preparation of a water budget involves the identification and quantification of all flow magnitudes and directions of the source of water to the groundwater system as well as the outflow from the system. The field estimated inflows include groundwater recharge from precipitation, overland flow, or recharge from surface water bodies that have interaction with the groundwater system. Artificial recharge or injection will be also involved if there is. Outflows from the system may be defined as springflow, baseflow, evapotranspiration, and extraction.
- d- To understand the groundwater movement throughout the hydrogeological system, it is essential to define the flow system. Water level measurements are used to estimate the dominant directions of groundwater flow, the hydraulic gradient, locations of recharge areas, location of discharge areas, and the connections between groundwater aquifers and surface water systems. As in the water budget preparation, water quality analyses are also employed to quantify recharge and baseflow. The definition of the flow system may be based exclusively on the physical hydrologic data, but it is better to use geochemical data or isotope techniques whenever possible to strengthen the conceptual model.

However, the quantity, quality, and distribution of the available data are governing factors regarding groundwater modeling. Therefore, parameter estimation is a vital task in groundwater modeling. When the availability of enough hydrogeologic information is not the case within a groundwater modeling scheme, the optimum results against a pre-established criteria still can be ultimately (Hill 1998) reached using a range of methods and

assumptions: i.e., the deterministic method and the geostatistical methods. Geostatistical methods are more feasible in hydrogeological applications and parameter regionalization, as they were developed mainly to quantify spatial uncertainties. The statistical and geostatistical fundamentals and methods are described intensively in Davis (1986), Isaaks and Srivastava (1989), Journel (1989), Cressie (1990, 1991), Keidser and Rosbjerg (1991), Deutsch and Journel (1992), Dagan (1997), Myers (1997), Neuman (1997), Chiles and Delfiner (1999), and Schatzman (2002).

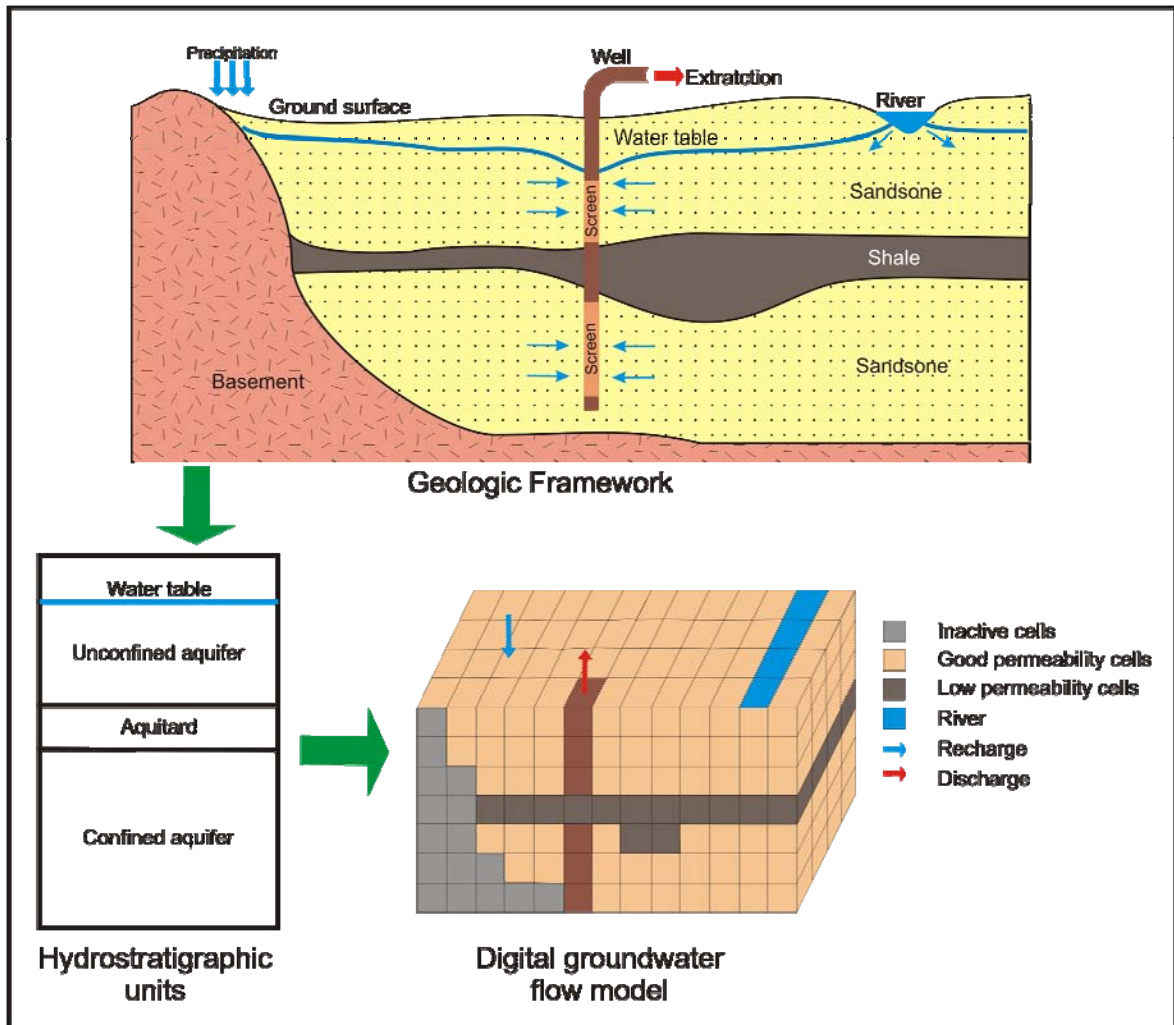


Figure 5.1. Schematic illustration showing the procedure of translating the geologic framework of the real world into digital form.

5.4 Interpolation

Interpolation is a process to construct, estimate, intermediate, and fill new data values in some space from a discrete set of known data points. The most known and representative statistical method concerning hydrogeological information is the kriging that was first developed by the South African geologist Danie G. Krige (Krige 1951, 1952).

5.4.1 Kriging

Kriging is a geostatistical regression gridding technique used to flexibly approximate or interpolate data. Kriging can be either an exact or a smoothing interpolator depending on the user-specified parameters. It incorporates anisotropy and underlying trends in an efficient and natural manner. Kriging can be custom-fit to a data set by specifying an appropriate variogram model.

5.4.2 Variograms

The variogram is a three dimensional function, as it is used to match a model of the spatial correlation of the observed variables. The variogram is a measure of how quickly things change on the average. One is thus making a distinction between the experimental variogram that is a visualization of a possible spatial correlation and the variogram model that is further used to define the weights of the kriging function (Figure 5.2 a, b).

The fundamental principle of a variogram model is that, on the average, two observations closer together are more similar than two observations further apart. Because the underlying processes of the data often have preferred orientations, values may change more quickly in one direction than another. As such, the variogram is a function of direction.

As illustrated in Figure 5.2 a, let us consider two independent random variables $Z(x)$ and $Z(x+h)$ that are separated by the lag distance h , so the variability between these two quantities can be in probabilistic notation characterized by the dependent variogram function $\gamma(x,h)$ as follows:

$$2\gamma(h, x) = E \left\{ [Z(x+h) - Z(x)]^2 \right\} \quad [\text{Eq 5.11}]$$

It is possible to consider the variogram $2\gamma(h)$ as the arithmetic mean of the squared differences between two experimental measures $Z(x_i)$ and $Z(x_i+h)$:

$$\gamma(h) = \frac{1}{2N(h)} \sum_{i=1}^{N(h)} [Z(x_i+h) - Z(x_i)]^2 \quad [\text{Eq 5.12}]$$

Where $N(h)$ is the number of experimental pairs of the data with lag distance h .

5.5 Boundary conditions

The boundaries of a groundwater model are the domains or points at which the dependent variable (head) or the derivative of the dependant (flux) is known. The boundaries can be inner and/or outer boundaries. In model construction it is actually critical (Franke et al. 1987) to select the right boundary conditions. The presence of an impermeable body of rock or a large body of surface water forms the *physical boundary* of the groundwater flow

systems. Groundwater divide or streamline forms the *hydraulic boundary* of the groundwater flow systems (Anderson and Woessner 1992, Diersch 1998).

The hydrogeologic boundary conditions can be explained by the following mathematical conditions (Figure 5.3):

- **1st type: Dirichlet condition**, specified head boundary:

The key assumption for the Dirichlet boundary condition is that regardless of the groundwater flow within the flow domain and at the boundary, there will be no influence on the potential of the outside water body, in such a way that this potential remains fixed as determined by the boundary condition (Delleur 1999). The mathematical expression of the Dirichlet boundary condition, for stationary groundwater modeling, is shown in the following equation (Diersch 1998):

$$h(x_i, t) = h_1^R(t) \quad \text{on } \Gamma_1 \times t(0, \infty) \quad [\text{Eq 5.13}]$$

where t is the time [T], h_1^R is the prescribed boundary values of hydraulic head h , and Γ is the given boundary.

The hydraulic head at the boundary is known. Examples are a river, lake, or occasional water body in contact with an aquifer. In the case that this boundary type has no direct contact with the aquifer, the boundary can still be applied by placing a fixed or specified head cell or cells, in which the allocated head is known.

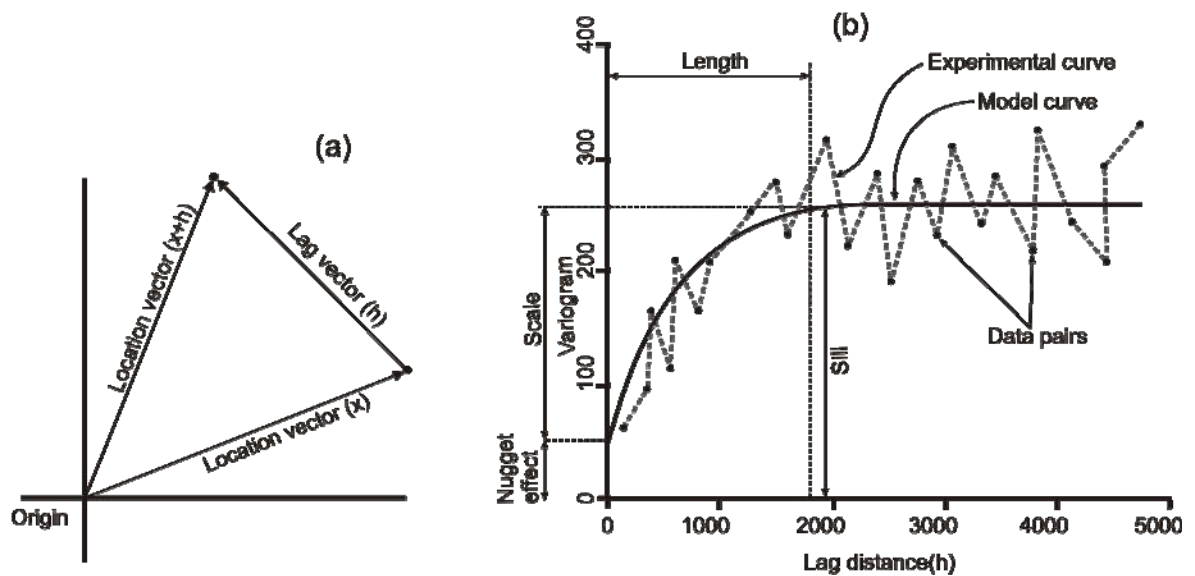


Figure 5.2. (a) Diagram showing the spatial distribution of the independent random variables and the separating lag distance between them; (b) diagram represents the variogram components and a typical and experimental curve. Compiled from Surfer® 8 User’s Guide (2002) and Bohling (2005).

- 2nd type: Neuman condition, specified flow boundaries:

A flux boundary condition implies that regardless of the state and flow of the groundwater inside the flow domain and at the boundary, the normal flux is fixed by external conditions and remains as determined by the boundary condition (Delleur, 1999). This can be expressed by:

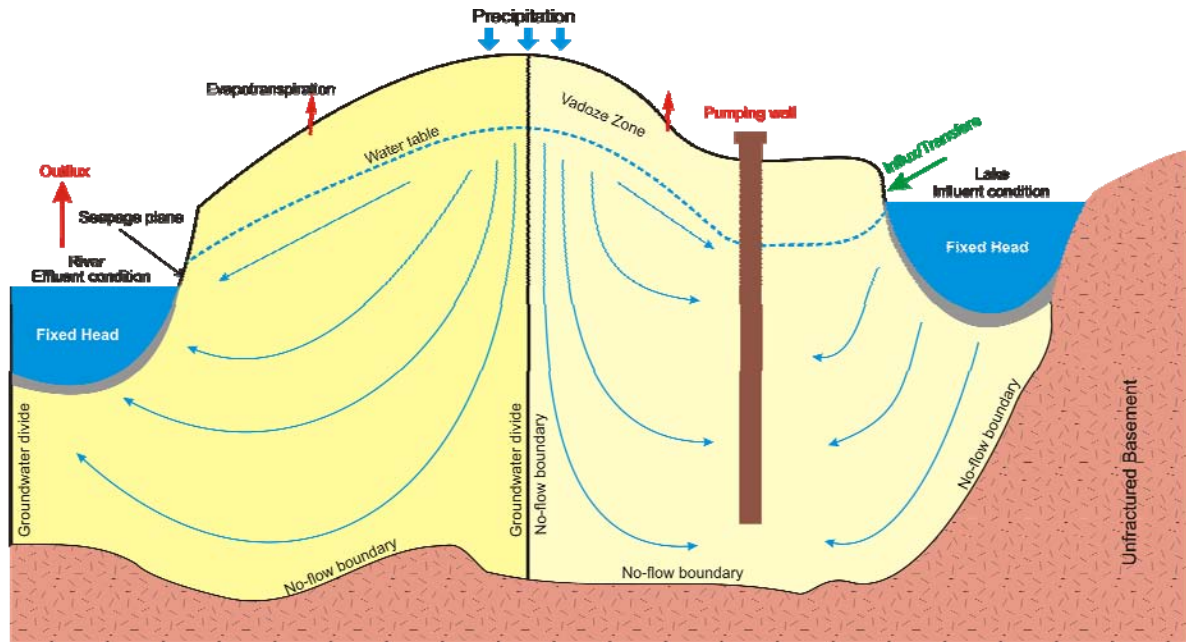


Figure 5.3: Diagram of regional groundwater flow system representing the physical and hydraulic boundary conditions. Modified after Anderson and Woessner (1992).

$$q_{n_h}(x_i, t) = q_h^R(t) = -k_{ij} \frac{\partial h}{\partial x_j} n_i \quad \text{for 2D horizontal unconfined} \quad [\text{Eq 5.14}]$$

$$\bar{q}_{n_h}(x_i, t) = \bar{q}_h^R(t) = -T_{ij} \frac{\partial h}{\partial x_j} n_i \quad \text{for 2D horizontal confined}$$

on $\Gamma_2 \times t(0, \infty)$

where q_{n_h} represents the Darcy flux of the fluid, \bar{q}_{n_h} represents the vertical averaged Darcy flux of the fluid, q_h^R and \bar{q}_h^R are the normal boundary fluid flux for 3D and 2D, respectively, T_{ij} is the transmissivity tensor, and n_i is the normal unit vector.

The flux across the boundary is known. It includes no flow boundaries between geological units (boundaries where flux is specified to be zero), interactions

between groundwater and surface water bodies, springflow, underflow, and seepage from bedrock into alluvium. The most commonly applied form of a Neuman Boundary is a No-flow boundary, often occurring between a highly permeable unit and a unit of much lower permeability or from water divide.

A difference in hydraulic conductivity of two orders of magnitude or greater between two adjacent units is enough to rationalize assignment of a no-flow boundary, as this contrast in permeability causes refraction of flow lines such that flow in the higher conductivity layer is essentially horizontal and flow in the lower conductivity layer is essentially vertical (Freeze and Witherspoon 1967; Neuman and Witherspoon 1969).

This case is also applicable if the hydraulic gradient across the boundary is also low, as flow out of the higher conductivity layer is negligible, and the boundary can then be set to impermeable. Saltwater interface at some coastal aquifers, some faults, and regional groundwater divides form typical no-flow boundaries (Zheng et al. 1988).

▪ **3rd type: Cauchy condition**, head-dependent flow boundary:

For which the flux across the boundary is dependent on the magnitude of the difference in head across the boundary, with the head on one side of the boundary being input to the model and the head on the other side being calculated by the model. The mathematical expression of this boundary type is as follows:

$$\begin{aligned} q_{n_h}(x_i, t) &= -\Phi_h(h_2^R - h) && \text{for 3D and 2D vertical and unconfined} \\ \bar{q}_{n_h}(x_i, t) &= -\bar{\Phi}_h(h_2^R - h) && \text{for 2D horizontal confined} \end{aligned} \quad [\text{Eq 5.15}]$$

on $\Gamma_3 \times t(0, \infty)$

Where Φ_h and $\bar{\Phi}_h$ are the fluid transfer coefficients.

Here the transfer coefficients Φ_h and $\bar{\Phi}_h$ represent two directional functions of the form:

$$\Phi_h = \Phi_h^{in} \quad \text{for } h_2^R > h \quad \text{and} \quad \Phi_h = \Phi_h^{out} \quad \text{for } h_2^R \leq h \quad [\text{Eq 5.16}]$$

$$\bar{\Phi}_h = \bar{\Phi}_h^{in} \quad \text{for } h_2^R > h \quad \text{and} \quad \bar{\Phi}_h = \bar{\Phi}_h^{out} \quad \text{for } h_2^R \leq h \quad [\text{Eq 5.17}]$$

Cauchy Boundary can be applied to leakage from a surface water body where the flux is dependent on the difference of hydraulic head between the surface water and groundwater level and the vertical hydraulic conductivity of the boundary;

and evapotranspiration where the flux is proportional to the depth of the water table in an unconfined aquifer.

▪ **4th type: Pumping/Injection Wells:**

For which the groundwater aquifer system is stressed by undergoing extraction or injection schemes, which in turn cause changes in hydraulic head, and can be mathematically represented as:

$$Q_p^w(x_i, t) = \sum_m Q_m^w \prod_i \{\delta(x_i - x_i^m)\} \quad \text{for } \forall (x_i, x_i^m) \in \Omega \quad [\text{Eq 5.18}]$$

where Q_p^w represents the well function, Q_m^w is the pumping or injection rate of a single well m , and x_i^m is the coordinate of a single well m (Diersch 1998).

5.6 Initial conditions

The head distribution everywhere in the system at the beginning of the simulation forms the initial conditions; thus, they are boundary conditions at the first time step. Initial hydraulic heads must be input before running the simulation. In the case of a steady state model the heads can be estimates or averages of all the available data; however, for transient models the heads can be real values or can be the result of a steady state simulation. Heads at fixed head cells must be real values. Steady state problems require at least one boundary node with a known head in order to give the model a reference elevation from which to calculate heads. In transient solutions the initial conditions provide the reference elevation for the head solution, also taking into account the groundwater balances, as they are a key function for the transient simulations and calibration. The initial conditions may be expressed by the following equation (Diersch 1998):

$$h(x_i, 0) = hI(x_i) \quad [\text{Eq 5.19}]$$

in the domain Ω , where hI is a known spatially varying initial head distribution.

5.7 Discretization

The discretization concerns the spatial and temporal transformation of the geometric and time-dependent components of the groundwater model into discrete elements. The discretization of the geometry is crucial where boundary conditions or stresses are to be applied. The model cells should be small enough to stand the detailed hydrogeologic parameters, to reflect the curvature of the water table and the hydraulic gradient, and also the effects of point stresses on the hydrogeological system such as recharge, evapotranspiration, and pumping from well nodes.

The spatial distribution and heterogeneity of aquifer properties has also to be considered when choosing an appropriate grid or mesh size. The more variable the aquifer properties, the finer the model grid should be to express these variations. The modeling objectives are the main factor of the grid or mesh size, despite the fact that the information availability of the aquifer properties is in most cases a constraint factor. With lower resolution data on the distribution of aquifer properties, a larger grid or mesh size should be used. However, simulating the hydrogeological systems for the groundwater management and sustainability strategies, great attention must be paid to the choosing of the groundwater flow system and according to what can it offer when special simulations or very fine cell sizes are of interest.

It is always impractical to employ grids or cells that are comparable in size and dimension to the pumping wells, although predicting head or drawdown in the close proximity to pumping well is of high rank in case of application of groundwater management and sustainability schemes. In a finite element model the pumping rate is assigned to the node itself, which reflects representatively the head changes and hydraulic gradient in the vicinity of the well. However, in finite difference models the pumping rate is applied to the cell that contains the pumping point, and the well diameter is typically much smaller than the cell size.

A number of analytical methods have been implemented in an attempt to improve the head solutions: i.e., the analytical method (Prickett 1967; Peaceman 1978; Garg et al. 1980), the grid refinement such as the local grid refinement (LGR) (Mehl and Hill 2002), and the telescoping grid refinement (TGR) (Ward et al. 1987; Leake and Claar 1999).

Nonetheless, although these methods are of valuable appreciation in dealing with problems of the groundwater flow modeling, they may have many of limitations, especially for applications that involve the developing of numerical models for large scales with complex hydrogeologic system and boundary conditions. Namely, the application of these techniques to complex systems may lead to slow convergence, numerical oscillations, computational inefficiencies, and solution failure.

Just as it is favorable to use small nodal spacing, ideally it is advisable to apply small time increments to obtain an accurate solution and to facilitate the minor changes of the aquifer behavior during time. This submission is illustrated in Figure 5.4. However, increasing the span of the time steps during the simulation is recommended, especially when simulating a stress, such as pumping, that is applied to the aquifer.

Under certain conditions, the numerical model is prone to oscillations in space and/or time. The use of too large time steps results in unstable time oscillations (Figure 5.5), as these oscillations grow larger with the simulation time progress and may cause the simulation not to converge thus fail. Unlike time oscillations, space oscillations do not tend to grow as

the simulation progress in time. The relationship between the temporal and spatial distribution is also important. It can be presented in the following equation (Poulsen 1994):

$$\Delta t_c = \frac{S (\Delta x)^2}{4T} \quad [\text{Eq 5.20}]$$

where Δt_c is the maximum time step allowed, (Δx) is the regular grid spacing, and S and T refer to storativity and transmissivity, respectively.

Proper selection of the timesteps can control both time and space oscillations. The Peclet and Courant Numbers are then essential assisting and constraint numbers that help prevent the simulation from failing due to oscillations (Figure 5.5). The relationship between Peclet and Courant Numbers is given as follows:

$$Cr \leq \sqrt{\frac{1}{Pe^2} + 1} - \frac{1}{Pe} \quad \text{and} \quad Cr \geq 1 - \frac{2}{Pe} \quad [\text{Eq 5.21}]$$

where the Courant Number (Cr) controls the oscillations in the solution arising from the discretization of time derivative and is defined as:

$$Cr = \frac{q\Delta t}{n\Delta x} \quad [\text{Eq 5.22}]$$

and the Peclet Number (Pe) is a measure of the ratio between the advective and the dispersive components of transport, and it controls the oscillations in the solution due to the spatial discretization of the domain. The Peclet number is defined as:

$$Pe = \frac{q\Delta x}{nD} \quad [\text{Eq 5.23}]$$

as q is the Darcy velocity, Δt is the timestep, Δx is the grid spacing, D is the dispersion tensor, and n is the material porosity.

The condition represented by equation [5.21] has to be valid at all nodes within the modeled domain to avoid the unpleasant oscillations.

A groundwater model may represent either steady state or transient aquifer conditions. In a steady state groundwater model all flows in and out of the model are assumed to be equal, and there is no net change in storage; accordingly, no storage terms are required in the input parameters. A steady state model may be run for different times, and the outcome will be the same as time is irrelevant under steady state conditions. A transient

groundwater model simulates the stresses on an aquifer over time and is therefore divided into time steps. The number of time steps can be input by the user and should reflect any temporal stresses on the aquifer such as climatic changes, recharge, or extraction, or can it be automatically controlled via the balances or head changes between the time steps.

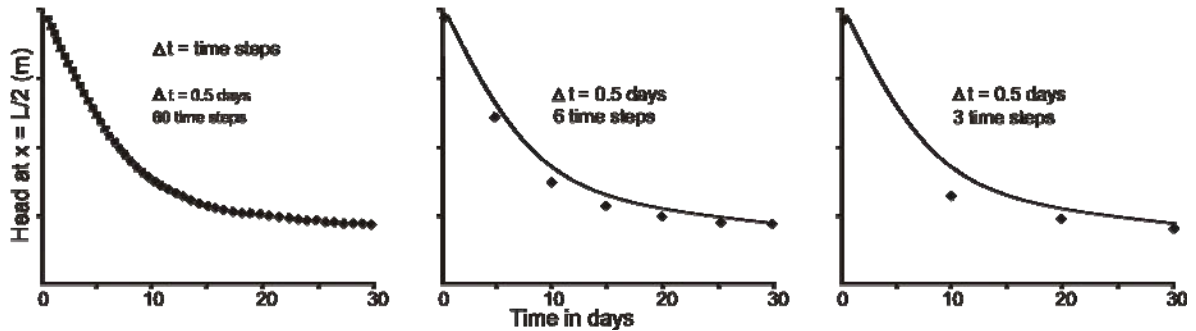


Figure 5.4. The concept of the effect of the size of the time steps on the simulation of the decay of the groundwater hydraulic head. Solid line represents the analytical solutions and the points represent the numerical solutions (modified after Townley and Wilson 1980).

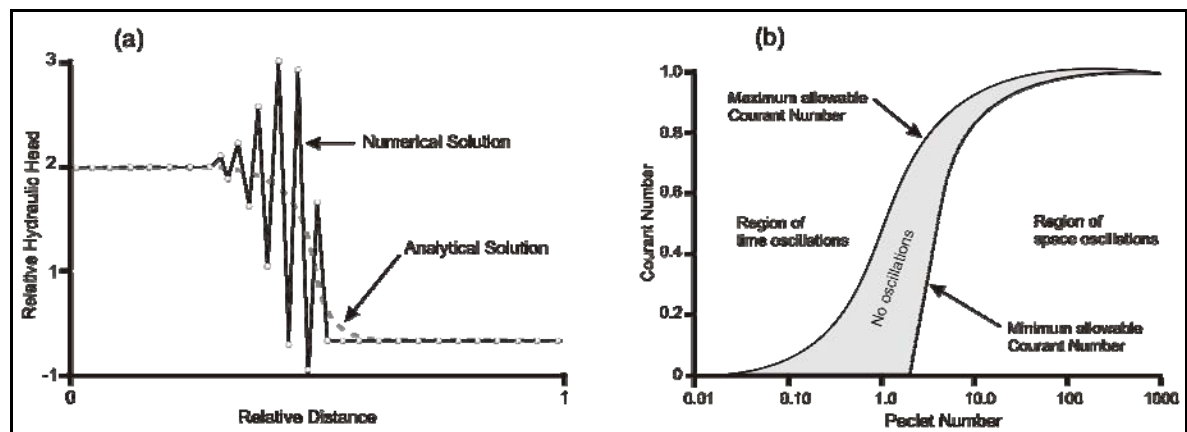


Figure 5.5. (a) Graph illustrating the instability of time oscillations; (b) maximum and minimum Courant Number criteria for one dimensional simulations (modified after Fabritz 1995).

5.8 Calibration

Generally, there are two types of groundwater flow models, the forward model and the inverse model. The *forward model* stands for the solution of the hydraulic head of an aquifer at any point of the aquifer and any time. This solution can be obtained when the aquifer parameters like transmissivity, storativity, hydraulic conductivity, and stresses on the aquifer and the initial and boundary conditions are known. In reality, the aquifer parameters are rarely found complete or representing the whole area of interest, as they are in most cases found as scattered measurements on the study area. So as to develop a

reliable forward groundwater flow model that can be used to predict the aquifer behavior, the aquifer parameters are to be interpolated.

The procedure in which a groundwater flow model is used to estimate the hydraulic parameters of an aquifer is known as the calibration. Model calibration is the process of modifying one or more aquifer parameters until the results of the simulation match the measured data. A steady state calibration is performed to water levels that represent steady state conditions such as long term mean water levels, mean annual water levels, or mean seasonal water levels for a particular season. A quasi-steady state calibration is conducted to water levels that represent the aquifer's behavior at a given point in time under certain stresses applicable at that time. Transient calibration is performed to water levels that represent the aquifer's response to stresses such as changeable recharge and (Anderson and Woessner 1992) extraction over time, and consequently it is required to have some handle on the magnitude of these fluxes for the duration of the modeling period in order to achieve accurate calibration.

The model that is used to estimate the aquifer parameters (Carrera and Neumann 1986), including boundary conditions and stresses, to create a precise match between the output of the forward model and the field data is described as an *inverse model*. The best known inverse model technique is PEST-model from Doherty et al. (1994). Further readings on the principles of the inverse problems and calibration procedures, techniques, and types can be found, for example, in Marquardt (1963), Fletcher (1980), Draper and Smith (1981), Seber and Wild (1989), Cooley and Naff (1990), Hill (1992), Doherty et al. (1994), Sun (1994), and Tarantola (2005).

To establish an inverse groundwater flow simulation, the *trial and error* or the *automated* methods (the automated methods can in turn be direct or indirect methods) can be used (Prickett and Lonquist 1971; Anderson and Woessner 1992; Doherty et al. 1994; Sun 1994; D'Agnese et al. 1999; Inoue et al. 2000).

5.8.1 Trial and error

This method is based initially on selecting value for the unknown parameters; hence, the forward model is run, and a comparison between the results of the calculated hydraulic head with the measured hydraulic head is carried out. This process should be repeated until a satisfactory result is obtained. Regardless of the fact that the trial and error method is generally slow in refinement for unknown parameter values, it enables the modeler to assess some assumptions about the model being calibrated.

5.8.2 Automated methods

The automated methods include the direct and indirect methods of the reverse problems.

▪ **The direct methods**

The direct methods in inverse groundwater flow modeling assume that the groundwater hydraulic head is known throughout the model domain, and then by rearranging the *continuity equation* [Eq 5.2] the unknown parameters can be calculated.

▪ **The indirect methods**

These use the output of the forward model as a trigger to estimate the aquifer parameters in the solution processes of the inverse model. Sun (1994) has categorized the indirect methods to be search, gradient or second order methods. All of these methods attempt to determine a search sequence. The search methods use an objective function for the determination of the search sequence. The gradient methods are those (Li and Yail 2000) that use the gradient of the objective function to determine a search sequence. The second order methods are the methods that use the second order derivative of the objective function for the determination of the search sequence. The indirect methods use an algorithm (Yeh 1986) that involves and accomplishes this loop of orders: guess or find an initial parameter value. Use one of the search, gradient, or second order methods to produce a search sequence. Compare the observed field data and the output from the forward model. Repeat the last step until the value of the objective function has reached minimal value.

Whether the calibration method is trial and error or automated, several techniques are normally employed to assess the calibration. To quantify the calibration, the difference between measured and calculated heads, otherwise known as residuals, may be compared graphically and statistically. When the mean of the residuals is less than some acceptable threshold value (difference is reduced to as close to zero as possible, and the standard deviation is reduced as much as possible), the model is calibrated. The standard statistical evaluation of the calibration method such as the Root Mean Square (RMS) Error should be applied [Eq 5.24].

$$RMS = \sqrt{\left[\frac{1}{n} \sum_{n=1}^n (h_o - h_c)^2 \right]} \quad \text{[Eq 5.24]}$$

where h_o represents the observed head for each observation, h_c is the calculated head for each observation, and n is the number of model observations.

It is necessary that only one parameter is varied at a time in order to have the ability to follow the effects of the changes on the solution. It is also necessary that any effects are evaluated by the same statistical methods used to evaluate the model calibration. The calibrated model is now deemed to be used to predict the aquifer behavior under different hydraulic stresses.

5.9 Data requirements

It may be disadvantageous that the numerical groundwater models need intensive, accurate, complete data sets covering the whole modeled area. But with the newly developed techniques of GIS and the sophisticated statistical methods, it should to a far extent no longer be a problem to model the area of interest even with data gaps. To develop a groundwater flow model, the following data sets have to be completely prepared: (a) model structure that includes slice elevations and complete layer discretization along the whole area in interest, (b) the aquifer parameters, and (c) the boundary conditions.

In general, the data requirements for a groundwater flow model can be listed as below (Moore 1979):

- Geologic map and cross sections revealing the geometry, extent and boundary of the system
- Topographic map showing surface water bodies and divides
- Digital Elevation Model
- Contour maps and cross sections of the aquifer layers
- Isopach maps showing the thickness of the aquifers
- Water table and potentiometric maps for all aquifers
- Hydrographs for groundwater head and surface water levels and discharge rates
- Data for the hydraulic conductivity and transmissivity
- Storage data for the aquifers and confining beds
- Information about the colmation beds
- Spatial and temporal distribution of rates of evapotranspiration, groundwater recharge, surface water-groundwater interaction, groundwater extraction, and natural groundwater discharge (seepage, etc.)

6

Regional Model

The main purpose of this thesis is to develop local groundwater flow models for the Dakhla oasis and the area of Lake Nasser as discussed in Chapter 1 (for localities refer to Figure 6.2). As the boundary conditions in the areas of interest are difficult to estimate, a regional groundwater flow model for the whole Nubian Sandstone Aquifer System had to be developed and calibrated to serve as a base model for the further modeling schemes. The regional calibrated model has then been refined at the stress areas, model boundaries or where required to facilitate the detailed input and output information. The refinement was designed to be as small as possible to reveal the minor aquifer responses to the adjusted hydraulic stresses as further discussed in this chapter.

In this chapter the development and design of a regional groundwater flow system for the Nubian Sandstone Aquifer System is introduced as well as the effect of anthropogenic activities on the regional groundwater flow system within the aquifer. The procedure and methods are schematically configured in Figure 6.1. An overview on the aquifer domain, extension, and different boundaries is illustrated in Figure 6.2.

6.1 Data acquisition

The primary data were collected and obtained from several authorities, organizations, and even individuals. Obviously, the data sets were obtained in different formats and commonly with continuity problems. These sources include the institute of geological sciences at Martin Luther University Halle-Wittenberg, Germany as a main source, Groundwater and Development Center in Kharga Oasis, Egypt, Branch of Academy of Scientific Research and Technology in Kharga oasis, Groundwater and Irrigation Center in Dakhla Oasis, Egypt, the General Authority for Lake Nasser Development, the General Company for Research and Ground Water (REGWA), Cairo, Tushka Project and the Kingdom Agriculture Development Company, Tushka, Egypt, as well as the published and internal technical and academic reports and literature, such as the Research Institute for Groundwater (RIGW), Ministry of Public Works and Water Resources (MPWWR) in

Egypt, Groundwater Authority (GWA), Great Man-Made River Authority (GMMRA) in Libya, and the documents of CEDARE, UESCO, and FAO (Appendix A.1).

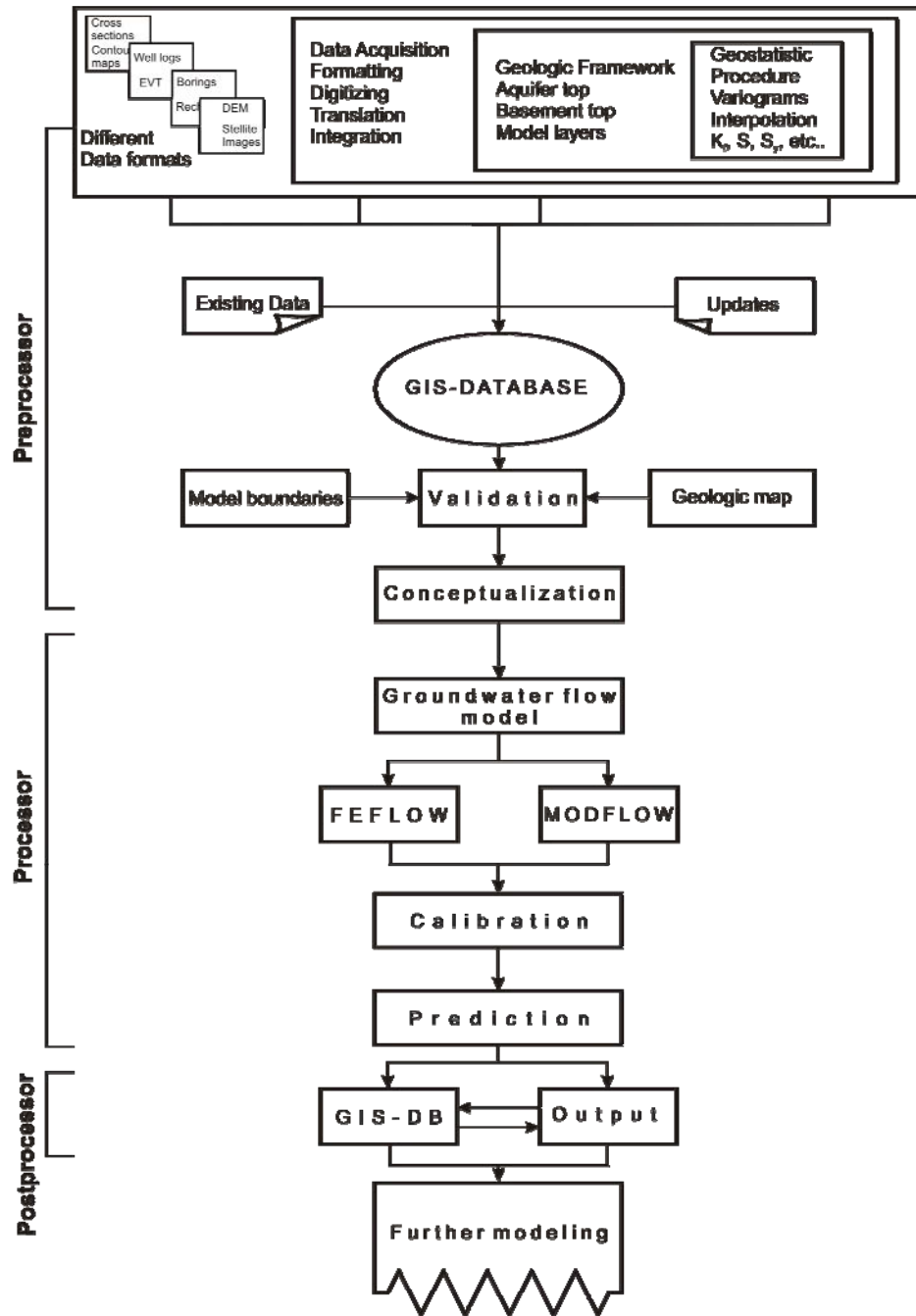


Figure 6.1. Schematic illustration of the procedure of developing a regional groundwater flow model for the NSAS.

6.2 Model development and design

The available data were collected and obtained as scattered distributions of data sets in assorted formats: for instance, well logs, geologic and hydrogeologic cross sections,

drilling data, topographic sheets, basement contour maps, geologic maps, and existing digital data sets from previous work. As a potential professional start with the groundwater flow modeling, a GIS-database coherent structure has been built to accomplish a trustworthy and logical data set and to facilitate the further work. Actually, this GIS-database was constructed to form a comparable structure to the Hydrogeological Information System. As can be seen in Figure 6.2, the following steps have been achieved to construct the GIS-database, for which ArcMap/ArcInfo (ESRI® ArcMap™ 8.2, ArcInfo™ 8.2, 1999-2002) was used:

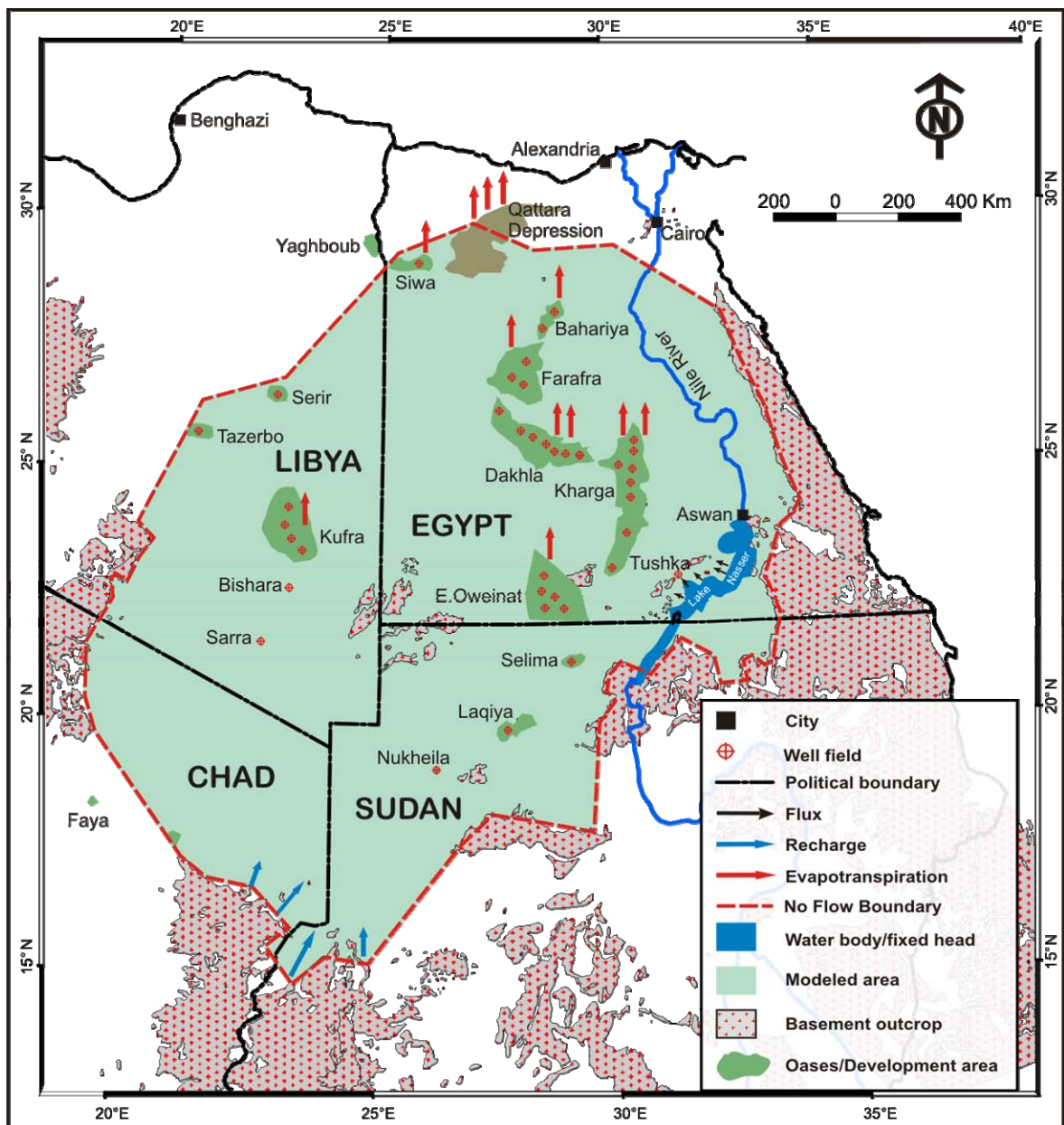


Figure 6.2. Schematic drawing shows the location, extent, development areas, and boundary conditions of the NSAS.

6.2.1 Digital encoding and translation

The main tasks in generating a GIS-Database are scanning, digitizing and georeferencing. All the raw analog signals of the data sets (analog maps, sheets, cross sections, etc.) were gently converted to digital bitmaps (raster data .TIF). These bitmaps are formed of pixels that bear no relationship with the dimensions of the drawings that the raster represents: hence, the bitmaps were subjected to a process of scaling and translating of their pixels to match a particular size and position in a procedure of georeferencing.

This step had to be achieved very cautiously, since it is always the bridge between the analog features of the real world and the digital ones and it forms the conjunction of the different data sets and its spatial distribution. Thus, careless or inaccurate translation leads to misplacement and dislocation of the target features. Consequently, this results in wrong further calculations on one hand; on the other hand, the features will never spatially overlay on each other, which certainly should be avoided.

The bitmaps were spatially georeferenced essentially with the coordination system they show, which in the majority was the geographic coordination system as an international coordinate system (World Geodetic System 1984: WGS-84 (Malys and Slater 1994; DMA TR8350.2, 1997)). Geologic cross sections were also georeferenced by setting the x-axis to the calculated real direction of the profile and the y-axis to the elevations given in the cross section multiplied by an appropriate factor for the vertical exaggeration. WGeo 4.0 (WGeo © WASY GmbH) and the georeferencing tool of ArcMap 8.2 were primarily used for the process of georeferencing.

As a subsequent step, the raster data had to be converted into a digital vector format by a way of sampling at discrete intervals known as digitizing. Without georeferencing, the vectorized GIS drawing size is determined by the pixel dimensions of the raster (the width and height of the raster in pixels). This is in turn determined by the image resolution, which obviously has nothing to do with the real world.

The digitizing procedure involved the attributing of the vector data that is an advantageous as well as an initiative process in building the GIS-database, as the data yet include the x and y Cartesians and the appropriate variables. This step included the construction of vector data for the top, bottom, and slices of the aquifer, initial conditions and boundary conditions as well. For the unity and straight forwarded work purposes, all the vector data were created originally in the UTM (Universal Transverse Mercator) coordination system (DMA-TM8358.2, 1989).

An instant result of the encoding and translation procedure was the production of the geologic map of the Nubian Sandstone Aquifer System as illustrated in Figure 3.3. This digital version of the geologic map was digitized and acquired from the Conoco maps (Conoco 1987) and the Geological Data Explorer (GEODE) of the U.S. Geological Survey (USGS 2004).

6.2.2 Conceptual model

A model concept is a set of assumptions and hypotheses that facilitate the quantification process of the real system under consideration. Several assumptions were considered in this study to describe the real aquifer system based on the available data.

On the basis of the knowledge of the NSAS, as well as the previous modeling attempts, it is clear that in order to be trustworthy, the conceptual model has to be three dimensional and incorporate as much of the geologic structure as available. As such, the extensive base of raw data was to be transformed into a self-consistent three dimensional conceptual model. The attitude for development of the conceptual model is schematically illustrated in Figure 6.3. The understanding of the hydrogeology of the region formed the basis for determining model boundaries, the number of aquifer layers to be modeled, and the location and extent of each aquifer layer.

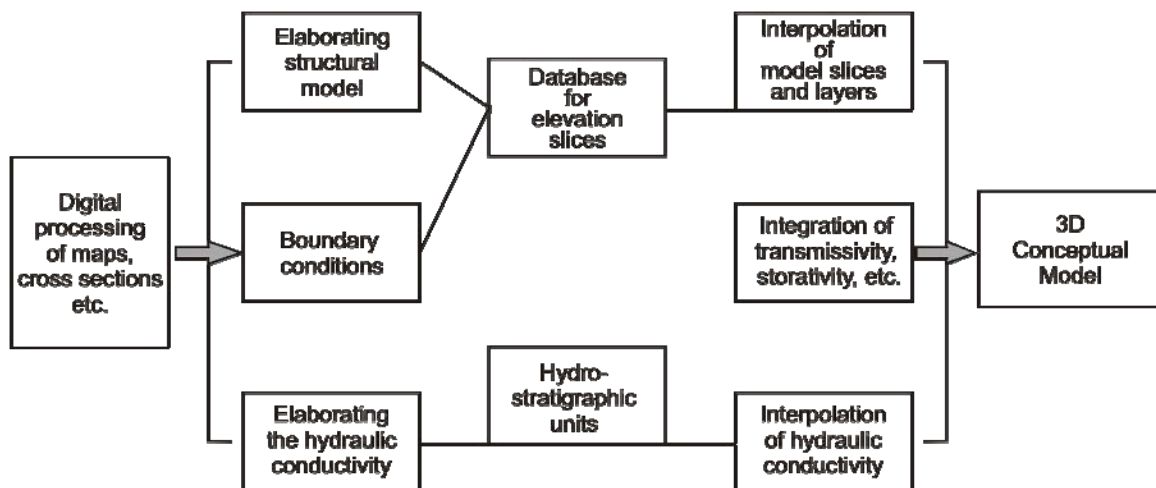


Figure 6.3. Block representation of a flowchart for the typical steps for the development of the 3D conceptual model.

The available cross sections were linked to the boreholes, geology, and the constructed cross sections by the author to allow and enhance the continuous interpolation of the stratigraphy and model layers. Considerable hydrogeologic judgment was necessary to produce meaningful, representative hydrogeologic cross sections and to correct erroneous data.

As can be seen in Figure 6.2, a set of boundary types was chosen and defined for the domain; these will be discussed more deeply in section 6.2.5, and also the recharge areas, pumping locations, evapotranspiration, and water bodies are illustrated.

The cross sectional analysis resulted in a number of stratigraphic units. They differ in number and lithologic description according to their location (Figure 3.2), and these in turn are interpreted into mainly eight hydrostratigraphic units (three aquitards and five aquifers) in light of the given hydraulic parameters, geology, as well as depositional environment information. The number of the hydrostratigraphic units differs naturally from one location

to another. Figure 6.4 illustrates the typical cross sections showing the hydrostratigraphic interpretation of the lithologic, hydrogeologic, and borehole data.

The continental sandstone of Paleozoic to Cretaceous age was assigned to five different aquifers with hydraulic conductivities ranging fairly between 10^{-4} and 10^{-6} m/s. The lateral continuity of each aquifer within the different basins, as well as among these basins, is proved. Some lateral variations and heterogeneity in hydraulic conductivities of the Paleozoic sediments between Dakhla and Kufra Basins are noticed and interpreted (Figure 6.4). Aquifer 2 in the Egyptian areas and aquifer 4 in the Libyan areas are the most productive. Consequently, they are the most stressed or penetrated aquifers of the system. Both aquifers are revealing unconfined conditions among the Egyptian oases as well as all over the Libyan domain.

The sediments of marine origin that intercalate the sandstones are forming three aquitards and confining the above mentioned aquifers along almost the whole extent of the aquifer. The topmost aquitard is formed of Tertiary shale, clay, and limestone and possesses the most impermeable strata of the aquifer, since its hydraulic conductivity is less than 10^{-8} m/s. The other two aquitards form reasonably confining beds at different altitudes with hydraulic conductivity of about 10^{-7} m/s (Figure 6.4). Despite the discontinuity condition, both were noticed all over the domain, excluding some localities to the south of the aquifer domain.

Because of the uneven distribution, quality, reliability, and the scarcity of the data sets from various sources, screening and data quality control were essential in the development of the conceptual model, consequently the database. The interfaces between the different units and the hydraulic conductivity fields within each unit were defined on the basis of borehole data. To obtain laterally continuous layer elevations and hydraulic conductivities throughout the whole domain, the spot elevations and conductivities were interpolated using universal kriging, as will be discussed further in section 6.2.4.

The availability of large volumes of highly representative, quality data strongly controls the reliability, validity, and continuity of the groundwater investigations. Therefore, engaging all data into a coherent and logical GIS structure is a crucial step in this work.

6.2.3 GIS-Database

Once the processes of digital encoding, vectorization, and conceptualization have been started, big data sets are developed. These data sets had then to be compiled in a unique structure that allows “one to one” or “one to many” spatial and temporal relationships. This can be obviously supported by the GIS. Considering that large spatially and temporally related data storage and processing are necessary for the groundwater flow modeling of this work, GIS is adopted to provide a basic platform and powerful tool for all spatial and temporal data processing and analysis as well as the creation of digital geographic

databases to manipulate and prepare data as input for different groundwater modeling systems.

Since the establishment of 3D groundwater flow modeling is a vital bridge objective in this work, GIS is actively used in the following roles: (a) to store, manipulate, and analyze the spatial distribution of each factor in connection with groundwater flow; (b) to quantitatively process and prepare the spatial data and provide for 3D groundwater models; (c) to support the discovery and verification of possible problems or conflicts during groundwater flow simulation and to assist in tedious model modification; and (d) to display the results by overlaying other theme maps for various kinds of applications.

All necessary data, such as DEM, geology, hydrogeologic units, terrain, hydraulic conductivities, and specific yield parameters distribution, initial groundwater contours, infiltration quantity, evapotranspiration, well locations, extraction rates, etc., have been built as GIS data layers and used for groundwater flow model establishment and flow simulation. The data transformation from GIS to the groundwater flow simulation codes was realized by GIS data export in the appropriate format that is required by the modeling code in question. The data sets for the slice elevation and aquifer parameters were created in ArcGIS as point data features with their spatial references and appropriate attributes in order to facilitate the geostatistical analysis procedure afterwards.

All the GIS data layers are put into the same ArcGIS-personal database with the same coordinate system, which is UTM, zone 35N. This database is used for information query, search, and analysis during and after the establishment of the model. When the simulation results of 3D groundwater flow simulation are problematic, it is particularly convenient and effective to use this database to find the possible reasons and make model modifications. The amount of work could be noticeably reduced, and considerable time could be saved by using the database during and after the establishment of the model.

6.2.4 Interpolation and layer generation

In the real world it is impossible to get exhaustive values of data at every desired point because of partial constraints. It is a question of data availability for the NSAS, since it is scarce and rigorously constrained to the oases and development areas of the aquifer. On account of this scarcity, discontinuity, and the scattered distribution of the data needed for the establishment of 3D groundwater flow model as intended in this work, a great effort was given to statistical management of the available data. It was a crucial phase to approximate, analyze, understand, and graph the values of the data gaps and to plot an indiscrete, reasonable database for the NSAS.

The word "kriging" is synonymous with "optimal prediction". It is a method of interpolation which predicts unknown values from data observed at known locations.

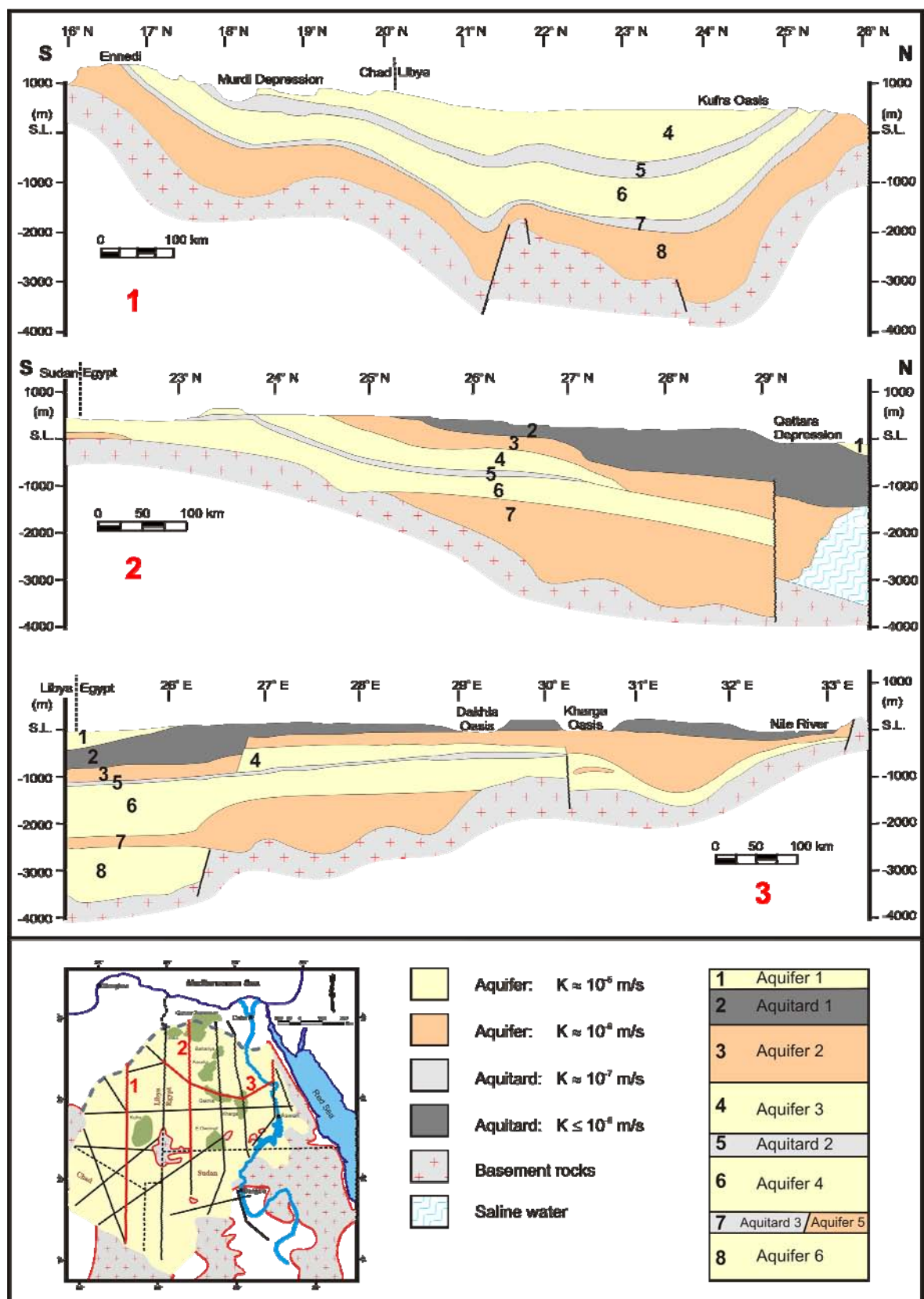


Figure 6.4. Schematic example configurations the conceptualization idea and the location of some regional cross sections in plan view.

This method uses variograms to analyze the spatial variation and surfaces' roughness and continuity (Barnes 1991; Zimmerman 1991). It minimizes the error of predicted values which are estimated by spatial distribution of the predicted values as well (Figure 6.5).

At this stage, all spatial data for each data factor (elevations, parameters, hydraulic head, etc.) were exported from ArcGIS as ASCII-x,y,z data format. These were afterward adjoined to the statistical treatment using software Surfer (Surfer 8.0, Golden Software ©, Inc. 1993-2002). The data were interpolated using kriging with an appropriate variogram for each data set. The exponential (Cressie 1991), spherical (Pannatier 1996), Gaussian (Pannatier 1996), and cubic (Olea 1999) variograms were the best matching model curves for the interpolated surfaces. The result grids were designed to have a resolution of 1 km for both horizontal and vertical spacing. This resulted in grids covering the whole modeled area and forming 1,690 rows and 1,600 columns or 2,704,000 data points for every interpolated surface.

6.2.4.1 Generation of layers and slices

Establishment of a geologic framework is an essential phase in the development of a 3D groundwater model. This step requires elevation data covering the whole modeled domain, whereby the sophisticated expression of spatial variation of the data represented here by kriging and its related variograms is one of the best known tools to achieve this objective.

As mentioned before, ArcGIS was used to elaborate and link all available data for elevations and surfaces in different point shape features. These were further applied to the interpolation procedure as ASCII-TXT data sets.

As more data were engaged, evaluated, and corrected, the surfaces were better constrained and became increasingly accurate. Once cross sections and data validation procedures are completed, new surfaces were built to provide a final model with maximum geological consistency. Cross sections and geological map contacts are used here as the main expert knowledge constraints, even though other constraints were also applied to take into account reliable data between cross sections in order to increase the accuracy of interpolated surfaces. These include topographic data, rock outcrops, and contacts from boreholes.

Since building surfaces separately does not ensure that they are consistent in the correct stratigraphic order away from cross sections, minimum thickness constraints were applied locally to remove most crossovers. These crossovers were frequent where units are thin, especially if the variability of the top or bottom elevation of a unit is greater than its thickness. In order to respect minimum thickness constraints, special attention was also given to reliable boreholes that do not reach bedrock.

Crossovers and other thickness problems were thus corrected locally depending on the specific problem, when and where it is, instead of taking a reference surface, calculating its

thickness, and then adjusting all the others to fit that layer upwards or downwards. Therefore, surfaces are not regionally modified on the basis of a reference layer as opposed to what is often done in multi-layered modeling using standard GIS tools.

- **Aquifer top**

Slice number one (ground surface) was the first created (Figure 6.5), since it was extracted from the SRTM-03 (Shuttle Radar Topography Mission-03 Arc Seconds (Farr and Kobrick 2000; USGS 2004; NASA 2005)). These are DEM (Digital Elevation Model) data with a resolution of about 90x90 m and distributed free of charge by U.S. Geological Survey.

The archival surface elevation of the available boreholes was then compared to the Digital Elevation Model, where maximum differences of ± 9 m were encountered. The elevations of the DEM were substituted with those of the boreholes at localities where they occurred.

- **Aquifer bottom**

The aquifer bottom or basement top was created from different data sources. These are boreholes, cross sections, basement outcrops, basement relief contour maps, geologic map, Isopach maps, and DEM. Figure 6.5 illustrates the top and bottom of the aquifer and the spherical variogram used for bottom slice.

- **The other slices**

The same procedure was used to create the other six slices of the aquifer. Once the interpolation process was finished, all elevation slices were imported again to ArcGIS for the application of the control and validation procedure. At the places where the crossovers and extrapolation probabilities occurred, the crossovers were controlled and corrected and the thickness constraints were applied.

6.2.4.2 Aquifer parameters

Groundwater management is mainly based on proper characterization of hydrogeological parameters. In this respect, a major problem comes up, namely, the identification of various hydrogeologic parameters and their spatial variability. As discussed in Chapter 5, the aquifer tests and hydraulic parameter investigations are restricted to the oases and development areas within the NSAS. A hydrogeological outline of the entire area shows, in general, spatial variability in hydraulic conductivities in the different aquifer units.

The available records for the hydraulic conductivities were first imported into an ArcGIS point data feature, these subsequently were delogarithmized. The interpolation was held on the delogarithmized values of the hydraulic conductivities. At this step, a lot of constraint points had to be situated prior to the interpolation procedure to avoid problems of extrapolation. The best variogram model that matched the hydraulic conductivity curves was the spherical variogram. The interpolated values of the hydraulic conductivities for the

entire domain are shown in Figure 6.6. An example variogram for aquifer bottom (layer 8) is also given.

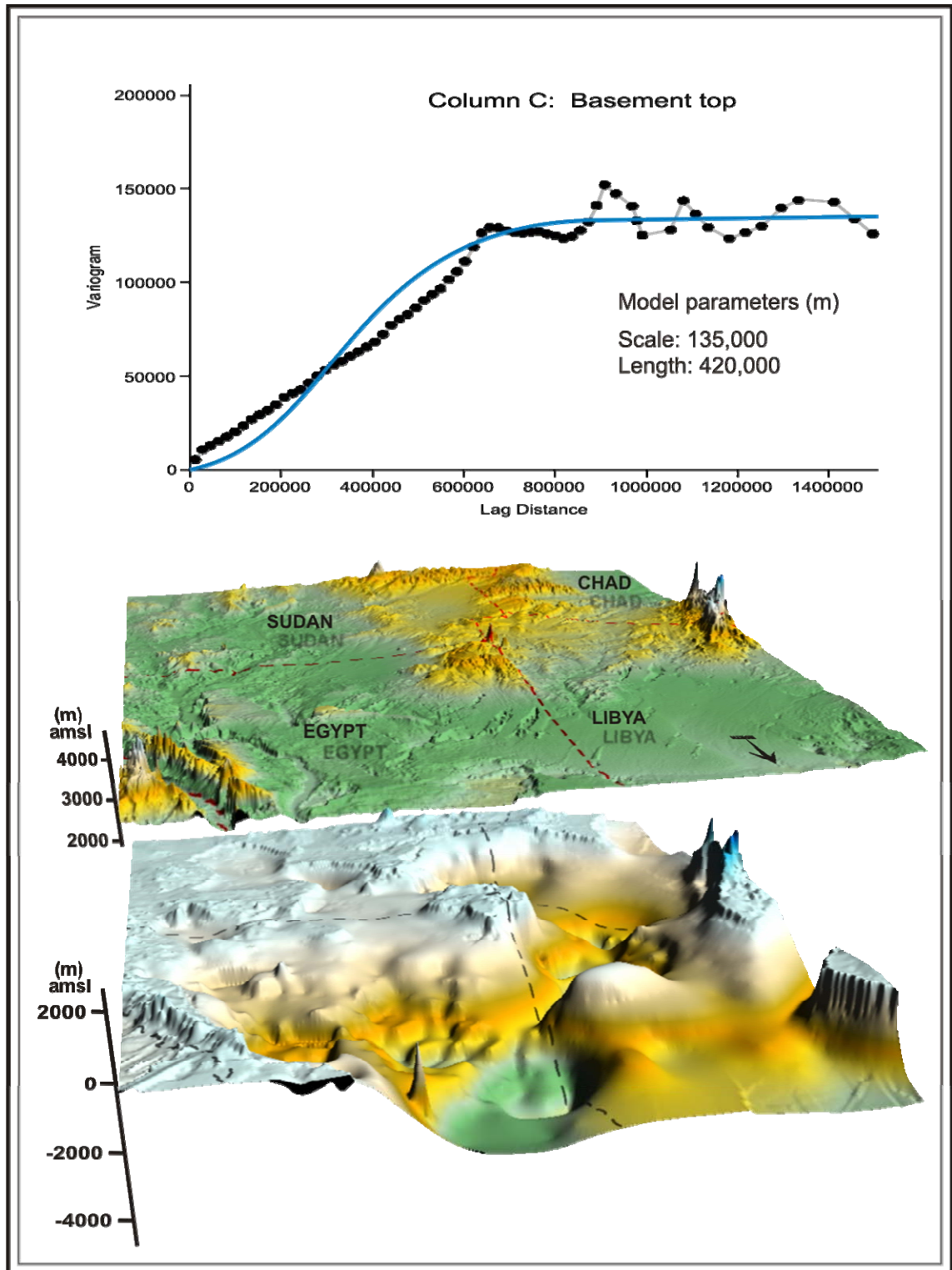


Figure 6.5. Digital Elevation Model and basement relief of the NSAS, as well as a corresponding Gaussian variogram for the basement relief.

The other aquifer parameters (transmissivities, storativities, and porosities) were assessed from the hydrogeological characteristics of Nubian facies as well as from the results of former modeling studies (Hesse et al. 1987; Heintz and Thorweihe 1993; Ebraheem et al. 2002; Sefelnasr 2002). These were afterwards prepared and interpolated just in the same manner as the hydraulic conductivities, yet without the need for delogarithmizing.

6.2.5 Boundary conditions

The whole aquifer domain is considered a closed system due to the natural (physical) boundaries consisting of the unfractured basement outcrops that bound the aquifer to the east, south as well as the west. In addition, the aquifer is bounded to the north by a hydrogeological boundary which is the Saline-Freshwater Interface. Yet this interface is considered unmovable or fairly constant in space by most of the scientists, even though its displacement is not absolutely ruled out.

6.2.5.1 1st type: Dirichlet boundary condition

The fixed head boundary condition was applied to the surface water body represented by Lake Nasser and to the Nile (Figure 6.2). The average surface water level of Lake Nasser is about 175 m (amsl). Despite the fact that this level changes over time, it is considered constant for the simulation course of the regional model; even so, it will be defined as a time-dependent boundary condition in the local modeling as discussed in Chapter 8. Lake Nasser forms a vast water body with a length of about 550 km, and an average width of 15 km, and an average depth of 25 m (Elewa 2006). The contact layer is formed mainly of the Nubian sandstone of about 100 m thickness. The groundwater level at the west of the lake ranges from 60-190 m (amsl).

The Nile was also considered a constant head boundary condition with changeable influent and effluent states depending on the exposed hydrogeological conditions. As north of Aswan High Dam to the latitude of 25° N, the Nile is running over the unconfined Post Nubian Aquifer System exhibiting effluent condition (the influent/effluent conditions are presented in this article from the hydrogeological point of view that is opposing the hydrological definition of these terms). The water level of the Nile ranges from 100 m (amsl) at the vicinity of Aswan High Dam (AHD) to 30 m (amsl) at the northern boundary of the aquifer, where the Nile crosses the aquifer boundary out of the model domain.

The Groundwater-Surface water (GW-SW) interaction between Lake Nasser water body and the Nubian Sandstone Aquifer System will be further discussed in depth in Chapter 8.

6.2.5.2 2nd type: Neuman boundary condition

The flux boundary condition is represented in this modeling scheme by the “no flow boundary” that was set to the model outer boundary due to the physical and hydrogeological boundaries as discussed in section 6.2.5.

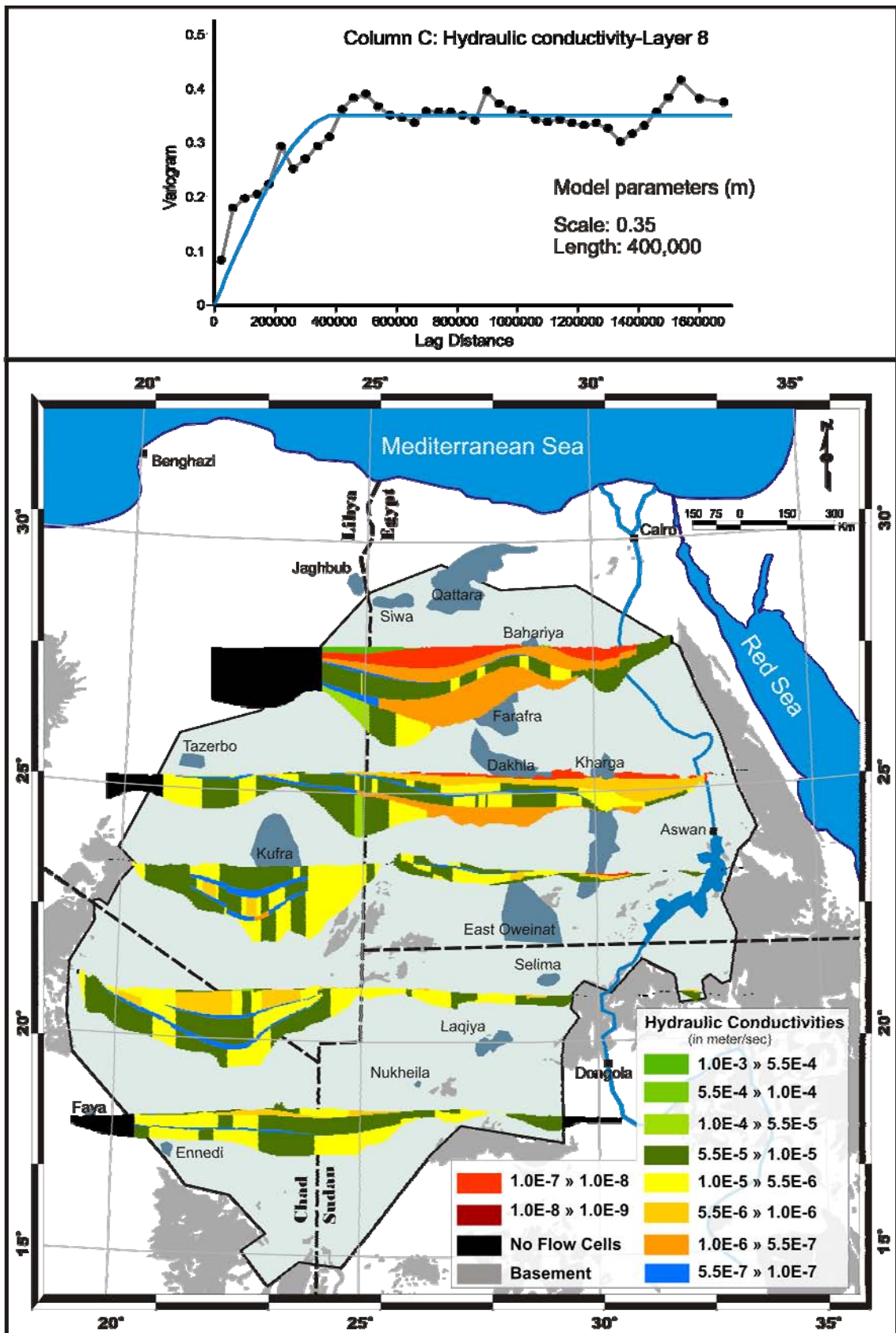


Figure 6.6. The distribution of the hydraulic conductivities as obtained from the appropriate statistical procedures. A matching spherical variogram is shown at the top of the figure.

6.2.5.3 4th type: Well boundary condition

This type of hydrogeological boundary condition is presented by the artificial discharge through pumping wells in the oases and development areas of the NSAS. As shown in Figure 6.7, there are two major extraction schemes: the actual and the planned. The actual scheme was driven from the actual groundwater exploitation at every stressed region as given from the official records of groundwater extraction for irrigation, industrial, and domestic water supply. These data were then used to calculate the daily artificial discharge for each individual stressed region (for sources refer to section 6.1).

The planned groundwater extraction rates are given from the reported proposals of the MPWWR and RIGW in Egypt, and the GMMRA in Libya. Based on these two schemes, different groundwater flow modeling scenarios were developed for the aquifer, as will be further discussed in this Chapter and the next Chapter.

In the regional modeling, the extraction rates were given as several pumping centers for each stressed region in cubic meters per day. For the areas where only planned extraction schemes were available, these were used also as actual extraction rates. Table 6.1 summarizes the extraction rates of each stressed area; both the actual (scenario 1) and planned (scenario 5) extraction rates are given as well as the extraction scenarios suggested by the author. Scenario 2, 3 and 4 are obtained by an increase of scenario 1 by 25%, 50% and 75% of scenario 5, respectively.

Table 6.1: The different extraction scenarios (Mill m³/y) for the different stress areas within the NSAS.

Area	Scenario 1	Scenario 2	Scenario 3	Scenario 4	Scenario 5
Siwa	26	71	116	161	206
Bahariya	34	70	105.5	141	177
Farafra	283	330	377	424	471
Dakhla	439	485.5	532	578.5	625
Kharga	93	120.5	148	175.5	203
E. Oweinat	164	423	682	941	1200
Tushka	7.3	7.3	7.3	7.3	7.3
Kufra	183	685	1186.5	1688	2190
Tazerbo	126	189	252	315	378
Serir	73	110	146.5	183	220
Selima	102	102	102	102	102
Laqiya	95	95	95	95	203
Nukheila	95	95	95	95	95

Sources: MPWWR (1999), RIGW (1999), Pallas and Salem (2001), CEDARE (2002) and Bakhbakhi (2006).

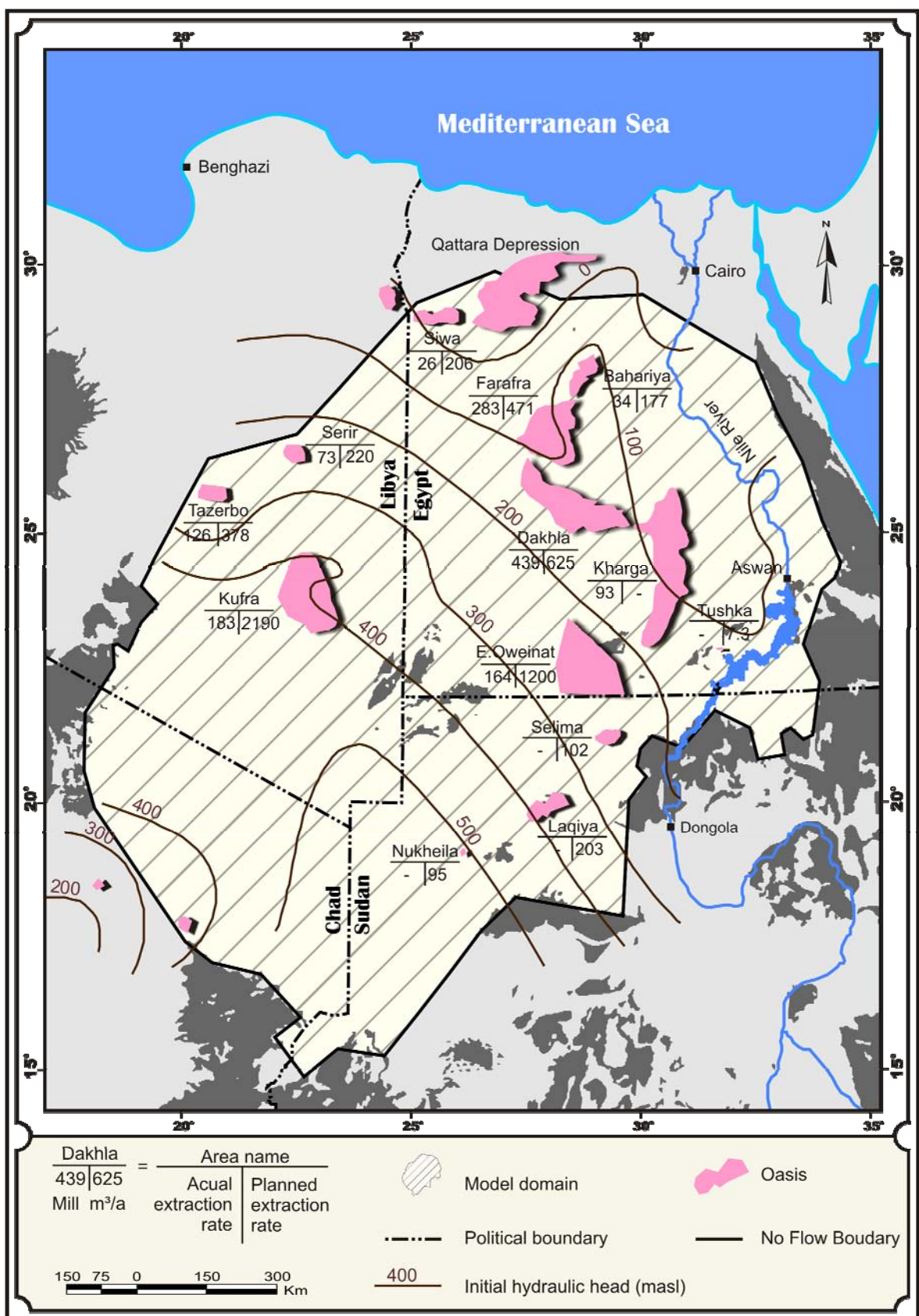


Figure 6.7. The distribution of the initial potentiometric head in the NSAS and the schemes of the extraction rates. Initial heads adapted from Ball (1927) and Sandford (1935).

The total actual extraction rates of Dakhla oasis given in cubic meter per day are illustrated by a chart in Figure 6.8. The groundwater extraction scenarios are based on the anthropogenic groundwater demand for domestic, agriculture, and industrial use, as well as the depth to groundwater owing to this discharge in every stressed area in each.

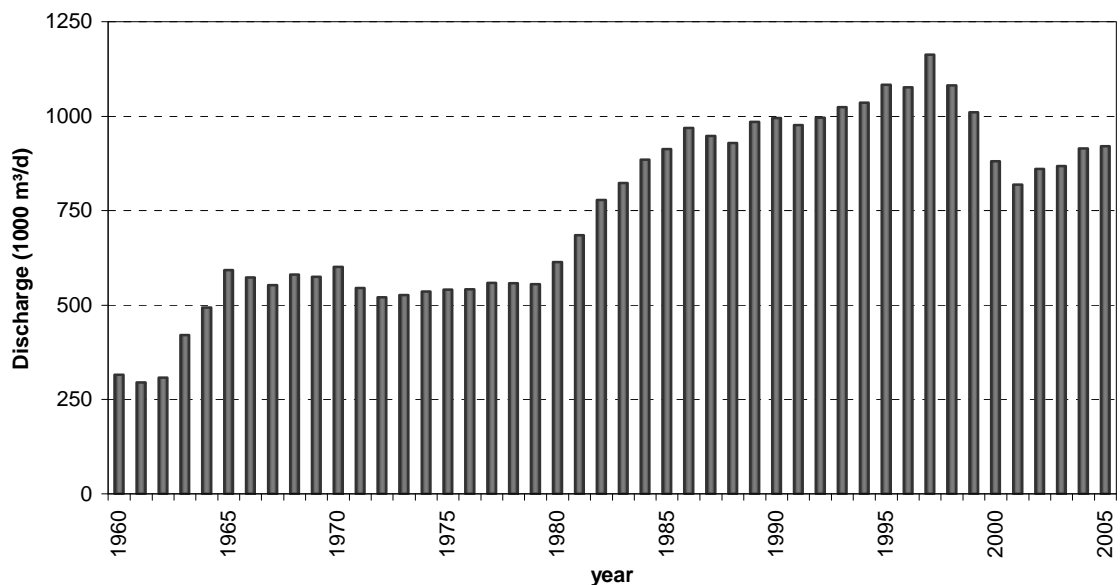


Figure 6.8. Cluster chart represents the total extraction rates of the Dakhla oasis in time since 1960. Source MPWWR (1999) and personal contact (2005).

6.2.6 Initial conditions

The initial conditions and historical groundwater levels are compulsory input items so as to have the ability to start the calculations or the calibration processes in the transient modeling schemes. For this purpose contour maps of potentiometric levels for the aquifer have been derived from the groundwater contour map of Ball (1927) and its modification that was presented by Sandford (1935). In addition, the available individual records of the groundwater levels before or around the year 1960 were also taken into account. As the New Valley project had started first in 1960, these maps are considered representative data inputs for the initial head records (Figure 6.7).

6.2.7 Recharge

As discussed in sections 4.5.2.1 and 4.5.2.2, the only possible modern recharge for the NSAS is represented by the seepage from the surface water of Nile and Lake Nasser, and the episodic infiltrations occur at the more humid regions in the most southern corner of the aquifer. Recharge through infiltration is estimated by 5-15 mm/y (Sonntag 2001). This amount was applied to the model as three recharge regions increasing in rate to the south.

6.2.8 Evapotranspiration

The evapotranspiration is commonly applied to the oases and depressions (refer to section 4.6), where the groundwater level occurs immediately close to or above the ground surface (Figure 6.2). The estimation of the evapotranspiration of the NSAS corresponds to a mean of 10-15 mm/year (Ahmad 1983; Sonntag 1986; Sonntag and Christmann 1987; Nour 1996).

6.2.9 Discretization

An advantageous ability in the finite element modeling systems is that they allow the independently spatial refinement of the areas in consideration within the whole model. The model was refined in the Dakhla oasis and Lake Nasser to have a mesh net with lateral size of the mesh elements up to 500 m. In the other oases and along the Nile the elements' size ranges from 500 m-6 km according to data density. In general the model has over 1.3×10^6 triangular prismatic mesh elements with 702×10^3 mesh nodes for every model slice. The finite element grid was generated manually by applying different region classes according to the hydrogeological conditions and modeling interests.

Based on the available data, the model was discretized vertically into eight layers as shown in Figure 6.4. So as to rectify the hydraulic conductivities these layers were further discretized into three layers each, except for the first and the last one, where each of them became two layers. Digitally the model, therefore, had 22 layers or 23 slices.

The time discretization was applied using the automated time step control, which is often appropriate for non-linear unsaturated simulations where the estimation of a time step history is usually difficult to find and the updating effort of the matrix systems occurs in any case.

6.3 Calibration

The groundwater flow model of the NSAS was calibrated principally under transient conditions by use of the available historical hydraulic head records as calibration targets and was adjusted using a trial and error parameter estimation method through a series of groundwater flow simulations. Automated parameter estimation techniques were attempted, but there are not enough different types of complete observation data for these techniques to be successful. The calibration process was designed for the period 1960-2005 (from the beginning of the New Valley Project until the last available field record).

Some of these records, however, endure temporal discontinuities and are poorly distributed spatially relative to the extent of the whole study area. For the areas where no observation data are available, the calibration relied principally on the hydraulic gradient and flow direction (Figure 6.9). Other factors were considered during the calibration, including the following: 1) Matching the simulation results to the conceptual model of the groundwater

acceptable margin of error (Table 6.2). Because too few complete records exist for the NSAS, most of the observations are analyzed as a single set.

For the complete head records (records from 1960-2005, some of them with gaps), the residuals, or difference between simulated and observed heads, ranged from -12.02 to 11.95 meters with a mean of 0.42 m, a root mean square of 2.22 m, and a calibration fit (Kuniansky and Danskin 2003) of 0.005 (Table 6.2, Figure 6.10). The mean of residuals indicated that the mean difference between computed and observed water level is skewed slightly positive (Figure 6.10). The root mean square is the square root of the average deviation of residuals from zero. The residuals are assumed normally distributed over the 1:1 line of the scatter diagram (refer to the histogram in Figure 6.10). The histogram shown in Figure 6.10 depicts the frequency range of the projections of the residuals on the axis perpendicular to the 1:1 line. It is skewed to the simulated heads, which indicates that simulated heads are slightly higher than the measured heads. This is supported with the positive overall mean residual error shown in Table 6.2.

The highest head discrepancies were located within or in the vicinity of the depressions, where steeper hydraulic gradients occur. At these spots, small changes to the calibration parameters led to large head variations. Hydrographs of history matching (referred to by others as model verification) were used for wells in locations of the model for which long-term water-level data were available (Figure 6.11).

Table 6.2. Calibration statistics for simulated hydraulic heads of the NSAS.

Calibration statistics	
Number of observations	928
Range of residuals (m)	23.97
Minimum residual (m)	-12.02
Maximum residual (m)	11.95
Mean residuals (m)	0.42
Standard deviation of residuals (m)	2.19
Root mean square residuals (m)	2.22
Calibration fit: standard deviation of residuals divided by average range of observed values	0.005

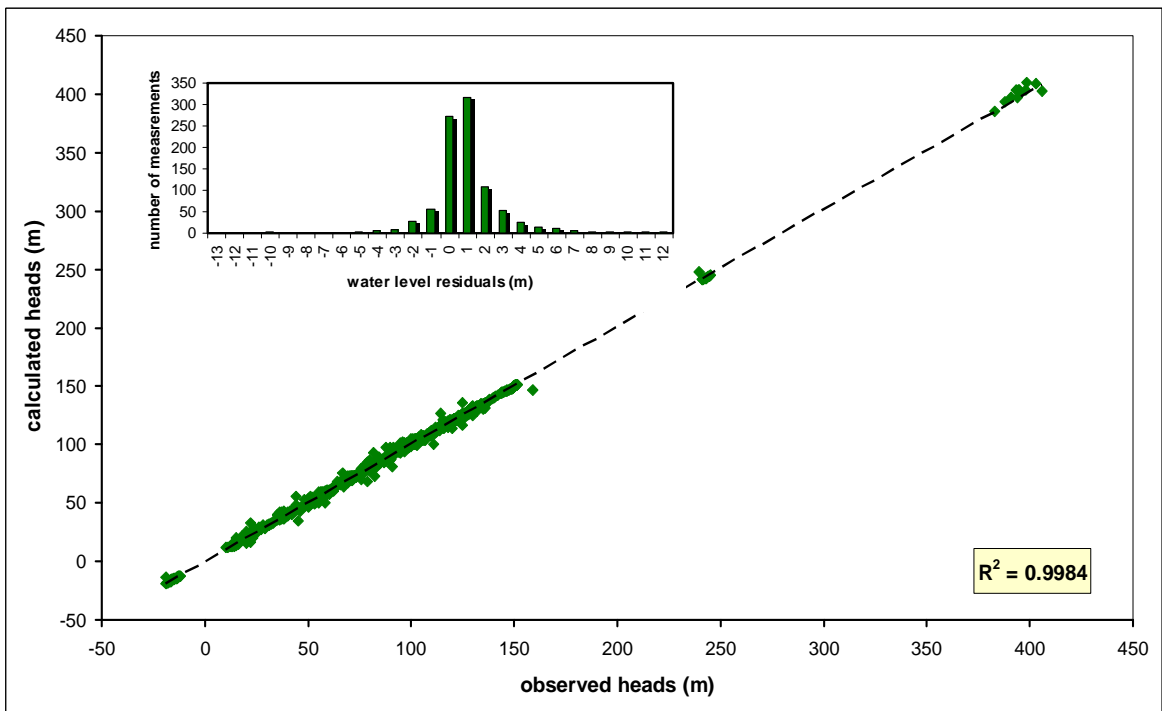


Figure 6.10. Scatter diagram showing simulated vs. measured heads at calibration targets. The histogram represents the frequency range of the residuals.

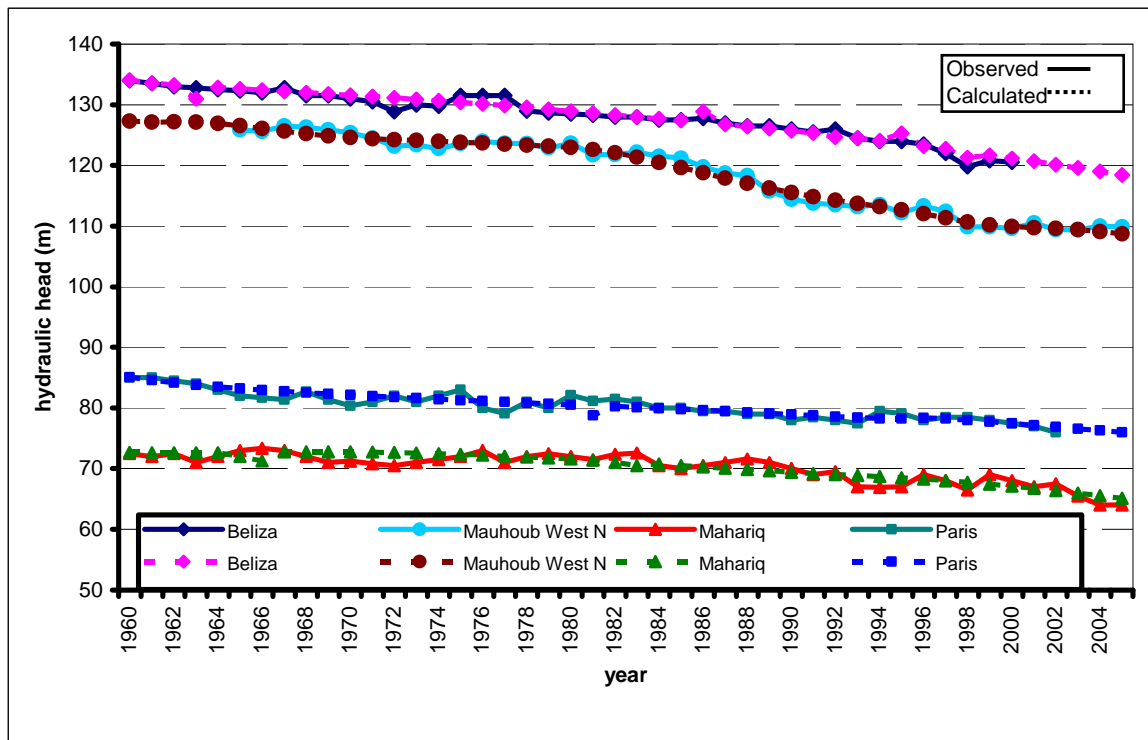


Figure 6.11. Hydrograph of history matching, a comparison between observed and computed heads with time (time scale represents the calibration period from 1960 until 2005).

6.4 Linkage with modeling systems

Computational grids for numerical models must be optimized to produce accurate and stable numerical solutions such that some geometric generalizations may be done in practice (Anderson and Woessner 1992). As a result, multi-layered hydrostratigraphic models are usually designed to fit the specific requirements of both the numerical modeling strategy and a particular software package (e.g., MODFLOW or FEFLOW). The main advantage is that the hydrostratigraphic model is readily available for numerical modeling. With such an approach, a model tends to have, as much as the data allow, the stratigraphic details required by the most demanding application of the project.

The first attempt in this work was to create a groundwater flow model using visual MODFLOW. The model was built and designed to have 320 columns and 338 rows with equal dimensions of 5 km in each layer. Vertically it was divided into 23 slices. During the calibration phase MODFLOW ran completely unstably and proved extreme unexpected fluctuations due to the resulting dry cells in the vadose zone (which emphasizes the unsuitability of MODFLOW for the complex saturated/unsaturated zone problems).

Attention was then paid to further development of groundwater flow modeling using FEFLOW. FEFLOW is especially suitable for problems involving complex model architecture and can deal conveniently with saturated/unsaturated problems. The database was oriented to help produce proper input data sets for FEFLOW. The discretization attempted for FEFLOW was discussed in section 6.2.9.

6.5 Regional model output

The calibrated regional model was first used to forecast the changes in the flow regime that result from the natural stresses and the anthropogenic activities on the aquifer resources during the coming 100 years. In the analysis procedure of the simulation results, emphasis was given to the changes in hydraulic head, drawdown, depth to groundwater, as well as the groundwater balance to evaluate the potential and response of the aquifer to the stresses above mentioned within the prediction period. The current hydraulic head distribution and drawdown (state 2005) are represented by Figures 6.12 and 6.13, respectively.

6.5.1 Hydraulic head

In general, the direction of groundwater flow within the regional model area is kept by the original trend of the initial head postulated by Ball (1927) and Sandford (1935) that is shown in Figure 6.7. However, as expected, the values and local trends of these contours have some changes within the depressions like the Dakhla and Kharga oases and development areas like East Oweinat, where new contour lines with lower values appeared. Table 6.3 gives a representation of the average hydraulic head, drawdown, and depth to groundwater in the stressed area within the aquifer.

The major changes in the pattern of the groundwater contour lines for scenario 1 and scenario 5 for the years 2050 and 2100 (refer to Table 6.1 for the extraction values) are shown in Figures 6.14 to 6.17. For scenario 1, the contours started to change slightly, especially in the Egyptian oases (i.e., Kharga, Dakhla, Farafra, and Bahariya), by 2050 to expose further slight changes by 2100. However, these changes are still local changes and do not extend the depression to the neighboring one.

The situation is completely different with the results of scenario 5, as the full capacity extraction rates induce noticeable changes in the groundwater flow directions and patterns at almost all of the stressed areas by 2100 as seen in Figure 6.17.

6.5.2 Drawdown

Before the project of the development of the New Valley has started, or rather before year 1960, there was no obvious drawdown within the studied depressions. Once the successive groundwater extraction was in progress, the amount of the groundwater stored in the aquifer started decreasing, leaving a noticeable decline in the potentiometric level. The performed simulations helped in reading and trailing this decline in hydraulic head within the interest areas (Table 6.3).

The results obtained from scenario 1 indicate that the major cones of depression are centered in the Kharga and Dakhla oases with average drawdown of 40 m and 42 m by 2050, respectively. This amount of decline in hydraulic head increases further for both oases to reach an average of 55 m by 2100. Nonetheless, the amounts mentioned above are an average drawdown, which does not hinder the existence of drawdown values that exceed 50 m by 2100, for example, within the well fields of Kharga city in the Kharga oasis or east of the Dakhla oasis. At the other depressions and the East Oweinat area, gentle cones of depression are formed without exposing anomalies of the hydraulic gradient or deepness of the cones of depression (Figures 6.18, 6.19).

However, with application of scenario 5, very steep hydraulic gradients and wide, deep cones of depression were created around the well fields by 2100 in Kharga, Dakhla, and East Oweinat in Egypt; Kufra, Serir, and Tazerbo in Libya; and Laqiya in Sudan (Figures 6.20, 6.21). The cones of depression around Dakhla, Farafra, and Bahariya are now extended to build a huge single cone of depression gathering the whole area occupied by the three oases. The two meter drawdown line is now located about 145 km south of the well fields of the Dakhla oasis. In the East Oweinat area, the cone of depression extends to the south beyond the state boundary between Egypt and Sudan to form a very deep cone of depression with an average value of 162 m (Table 6.3) and a maximum value exceeding 200 m at several locations by year 2100 within the East Oweinat area (Figure 6.21).

Table 6.3. Average changes in hydraulic head, drawdown and depth to groundwater for the stressed areas of the NSAS.

Location	Initial head (m amsl)	Scenario	Hydraulic head (m amsl)			Drawdown (m)			depth to groundwater (m bgl)		
			2005	2050	2100	2005	2050	2100	2005	2050	2100
Dakhla (63 m)	140	1	115	98	85	25	42	55	-9	8	21
		5	115	80	55	25	60	85	-9	26	51
Kharga (38 m)	75	1	45	35	20	30	40	55	11	21	36
		5	45	35	20	30	40	55	11	21	36
Farafra (115 m)	135	1	127	115	102	8	20	33	-17	-5	8
		5	127	105	80	8	30	55	-17	5	30
Bahariya (124 m)	128	1	121	112	104	7	16	22	-12	-3	5
		5	121	100	81	7	28	47	-12	9	28
Siwa (125 m)	-5	1	-11	-15	-20	6	10	15	-4	2	7
		5	-11	-22	-29	6	17	24	-4	7	14
E. Oweinat (100 m)	250	1	245	239	232	5	11	18	22.5	29	35
		5	245	170	105	5	80	145	22.5	98	162
Kufra (113 m)	405	1	398	393	388	7	11	16	5	9	15
		5	398	335	275	7	70	130	5	68	128

-ve sign means flowing well. (63 m) is the economic lifting depth for each area (Euro and Pacer Consultant 1983). bgl = below ground

The Kufra oasis is not that much different from the situation in East Oweinat, as the average drawdown there is about 128 m and a maximum drawdown value that exceeds 200 m is also recorded. Selected results of scenarios 2, 3 and 4, are shown in Appendix A.

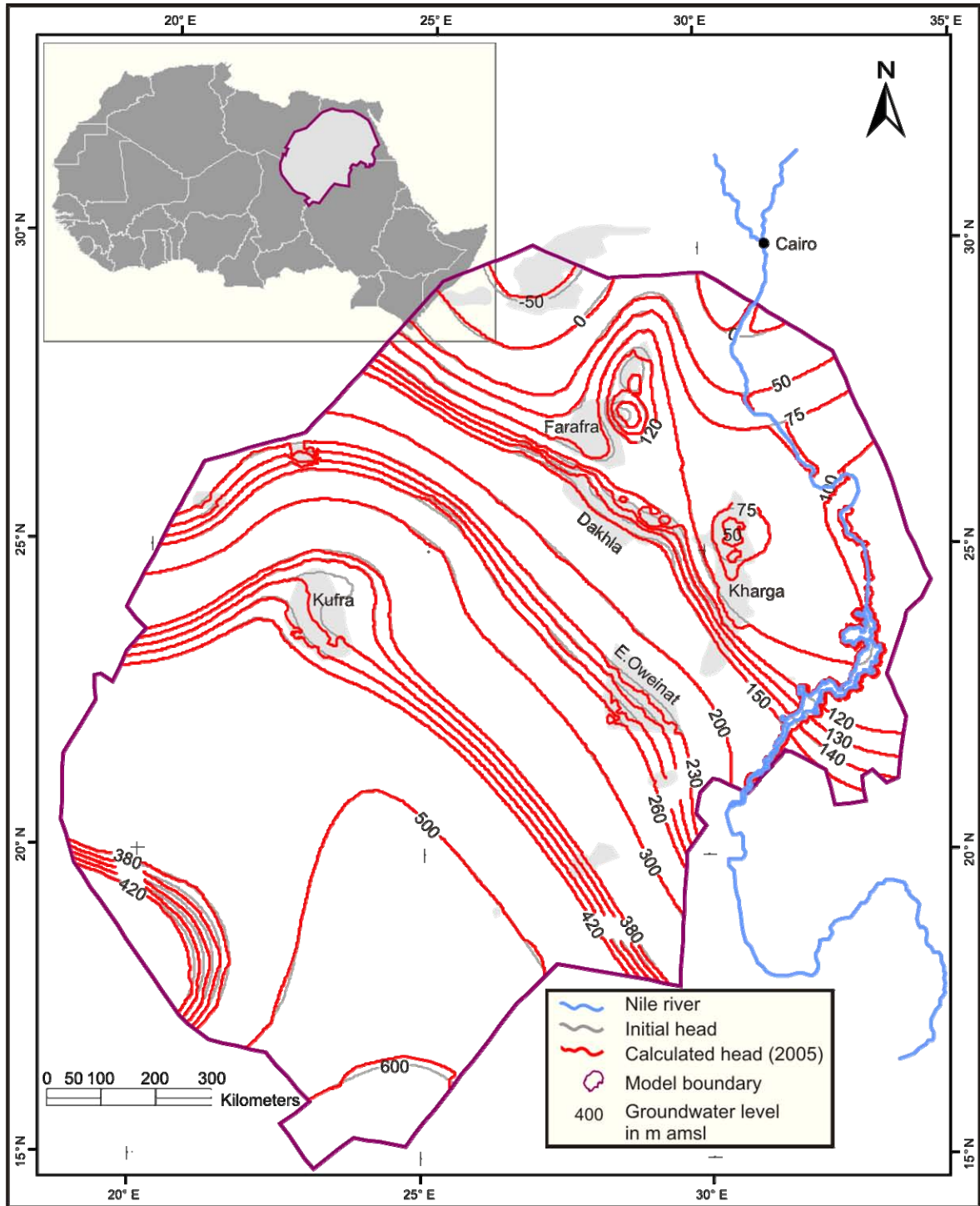


Figure 6.12. The distribution of the simulated hydraulic head of the NSAS by 2005 in comparison to the initial heads of year 1960.

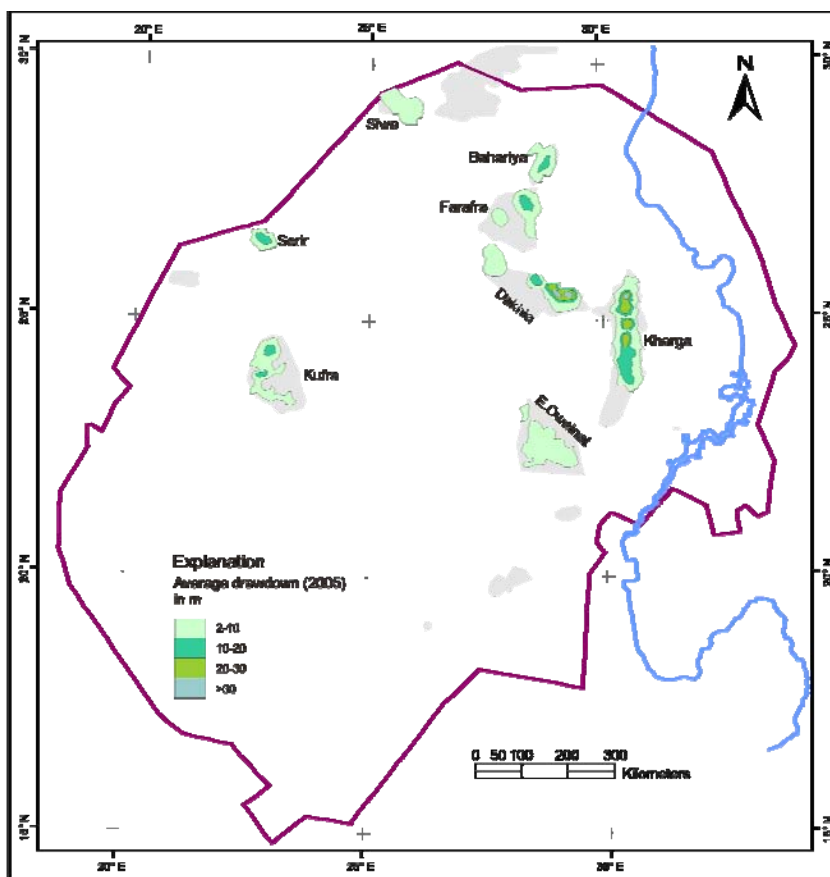


Figure 6.13. The decline of the groundwater head (drawdown) within the depressions of the NSAS by 2005.

6.5.3 Depth to groundwater

The calculated water depths within scenario 1 in all stressed areas (except for the Kharga oasis) indicate that the simulated groundwater exploitation rates in this scenario for these areas are obviously lower than the permissible/potential rates for the coming 100 years. As for all simulated areas, except for the Kharga oasis, the groundwater depths are still away from the postulated economic lifting depth for irrigation (Euro and Pacer Consultant 1983; RIGW 1999) (Table 6.3). In the Kharga oasis, only at the middle and north of the oasis should the extraction rates be slightly decreased.

In scenario 5, the extraction rates are still feasible for Siwa, Bahariya, Farafra, and most of the area of the Dakhla oasis, where the economic lifting depths are not exceeded. The simulation results indicate that the extraction rates in the East Oweinat area and the Kufra oasis are much higher than the affordable rates to keep the economic development of these areas. The depth to groundwater in the East Oweinat area will exceed 98 m by 2050 and 162 m by 2100 if the full capacity of extraction rate (1.2 km³/year) is applied. A similar negative impact was obviously shown in the Kufra oasis. Therefore, it is concluded that the extraction rates of scenario 5 (the planned extraction rates) for both the East Oweinat area and Kufra could be feasible, but only for too short time and not for the long sustainable development of the NSAS.

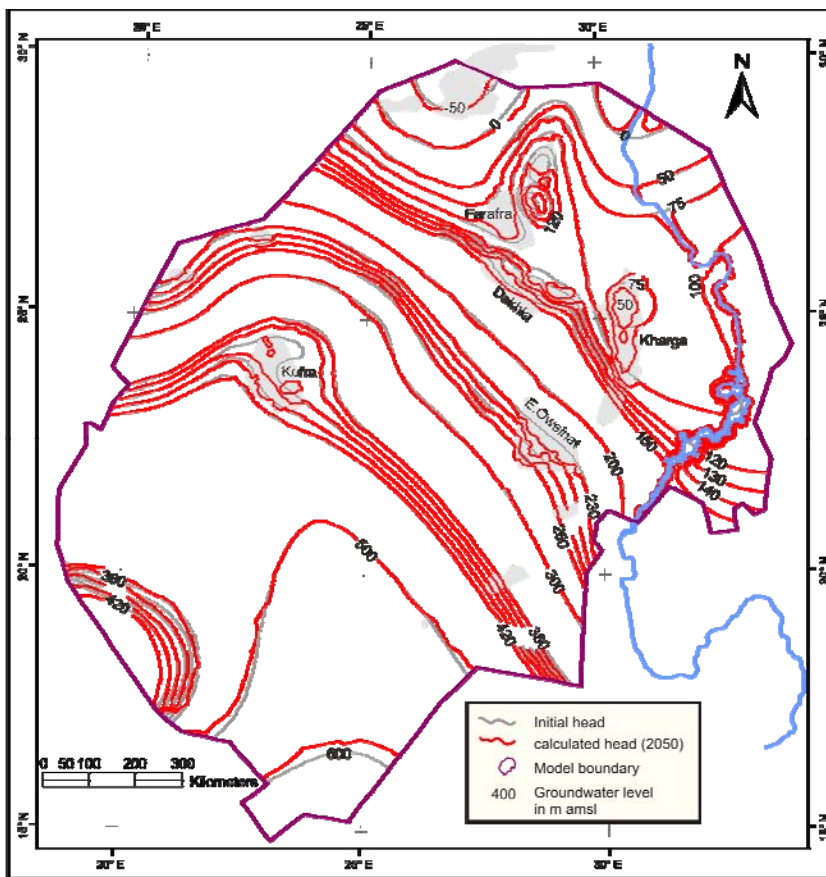


Figure 6.14. Simulated hydraulic head for the lower aquifer of the NSAS by 2050. The extraction rates of scenario 1 are proposed to be constant until 2100.

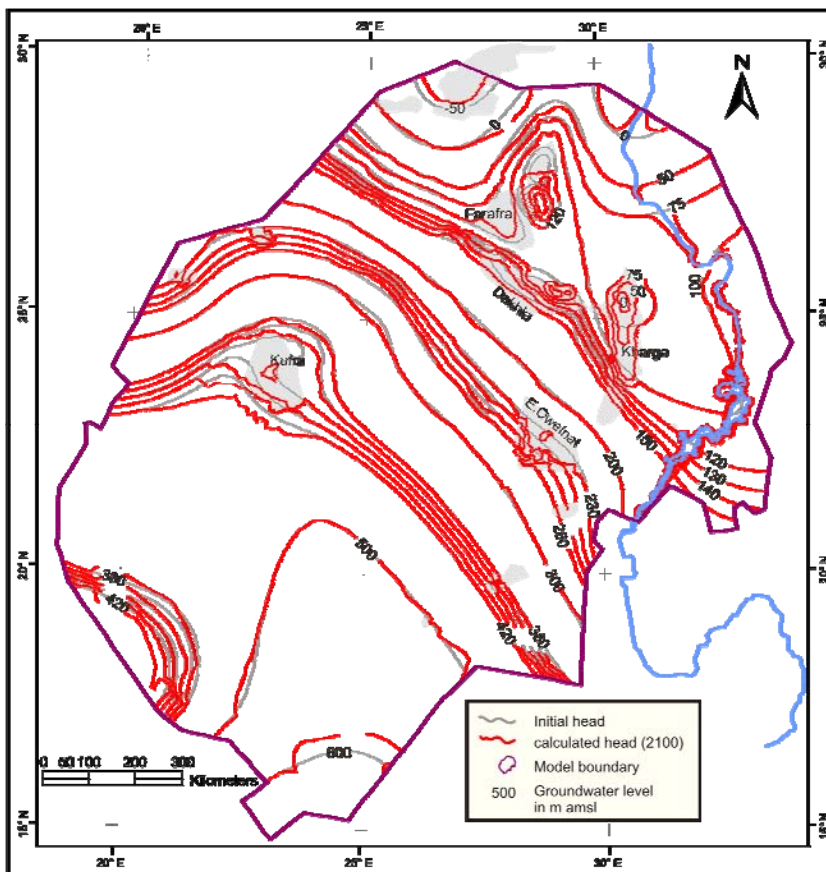


Figure 6.15. Simulated hydraulic head for the lower aquifer of the NSAS by 2100. The extraction rates of scenario 1 are proposed to be constant until 2100.

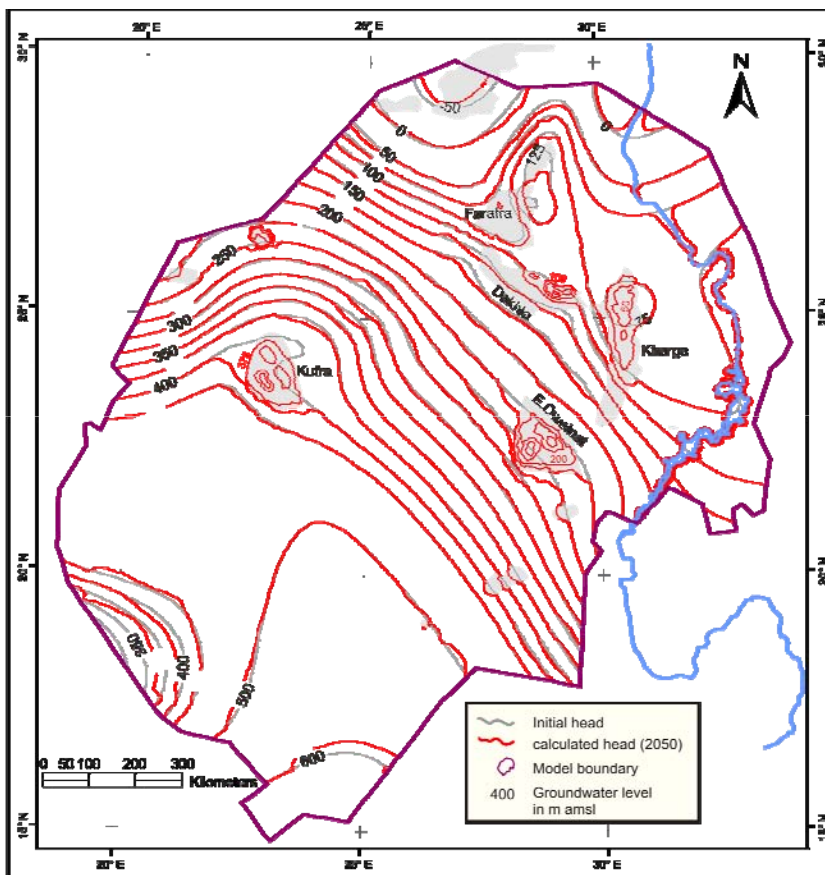


Figure 6.16. Simulated hydraulic head for the lower aquifer of the NSAS by 2050. The extraction rates of scenario 5 are proposed to be constant until 2100. Contour interval 25 m.

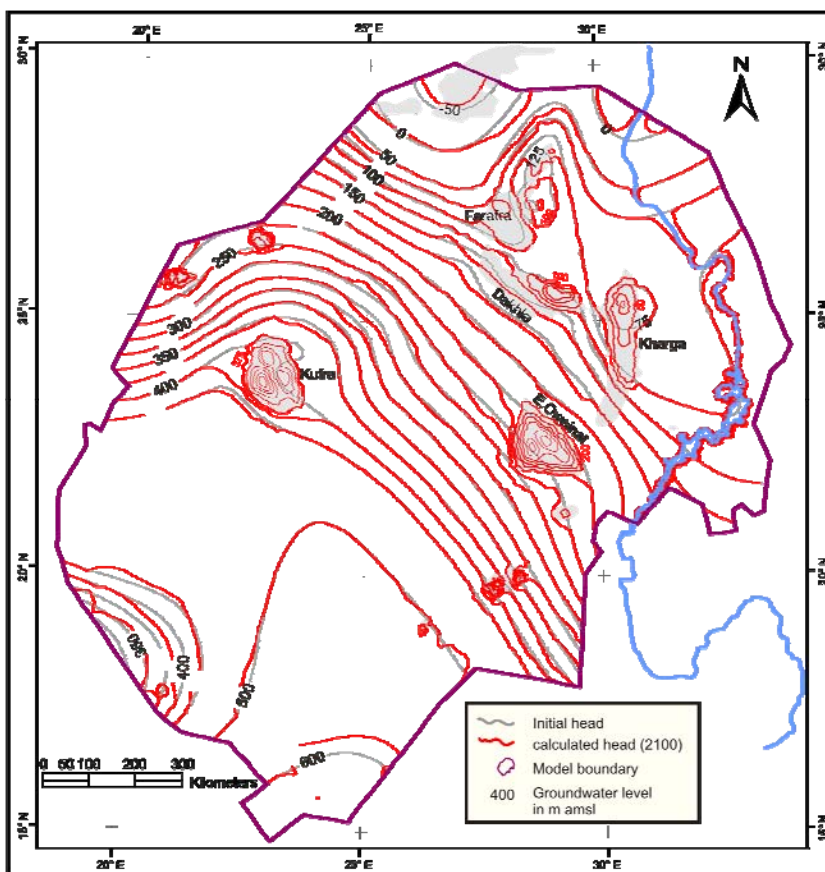


Figure 6.17. Simulated hydraulic head for the lower aquifer of the NSAS by 2100. The extraction rates of scenario 5 are proposed to be constant until 2100. Contour interval 25 m.

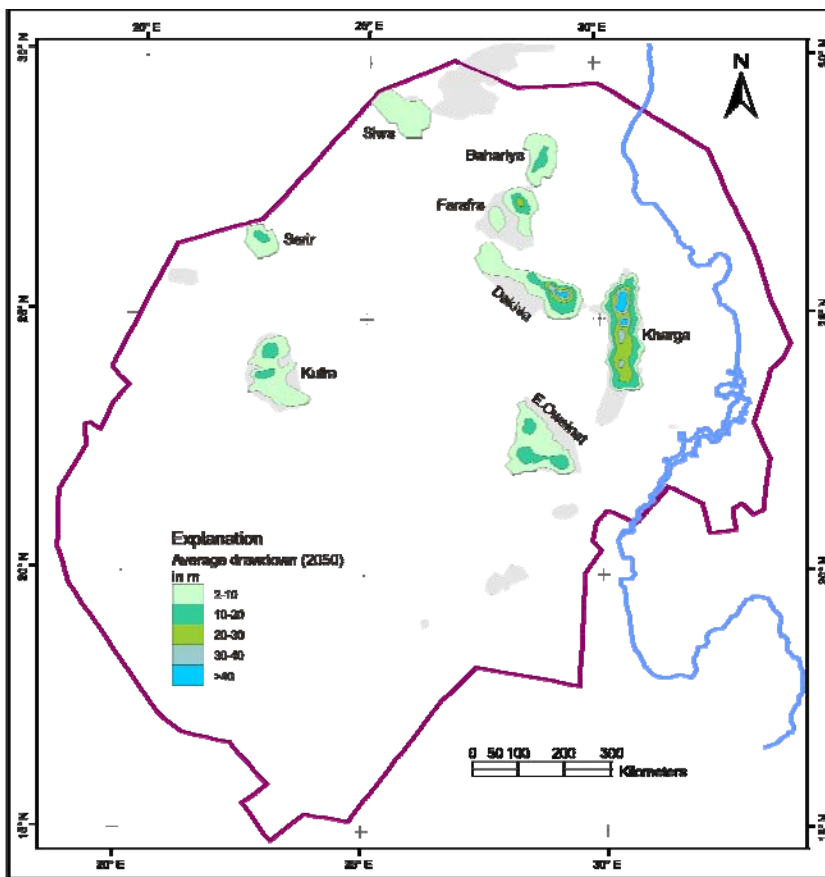


Figure 6.18. Resulting drawdown by 2050 in the NSAS, suggesting the extraction rates of scenario 1 are constant until 2100.

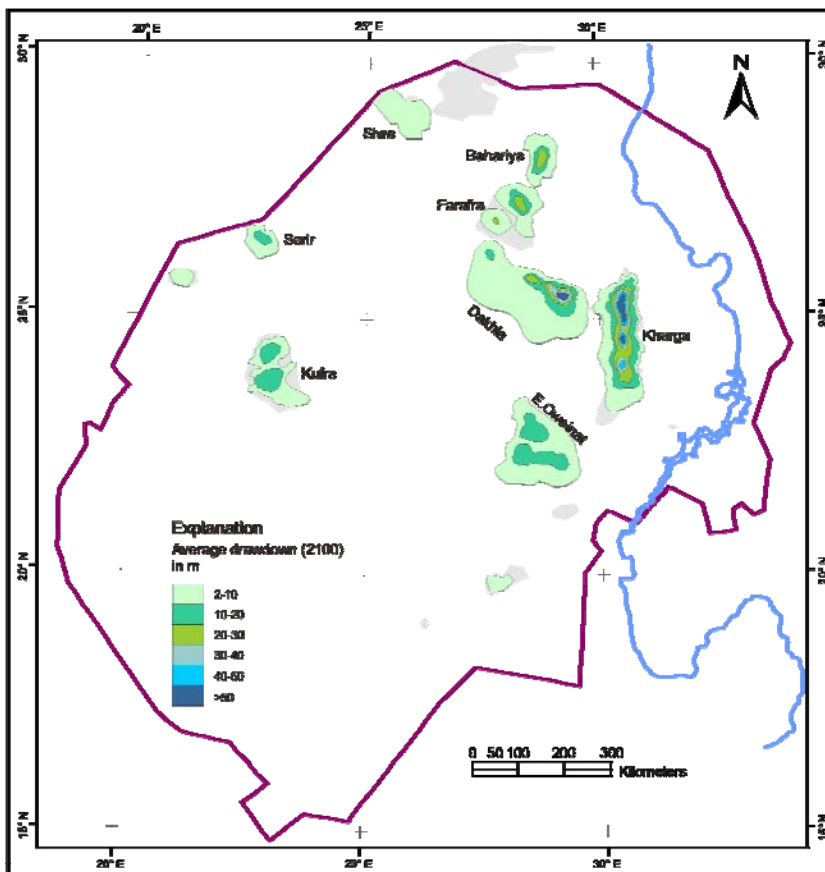


Figure 6.19. Resulting drawdown by 2100 in the NSAS, suggesting the extraction rates of scenario 1 are constant until 2100.

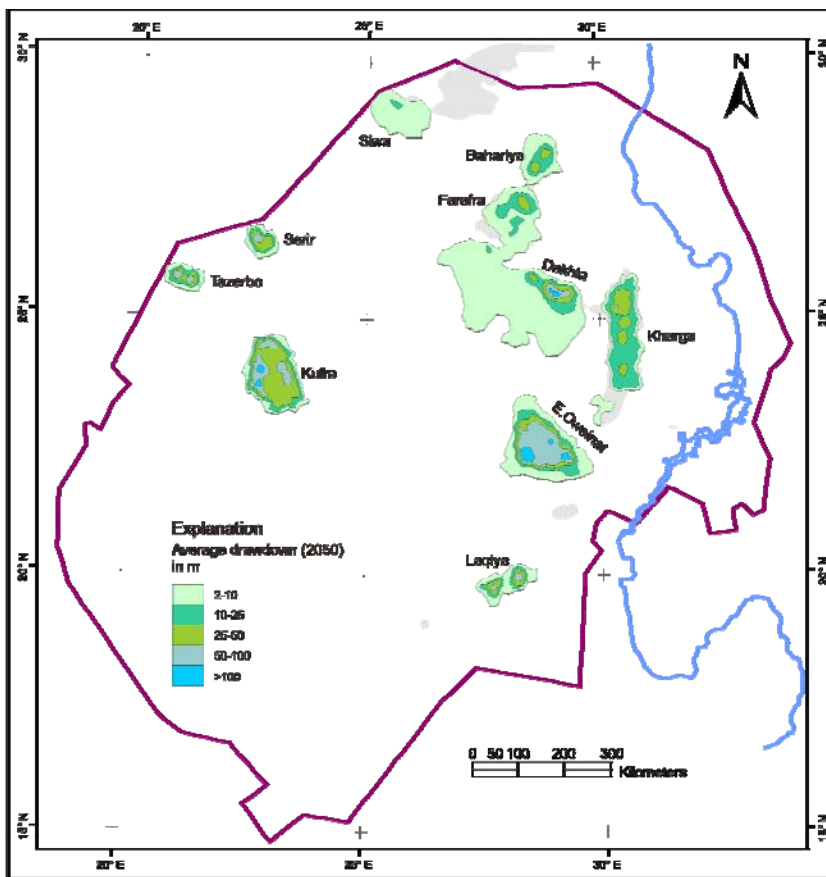


Figure 6.20. Resulting drawdown by 2050 in the NSAS, suggesting the extraction rates of scenario 5 are constant until 2100.

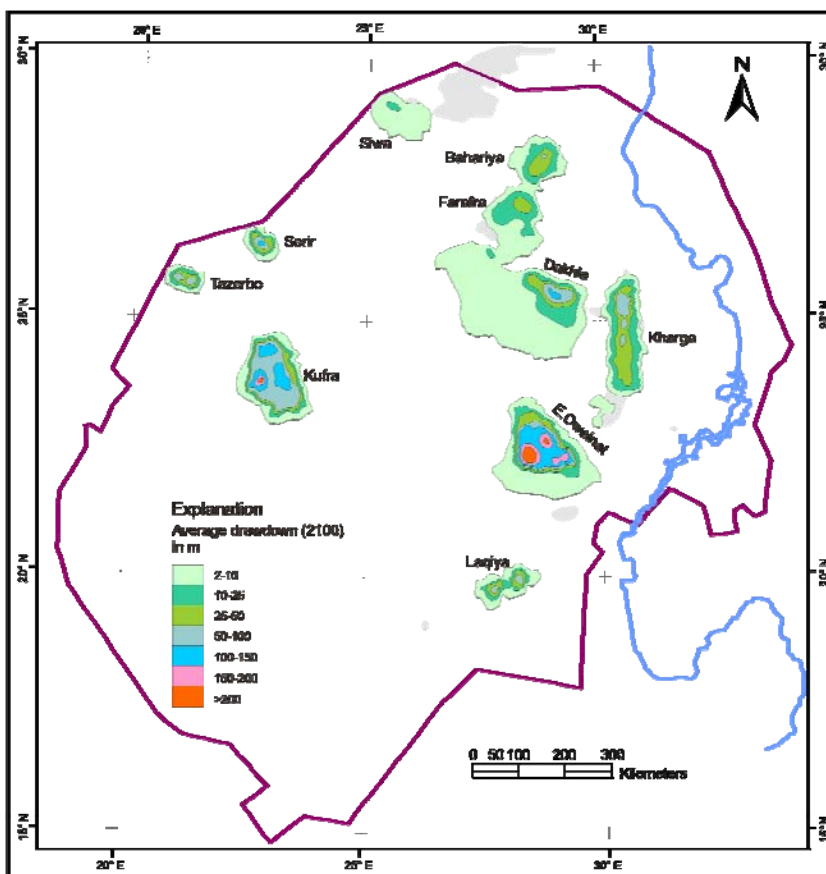


Figure 6.21. Resulting drawdown by 2100 in the NSAS, suggesting the extraction rates of scenario 5 are constant until 2100.

The optimization process of the model for East Oweinat area and Kufra oasis in terms of the abstraction rates shows that scenario 3 (Table 6.3) is the best option for the groundwater management. The average depth to groundwater by 2100 will not exceed 90 m and 85 m for Kufra and East Oweinat, respectively, in this scenario. So it is concluded that scenario 3 is economically the optimal development scenario at these areas.

6.5.4 Groundwater balance

It was proven by referring to the radiocarbon age dating and the stable isotopes that the groundwater in the NSAS is fossil water (age >5,000 years), and no recent formation is detectable. Nonetheless, this does not exclude the possibility of groundwater influx between the adjacent reservoirs within the system. If there is any groundwater supply from the south, this should be attributed to groundwater recharge within and/or surface runoff from a fairly narrow band of rainy, mountainous terrain along the Tibesti-Ennedi-Darfur water divide between northern and central Africa.

A groundwater balance for the NSAS for the period 1960-2100 was calculated using both the actual extraction rates (scenario 1) and the planned extraction rates (scenario 5) for the prediction period to obtain a more general picture of the behavior of the aquifer system to the different anthropogenic activities. The groundwater balance can be expressed as change in storage which equals the sum of the inflow and outflow from the system. The inflow is represented by the limited areal recharge in the south and the influx from the water body of the Nile and Lake Nasser to the aquifer. The outflow is the sum of the natural discharge into and from depressions (seepage, evaporation, and/or evapotranspiration), water outflux to the Nile, and the artificial discharge from pumping wells. Figures 6.22 and 6.23 represent the flow components of the NSAS for scenario 1 and 5, respectively, while Figures 6.24 and 6.25 show the decrease in groundwater volume as a response to the application of the discharge rates of scenario 1 and 5, respectively.

It can be concluded that the annual change in storage is typically contingent on the changes of the extraction rates in both scenarios, except for the very beginning of the simulation, where the extraction rates were relatively small and the change of storage was affected to some extent by the inflow component. For example, in scenario 1 (Figure 6.22) the extraction rate decreases gently to reach about -0.5 km^3 by 1980. In the same case the annual change in storage reaches about 0.3 km^3 after a little swaying from positive to negative values at the very beginning of the simulation. The parallelism between these two components indicates that every additional extraction is groundwater mining.

It is also concluded that during the period from 1960-2005, the total artificial discharge by pumping increased from $0.16 \text{ km}^3/\text{y}$ to $1.8 \text{ km}^3/\text{y}$ (about 1500%), while inflow stayed still almost the same (this is the case if the actual extraction rates are still constant until 2100).

From figure 6.24, it can be seen that the groundwater volume decreased by about 42 km³ by 2000. If the present extraction rates are kept the same, the predicted decrease of groundwater volume will be about 354 km³ by 2100. However, by applying scenario 5, the groundwater volume decreased about 10 times to have a value of 1,491 km³.

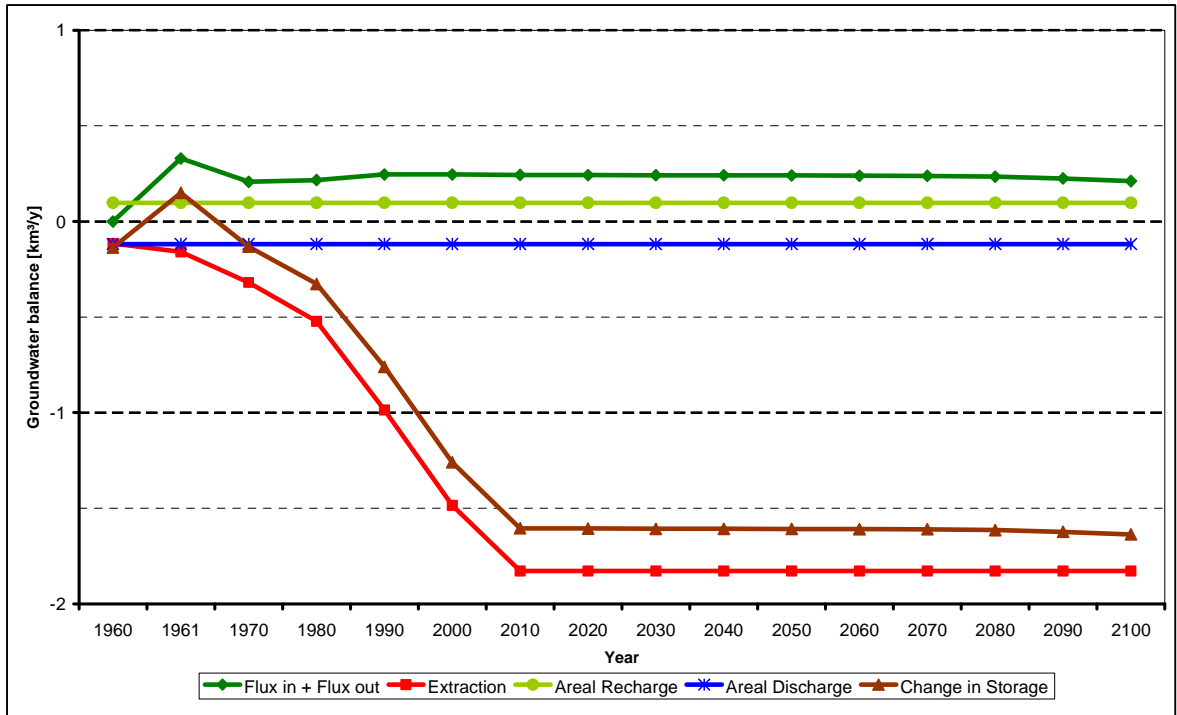


Figure 6.22. Groundwater balance for the NSAS for the period 1960-2100, scenario 1.

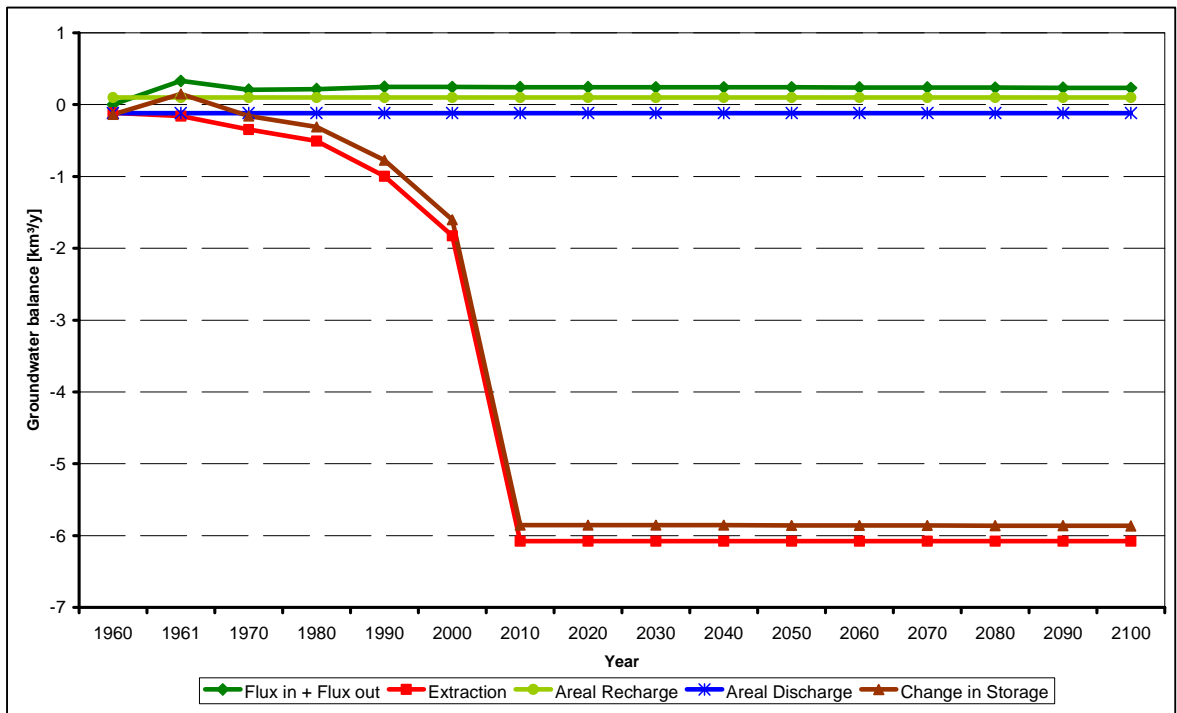


Figure 6.23. Groundwater balance for the NSAS for the period 1960-2100, scenario 5.

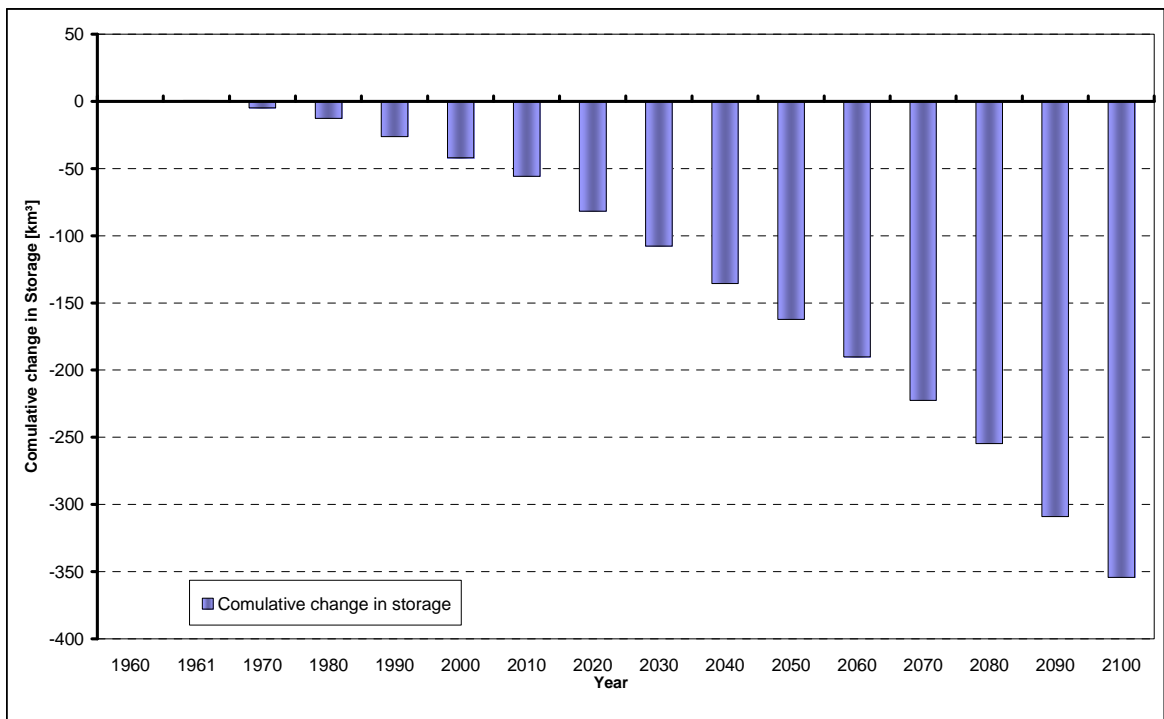


Figure 6.24. Cumulative decrease in groundwater storage of the NSAS for the period 1960-2100, scenario 1.

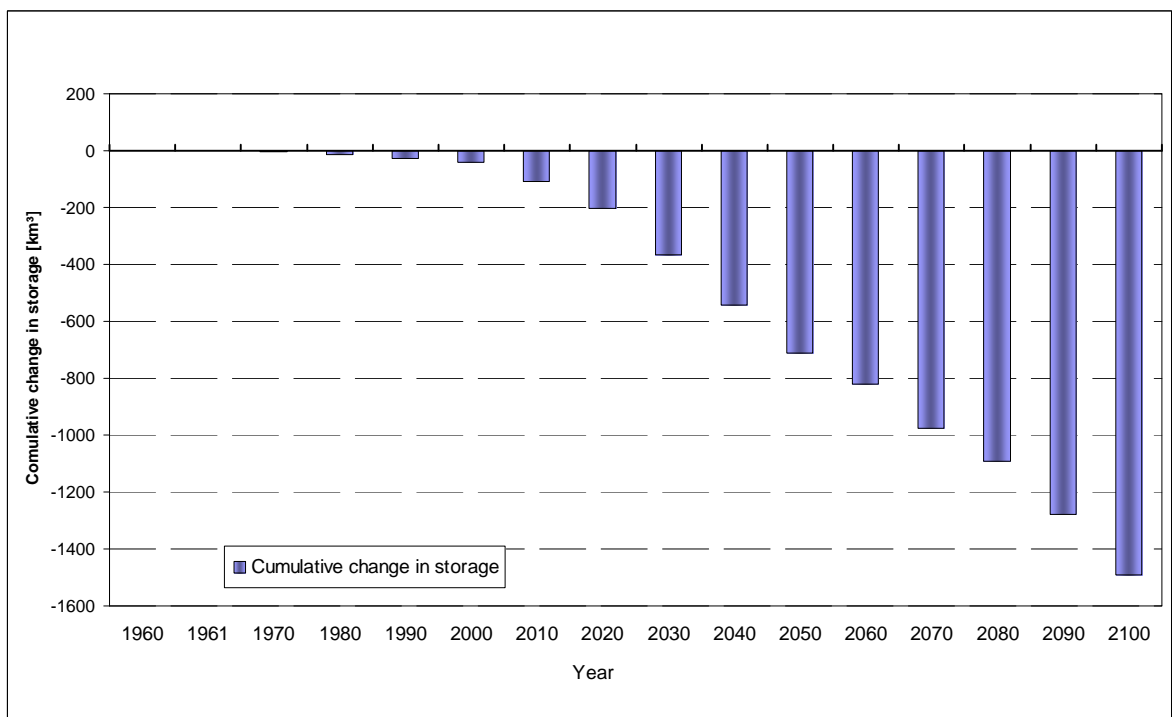


Figure 6.25. Cumulative decrease in groundwater storage of the NSAS for the period 1960-2100, scenario 5.

7

Local Model Dakhla Oasis

7.1 Introduction

The populated areas in Egypt constitute only 6% of Egypt's total area. Some 99% of all Egyptians live in the Nile valley. Therefore, the quickly growing development in Egypt has required big movements of investments and people from the Nile valley towards the Western Desert. In that case, fresh water supply is an essential and feasible option that can cover the wide gap between the available capacities and the accelerating demands.

Geographically, the Western Desert, including the Mediterranean littoral zone and the New Valley, comprises 68% of Egypt's total area. The New Valley consists of three oases, Kharga, Dakhla, and Farafra (Allam et al 2002).

Dakhla is the biggest oasis in the Western Desert and lies farthest away from the main settlements of Egypt with about 75,000 inhabitants (2003 estimate) who live in 17 different settlements. The whole depression of the Dakhla oasis comprises a number of smaller oases, separated by hills or desert, but never far in between. Among the 17 settlements, only Mut and Qasr qualify as towns (Brookes 1993). Villages of Tenieda and Balat dominate the east. Mut, in the middle, is the largest settlement in the oasis with 15,000 inhabitants, while Qasr and Mawhoub are located in the west (Figure 7.1).

Dakhla is situated above sea level, as high as an average of 122 meters. The lowest point of the Dakhla oasis, about 88 m (amsl), lies in West Mawhoub (Figure 7.1), and the oasis' surface rises gradually southeastward. Altitudes range from 110 to 140 m above sea level (Kleindienst et al. 1999).

Originally, Dakhla was fed by about 520 springs and ponds, but in modern times many have dried out, and others only work with electric pumps. The economy of Dakhla is based on agriculture, production of handicrafts, and some tourism. Before the road was constructed, Dakhla must have felt like a planet of its own, where only a few inhabitants ever came as far as the neighboring oases Kharga and Farafra.

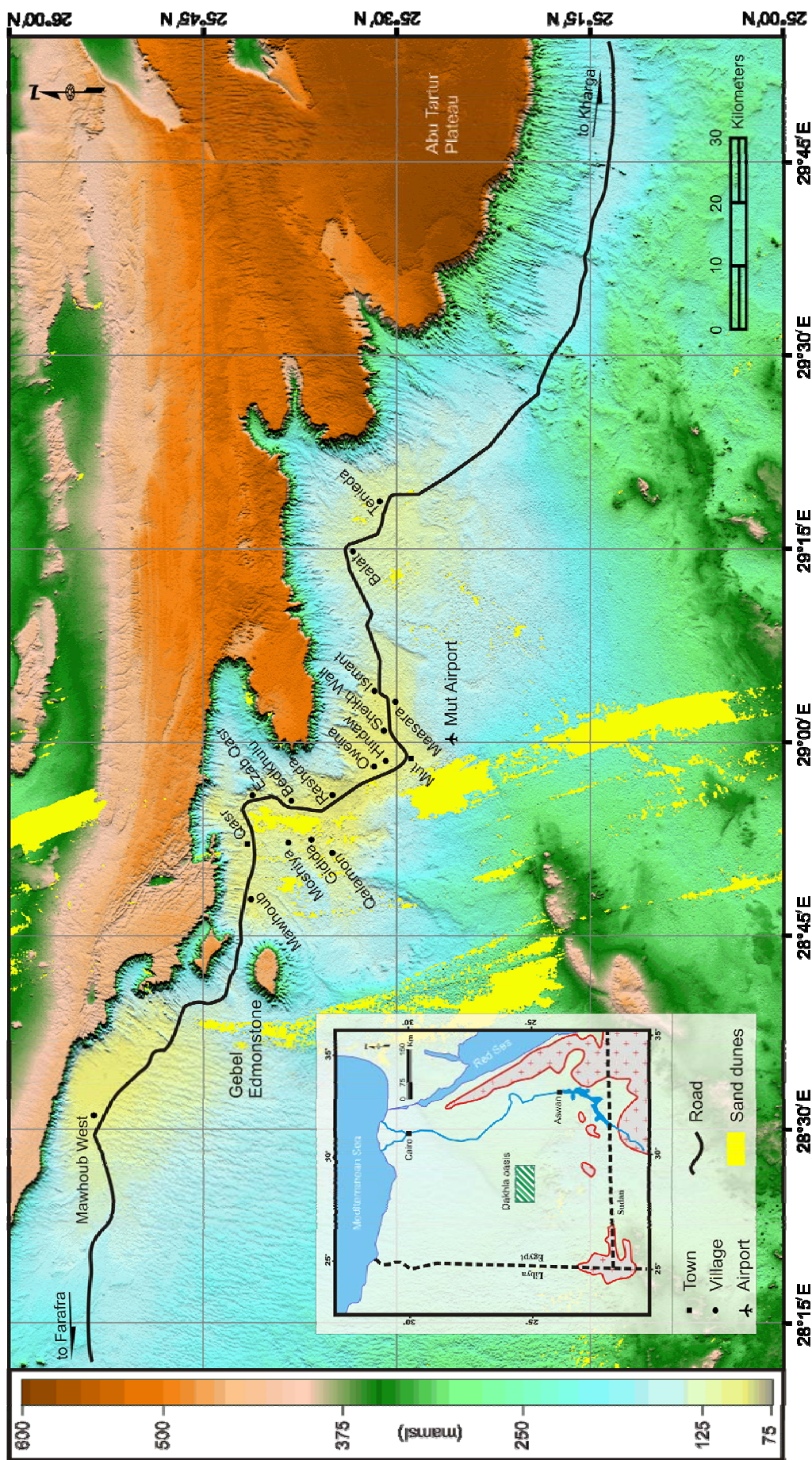


Figure 7.1. Location map of the Dakhla oasis showing the depression, settlements, and topography. The topography is obtained from the DEM of the SRTM-03 (USGS 2004; NASA 2005).

As to climate, the Dakhla oasis belongs to the rainless part of Egypt (Brookes 1993; Kleindiest et al. 1999). The hottest months are June, July, and August (with a mean maximum temperature of 37.7°C). The coldest month is January (with a mean minimum temperature of 4.0°C).

7.2 Locality

The Dakhla oasis is located in the South Western Desert of Egypt, ca. 120 km west of the Kharga oasis, about 300 km west of the Nile valley and about 300 km southeast of Farafra oasis, between longitudes 28°15' - 29°40' E and latitudes 25°00' - 26°00' N (Figure 7.1). Dakhla is connected by a main road with the Farafra oasis 300 km northwest and the Kharga oasis 190 km east. The oasis is about 155 km long from southeast to northwest, with a maximum width of about 60 km.

7.3 Geomorphological background

The topography and geology of the New Valley in general and the Dakhla oasis in particular has been a subject of different studies (e.g., Beadnel (1905), Mitwally (1953), Hermina et al. (1961), Said (1961), Awad and Ghobrial (1965), Hermina (1967), Mansour (1973), Ezzat (1975,1976), El-Younsy (1978, 1984), Klitzsch et al. (1987), Hermina (1990), Brookes (1993), and Wycisk (1993)). A brief discussion is given below.

The main topographic feature of the Dakhla oasis is the steep scarp, which bounds and overlooks the depression of the oasis on its northern side. It is irregular in its outline, but generally it extends in a WNW-ESE direction for more than 250 km. It is broken into a number of promontories by well-marked indentations, the most important of which occur to the east of Qasr, northeast of Balat, and to the east of Tenieda. A gradual slope is formed up to the plateau at these indentations (El Younsy 1984). The face of the scarp is essentially composed of Upper Cretaceous to Paleocene shale and mudstone and is generally capped by limestone and chalky limestone. The height of this scarp ranges from 400 m (amsl) to the west and rises gradually to reach about 580 m (amsl) northeast of Tenieda village (Figure 7.1).

The depression of the oasis extends from Tenieda in the east to Mawhoub West in the west. It is excavated in the Nubian red clays. The depression is represented by an immense plain, which extends from the Kharga oasis in the east to the farthest west of the Dakhla oasis and is still opened to the south and southwest, where its floor gradually merges southward into the Nubian Sandstone higher plain (Brookes 1993). The plain has a floor that consists mainly of red clays related to Quseir Shale-Formation (refer to section 7.4) and covered in some localities by alluvium deposits, which are partially cultivated (El-

younsy, 1984). Sand dunes frequently cover the scarp face in various localities, as well as areas in the depression of the oasis. The major sand dunes form a north-northwest/south-southeast trend extending to the west of Qaret El-Mawhoub (Edmonstone). Gebel Edmonstone is a single isolated hill in the whole depression of Dakhla. It is a detached portion (or an outlier) of the plateau and occurs about 18 km west of Qasr. This conspicuous hill has a height of about 465 m (amsl) and about 300 m above the depression plain (Brookes 1993).

7.4 Geological background

Commonly, the successive sedimentary formations within the Dakhla depression dip steadily northward at a very small inclination. Consequently, every formation has a wide outcrop. In general, these formations crop out at the cliff to the north of the depression and they do not appear in the oasis depression itself (Ezzat 1976). The late Mesozoic-Early Cenozoic rocks, which build the primary sedimentary cover in the area under discussion, are subdivided into a number of mappable lithostratigraphic units. The units are classified generally into two categories: (a) a Jurassic-Campanian sequence, predominantly continental but with marine intercalations, and (b) a Campanian-Lower Eocene transgressive-regressive open marine sequence. A summary of the depositional history in the Dakhla oasis is given below as discussed in Hermina (1990).

(a) Jurassic-Campanian sequence

The Jurassic-Campanian sequence includes the predominantly continental sandstone and clay beds that were formerly lumped under the term “Nubia”. These are from base to top: The Six Hills Formation (Late Jurassic-Lower Cretaceous), the marine shale of Abu Ballas Formation (Aptian), Sabaya Formation (Albian-Early Cenomanian), the marine claystone of Maghrabi Formation (Cenomanian) and Taref Formation (Early Turonian) (El Nagggar 1970; Barthel and Boettcher 1978; Barthel and Hermann-Degen 1981).

(b) The Campanian Transgression

The sequence from base to top is described in brief as follow:

- *Quseir Formation = Mut Formation (Youssef 1957)*. It is composed of variegated shale, siltstone, claystone, and flaggy sandstone containing freshwater gastropods and plant remains. It covers extensive areas in the Dakhla depression and participates as well, with varying thickness, in the formation of the foothills of the bordering scarp. The Quseir Formation forms the floor of the excavated depression (Hermina et al. 1961).
- *Dawi Formation = Phosphate Formation (Awad and Ghobrial 1965)*. The Dawi Formation is a phosphate-bearing unit alternating with black shale and limestone.
- *Dakhla Formation (Said 1961)*. The Dakhla Formation consists of dark-grey shale, marl, and clay with intercalations of calcareous sandy and silty beds along the scarp face; it also covers parts of the plain in the west of Dakhla. The total thickness at the type section north of Mut town is about 230 m.

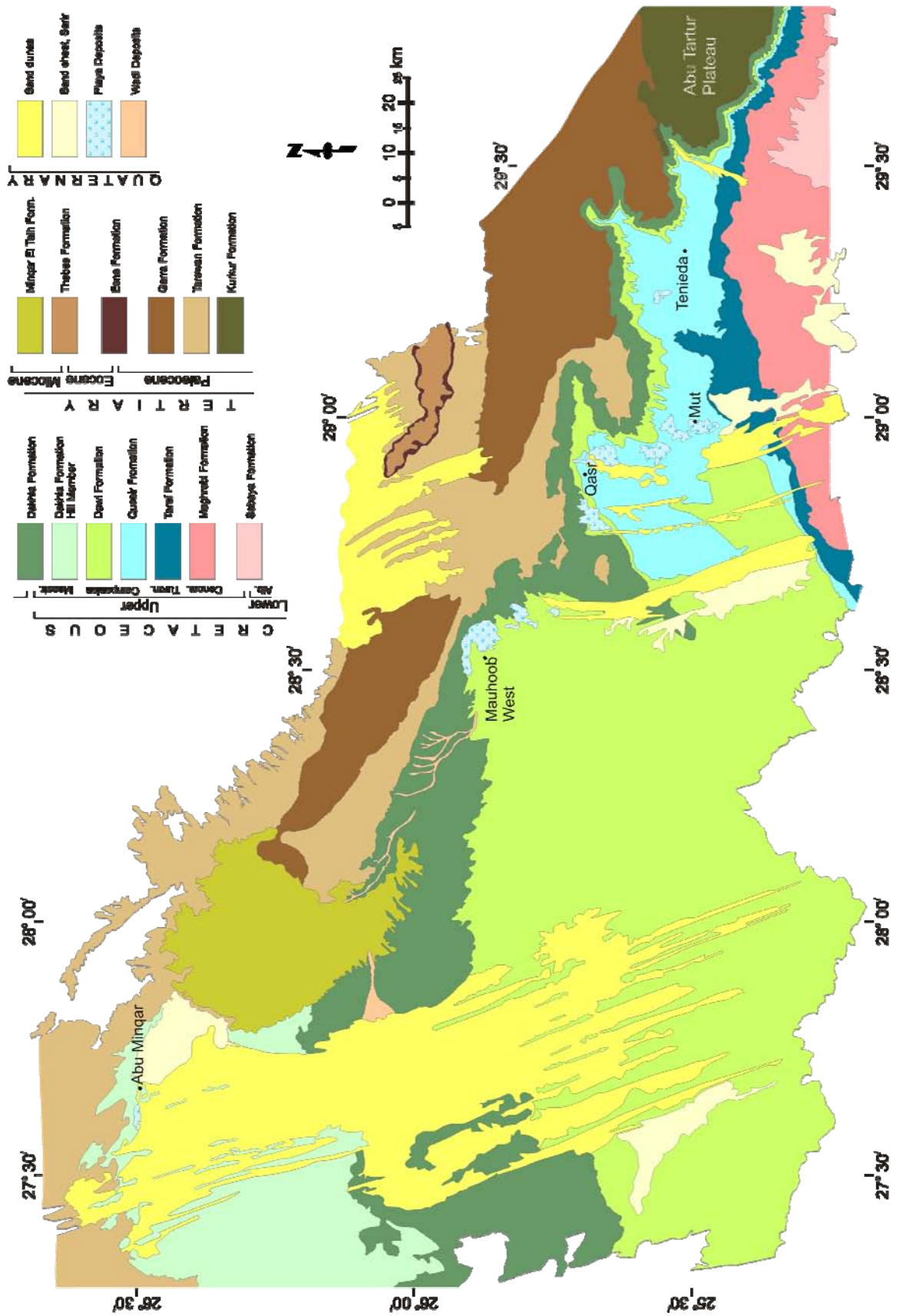


Figure 7.2. Geological map of the Dakhla oasis. Digitized from Conoco (1989), lithostratigraphic units adapted from El Khawaga et al. (2005).

- *Kurkur Formation (Issawi 1969)*. It is formed by successions of marl, marly limestone, and dolomite laterally replacing the upper part of the Dakhla Formation. It forms the top of the scarp; it gradually decreases in thickness and disappears in the sections to the northwest of Mut.
- *Tarawan Formation (Awad and Ghobrial 1965)*. It consists of fossiliferous, partly marly, or chalky, yellowish white limestone grading into limestone, impure limestone, or dolomite.
- *Garra Formation (Issawi 1969)*. White, thick-bedded, partly chalky limestone beds make up Garra Formation.
- *Esna Formation (Said 1960)*. It is composed of greenish-grey open marine shale with allochthonous calcareous intercalations becoming more common towards the top.
- *Thebes group (Said 1962)*. The Thebes group is composed of brown limestone with shale interbeds laterally grading into greenish-white limestone with chert.
- *Minqar El Talh Formation (Hermina and Lindenberg 1989)*. This is a light colored continental to lacustrine sandstone with root marks and yellow siltstone capped by platy lacustrine limestone.

The Quaternary sediments are represented by the significant aeolian accumulations that occur in the depression. The playas in the area under discussion are found in the area between Tenieda and west of Mawhoub. The lacustrine playa deposits are made up of horizontal alternating bands of soft, friable sand, clay and silt with plant remains. Salt crusts resulting from capillary rising groundwater build up 10-20 cm thick layers and in some places intercalate the lacustrine deposits (Embabi 1982; Maxwell 1982; Kroepelin 1990; Pachur 1999).

7.5 Water quality

The salinity of groundwater of the NSAS in Egypt changes both horizontally and vertically. The salinity of water increases from SW to NE as well as the hydraulic gradient and usually decreases with depth: e.g., the Kharga and Dakhla oases, where the salinity decreases from about 500 ppm in the upper aquifer to about 200 ppm in the lower one (Dahab 1998; Allam et al. 2002).

Generally, the groundwater of the Nubian series of the Dakhla oasis is mainly fresh. The groundwater temperature ranges between 27 °C and 38 °C, depending on the depth. The TDS (Total Dissolved Solids) of the groundwater in most parts of the Dakhla area is fairly less than 500 ppm, representing great differences in salinity from one place to another (Idris and Nour 1990; Dahab 1998). It can be concluded that the water in general is marked by low salinity in the eastern part of the oasis, where the TDS has an average of 150 ppm: e.g., in Tenieda and Balat (two villages existing to the farthest east of the oasis (refer to

Figure 7.1). However, the salinity increases westward until it reaches its maximum values in Mut, Hindaw, and Rashda (average value is 2,000 ppm) (Diab 1972; Soltan 1997). The ion content of the groundwater of the Dakhla oasis ranges from low to high depending on the area.

The electrical conductivity (EC) exposes enormous values, especially in the west of the oasis. On the contrary, in the east of the oasis, moderate EC values are dominating. The EC ranges from 133.3 $\mu\text{S}/\text{cm}$ in the eastern part of the oasis to a highest value of 7,000 $\mu\text{S}/\text{cm}$ in some parts to the western area of the oasis (Dahab 1998). Hard water is the dominant feature of water within the Dakhla oasis, where the total hardness of most localities exceeds 150 mg/l, so water is designated as hard (maximum permissible limits are set according to the World Health Organization, WHO, European Standards, 1984). These relatively high values of TDS and EC are related mainly to the occurrence of playa deposits and salt crusts in the middle and west of the oasis.

7.6 Model input and structure

As discussed in Chapter 6, a regional groundwater flow model for the whole NSAS was developed and calibrated to help correctly define the boundary conditions of the area of interest as well as to serve as a base model for the local modeling approach. Consequently, the data input is also valid and further used for the local modeling with some additional adjustments and refinement for the Dakhla area according to the locations of the pumping wells. This approach allowed precise analysis of the pumping and the resulting drawdown in the Dakhla oasis during the simulation period 1960-2100.

There are 523 private and/or shallow wells and 313 deep wells extracting the upper and lower aquifers, respectively, in the Dakhla oasis. These wells are entered into the model based on their horizontal and vertical coordinates. For the wells that numerically overlap (when they are too close to each other) or fall in the same numerical cell, their extraction rates are summed up and gathered to one pumping center. If a certain well is tapping both the shallow and the deep aquifer, then it is divided into two numerical wells at the same node. The actual extraction rates are given to the model for scenario 1 (refer to section 6.2.5.3) and the extraction rates from the other scenarios are shared out on the wells proportionally. Figure 7.3 illustrates the horizontal distribution of the pumping wells/pumping centers within the Dakhla oasis; on the other hand, Figure 7.4 represents simplified cross sections for selected locations in the area.

7.7 Model output

The local prediction simulation was used to evaluate five possible future development plans for the NSAS in the Dakhla oasis in an attempt to explore the hydrologic feasibility of these plans and the sustainability of the aquifer under each extraction scheme.

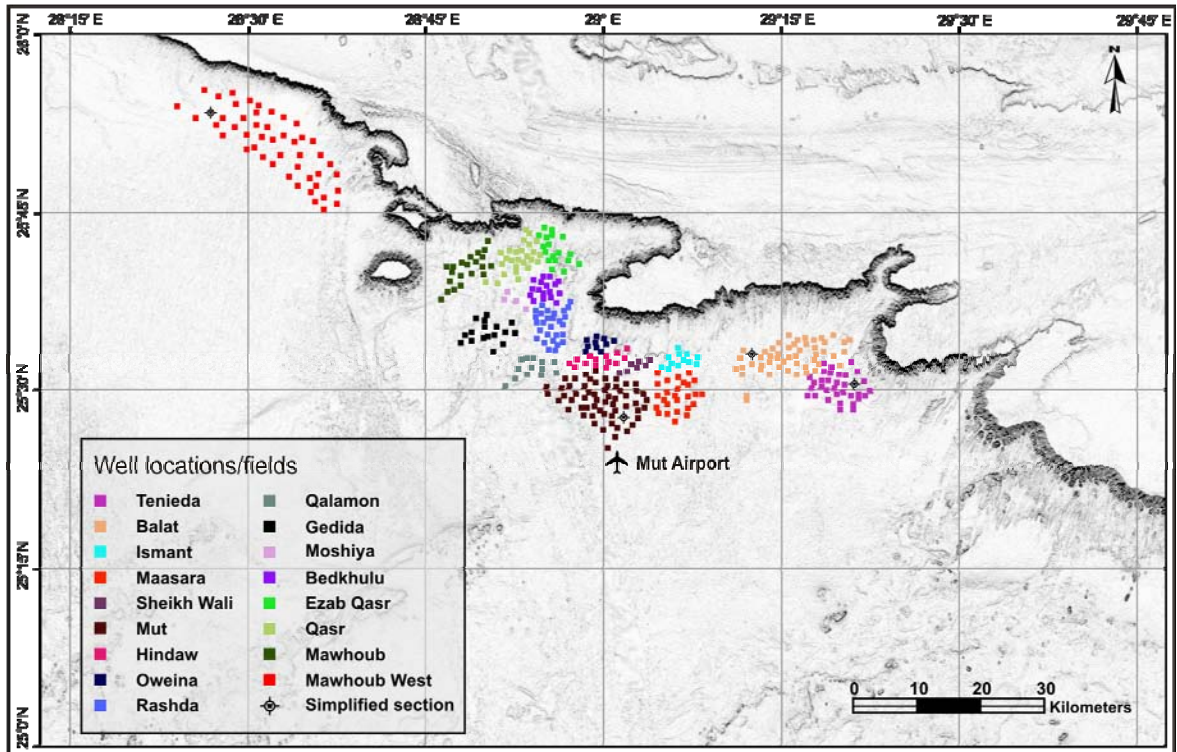


Figure 7.3. Location map of the Dakhla oasis showing the distribution of pumping-well fields and locations of wells of the simplified cross sections.

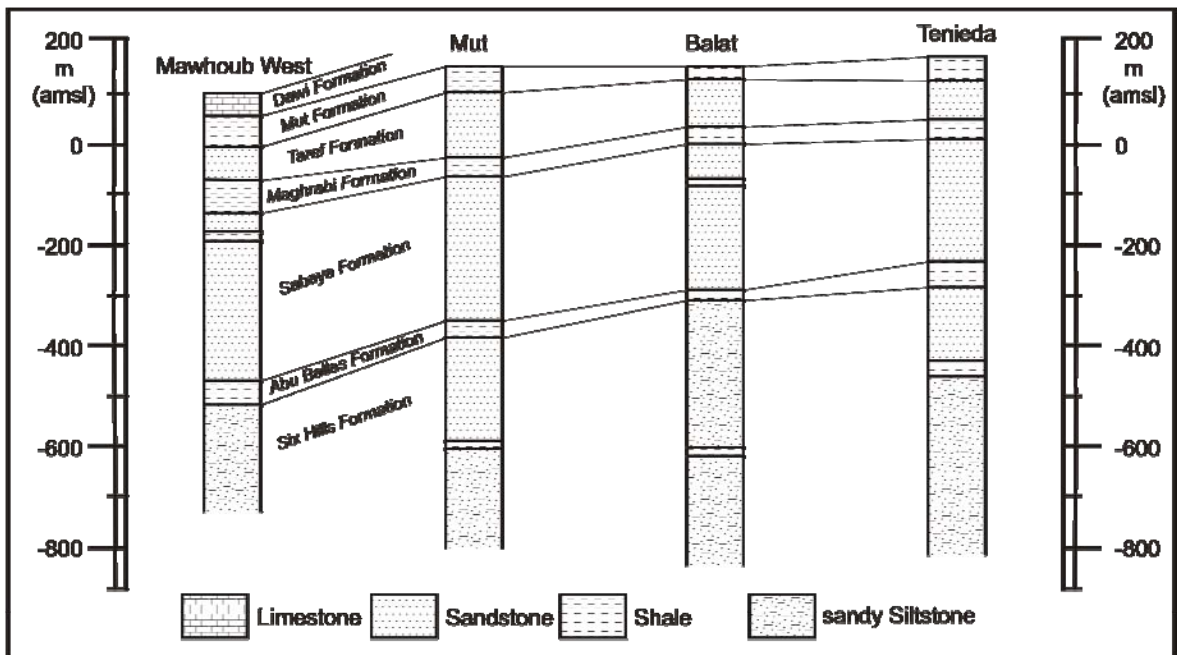


Figure 7.4. Simplified cross sections of selected locations in the east, middle and west of the Dakhla oasis based on the well logs (modified after Sefelnasr 2002).

The prediction period extended from year 2005 to 2100. The assumed groundwater extraction rates for each scheme are presented in Table 6.1 and Appendix B1.

7.7.1 Scenario 1

In this scenario the actual extraction rates of 1.2×10^6 m³/d for the Dakhla oasis (Table 6.1 and Appendix B.1) are considered constant during the prediction simulation. As can be seen from the initial hydraulic head (Figure 7.5), the original groundwater flow direction in the Dakhla oasis was generally from southwest to northeast and followed the regional trend of groundwater flow direction in the whole NSAS. This general trend is still roughly kept by year 2005. However, cones of depression (COD) have appeared just around the well fields of Tenieda, Balat, Mut, Qasr, and Mawhoub West (the east, middle, and west of the oasis). This change in the flow direction is obviously noticed from the 120-m contour line of hydraulic head. It shows that the flow direction changes and new locally closed contour lines with lower head values of 110 and 100 m appear around the well fields (Figure 7.5).

These changes in the hydraulic head pattern will be further developed by year 2050 and 2100, as the hydraulic gradient changed from 4.6×10^{-4} by year 2005 to 2.0×10^{-3} by year 2100 in the middle of the oasis, which induces the COD to be wider and deeper with time (Figures 7.6 and 7.7). The COD are centered on the well fields (around major population communities), forming an elongated shape from northwest to southeast following the general depression trend of Dakhla oasis. By year 2005, the 3 m drawdown line lies about 30 km away from centers of the COD. The major decline in potentiometric surface is observed around the well fields of Tenieda, Balat, and Mut, where the drawdown reaches 35 m at the center of the COD. Nevertheless, it is only about 12 m at Mawhoub West. This indicates that the groundwater potentiality in the Dakhla oasis is rather good at the eastern side of the oasis and gets obviously better westward, especially at the area of Mawhoub West.

Further simulation shows the decline of potentiometric surface increases to reach 50 m at the east of the oasis, 60 m at the middle, and 20 m in the west by 2050 (Figure 7.9). The COD developed further by 2100 to overtake the oasis boundaries. The maximum drawdown of 75 m is recorded at Maasara village, whereas the 50 m COD covers the whole east and middle of the oasis from Tenieda village to Qasr city (Figure 7.10). With an average drawdown of 55 m for the oasis, the average annual change in hydraulic head of the entire simulation period would be 0.57 m per year. Most of the wells in the middle and west of the oasis were still flowing by year 2005 (Figure 7.11). This case changes completely at the end of the simulation, as only a few wells in Mawhoub west will still be flowing and the rest will dry out (Figure 7.12).

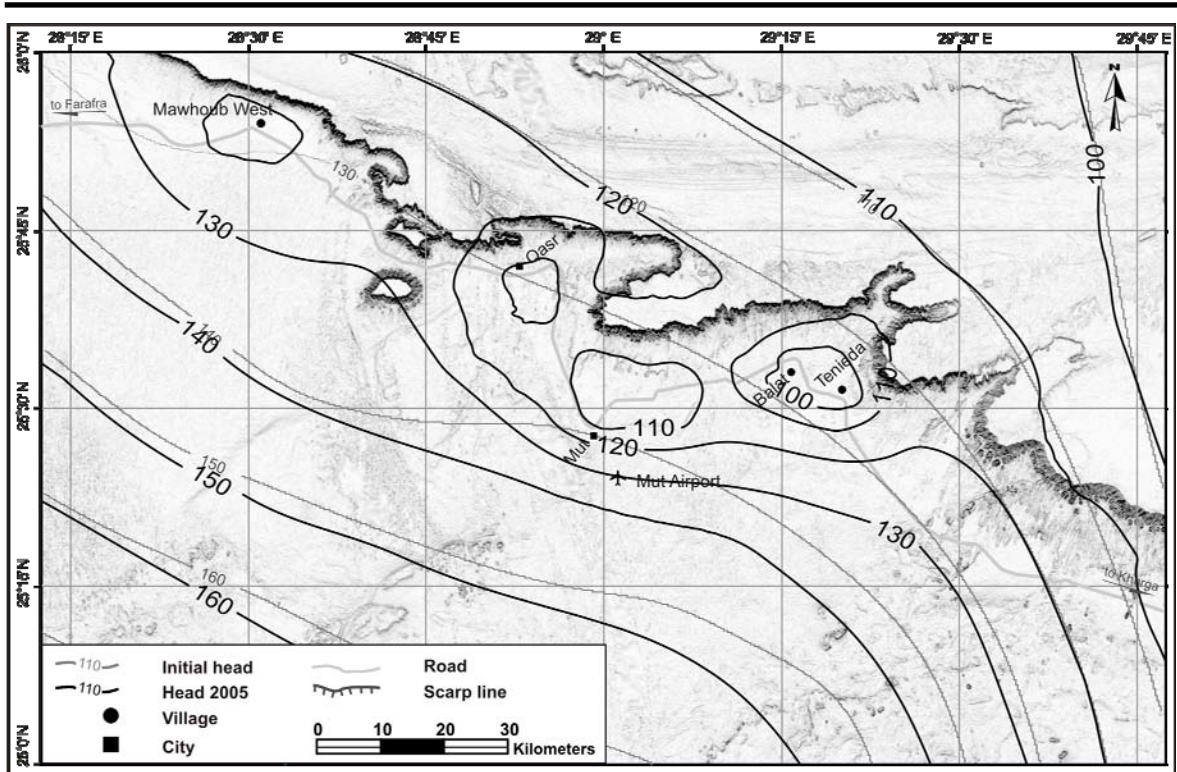


Figure 7.5. Simulated hydraulic head m (amsl) for the NSAS in the Dakhla oasis 2005.

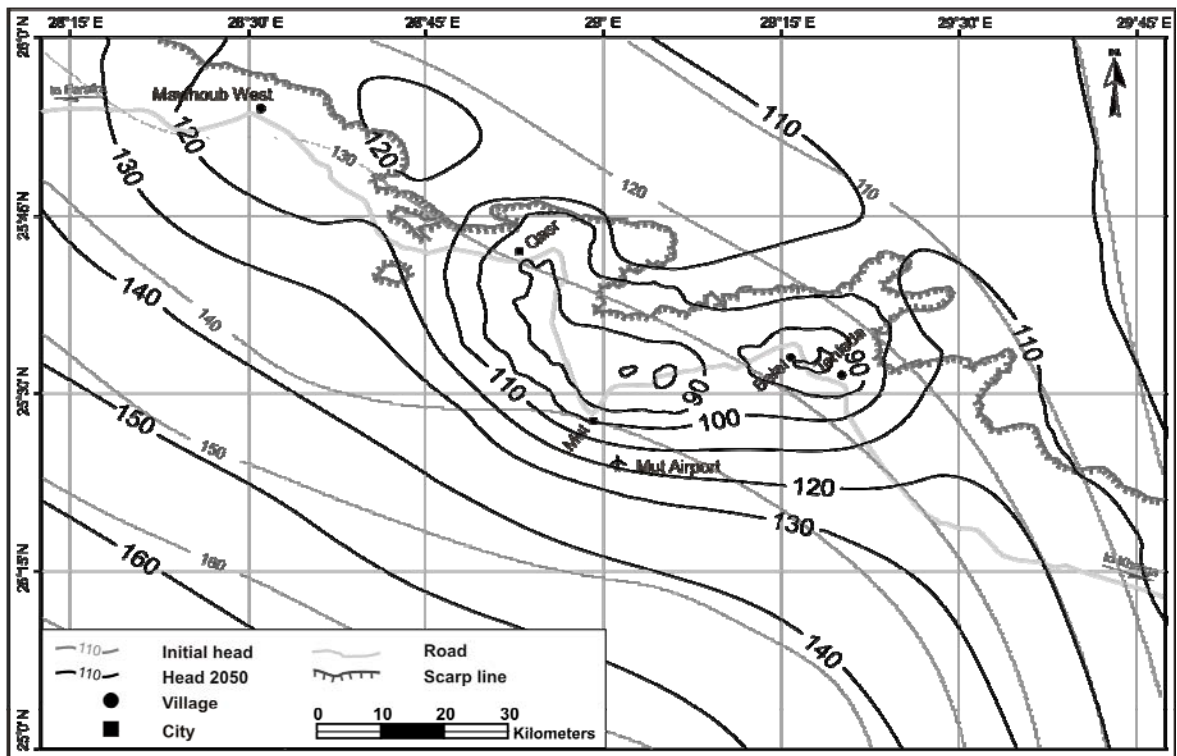


Figure 7.6. Simulated hydraulic head m (amsl) for the NSAS in the Dakhla oasis 2050, scenario 1.

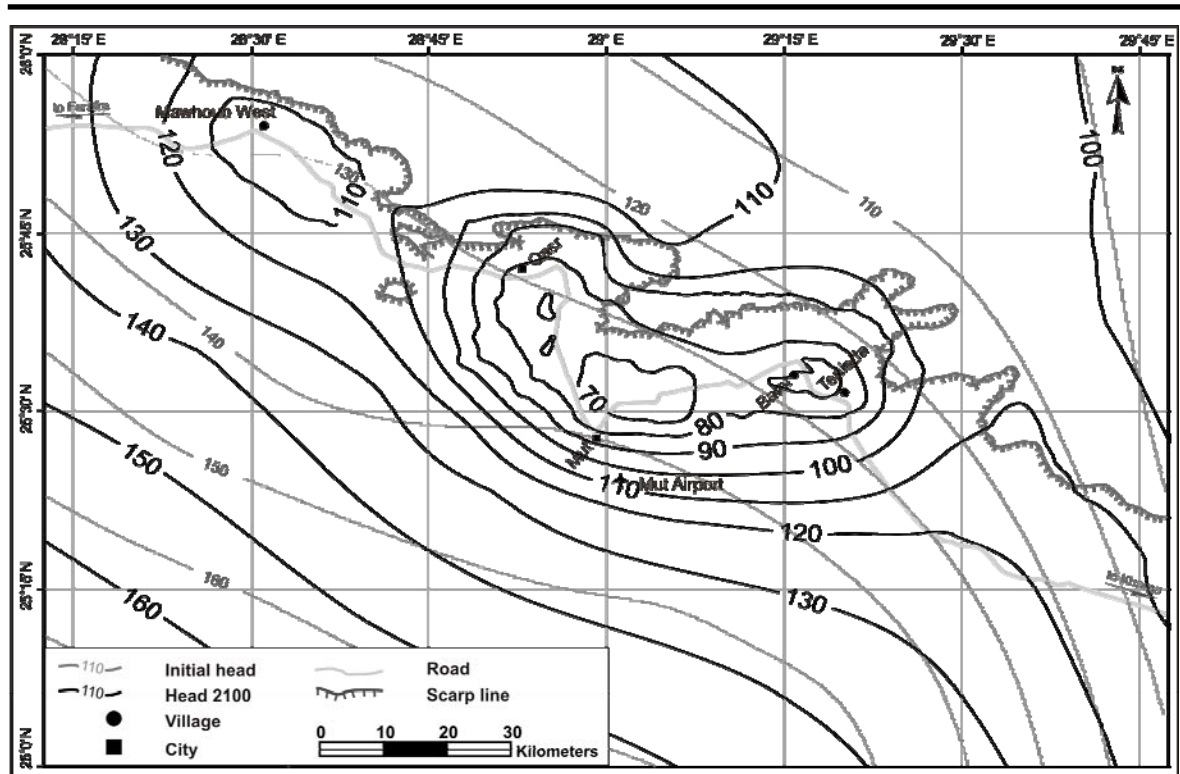


Figure 7.7. Simulated hydraulic head m (amsl) for the NSAS in the Dakhla oasis 2100, scenario 1.

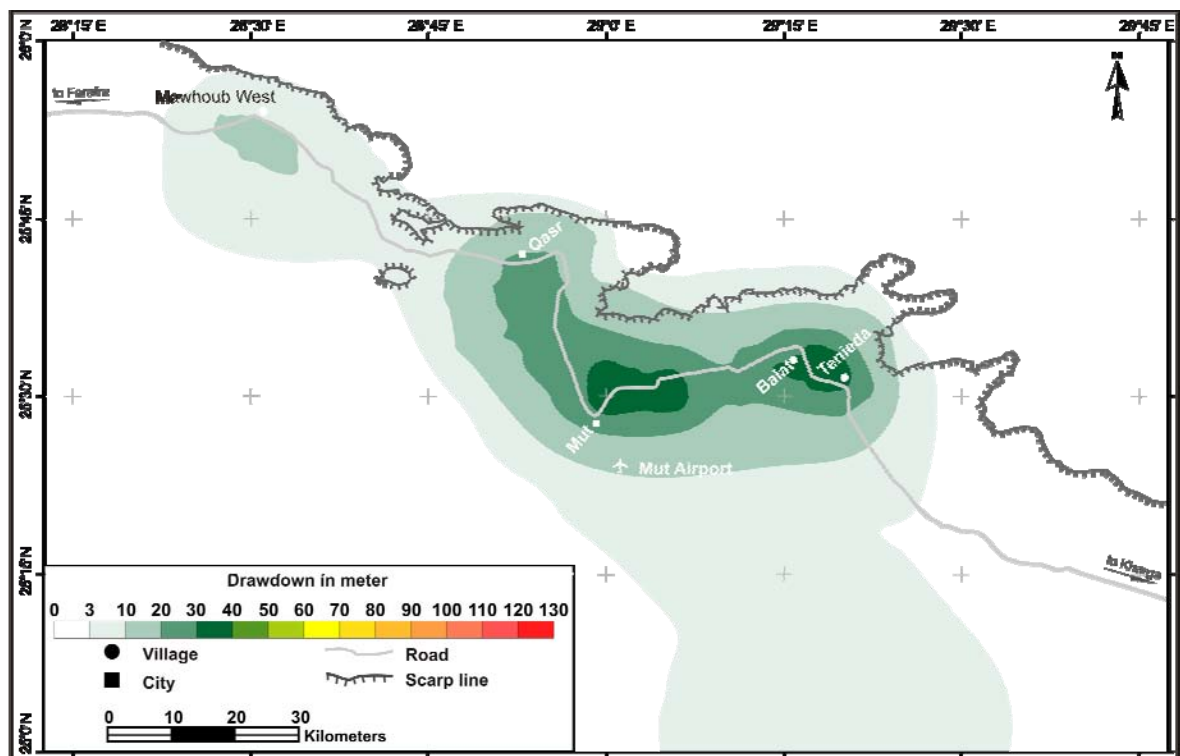


Figure 7.8. Simulated decline in potentiometric surface for the NSAS in the Dakhla oasis by 2005.

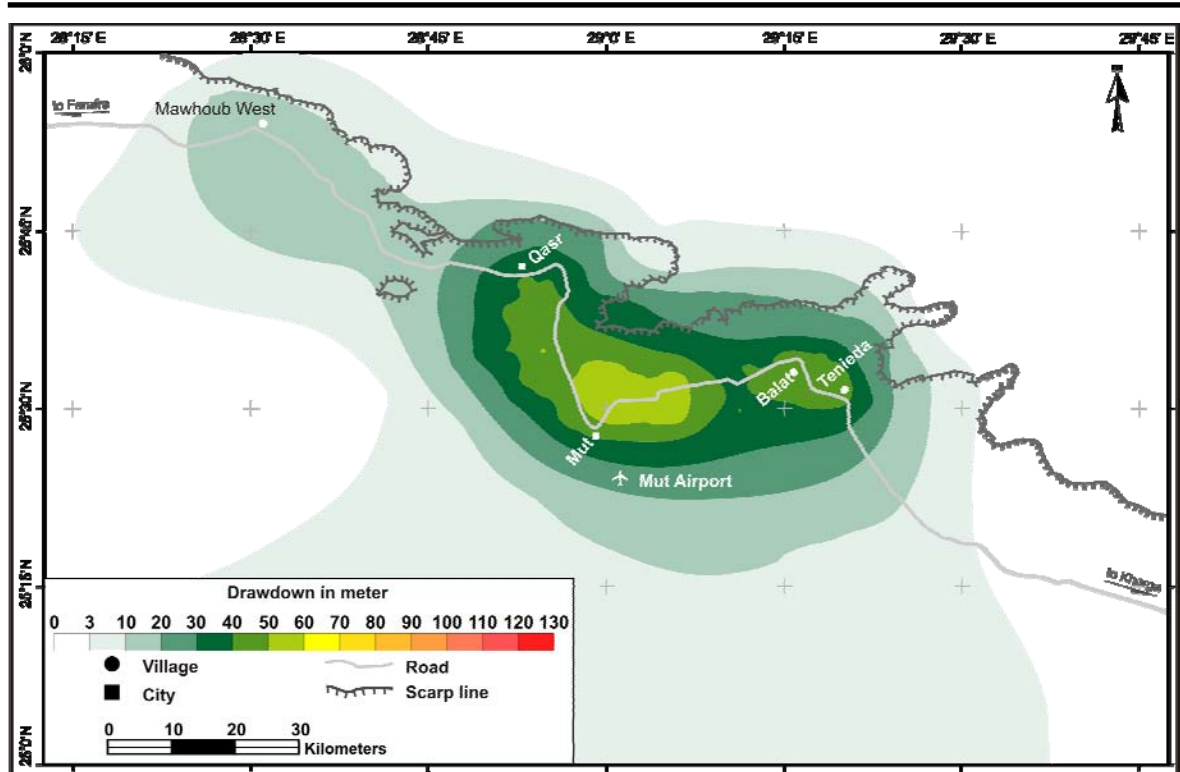


Figure 7.9. Simulated decline in potentiometric surface for the NSAS in the Dakhla oasis by 2050, scenario 1.

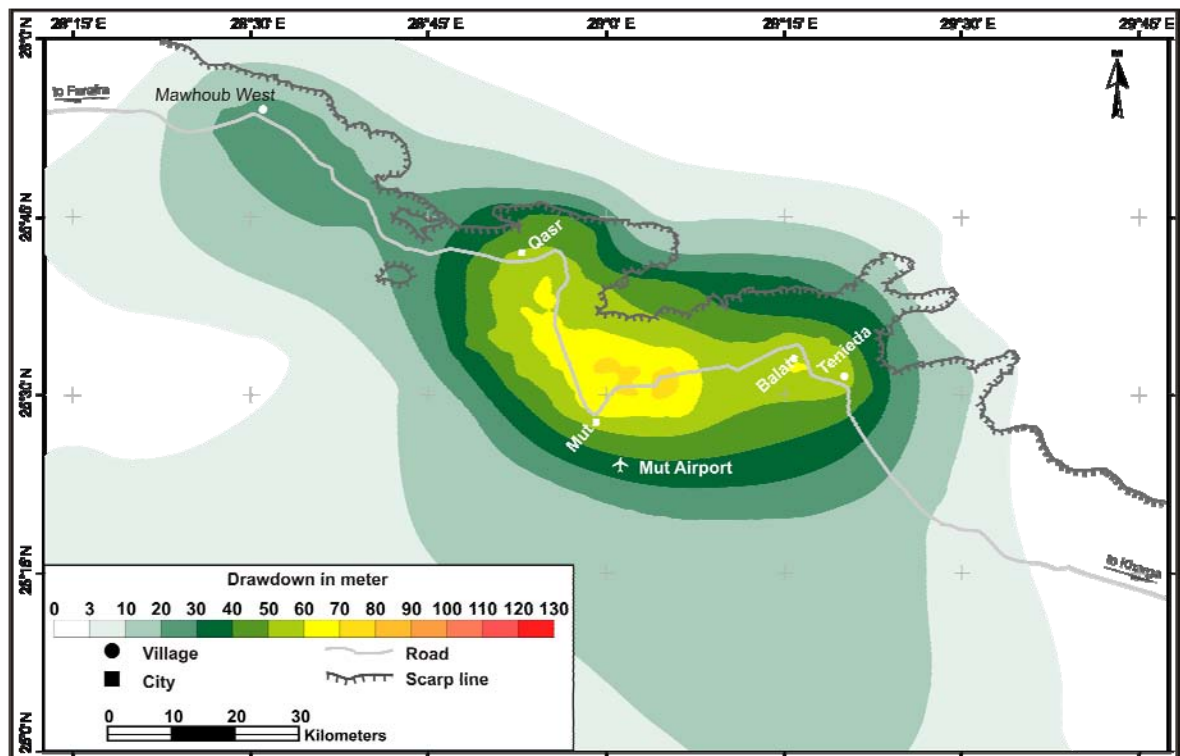


Figure 7.10. Simulated decline in potentiometric surface for the NSAS in the Dakhla oasis by 2100, scenario 1.

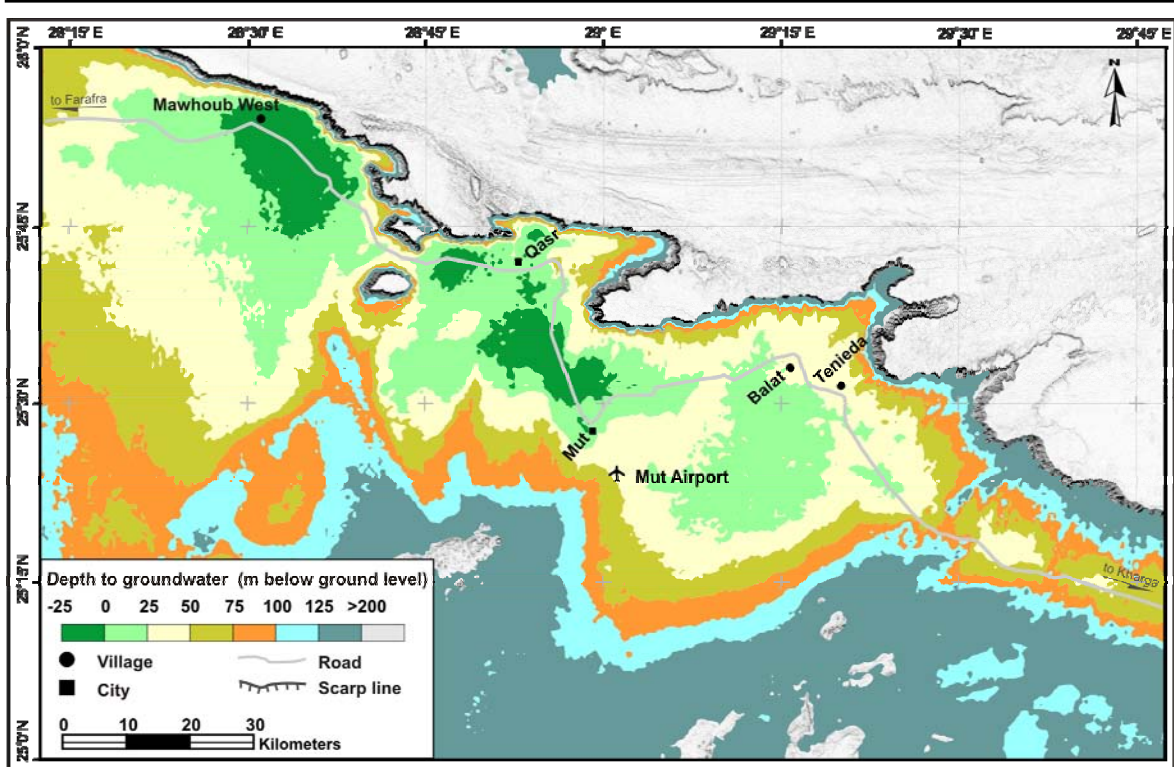


Figure 7.11. Calculated depth to groundwater for the NSAS in the Dakhla oasis by 2005.

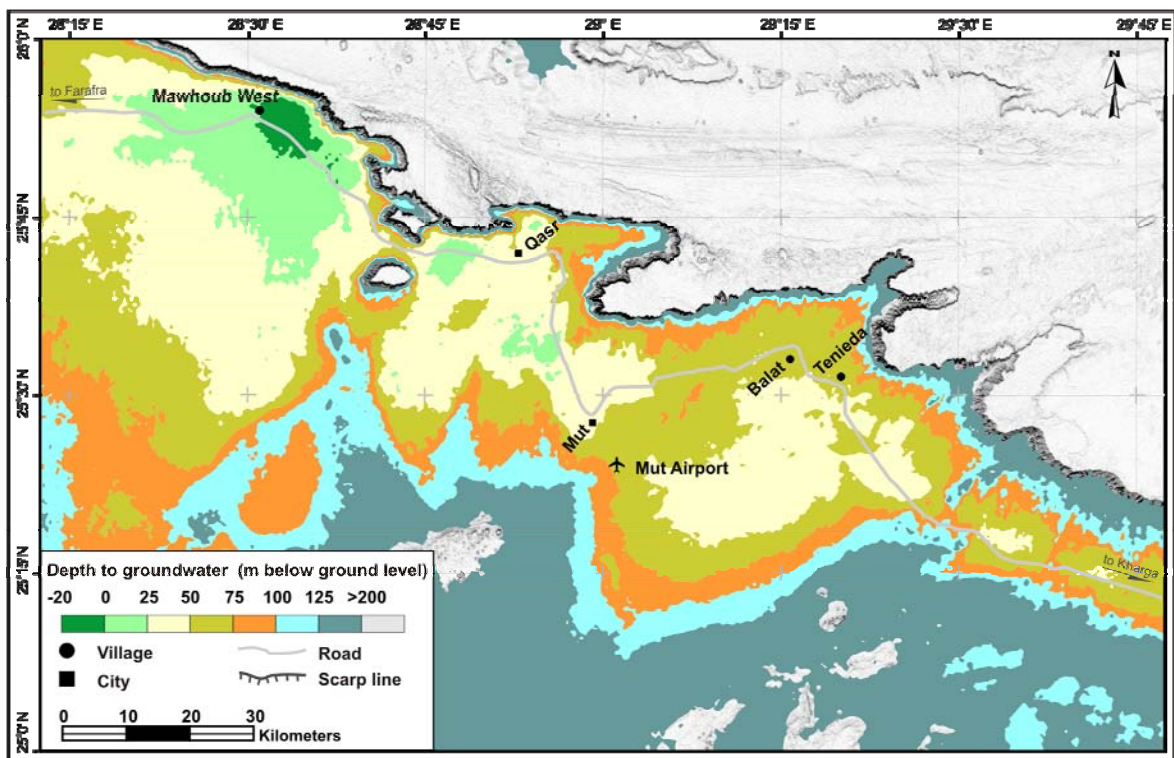


Figure 7.12. Calculated depth to groundwater for the NSAS in the Dakhla oasis by 2100, scenario 1.

However, the depth to groundwater in all the cultivatable areas within the oasis will be still less than 75 m. At present, the depth to groundwater less than 100 m is considered economical; hence, the application of this scenario is affordable for the groundwater development in the Dakhla oasis. Yet this scenario is still under the permissible potentiality of the NSAS in the Dakhla oasis.

7.7.2 Scenario 2

The total extraction rates were here increased by the a quarter of the full capacity extraction rates of the planned development to be 1.33×10^6 m³/d. These rates were shared out between the production wells proportionally according to their actual extraction rates. Even so, in different locations in the oasis, some extra virtual wells were set up. As a consequence, the hydraulic head pattern started to change its direction locally from south to north by the simulation year 2100 (Figure 7.13). As expected, the decline of the potentiometric surface increased to reach its maximum value of 100 m at several localities within the oasis by the same year, as shown in Figure 7.14. The depth to groundwater did not exceed the 80 m limit at the east Dakhla depression, 60 m at the middle, and 35 m at the west, which in turn indicates substantial system potential for additional water production although with the forecasted consequences such as further decline in potentiometric surface.

7.7.3 Scenario 3

This scenario was considered to predict the consequences of the future development when the artificial discharge is increased by half of the full capacity planned extraction rates. An extraction rate of 1.46×10^6 m³/d was subsequently applied.

Figures 7.15 and 7.16 represent the successive changes in hydraulic head during the simulation by year 2050 and 2100, respectively. The core of COD reached the maximum value of 80 m around Mut city by year 2050, as shown in Figure 7.17. At the same time, it did not exceed 30 m at Mawhoub West and an average decline of the potentiometric surface of 45 m over the whole oasis. The abstraction at the current pumping scheme was found to balance the local inflow at the end of the simulation with a 75 m average decline in the potentiometric surface in Dakhla oasis (Figure 7.18) and a maximum drawdown of 105 m at the middle of the oasis (the area between Ismant and Mut). Nevertheless, the drawdown did not exceed 30 m at the Mawhoub West area.

At the end of the prediction, depth to groundwater at Mawhoub West area will mostly be around the ground level at all well fields and will not exceed 25 m. In the Mawhoub area the maximum depth to groundwater will be 50 m. However, between Qasr city and Mut city the average water depth ranges from 50-75 m below ground level.

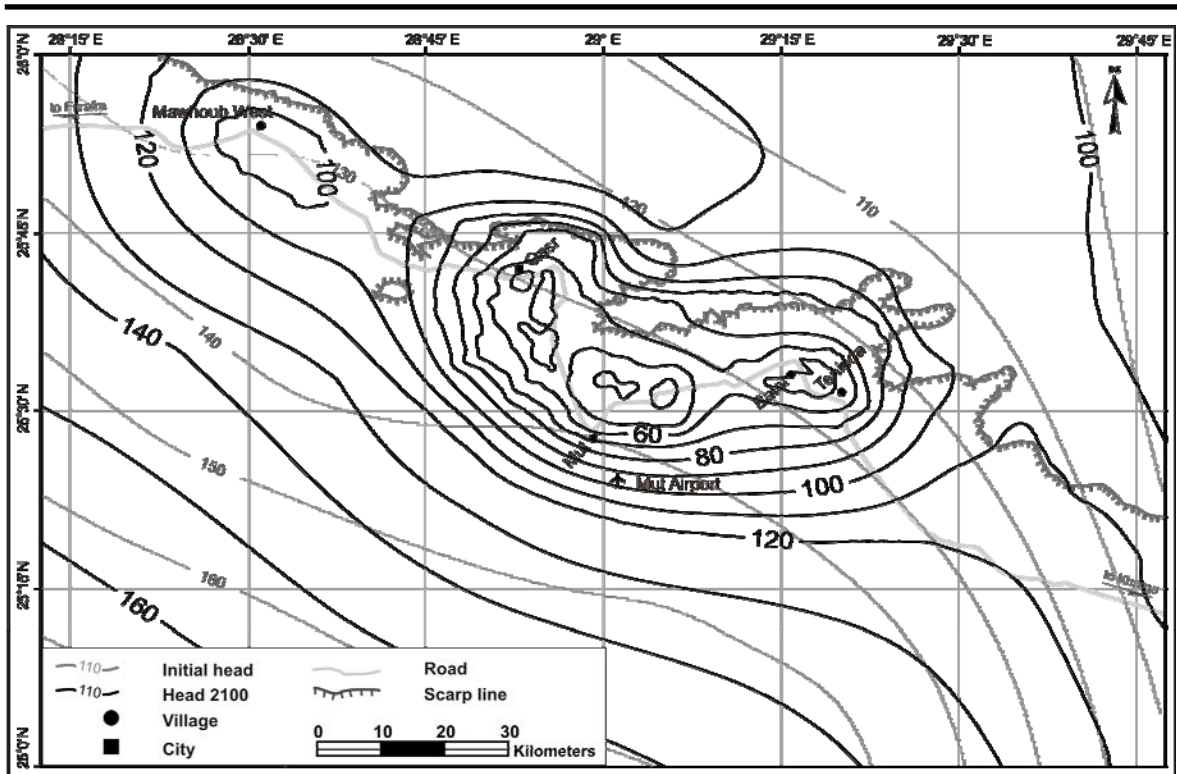


Figure 7.13. Simulated hydraulic head m (amsl) for the NSAS in the Dakhla oasis by 2100, scenario 2.

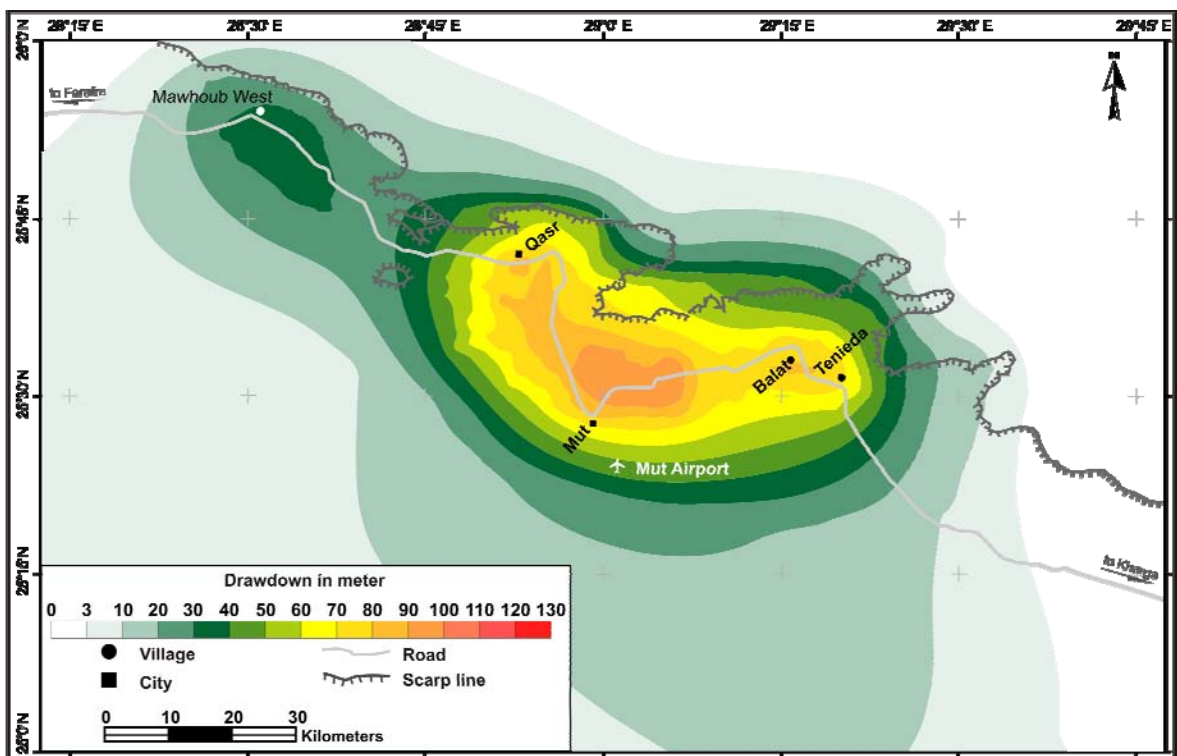


Figure 7.14. Simulated decline in potentiometric surface for the NSAS in the Dakhla oasis by 2100, scenario 2.

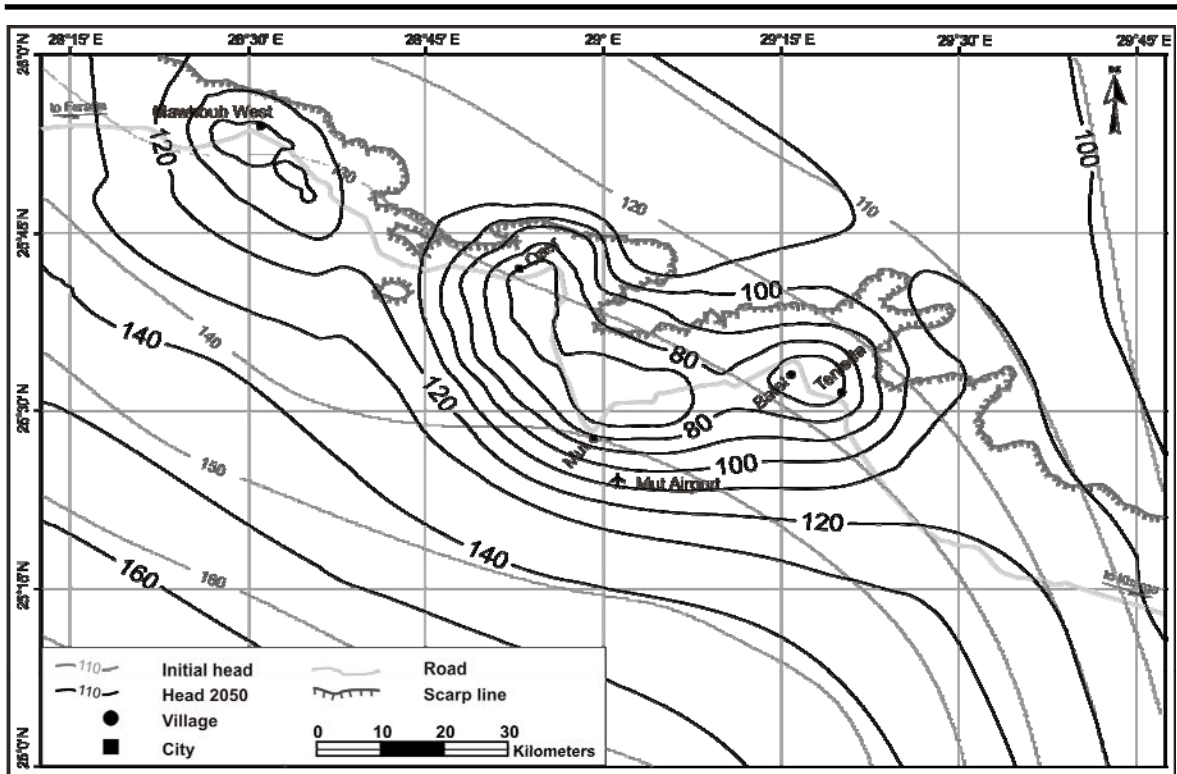


Figure 7.15. Simulated hydraulic head m (amsl) for the NSAS in the Dakhla oasis by 2050, scenario 3.

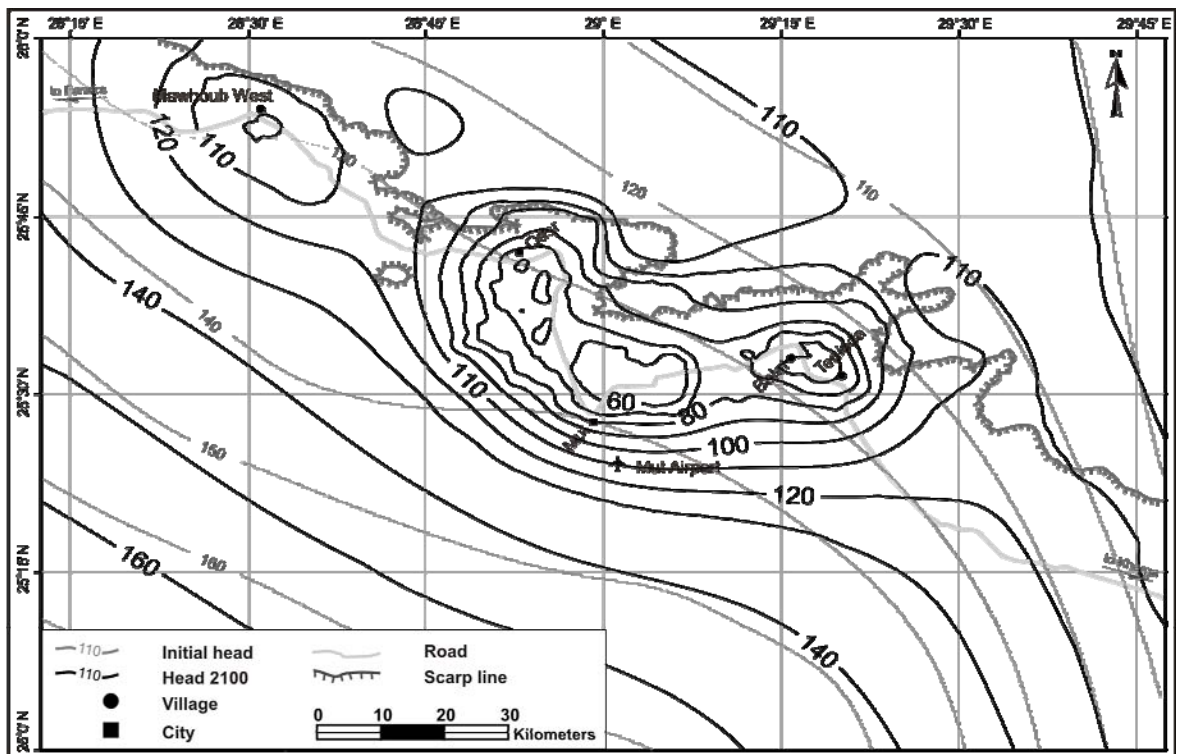


Figure 7.16. Simulated hydraulic head m (amsl) for the NSAS in the Dakhla oasis by 2100, scenario 3.

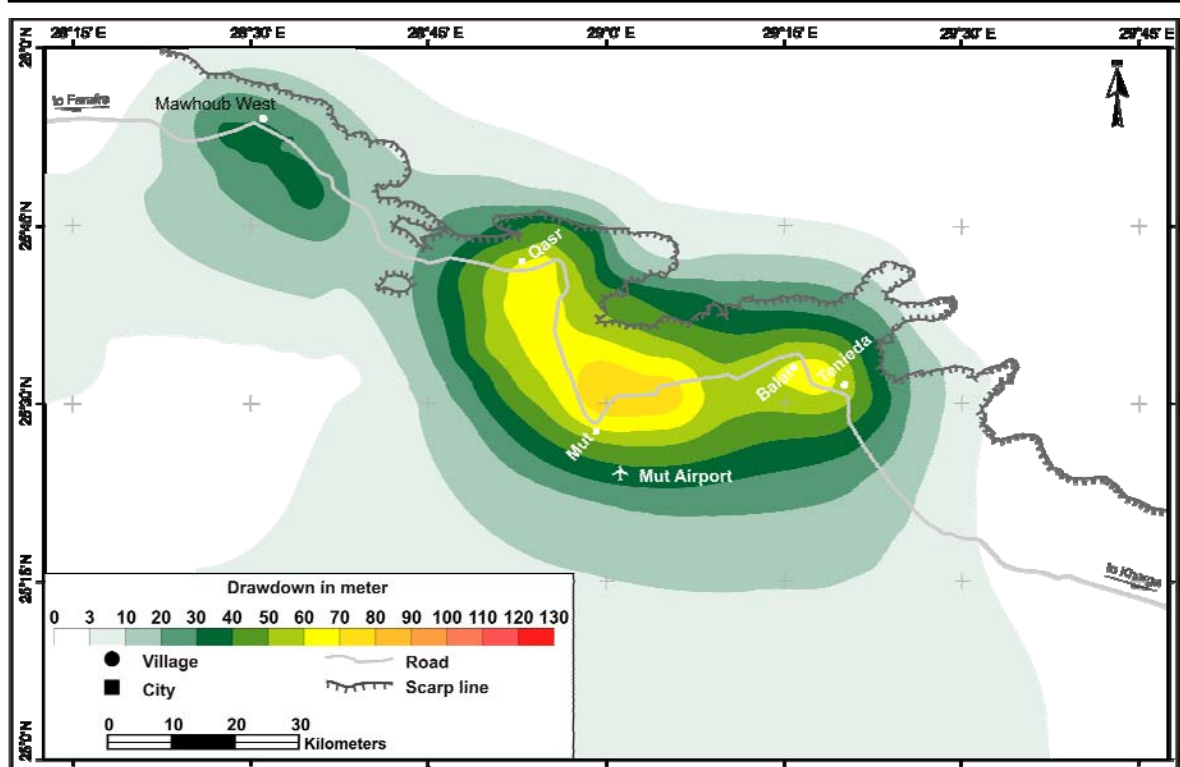


Figure 7.17. Simulated decline in potentiometric surface for the NSAS in the Dakhla oasis by 2050, scenario 3.

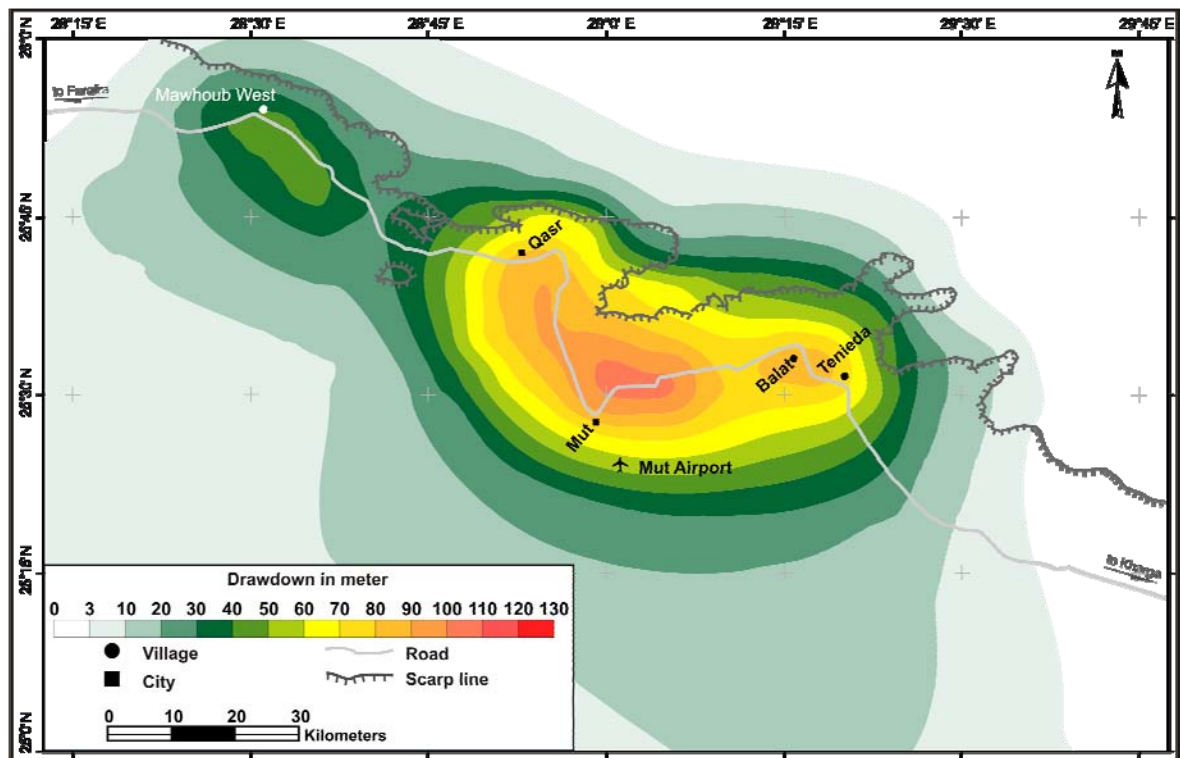


Figure 7.18. Simulated decline in potentiometric surface for the NSAS in the Dakhla oasis by 2100, scenario 3.

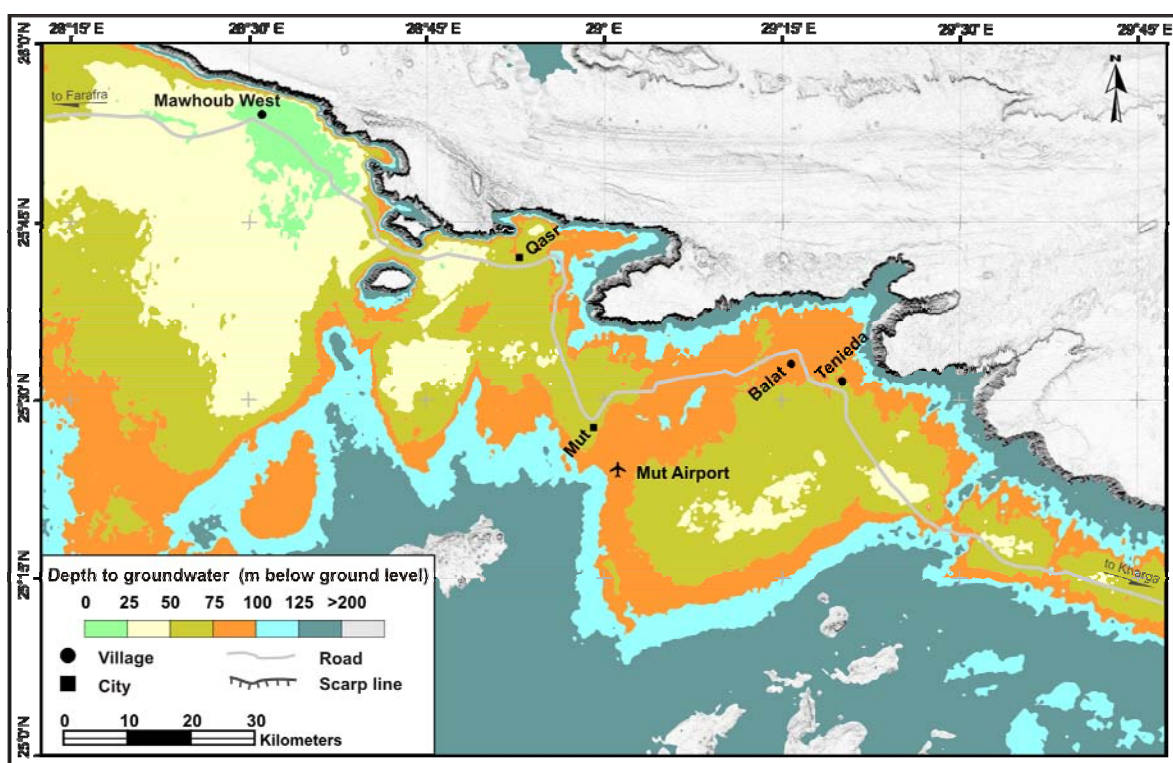


Figure 7.19. Calculated depth to groundwater for the NSAS in the Dakhla oasis by 2100, scenario 3.

To the east of Mut city the water level lies a little bit deeper, as the water depth ranges from 50-100 m below ground level (Figure 7.19). The productivity of the aquifer at implementation of this abstraction scenario is still high to very high, as it reaches 19,500 m³/day/m of drawdown. Based on the groundwater potentiality and development ambitions in the Dakhla oasis, this scenario was found to be the best development option for the domestic, agricultural and industrial activities for the coming 100 years.

7.7.4 Scenario 4

An extraction rate of 1.6×10^6 m³/d was simulated in this scenario, which corresponds to an increase of the extraction to 75% of the planned rates (Table 1). Successive changes in the hydraulic head contour courses and the COD by year 2100 are shown in Figures 7.20 and 7.21. A distinct successive drop in the potentiometric levels is apparently noticed as a response of the increase of the abstraction rates of this scenario. The core of the COD will reach as so far as 120 m at the middle of the oasis. On the other hand, the 100 m COD will cover the entire populated and planned reclaimed area of the Dakhla oasis, excluding the Mawhoub West area, where the decline of the potentiometric level reaches 50 m as shown in Figure 7.21. The depth to ground water will roughly reach 120 m below ground level at the area east of Mut city, where the limit of 100 m water depth will be overtaken amongst the most populated areas in the Dakhla oasis, evidently excluding Mawhoub West village.

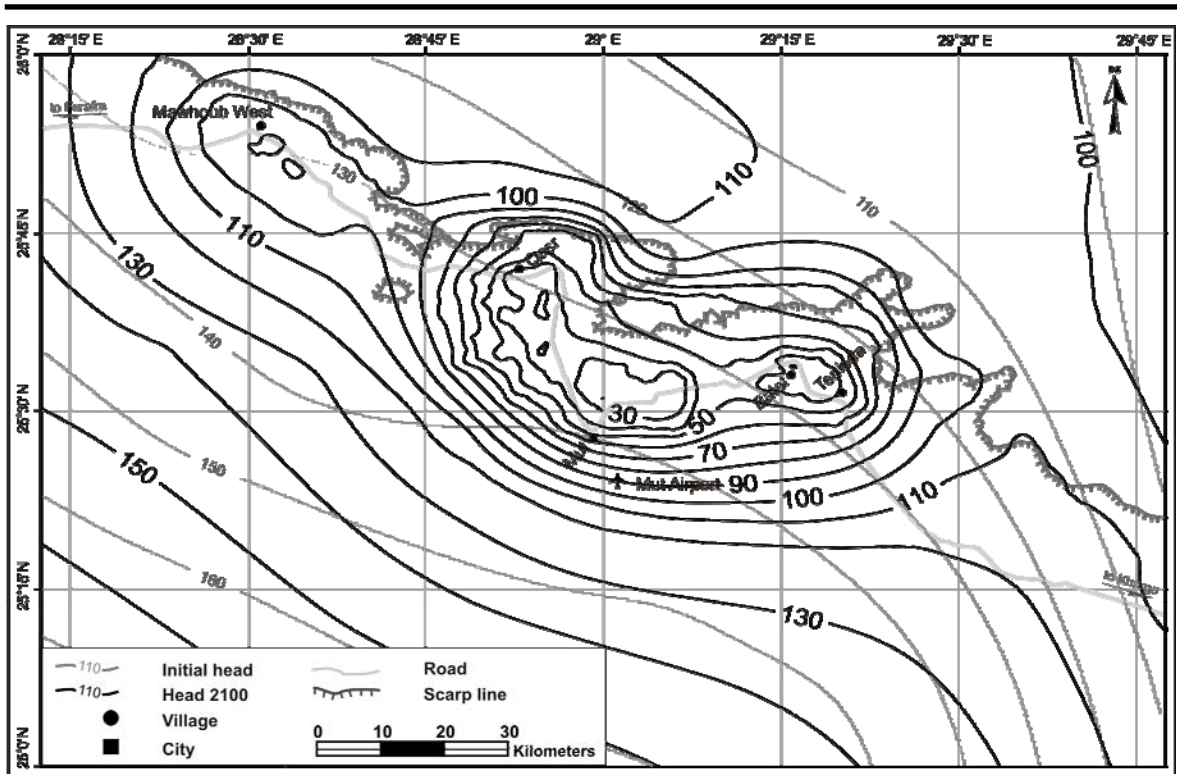


Figure 7.20. Simulated hydraulic head m (amsl) for the NSAS in the Dakhla oasis by 2100, scenario 4.

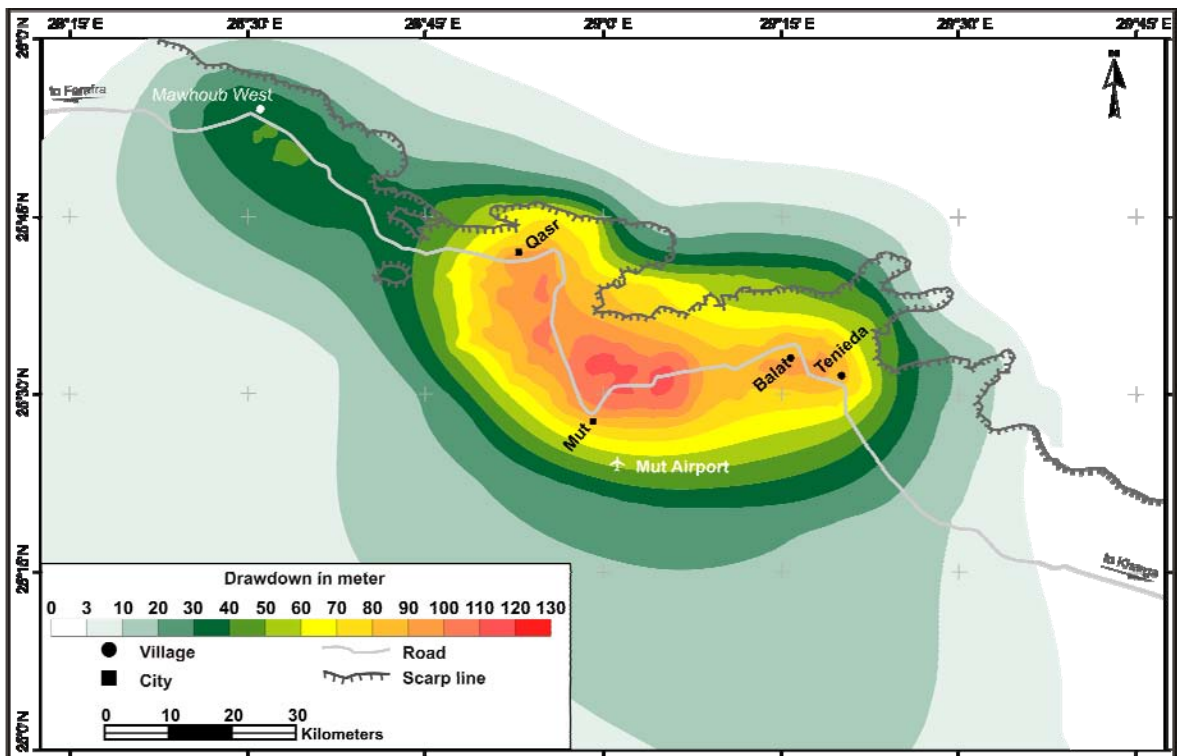


Figure 7.21. Simulated decline in potentiometric surface for the NSAS in the Dakhla oasis by 2100, scenario 4.

This indicates that the implementation of this abstraction scenario (scenario 4) is not feasible for the development strategies in the Dakhla oasis.

7.7.5 Scenario 5

The attempt to simulate this scenario is to investigate the consequences of expanding the groundwater abstraction rates in the Dakhla oasis to their full capacity planned rates of 1.7×10^6 m³/d. It is already expected from the simulation results of scenario 4 that the simulation results would be even worse with the application of this scenario concerning the decline in potentiometric surface and depth to groundwater. The changes in hydraulic head and drawdown by years 2050 and 2100 are shown in Figures 7.22-7.25. Figure 7.26 illustrates the depth to groundwater from ground level by year 2100.

The drawdown will reach 95 m and cover the area between Ismant to Qasr by year 2050, whereas this area will be covered by a 125 m drawdown by year 2100. The average drawdown over the oasis at the end of the simulation will then be about 85 m, which means that the average annual decline in hydraulic head is about 0.90 m/year. The areas of depth to groundwater exceeding 100 m due to this scheme of abstraction will expand to cover most of the villages east of Mut city.

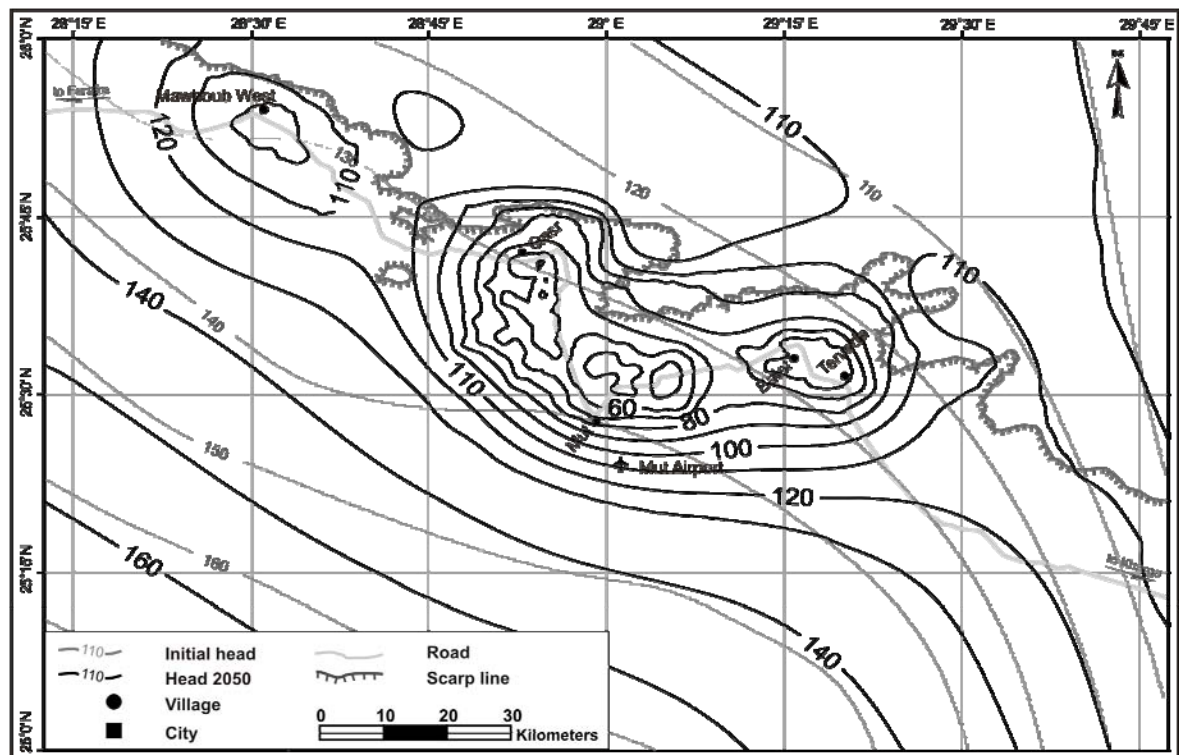


Figure 7.22. Simulated hydraulic head m (amsl) for the NSAS in the Dakhla oasis by 2050, scenario 5.

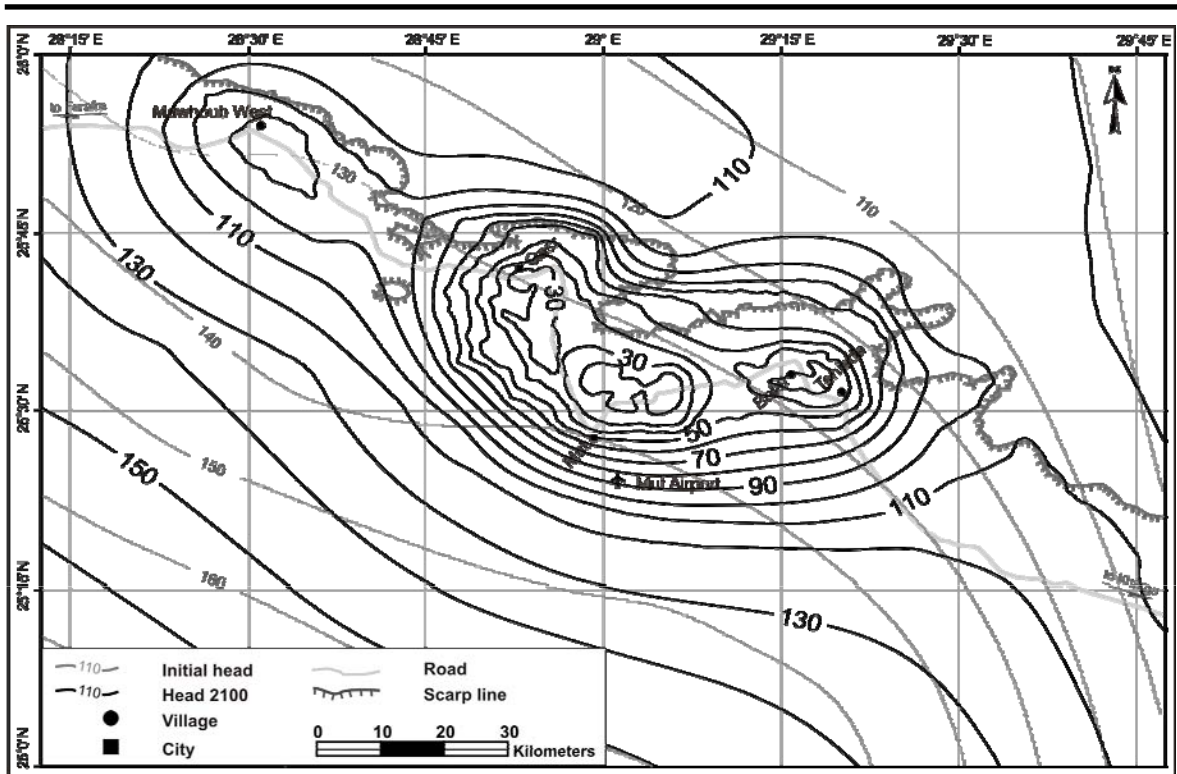


Figure 7.23. Simulated hydraulic head m (amsl) for the NSAS in the Dakhla oasis by 2100, scenario 5.

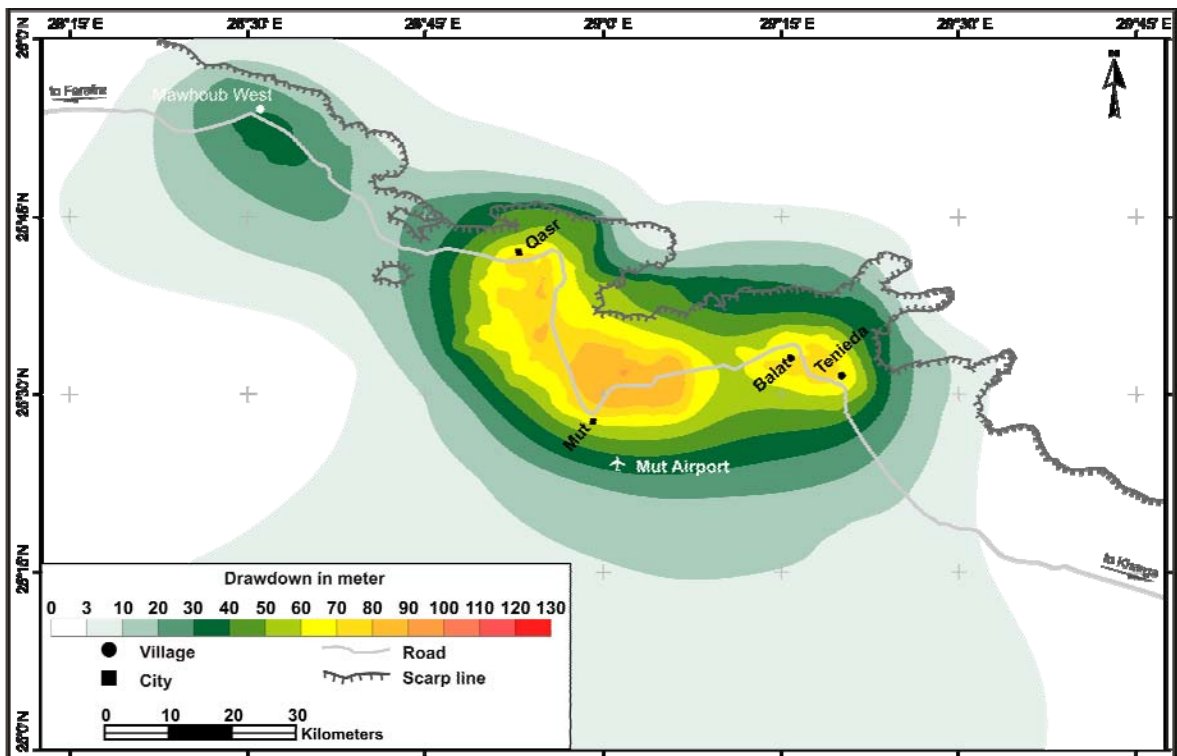


Figure 7.24. Simulated decline in potentiometric surface for the NSAS in the Dakhla oasis by 2050, scenario 5.

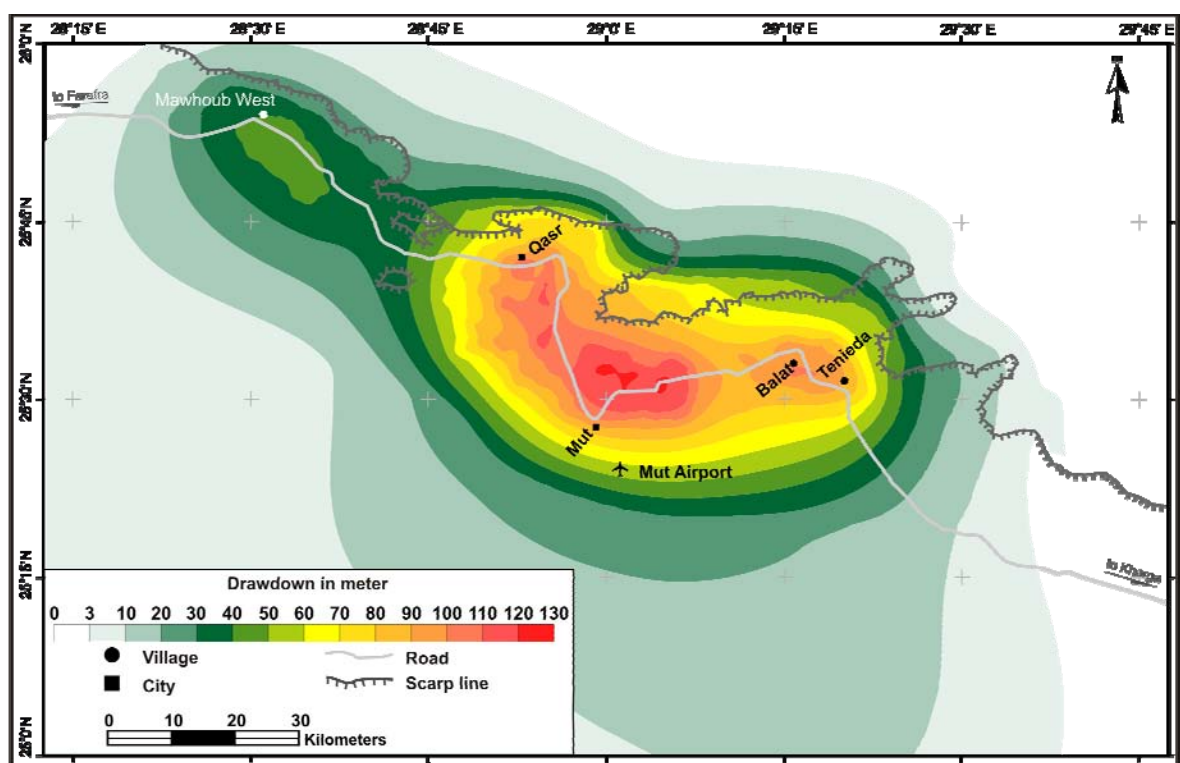


Figure 7.25. Simulated decline in potentiometric surface for the NSAS in the Dakhla oasis by 2100, scenario 5.

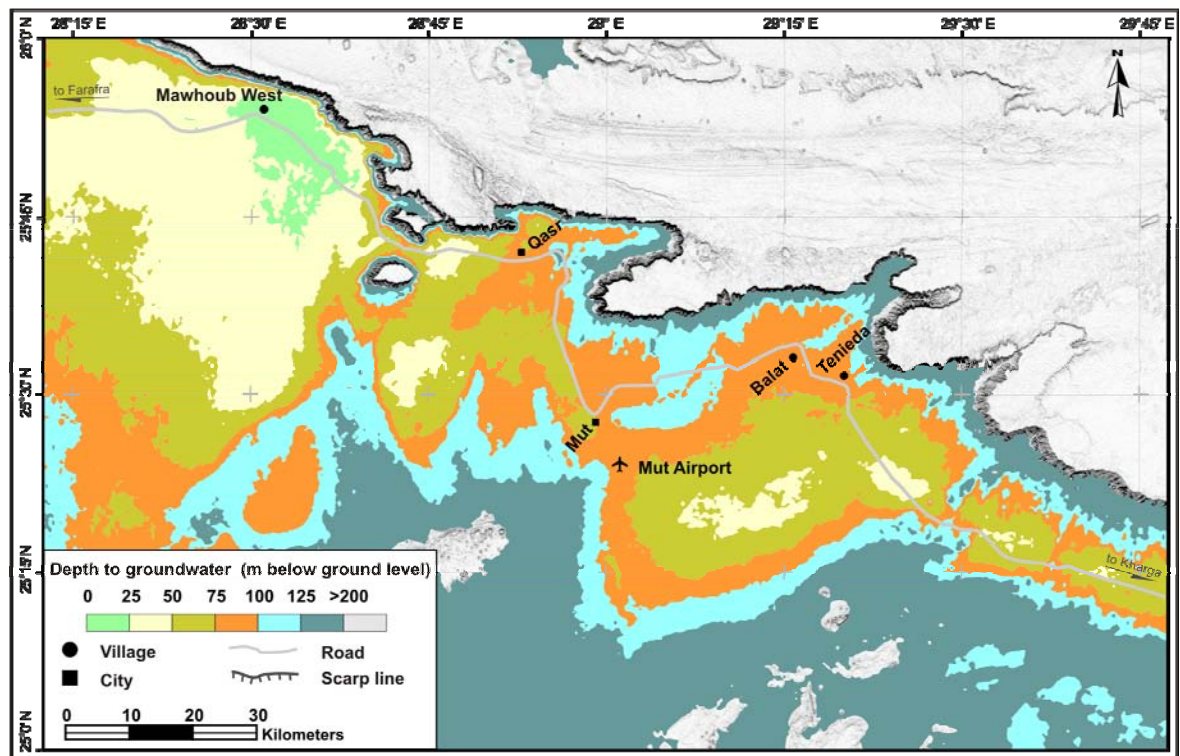


Figure 7.26. Calculated depth to groundwater for the NSAS in the Dakhla oasis by 2100, scenario 5.

It is also obvious, as discussed in the regional modeling, that every extracted cubic meter from the NSAS is groundwater mining, which is clearly emphasized with the local modeling of the Dakhla oasis and supported by the obvious successive decline of potentiometric surface as a response to each abstraction scenario.

7.8 Socio-economic feasible use

The changing nature of social sustainability and inter-related risk of resource degradation are the critical considerations when developing plans for the use of non-renewable groundwater resource. Social sustainability contemplates the society's needs and goals, which are here certainly a factor of the groundwater resource availability, time, place, and anthropogenic activities. However, there is no rigorous definition of the social sustainability. For these reasons, the use of "sustainability" in the context of "mining aquifer storage" needs some clarifications. In this study the term sustainability is interpreted in the "social context" and thus sustainability is not meant to imply preserving the groundwater resource for generations to come but instead reconciling the use of the non-renewable resource of the NSAS with the sustainability of human life.

As mentioned before, a depth to groundwater up to 100 m is considered economical today. Based on this contemplation and the results discussed in section 7.7, it is concluded that the best option for groundwater management in the Dakhla oasis in terms of groundwater extraction is the implementation of an extraction rate of 1.46×10^6 m³/d as introduced by scenario 3 (section 7.7.3). The results of this scenario emphasize not only that the economic depth to groundwater could be retained during the simulation period and maybe beyond but also that the potentiality of the aquifer could be better utilized to meet the proposed development plans. The implementation of scenarios 4 and 5 will be responsible for creating a huge cone of depression that extends far away beyond the oasis borders, and the depth to groundwater will exceed 100 m (bgl). Besides, the potentiometric head will drop below the bottom of the first aquifer. This, in turn, will affect the phreatic water levels and springs. Therefore, the wells extracting the first aquifer will dry out.

8

Local Model Lake Nasser -Tushka

8.1 Introduction

Groundwater and surface water are not isolated components of the hydrologic system but instead interact in a variety of physiographic and climatic landscapes. Thus, development or contamination of one frequently affects the other. Groundwater flow to and/or from lakes and rivers has always been estimated using simple flow nets (Hunt et al. 2003). However, groundwater interaction with lakes and rivers can vary spatially (Krabbenhoft 1986) and/or temporally (Sacks et al. 1999). To understand these interactions, a sound hydrogeological framework is needed. Moreover, the groundwater flow pattern in the vicinity of such hydrologic interaction domains is controlled not only by the configuration of the groundwater and surface water level but also by the distribution of hydraulic conductivity in the rocks, and the topographic and geologic effects as well (Sophocleous 2002). The best way for investigating interaction of groundwater with lakes is to integrate the lake water levels into groundwater flow models.

In this chapter the groundwater-lake interaction in the area of Lake Nasser and Tushka was investigated. A great effort was given to estimate the influent/effluent balances and localities of Lake Nasser to/from the NSAS. Furthermore, the consequences of the development of the new Tushka lakes at the west of Lake Nasser on the NSAS in terms of the possibility of whether these water bodies recharge the aquifer have to be elaborated.

Lake Nasser is one of the largest man-made fresh water reservoirs in the world. It was formed due to the construction of the Aswan High Dam (1959-1969). It formed of an elongated water body of about 560 km long behind the Aswan High Dam, 196 km of which are in Sudan (Lake Nubia), and a maximum width of 35 km, which is near the Tropic of Cancer with an average width of 15 km (Kim and Sultan 2002). The water volume in the lake fluctuates greatly seasonally and from year to year, depending on the

net annual volume of water it receives (Elewa 2006). The highest recorded water levels are 178 m above sea level (in 1996) and 182 masl (in November 1998), while the lowest level recorded so far was 158 masl (in July 1988).

The lake covers a total surface area of 5,270 km² (85 % of which is in Egypt) and has a storage capacity of some 157 km³ of water. The average depth is about 25 m and maximum depth is 130 m (Elewa 2006). During the irrigation seasons, seepage losses by distribution canals in irrigated fields contribute to elevated groundwater levels. Lake Nasser has a huge resource of fish, with all its relative advantages.

The study area caught the attention of several authors, scientists, and even governmental authorities, as geological, hydrogeological, hydrological, and climatic studies were frequently held, among them Shatta (1962), El-Shazly et al. (1977), Tamer et al. (1987), Aly et al. (1993), GARPAD (1998), Altorkomani (1999), RIGW (2001), Sallam (2001), Kim and Sultan (2002), and Elewa (2006). A general discussion of the outlines, geological, hydrogeological, and hydrological features of this area is presented in section 8.2.

8.2 Site description

The study area is located between latitudes 22° N and 24° N and longitude 30° E and 33° E, as shown in Figure 8.1a. The area west of Lake Nasser is commonly flat plain with hills, ridges and scarps which are generally rugged and rough. The ground level ranges from about 125 to 250 m amsl. A remarkable depression called the Tushka depression is located to the west of the lake with a ground level that ranges from 125 to 200 m amsl. This depression is used as a secondary fresh water reservoir of Lake Nasser. Once the water level exceeds 178 m amsl in Lake Nasser, the excess of water storage is discharged into this depression through a side canal, preventing the water level in Lake Nasser from reaching dangerously high levels and acting as a safety valve for the High Dam. Accordingly, four other lakes were formed in the Tushka depression.

The geology of the study area is dominated by a sedimentary succession ranging in age from Jurassic to Quaternary, with exposures of igneous and metamorphic rocks belonging to the Late Precambrian basement, in addition to the Tertiary foreland volcanics of the Late Cretaceous and mid-Tertiary age (Elewa 2006). Figure 8.1 shows the location, a schematic cross section along line SE-NW, and the geologic map of the area of interest. The basement surface is uneven. It crops out near Lake Nasser in the middle of the study area (Kim and Sultan 2002). The basement surface forms an impervious lower boundary for the aquifer and acts as a barrier to the lateral groundwater flow in some locations. The lower part of the sequence consists of undifferentiated conglomerate, sandstone and shale.

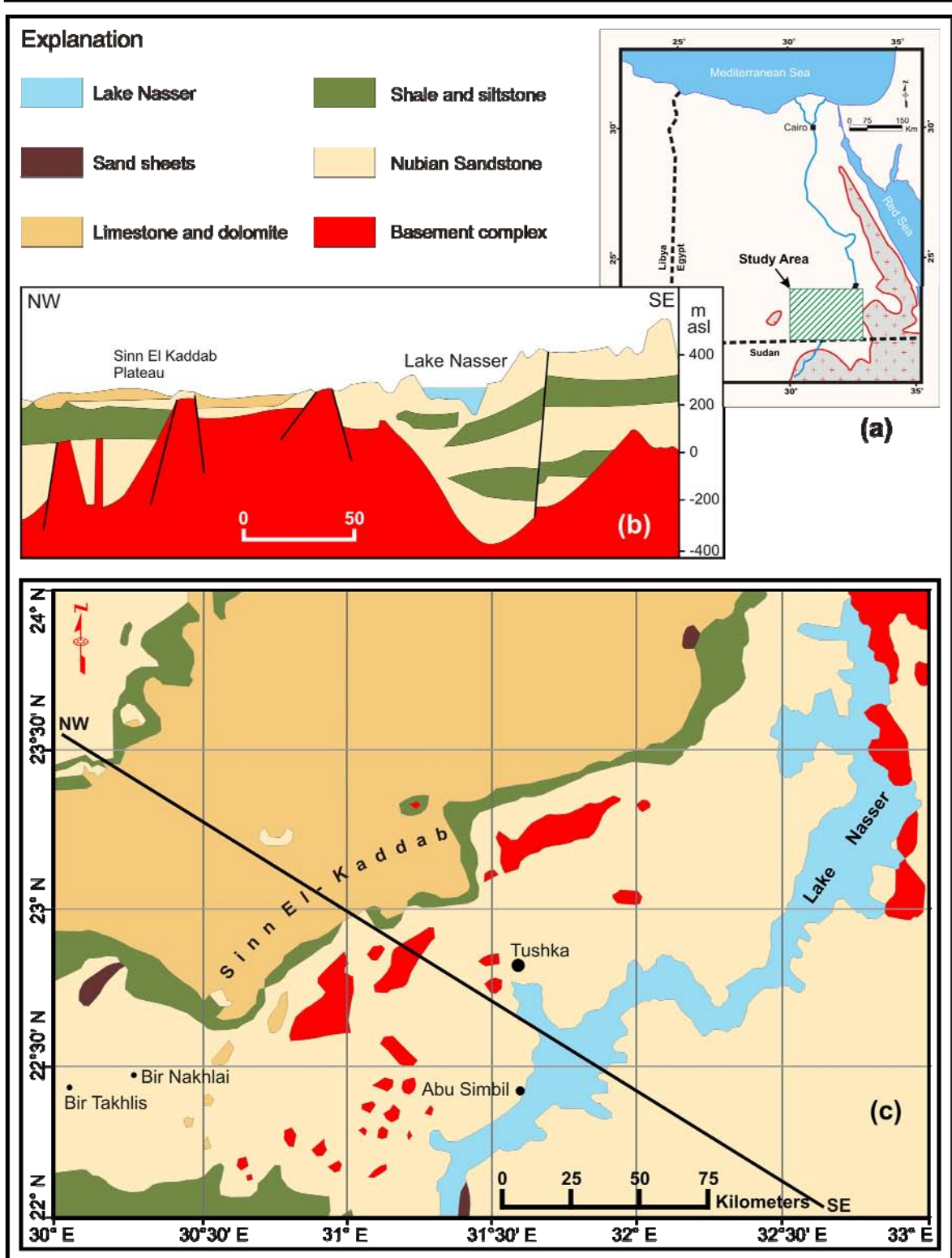


Figure 8.1. Location map showing (a) the study area, (b) a schematic cross section, and (c) a geologic map of the area with the location of cross section. (Geological map after Conoco (1987) and USGS (2004), the cross section after Kim and Sultan (2002)).

The middle part of the sequence is composed of coarse pebbly sandstone, fine sandstone with siltstone, and shale intercalations. The two sequences are of Upper Jurassic to Lower Cretaceous age. The upper part of the sequence is exposed in the northern part of the study area. It is formed of sandstone capped by karstified Tertiary limestone (Kim and Sultan 2002).

Hydrogeologically, the basin under the area of interest is interconnected. The penetrated Nubian section is formed of fining downward litho-facies. The relatively high water level of Lake Nasser and the difference between its level and the groundwater level induce the water body of Lake Nasser to expose influent conditions (Aly et al. 1993). The groundwater flow direction in the area south of Lake Nasser is from southwest to northeast, which means that it is following the general flow direction of the whole NSAS.

8.3 Model input and boundaries

The area of interest was already integrated in the calibrated 3D-regional groundwater flow model of the NSAS. The initial and boundary conditions of the regional model were also valid for this local modeling approach. Within the scheme of regional modeling, the water body of Lake Nasser was considered a time-constant head (fixed head-boundary condition-1st type). In the case of the local modeling approach, Lake Nasser is modeled a time-dependent head boundary, where the fluctuations of the water level of the lake were taken into account to simulate the response of the aquifer to these water level changes, especially along the contact section. The discretization attempt of the study area was carried out to produce mesh elements as small as possible. The resolution of these elements varied from 100 m to 500 m.

After the construction of Aswan High Dam, the surface water level in the lake rose from 116 m to 158 m amsl in 1970. Subsequently, the lake level fluctuated, reflecting the intensity of the Nile inflows as shown in Figure 8.2. During the period of 1970-2005, the lake level fluctuated between a minimum level of 158 m amsl (in 1987) and a maximum level of 182 m amsl (by 1997).

The latest rise in lake levels induced Lake Nasser to overflow a spillway that was constructed to channel excess lake water and create four lakes to the west of Lake Nasser (Figure 8.3). These lakes were modeled as constant head boundary starting from year 1998. The first lake covers an area of about 400 km² with a lake level of 172 m amsl. The further excess of water from Lake Nasser spread further west, forming three additional lakes across a lowland area of about 750 km² with lake levels of 162 m, 156 m, and 147 m amsl westward, respectively (Yan et al. 2003). Due to the large surface area exposed by the lake water, the average evaporation is high and is estimated to be about 16.4 mm/d (Aly et al. 1993). This high amount of evaporation equals roughly 20% of the lake inflow. On account of the aridity of the area under discussion, no areal recharge was considered except for what was applied to the regional model.

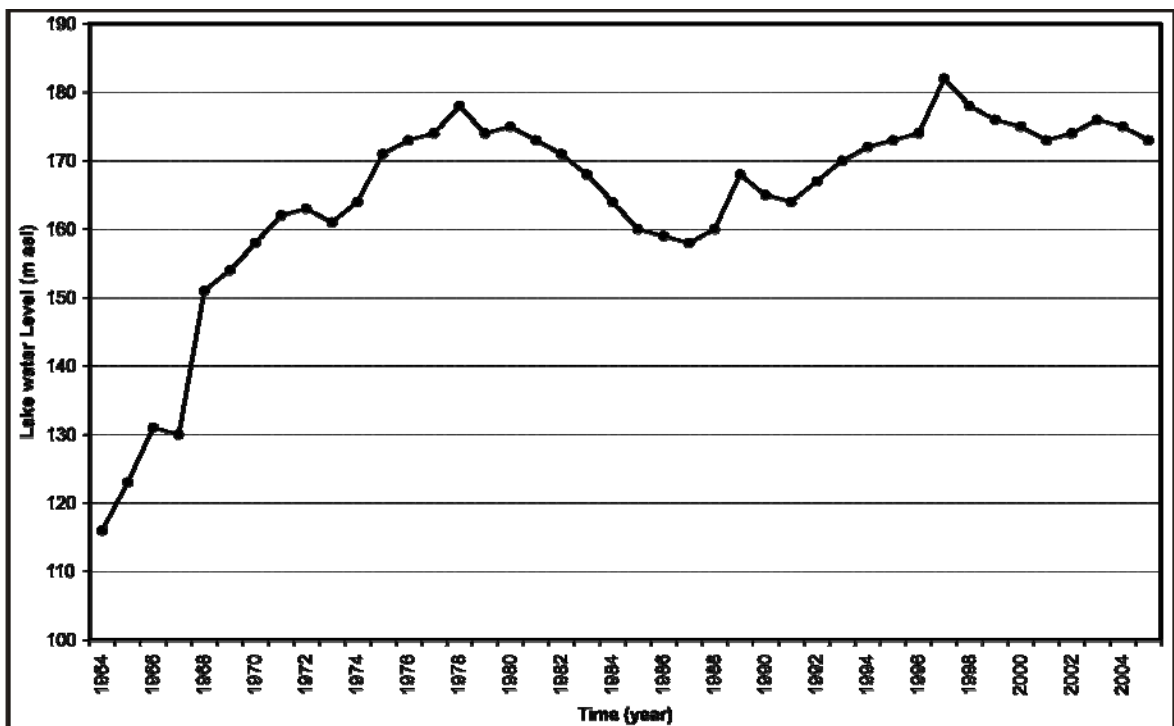


Figure 8.2. Fluctuations of Lake Nasser-water level from 1964-2005. Sources: GALND (1997), RIGW (1998), and personal contact (2003) and (2006).

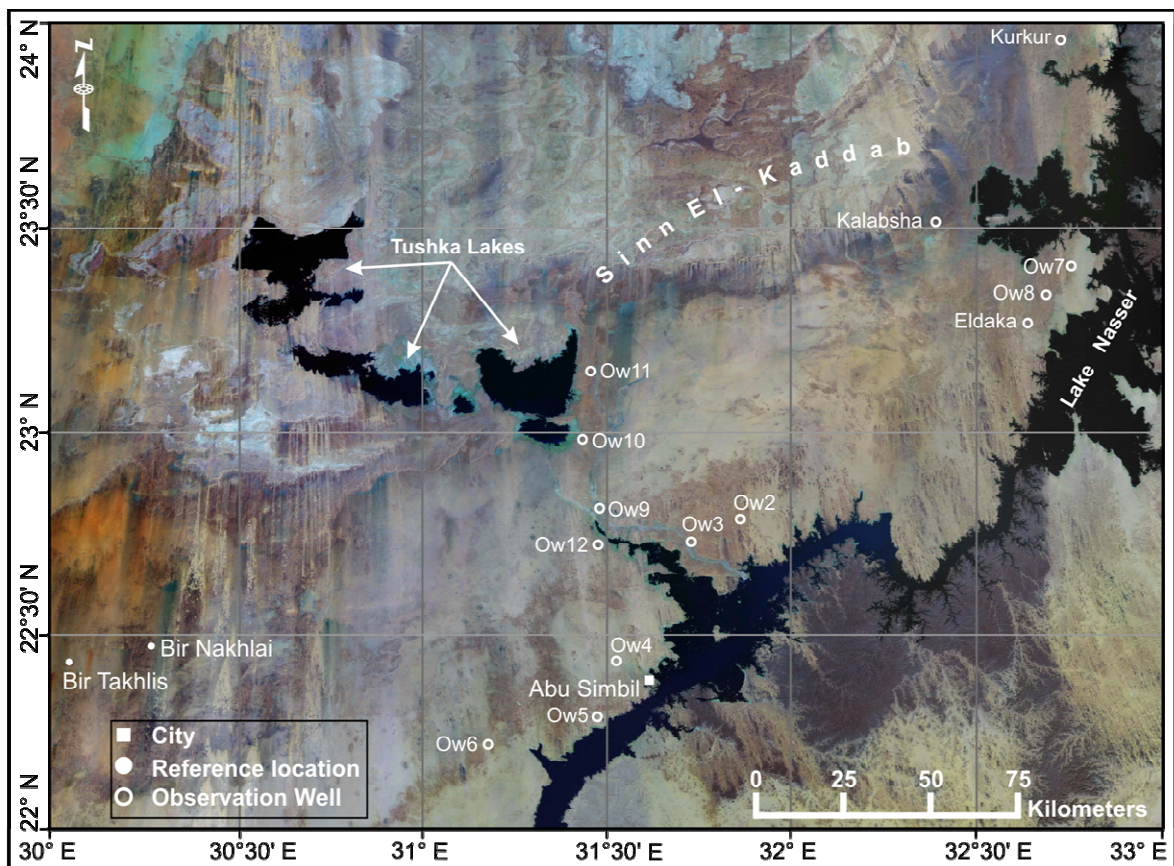


Figure 8.3. Location image of Lake Nasser, the Tushka lakes and the surrounding areas showing the location of the available observation wells. Satellite image from NASA (2005).

The aquifer was simulated as a free-surface boundary able to fluctuate in response to recharge from adjacent water bodies.

8.4 Model output

From the available observation records along the western side of Lake Nasser, it can be concluded that after the construction of the Aswan High Dam, the groundwater levels in the vicinity of the lake rose in response to the increase of water levels of Lake Nasser. This increase in groundwater levels varies from one site to the other along the lake bank and decreases westward as distance from the lake increases. The hydraulic head at most of the observation wells in the vicinity of the lake was not only considerably elevated on account of recharge from the lake, but it also reproduced the lake stage fluctuations as shown in Figure 8.4. The hydraulic head at the farthest observation wells reflected only slight increase in their values.

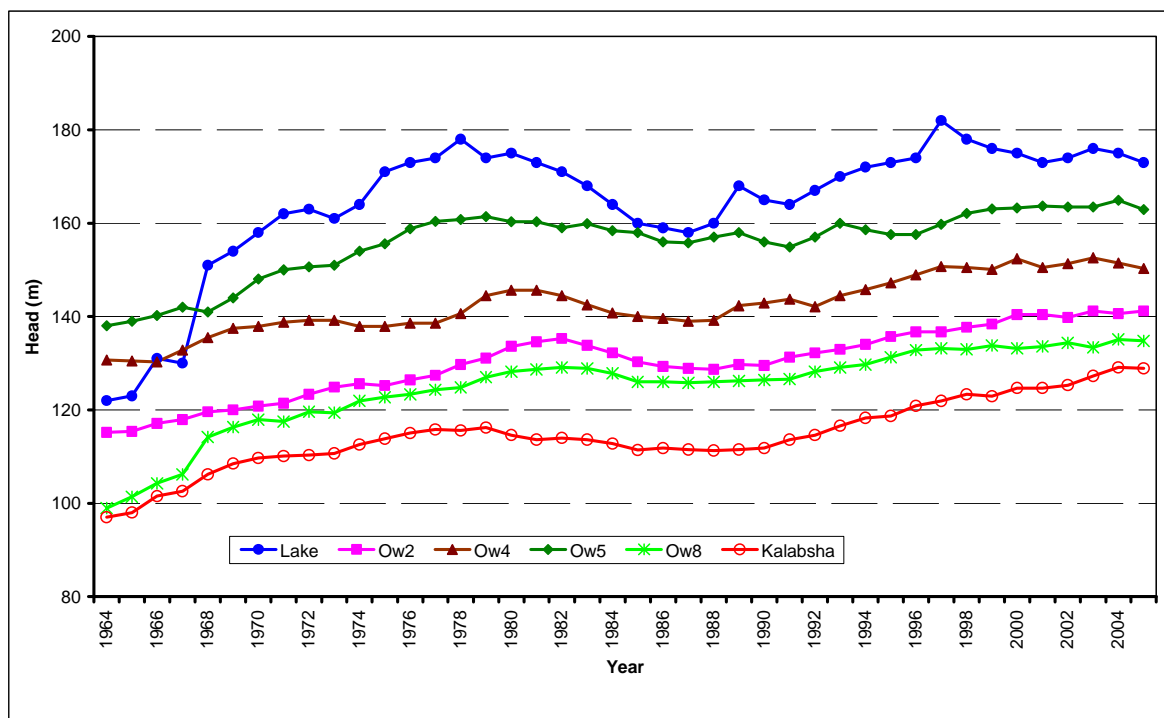


Figure 8.4. Hydrograph illustrating the changes in hydraulic head at selected observation wells west of Lake Nasser and how they reproduce the fluctuations of the lake levels.

The observation wells represented by Figure 8.4 lie within a maximum distance of 25 km from the lake (Figure 8.3). The groundwater level rose in these wells with an average value of 25 m. At the observation wells lying at different distances from the lake, the groundwater level is still affected by the recharge from the lake. Nonetheless, these wells are less sensitive to the fluctuations of the lake stage. However, the increase of the groundwater level did not exceed 0.3 m at the farthest available observation well (Ow11).

This 0.3 m increase in groundwater level at observation well Ow11 was obtained by the simulation until year 1998; after that, the Tushka lakes were included in the simulation. Therefore, the groundwater level was preferably affected by these lakes rather than Lake Nasser.

During the simulation from 1964-1998, the pattern of hydraulic head in the study area kept its direction from southwest to northeast. However, substantial changes occurred at the front of the hydraulic head contour lines in the vicinity of and along Lake Nasser. The recharge front of the 130-m contour line moved considerably westward from the lake to have a maximum noticeable distance of 55 km from the lake west of Abu Simbil (for locations refer to Figure 8.3). Figures 8.5 and 8.6 illustrate the progress of the recharge front along Lake Nasser as comparison examples between the initial hydraulic head (the hydraulic head of the study area until 1964) and the hydraulic head in year 1998, respectively.

The reason for choosing year 1998 as an output point is to expose the changes of the hydraulic head patterns and dynamics in the area just before the development of Tushka lakes. At Abu Simbil and Tushka depression, the average movement rates of the recharge front were 1.7 km/y and 0.8 km/y, respectively.

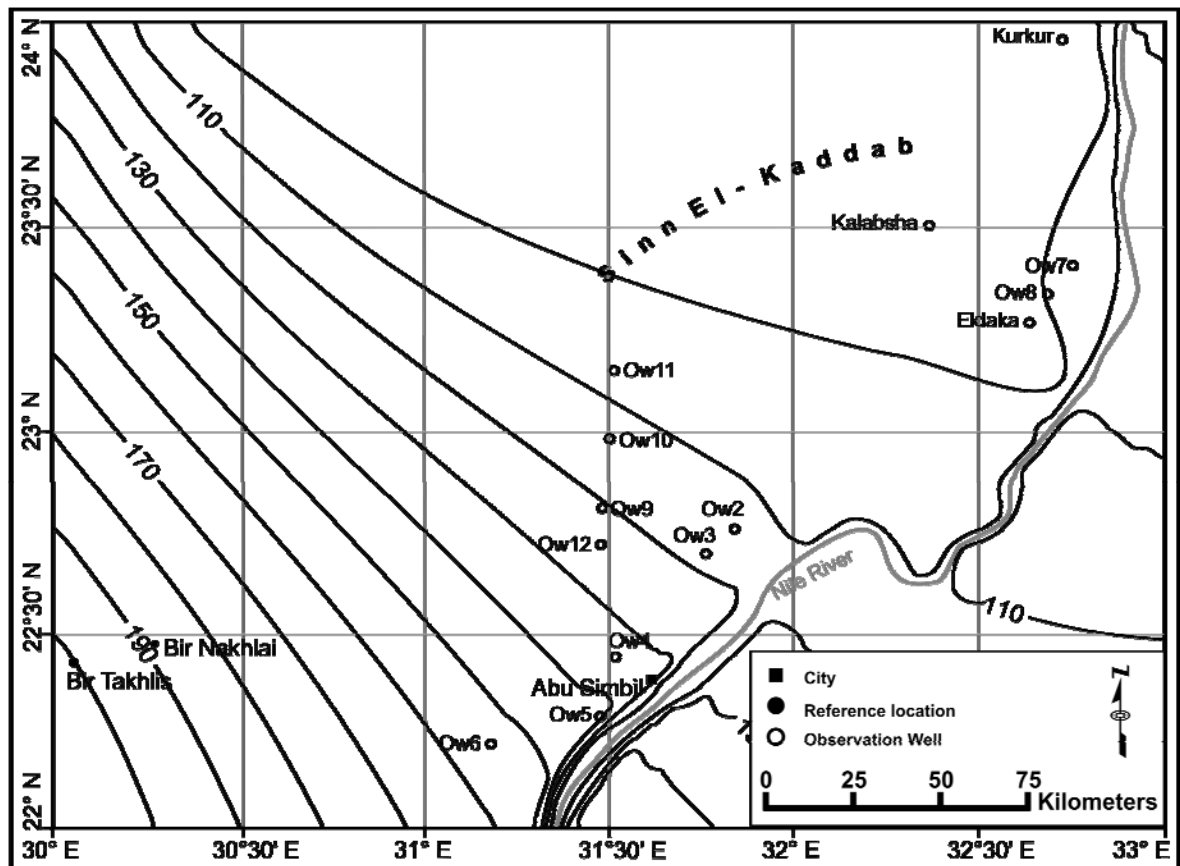


Figure 8.5. Contour map shows the distribution of the initial hydraulic head around Lake Nasser and the Tushka area before the construction of the Aswan High Dam.

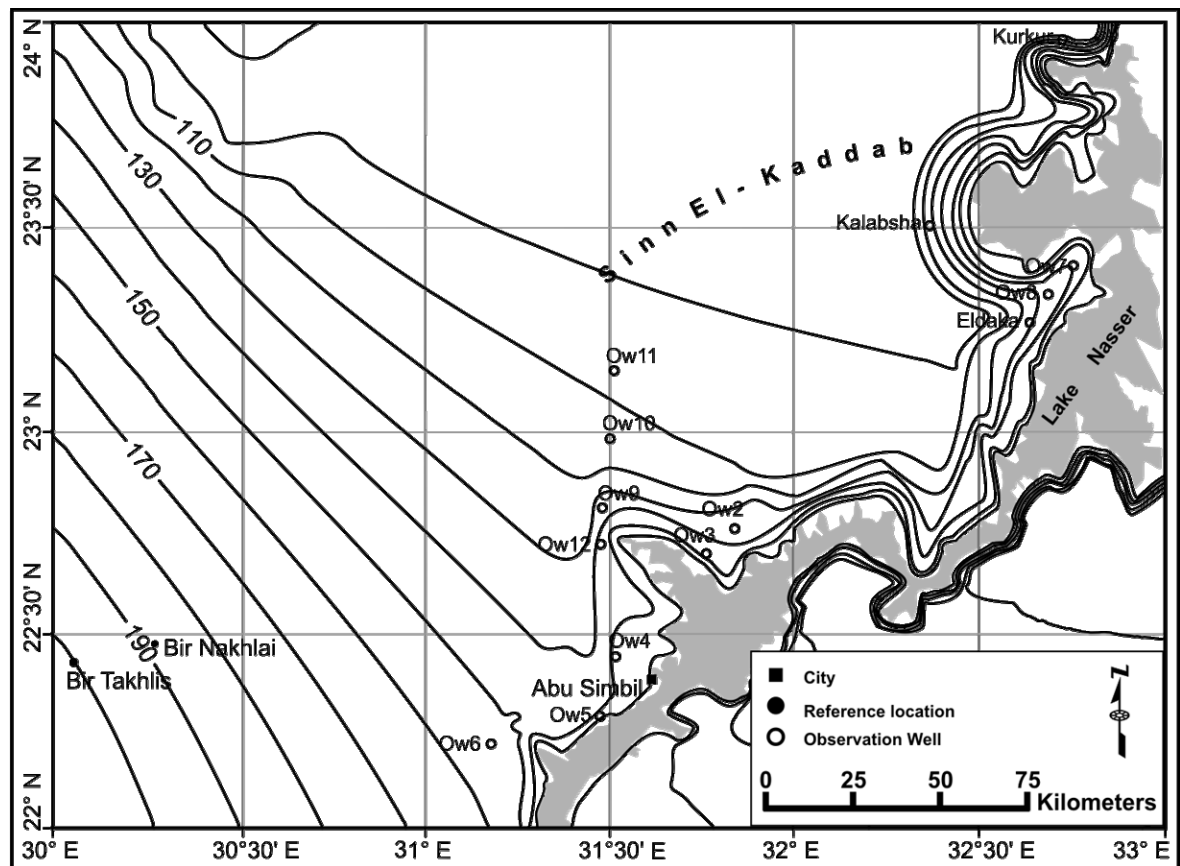


Figure 8.6. Contour map represents the distribution of the hydraulic head around Lake Nasser and the Tushka area in 1998 just before the development of the Tushka lakes.

At Kalabsha (in the north of Lake Nasser), the 100-m contour line moved about 35 km southward to lie just under the foot of the Sinn El-Kaddab plateau. The average increase in hydraulic head within the first inundated 20 km strip away from Lake Nasser is 32 m until 1998. Based on this conclusion, the groundwater volume that was added to the aquifer storage in this area is calculated to be about 281.5 km³.

After the development of Tushka lakes (Figure 8.3), those huge water bodies came in direct contact with the NSAS in the west of Lake Nasser. These new water bodies were modeled as a constant-head boundary condition starting from 1998, as discussed in section 8.3. Consequently, the hydraulic head pattern and direction as well as the aquifer storage were affected by the sudden accumulation of water head on top of it. Figure 8.7 presents the distribution of the hydraulic head in the study area in 2000 and 2005, respectively. From Figure 8.7, it can be concluded that the hydraulic head pattern west of Lake Nasser did not reveal significant changes from 1998 to 2000. Contrary to the expected dynamics, the recharge front regressed slightly at this time. This can be proved by the 150-m contour line passing through the observation well Ow4. This regression is due to the drop of the level of Lake Nasser from 182 m amsl in 1997 to 175 m amsl in 2000.

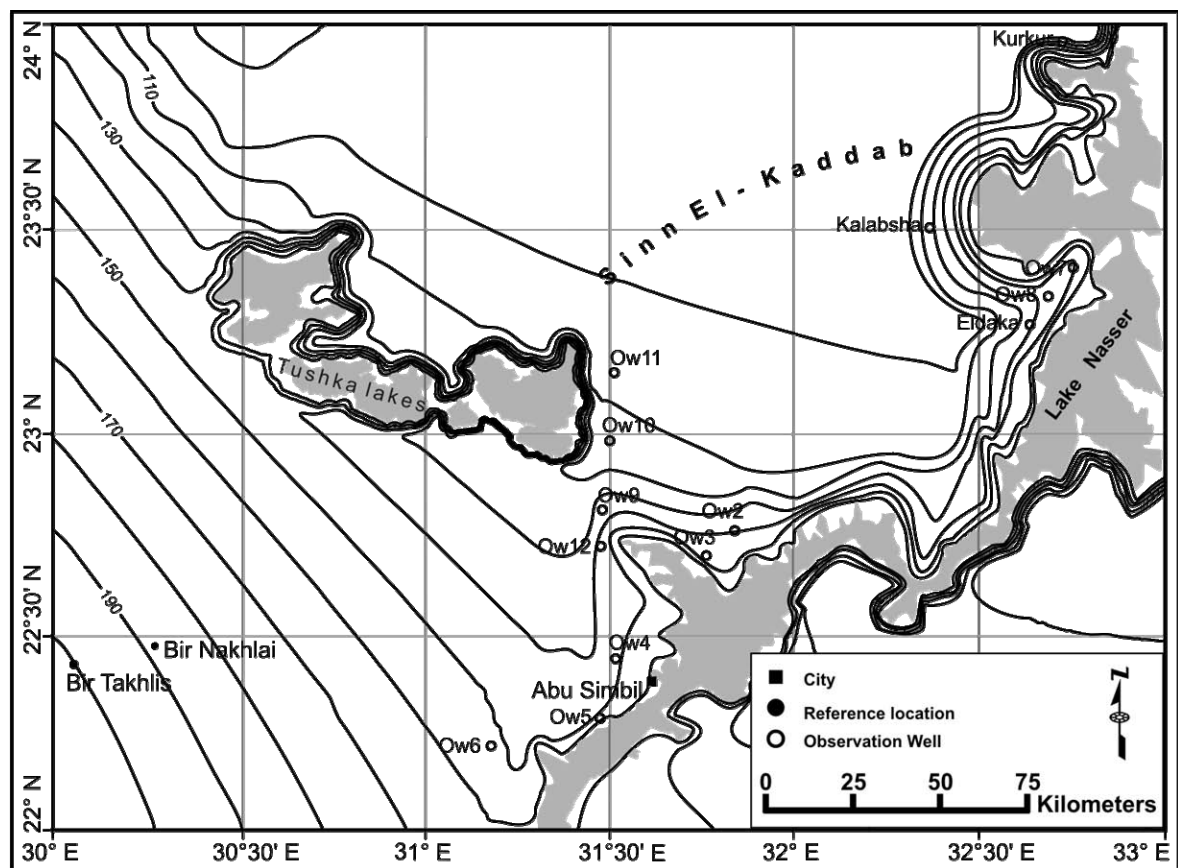


Figure 8.7. Contour map represents the distribution of the hydraulic head around Lake Nasser and the Tushka area in 2000.

In the Tushka depression, significant changes of the hydraulic head values and pattern have occurred on account of the creation of the Tushka lakes. An average increase of about 25 m in the hydraulic head at this depression is encountered. These changes are emphasized by the distribution of the hydraulic head in the study area in 2005 as shown in Figure 8.8. Figure 8.8 indicates that the recharge front moves preferably to the northwest, west, and southwest. These pretended directions of the recharge front are due to the fact that the rising water level of the lakes leads to a damming up of the groundwater flowing from southwest to northeast. The northeast of the lakes area is reduced because of basement outcrops. To the northeast the area is characterized by relatively bad hydraulic conductivity as well as the presence of uplifts that obstruct the lateral movement of the groundwater. Also to the east, the transmissivity is reduced due to the low thickness of sediments and basement outcrops (see Figure 8.1).

The recharge from the Tushka lakes directly affects the groundwater potentiality of the Darb El-Arbaein area south of the Kharga oasis. The recharge front moved about 3 km from 1998 until 2005 to the west and northwest away from Tushka lakes. That means it moves about 425 m/year towards the west and northwest.

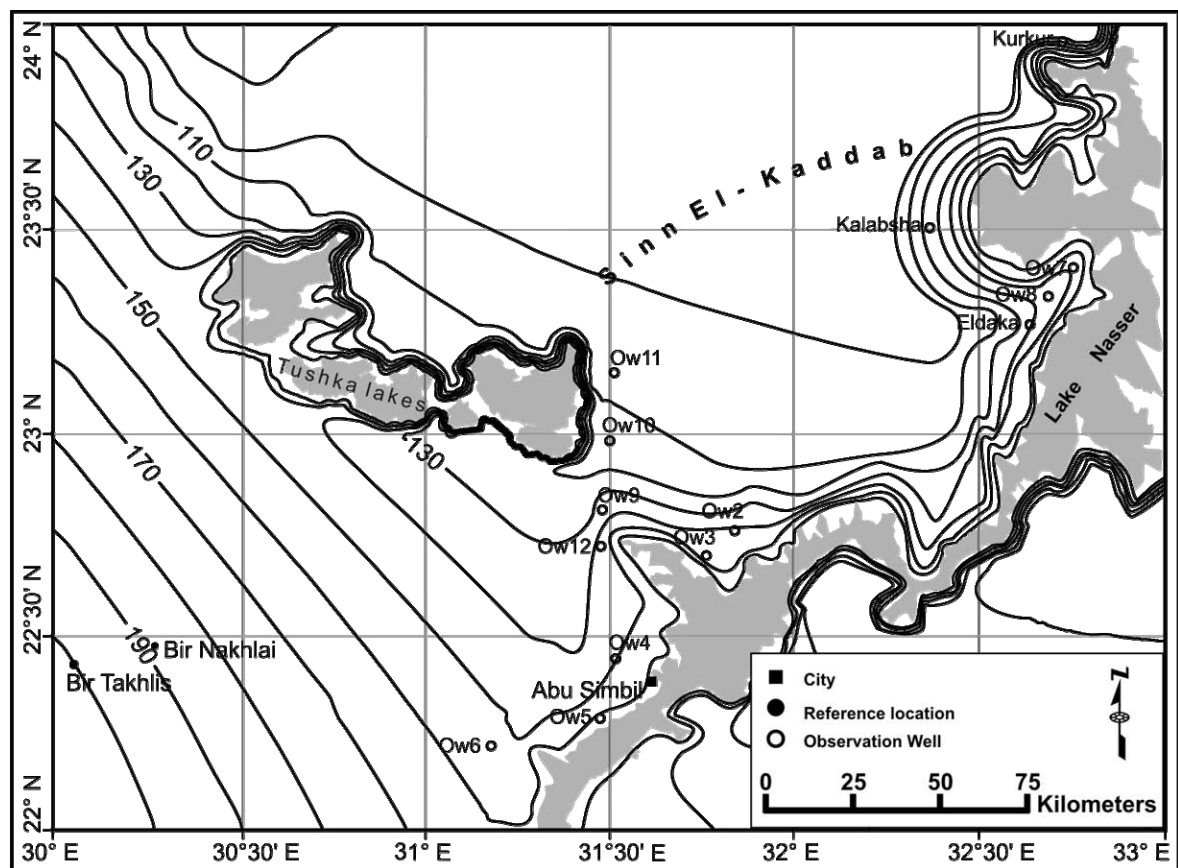


Figure 8.8. Contour map represents the distribution of the hydraulic head around Lake Nasser and the Tushka area by 2005.

8.5 Recharge from the lakes

The cumulative rise in surface water levels of Lake Nasser and the Tushka lakes, in conjunction with the comparatively low groundwater levels around these surface water bodies, encouraged a rapid increase in the hydraulic gradients and thus an increase in the interaction flows (fluxes) from the surface water bodies into groundwater. Therefore, surface water losses from Lake Nasser and the Tushka lakes contribute greatly to raising groundwater level, consequently, to recharge the NSAS close to them. The dynamic behavior of the system can be visualized by means of quantitative analyses in terms of water flux and mass balance. Figure 8.9 shows the cumulative flux from Lake Nasser and the Tushka lakes into the aquifer system during the simulation period from 1960-2005. Figure 8.9 indicates that the aquifer was recharged by an amount of $40.4 \times 10^{10} \text{ m}^3$ from Lake Nasser in just one year after the constructing of the Aswan High Dam. The cumulative recharge from Lake Nasser increased successively to reach an amount of $8.91 \times 10^{11} \text{ m}^3$ in 1998. The net cumulative recharge from Lake Nasser and the Tushka lakes in year 2005 is calculated to be about $9.66 \times 10^{11} \text{ m}^3$. Certain key parameters affect the sensitivity of the aquifer to recharge through the interactions between the lakes and the

aquifer. The most important factors are the lake levels, the hydraulic gradient of the groundwater, the aquifer thickness, and the hydraulic conductivity of the sediments.

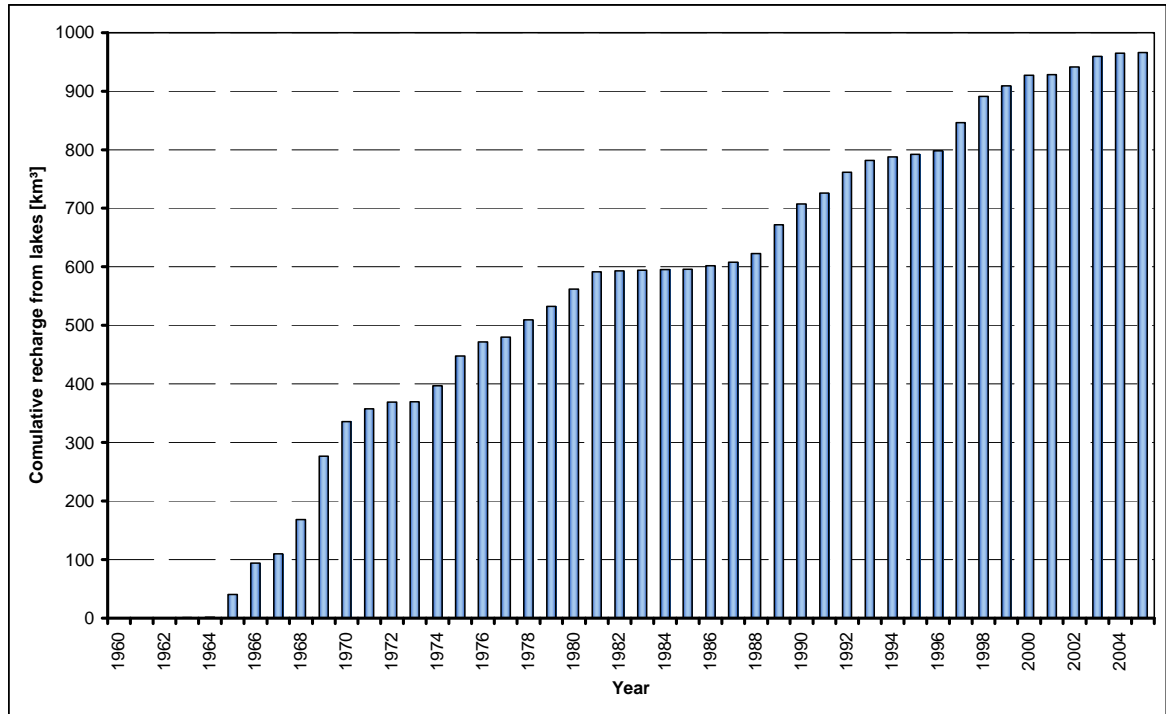


Figure 8.9. The cumulative recharge from Lake Nasser and the Tushka lakes to the NSAS for the period 1964-2005.

9

Summary and Conclusions

Outlines

The Nubian Sandstone Aquifer System is a closed, non-renewable transboundary groundwater system of a massive thickness and high water storativity but had been undergoing arid to hyperarid conditions and has no significant recharge since about 5,000 years. It has a wide extent over Egypt, southeastern Libya, northeastern Chad, and northwestern Sudan and lies between latitudes 14° and 30° N and longitudes 19° and 34° E. The NSAS consists mainly of four structural basins, the major among them are the Kufra Basin and the Dakhla Basin. The NSAS comprises an area of about 2.35×10^6 km² and has a maximum thickness of 4,500 m. The ground surface of the aquifer reveals a general slope from SSE to NNW and ranges roughly from about 3,000 m to -134 m (amsl). The hydraulic head ranges from 570 m (amsl) west of the Darfur area in Sudan and -78 m in the north of the system, in the Qattara Depression in Egypt. The modeled geometric volume is about 3.5×10^6 km³ and the calculated groundwater volume is about 212×10^3 km³. The exploitation of the aquifer resources is increasing rapidly forming large cones of depression around the groundwater extracting fields.

Objectives, model construction, and calibration

An integrated GIS-supported approach was proposed to create and develop a transient three-dimensional groundwater flow model for the NSAS in order to define and calibrate the regional boundary conditions, to simulate the groundwater management options for the different stressed areas within the aquifer, and to predict the environmental impact of the present and future groundwater extraction schemes on the different exploitation sites. A great effort was given to the development of a coherent, reliable conceptual model for the NSAS to mimic the real world as close as possible. The regional model was used afterward for the development and integration of local-scale (refined) models for the Dakhla oasis, Lake Nasser and the Tushka area. The regional model was calibrated under the transient

conditions using the trial and error method. The period 1960-2005 was chosen as a calibration period based on the availability and temporal distribution of the data. The calibration process indicated that the direction of the groundwater flow within the regional model area is kept by the original trend of the initial head postulated by Ball (1927) and Sandford (1935). However, the values and local trends of these contours showed some changes within the depressions; like in the Kufra, Dakhla and Kharga oases and the development areas; like in the East Oweinat, where new contour lines with lower values appeared.

Current situation

By 2005 the simulation indicated that the average decline in hydraulic head ranges from 5 m in East Oweinat area to 30 m in Kharga oasis. The depth to groundwater was five, 11 and 22.5 m (bgl) in the Kufra oasis, Kharga oasis and the East Oweinat area, respectively. While in the other Egyptian oases, the potentiometric level was still above ground level, which means that the extraction wells were still under free flowing conditions. The calibrated model was used for further prediction simulations to investigate the response of the aquifer to the different management options in the next 100 years. The scenarios of these prognostic calculations were elaborated disregarding the ongoing theoretical discussions about the admissibility of prognostic calculations. The parameters of the calibrated model were kept constant and the boundary conditions were adapted to the scenarios.

Prediction schemes and results of regional model

Based on the actual and full capacity, planned extraction rates of the NSAS, five extraction scenarios were suggested in an attempt to investigate the most feasible groundwater management option in terms of the economic depth to groundwater (economic lifting depth) and the groundwater demand.

The simulation of the actual extraction rates of scenario 1 ($1,828.3 \times 10^6$ m³/y) indicated that by 2100 the average drawdown in the Dakhla and the Kharga oasis will be about 55 m and in the Siwa oasis will be only 15 m, while in the Kufra oasis and the East Oweinat area the average drawdown will not exceed 16 and 18 m, respectively. At the end of the simulation the free flowing phenomenon will disappear all over the modeled area and the average depth to groundwater will range from 5 m (bgl) in the Bahariya oasis to 36 m in the Kharga oasis. In 2100 a groundwater volume of 354 km³ will be extracted from the aquifer storage. It is concluded that by 2100 the lifting depth will be still economic and the current extraction rates might be under the permissible, affordable rates for the groundwater management of the NSAS.

The simulation of the full capacity, planned extraction rates of scenario 5 ($6,077.3 \times 10^6$ m³/y) resulted in severe changes of the hydraulic head patterns within almost all of the

stressed areas of the NSAS during the simulation period. The resulted average decline in hydraulic head by 2100 will exceed 130 m in the Kufra oasis and the East Oweinat area. The average depth to groundwater will increase successively during the simulation to overtake the limit of 100-m (bgl) of the economic lifting depth in the Kufra oasis and the East Oweinat area by 2100. The phenomenon of the free flowing wells will disappear from the entire domain by 2030. Although the groundwater volume extracted from the aquifer storage until 2100 exceeds roughly 1,400 km³, which is only 0.66% from the total groundwater volume of the NSAS, the consequences are considered unpleasant, whereas, the most of this volume was extracted from the oases or populated areas. At these areas the decline in potentiometric surface and the depth to groundwater are increasing successively; accordingly, the groundwater withdrawal will be too expensive or probably impossible. The cones of depression that cover the Dakhla, Farafra, and Bahariya oases are engaged to form a huge, connected cone of depression, which, in turn, induces the drawdown to increase. In the East Oweinat area the cone of depression will overtake the state's boundary between Egypt and Sudan. Since the natural annual recharge to NSAS is too low to support the planned, large-scale irrigated agricultural development that rely on groundwater, the plan for groundwater development should be based upon an aquifer depletion concept, which means that every extracted cubic meter from the NSAS is groundwater mining.

Optimal management option, regional model

Based on the groundwater availability and demand, the proposed economic lifting depth, and the development ambitions for the NSAS, the application of the extraction rates of scenario 3 ($3,952.8 \times 10^6$ m³/y) was found to be the best management option that meets these topics. As by 2100 the average depth to groundwater will not exceed 90 m and 85 m (bgl) in the Kufra and the East Oweinat, respectively (where the highest extraction rates were applied).

Local model-Dakhla

The Dakhla oasis, which consists of 17 settlements, is the biggest oasis in southwestern desert of Egypt. The first scenario was implemented assuming the actual extraction rates (1.2×10^6 m³/d) are constant until the end of the simulation period (in 2100). By 2005 several changes could be seen in the hydraulic head patterns and flow directions, which are indicated by the development of local flow patterns and noticeable cones of depression as a response to the successive groundwater extraction in the last 45 years. A maximum drawdown of 35 m was reached at the east and middle of the oasis. In spite of that, most of the wells in the middle and west of the oasis are still free flowing. By 2100 the cone of depression will overtake the boundaries of the oasis. A maximum value of drawdown of 75 m was recorded in the middle of the oasis. Only few wells at the west of the oasis will be

still flowing and the rest will dry out. However, the depth to groundwater at all the cultivatable areas within the oasis will be still less than 75 m (bgl). The average annual change in hydraulic head of the entire simulation period would be 0.57 m per year. Based on these results, it is concluded that the implementation of scenario 1 is affordable for the groundwater management in the Dakhla oasis. However, this scenario is still under the permissible potentiality of the NSAS in the Dakhla oasis.

Optimal management option, Dakhla model

The simulation of scenario 3 (1.46×10^6 m³/d) resulted in an average decline in the potentiometric surface of 75 m in the Dakhla oasis and a maximum value of 105 m in the middle of the oasis by 2100. However, the drawdown did not exceed 30 m at the end of the simulation on the western side of the oasis. Depth to groundwater in the west of the oasis will mostly be close to the ground level in all well fields and will not exceed 25 m (bgl) by 2100. In the middle of the oasis, depth to groundwater will range between 50-75 m and will go deeper to the east of the oasis to reach a value of about 100 m. Based on the groundwater potentiality in and development ambitions in the Dakhla oasis, this scenario was suggested to be the best development option for the domestic, agricultural and industrial activities for the coming 100 years. The implementation of scenarios 4 and 5 will be responsible for creating a huge cone of depression that will be distant beyond the oasis' borders and the depth to groundwater will exceed 100 m (bgl). Besides, the potentiometric head will drop below the bottom of the first aquifer. This, in turn, will affect the phreatic water levels and springs. Therefore, the wells extracting the first aquifer will dry out.

Local model, Lake Nasser

Nasser Lake was formed due to the construction of the Aswan High Dam (1959-1969) and has a storage capacity of 157 km³. The rising water levels of Lake Nasser since 1964 helped raising the groundwater level of the NSAS in the vicinity of its bank. This rise in the groundwater level was calculated to have an average value of about 25 m in the observation wells lying within a distance of 25 km from the lake. These wells reflected the fluctuations of the lake level during the simulation. The average increase in hydraulic head within the first inundated 20 km strip away from Lake Nasser is 32 m until 1998. Based on this conclusion, the groundwater volume that was added to the aquifer storage in this area is calculated to be about 281.5 km³. In Abu Simbil and Tushka depression, the average movement rates of the recharge front were 1.7 km/y and 0.8 km/y respectively. After the development of the Tushka lakes, an average increase of about 25 m in the hydraulic head in the vicinity of the Tushka lakes (5 km strip) is encountered, especially to the west of the lakes. The recharge front moved about 3 km from 1998-2005 to the west and northwest away from the Tushka lakes. That means it moves about 425 m/year towards the west and northwest. The cumulative recharge from Lake Nasser increased successively to reach an

amount of 8.91×10^{11} m³ in 1998. The net cumulative recharge from Lake Nasser and the Tushka lakes in year 2005 is calculated to be about 9.66×10^{11} m³.

Outlook and prospects

Close to the northern boundary of the NSAS, the situation is a little bit complicated due to the presence of the Saline-Freshwater Interface. This boundary was considered in this study temporally constant, in spite of the fact that slight fluctuations are not completely excluded. At the end of the regional-model simulations in this study, the groundwater level decreased intensively in the Bahariya oasis, which means that the groundwater level gets close to the mean sea level. This fact, in turn, raises the question whether if the Saline-Freshwater Interface will be induced to move southward. Therefore, local groundwater flow/transport modeling is due to be carried out for this region to focus on this topic.

The groundwater mining will certainly affect the hydrochemical properties of the groundwater. Hence, Hydrochemical investigations are still needed in each stressed area within the NSAS to investigate the impacts of the successive groundwater withdrawal and irrigation activities on the water quality.

Isotope-dating techniques for the groundwater in the area west of Lake Nasser are to be carried out to help in combination with groundwater modeling for an accurate estimation of the water volume that is being recharged to the aquifer storage from Lake Nasser.

Further hydrogeological investigations in the Tushka depression should be carried out to determine the vertical hydraulic conductivity in this area to ensure the precise simulation of the groundwater-lake interaction between the NSAS and the Tushka lakes.

Due to the huge, modeled volume of the NSAS and the scarcity of the data, big data gaps are still to be filled to improve the consistency and reliability of the modeled aquifer geometry and parameters.

Since the current groundwater flow model for the NSAS is GIS-supported, it can easily be used for any further simulation purposes. It can also be updated to match the newly situations or to be improved when new data are obtained.

Bibliography

- Abu-Zeid, KM (1998). Modern Technology Tools for Water Management. Advanced Short Course on Applications of Modern Technology in Water Resources. MPWWR, internal report, Cairo, Egypt, 37 pp.
- Alaily, F, Bornkamm, R, Blume, HP, Kehl, H, Zieliski, M (1987). Ecological investigations in the Gilf Kebir, southwest Egypt. *Phytocoenologia*, 15: 1-20.
- Allam, A, Saaf, E, Dawoud, M (2002). Desalination of brackish groundwater in Egypt. *Desalination*, Vol. 152: 19-26.
- Altorkomani, G (1999). The geomorphology of Tushka and development potentialities. *Egypt Geographic Soc.*, N4: 218.
- Aly, A, Froehlich, K, Nada, A, Awad, M, Hamza, M, Salem, W (1993). Study of environmental isotope distribution in the Aswan High Dam Lake (Egypt) for estimation of evaporation of lake water and its recharge to adjacent groundwater. *Environmental Geochemistry and Health*, 15(1): 37-49.
- Ambroggi, RP (1966). Water under the Sahara. *Scientific American*, 241: 21-29.
- Amer, A, Nour, S, Meshriki, M (1981). A finite element model for the Nubian aquifer system in Egypt. *Proc. Int. Conf. Water Resources Management in Egypt*, Cairo, pp 327- 361.
- Anderson, MP, Woessner, WW (1992). *Applied Groundwater Modeling, Simulation of flow and advective transport*. Academic Press Inc., San Diego, 381 pp.
- Attia, FA (1985). Management of water systems in Upper Egypt. PhD thesis, Cairo University, Egypt.
- Attia, FA, (1998). Mediterranean Document on Groundwater. Groundwater resources management in Egypt, in the concept of IWRM. In: *Proceedings of 7th Nile conference 15-17 March*, Cairo, 11:1-16.
- Attia, MI (1954). Groundwater in Egypt. *Desert Inst. Bull.*, Cairo, 4 (1): 198-213.
- Awad, GH, Ghobrial, MG (1965). Zonal stratigraphy of Kharga Oasis. *Geol. Surv., U. A. R.*, Paper No. 34, 77 pp.
- Bakhbakhi, M (1999). Nubian Sandstone Aquifer System. IHP-V, Technical Documents in Hydrogeology, 42: 75-81. UNESCO, Paris.
- Bakhbakhi, M (2006). Nubian Sandstone Aquifer System. IHP-VI, series on groundwater, 10: 75-81. UNESCO, Paris.

- BALL, J (1927). Problems of the Libyan Desert. *Geographical Journal*, 70: 21-38, 105-128, 209- 224.
- Barberis, JA (1986). International ground water resources law. Food and Agricultural Organization Legislative Study, 40, 67 pp.
- Barnes, R (1991). The Variogram Sill and the Sample Variance. *Mathematical Geology*, 23(4): 673-678.
- Barthel, KW, Boethcher, R (1987). Abu Ballas Formation, a significant lithostratigraphic unit of former "Nubian Series". *Mitt. Bayer. Staats. Paleont. Hist. Geol.*, 18: 153-166.
- Barthel, KW, Hermann-Degen, W (1981). Late Cretaceous and Early Tertiary stratigraphy in the Great Sand Sea and SE margins (Farafra and Dakhla oases), South Western Desert, Egypt. *Mitt. Bayer. Staats. Paleont. Hist. Geol.*, 21: 141-182.
- Beadnell, HL (1905). The relation of the Eocene and Cretaceous systems in the Esna-Aswan reach of the Nile Valley. *Quat. J. Geol. Soc.*, 61: 667-678.
- Bear, J (1972). Dynamics of fluids in porous media. 1st ed. American Elsevier Inc., New York, 764 pp.
- Bellini, E, Giori, I, Ashuri, O, Benelli, F (1991). Geology of Al Kufra Basin, Libya. In (Salem, M, Sbeta, A, Bakbak, M). *The geology of Libya*, volume 6, Elsevier, Amsterdam, 2155 pp.
- Bellini, E, Massa, D (1980). A stratigraphic contribution to the Paleozoic of the southern basins of Libya. In. Salem, MJ, Brusrewi, MT (eds.). *The Geology of Libya*. Elsevier, Amsterdam, pp 1-289.
- BGR (2006). Draft of the Groundwater Resources Map of the World 1/25 M at IAH Congress, Beijing. Federal Institute for Geosciences and Natural Resources. <http://www.bgr.bund.de>
- Bohling, G (2005). Introduction to geostatistics and Variogram Analysis, unpublished. <http://people.ku.edu/~gbohling/cpe940/Variograms.pdf>.
- Bourne, C (1992). The International Law Commission's draft articles on the law of international watercourses: Principles and planned measure. *Colorado J. Int. Env. Law and Policy*, 3, 65–92.
- Brook, G, Embabi, N, Edwards, R, Cowart, J, Dabous, A (2002). Djara Cave in the Western Desert of Egypt. Morphology and Evidence of Quaternary Climatic Change. *Cave and Karst Science*, 29 (2): 57-65.
- Brookes, IA (1993) Geomorphology and Quaternary Geology of the Dakhleh Oasis Region, Egypt. *Quaternary Science Reviews* 12: 529–552.
- Carrera, J, Neuman, SP (1986). Estimation of aquifer parameters under transient and steady state conditions, 2, uniqueness, stability and solution algorithms. *Water Resources Research*, 22(2): 211-227.
- CEDARE (2001). Regional Strategy for the Utilization of the Nubian Sandstone Aquifer

- System. Volume II. Centre for the Environment and Development for the Arab Region and Europe, Hydrogeology, pp 1-142. Cario, Egypt.
- CEDARE (2002). Regional Strategy for the Utilization of the Nubian Sandstone Aquifer System. Draft final report, pp 22-82. Centre for Environment and Development for the Arab Region and Europe, Heliopolis Bahry, Cairo, Egypt.
- Chiles, JP, Delfiner, P (1999). Geostatistics, modeling Spatial Uncertainty. Willy, New York, 695 pp.
- Cloudsley-Thompson, JL (1984). Sahara Desert. 1st ed. Perhamon Press, Oxford, 384 pp.
- Conoco (1987). Geologic Map of Egypt. Egyptian General Authority for Petroleum (UNESCO joint map project), 20 sheets, scale 1:500 000. Cairo, Egypt.
- Cooley, RL, Naff, RL (1990). Regression modeling of groundwater flow. USGS, Techniques for Water Resourced Investigations, 03-B4, 232 pp.
- Cooper, HH, Jacob, CE (1946). A generalized graphical method for evaluating formation constants and summarising well field history. Transactions, American Geophysical Union. 27: 526- 534.
- Cressie, NAC (1990). The Origins of Kriging. Mathematical Geology, 22: 239-252.
- Cressie, NAC (1991). Statistics for Spatial Data. John Wiley and Sons Inc., New York, 920 pp.
- D'Agnese, FA, Faunt, CC, Hill, MC, Turner, AK (1999). Death Valley regional groundwater flow model calibration using optimal parameter estimation methods and geoscientific information systems. Advances in Water Resources, 22(8): 777-790.
- Dagan, G (1989) Flow and Transport in Porous Formations. 1st ed. Springer Verlag, Heidelberg, 465 pp.
- Dagan, G (1997). Stochastic modeling of Flow and transport: the broad perspective. In Dagan and Neuman, 1997(eds.). Subsurface flow and transport: a stochastic approach. International Hydrology Series, UNESCO, Cambridge University press, 255 pp.
- Dahab, KA (1998). Review on the hydrostratigraphic section in Egypt with special emphasis on their recharging sources. Bull. Geol. Survey, Cairo, Egypt, 45: 61-89.
- Darcy, H (1856). Les fontains publiques de la ville de Dijon. V. Dalmont, Paris, 647 pp.
- Davis, JC (1986). Statistics and data analysis in Geology. 2nd ed. John Willy, New York, 646 pp.
- Delleur, JW (1999). The Handbook of Groundwater Engineering. 1st ed. CRC Press and Springer, Boca Raton and Heidelberg, 949 pp.
- Deutsch, CV, Journel, AG (1992). GSLIB-Geostatistical Software Library and User's Guide, Oxford University Press, New York, 340 pp.
- Diab, M, Mahammed, MA, Rizk, ZS (1995). The role of geology, hydrogeology and

- human activities in the contamination of shallow water resources northwest of the Rosetta Nile Branch, Egypt. *J. Faculty Sci. Unite Arab Emirates Univ.* 8(2): 260-291.
- Diab, MS (1972). Hydrogeological and Hydrochemical studies of the Nubian Sandstone water-bearing complex in some localities in United Arab Republic. PhD Thesis, Assiut University, Egypt.
- DMA-TM8358.2 (1989). The Universal Grids: Universal Transverse Mercator (UTM) and Universal Polar Stereographic (UPS). Defense Mapping Agency, Technical Manual, 49 pp.
- DMA-TR 8350.2 (1997). World Geodetic System 1984: Its Definition and Relationship with Local Geodetic Systems. Defense Mapping Agency, Technical Report, Third Edition, 54 pp.
- Doherty, J (1994). PEST, Model-independent parameter estimation. User's Manual, 336 pp.
- Doherty, J, Brebber, L, Whyte, P (1994). PEST Model independent parameter estimation. User's Manual. Watermark numerical computing, Brisbane, 122 pp.
- Domenico, PA, Schwartz, W (1998). Physical and Chemical Hydrogeology. 2nd ed. John Wiley & Sons, New York, 506 pp.
- Draper, NR, Smith, H (1981). Applied regression analysis. 2nd ed. John Wiley & Sons, New York, 407 pp.
- El Gaby, S, Greiling, RO (1988). The Pan African Belt of Northeast Africa and Adjacent Areas. Vieweg, Braunschweig, pp 227-288.
- Ebraheem, A (2003). A large-scale groundwater flow model for the New Valley area with a telescoping mesh on Kharga oasis, SW Egypt. *N. Jahrb. für Geologie und Paläontologie Abh.*, 228: 153-174.
- Ebraheem, A, Garamoon, H, Riad, S, Wycisk, P, Seif El-Nasr, A (2003). Numerical modeling of groundwater resource management options in the East Oweinat area, SW Egypt. *Environmental Geology*, 44 (4): 433-447.
- Ebraheem, A, Riad, S, Wycisk, P, Sefelnasr, A (2004). A local-scale groundwater flow model for modeling ground-water resources management options in Dakhla Oasis, SW Egypt. *Hydrogeology Journal* 12 (6): 714-722.
- Ebraheem, A, Riad, S, Wycisk, P, Seif El-Nasr, A (2002). Simulation of impact of present and future groundwater extraction from the non-replenished Nubian Sandstone Aquifer in southwest Egypt. *Environmental Geology*: 43 (1-2): 188-196.
- Eckstein, Y, Eckstein, GE (2005). Transboundary Aquifers: conceptual models for development of international law. *Ground Water*. Vol. 43(5): 679-690.
- Edmunds, WM, Wright, EP (1979). Groundwater recharge and palaeoclimate in the Sirte and Kufra Basins, Libya. *Journal of Hydrogeology*, 40: 215-241.
- El Gaby, S (1985). On the relation between tectonics and ore mineral occurrences in the

- basement complex of the Eastern Desert of Egypt. Proc. 6th Int. Conf. Basement Tectonics, Santa Fe, N.M. USA, pp 652-671.
- El Gaby, S, List, F, Tehrani, R (1990). The basement complex of the Eastern Desert and Sinai. In Said, R (ed). The Geology of Egypt, Balkema, Rotterdam, pp175.
- El Khawaga, ML, Philobbos, ER, Riad, S (2005). Stratigraphic lexicon and explanatory notes on the geological map of the South Western Desert, Egypt, 81 sheets, scale 1:250,000. UNESCO, Cairo.
- El Naggar, ZM (1970). On a proposed lithostratigraphic subdivision for the Late Cretaceous- Early Paleogene succession in the Nile Valley Area, Egypt. 7th Arab Petrol. Congr. Kuwait, pp 1-50.
- El Ramly, M, Hussein, A (1985). The ring complexes of the Eastern Desert of Egypt. J. Afr. Earth Sci., 3: 77-82.
- El-Baz, F (1992). Origin and evolution of sand seas in the Great Sahara and implications to petroleum and groundwater exploration. In Sadek, A (ed). Geology of the Arab World, vol. II, Cairo University Press, Cairo, Egypt, pp 3-17.
- El-Baz, F (1998). Sand accumulation and groundwater in the Eastern Sahara. Episodes, 21(3): 147-151.
- El-Baz, F, Mainguet, M (1981). Dune forms in the Great Sand Sea and applications to Mars: reports of planetary geology program. NASA, Tech. Memo., 84211: 244-246.
- Elewa, HH (2006). Water resources and geomorphological characteristics of Tushka and west of Lake Nasser, Egypt. Hydrogeology Journal, 14: 942-954.
- El-Gezeery, N (1960). On the geology of Kharga Oasis, El-Kharga area. Internal report, Geol. Surv. and Min. Res. Dept., Cairo, pp 1-59.
- El-Sayed, M (1995). Duricrust and karst pinnacles in and around Farafra Oasis, Western Desert, Egypt. Sedimentology of Egypt, 3: 27-38.
- El-Shazly, E, Abdel Hady, M, El-Kassas, I, El-Amin, H, Abdel Megid, A, Mansour, S, Tamer, M (1977). Geology and groundwater conditions of Tushka basin area, Egypt, utilizing landsat satellite images. Remote Sensing Center, Academy of Scientific Research and Technology, EGS Journal, vol. 1, No.1, 57-64, Cairo, Egypt.
- EL-Younsy, AR (1978). The geology of the area northwest of Kharga Oasis, Western Desert, Egypt. MSc. Thesis, Assiut University, Egypt.
- El-Younsy, AR (1984). Contribution to the Geology of the New Valley area, Western Desert, Egypt. PhD Thesis, Assiut University, Egypt.
- Embabi, NS (1989). Barchans of the El Kharga depression. In El Baz, F, and Maxell, TA (eds). Desert landforms of South West Egypt, a basis for comparison with Mars. NASA, Cr-3611: 141-156.
- Euro and Pacer Consultant (1983). Regional development plan for the New Valley. Final

- Report, Vol. 1, Ministry of Development, Cairo, pp 32-54.
- Ezzat, MA (1974). Groundwater Series in the Arab Republic of Egypt. Exploitation of Groundwater in El Wadi El Gedid Project Area. General Desert Development Authority, Ministry of Irrigation, Parts I-IV. Cairo, pp 614.
- Ezzat, MA (1974). Groundwater Series in the Arab Republic of Egypt: Exploitation of Groundwater in El-Wadi El Gedid Project Area. General Desert Development Authority, Ministry of Irrigation, Cairo, pp 105.
- Ezzat, MA (1975). Hydrogeological conditions of Dakhla and Kharga area, Groundwater series in A. R. E. exploitation of groundwater in El-Wadi El-Gidid project area, part III, Gen. Des. Develop. Org., Cairo, pp 107.
- Ezzat, MA (1976). Exploration of Groundwater, Kharga Oasis. Desert irrigation, Ministry of Irrigation, Cairo, Egypt, pp 203.
- Fabritz, JE (1995). A two dimensional numerical model for simulating the movement and biodegradation of contaminants in a saturated aquifers. Msc. Thesis, the University of Washington, Seattle, Washington.
- FAO (1997). Treaties Concerning the Non-navigational uses of International Watercourses. Food and Agriculture Organization, Legislative Study No. 61, Rome, 291 pp.
- Farr, TG, Kobrick, M (2000). Shuttle Radar Topography Mission produces a wealth of data. Amer. Geophys. Union Eos, 81: 583-585.
- Fetter, CW (1994). Applied Hydrogeology. 3rd ed. Prentice Hall, New Jersey, 691 pp.
- Fletcher, R (1980). Practical methods of optimization. John Wiley & Sons, Chichester, 120 pp.
- Focazio, MJ, Plummer LN, Bohlke, JK, Busenberg, E, Bachman LJ, Powars, DS (1998). Preliminary estimates of residence times and apparent ages of ground water in the Chesapeake Bay watershed and water quality data from a survey of springs. USGS, Water-Resources Investigations, Report 97-4225, 75 pp.
- Foster, S, Loucks D (2006). Non-renewable groundwater resources. UNESCO, IHP-VI, Series on groundwater, No. 10, Paris, 81 pp.
- Francke, OL, Reilly, TE, Bennett, GD (1987). Definition of boundary and initial conditions in the analysis of saturated groundwater flow systems; an introduction. Techniques of Water Resources Investigations, 03-B5, USGS, pp 15-56.
- Freeze, RA, Cherry, JA (1979). Groundwater. Prentice-Hall, Englewood Cliffs, 604 pp.
- Freeze, RA, Witherspoon, PA (1967). Theoretical analysis of regional groundwater flow: 2. effect of water table configuration and subsurface permeability variation. Water Resources Research. 3: 623-624.
- GALND (1998). Statistics and information periodical about the authority activities. General Authority of Nasser Lake Development, internal unpublished report (in Arabic), p 150.

- Garg, SK, Pritchett, JW (1980). Determination of Effective Well Block Radii for Numerical Reservoir Simulations. *Water Resources Research* 16 (4):665-674.
- Ghobrial, MG (1967). The structural geology of Kharga Oasis. *Geol. Surv. Min. Res. Dept., Paper No. 43, Cairo, 39 pp.*
- Gossel, W, Ebraheem, AM, Wycisk, P (2004). A very large scale GIS-based groundwater flow model for the Nubian sandstone aquifer in Eastern Sahara (Egypt, northern Sudan and eastern Libya). *Hydrogeology Journal*, 12 (6): 698-713.
- Gourgaud, A, Vincent, PM (2004). Petrology of two continental alkaline intraplate series at Emi Koussi volcano, Tibesti, Chad. *Journal of Volcanology and Geothermal Research* 129(4): 261-290.
- Gras (1988). Geological Map of Sudan 1:1 Million, 16 sheets. Robertson Research, Llundudno.
- Halliday, W (2003). Caves and karsts of northeast Africa. *Int. J. Speleol.*, 32 (1/4): 19-32.
- Hantar, G (1990). North Western Desert. In Said, R (ed). *The geology of Egypt*, Balkema, Rotterdam, pp 293-319.
- Heath, RC (1983). Basic groundwater hydrology. USGS, Washington, Water Supply Paper 2220, 84 pp.
- Heinl, M, Brinkmann, PJ (1989). A Ground Water Model for the Nubian Aquifer System. *IAHS, Hydrological Sciences Journal* 34 (4): 425-447, Wallingford.
- Heinl, M, Thorweihe, U (1993). Groundwater Resources and Management in SW-Egypt. In Meissner, B, Wycisk, P (eds.). *Geopotential and Ecology: Analysis of a Desert Region*. *Catena Supplement* 26: 99-121.
- Hellstroem, B (1939). The subterranean water in the Libyan Desert. *Geofisika Annaler*, 21: 122-153. Stockholm.
- Hermina, M (1967). Geology of the northwestern approaches of Kharga Oasis. *Geol. Surv. Cairo*, 44: 87 pp.
- Hermina, M (1990). The surroundings of Kharga, Dakhla and Farafra oases. In Said, R (ed). *The Geology of Egypt*. Balkema, Rotterdam, pp 259-292.
- Hermina, M, Ghabrial, MG, Issawi, B (1961). The geology of the Dakhla area. Ministry of Ind. Geol. Surv. Mineral Resources, Cairo, 33 pp.
- Hermina, M, Lindenberg, HG (1989). The Tertiary. In Hermina et al. (eds). *Stratigraphic lexicon and explanatory notes on the geological map of Egypt*, 20 sheets, scale 1:500,000. Conoco Inc. Cairo, 264 pp.
- Hesse, KH, Hissene, A, Kheir, O, Schnaecker, E, Schneider, M, Thorweihe, U (1987). Hydrogeological investigations of the Nubian Aquifer System, Eastern Sahara. *Berliner Geowiss. Abh. (A)*, 75: 397-464.
- Hill, MC (1998). Methods and guidelines for effective model calibration; U.S. Geological Survey, Water resources investigations. Report 98-4005, 90 pp.
- Himida, IH (1970). The Nubian artesian basin, its regional hydrogeological aspects and

- palaeohydrological reconstruction. *Journal of Hydrology*, 9: 89-116.
- Hissene, AM (1986). *Geologie und Hydrogeologie des Erdis-Bekkens, NE-Tschad*. Berl. geowiss. Abh., (A), 76:1-67.
- Hughes, RH, Hughes, JS (1992). *A directory of African wetlands*. IUCN, Gland, Switzerland and Cambridge, UK, 820 pp.
- Hume, WF (1925). *Geology of Egypt, vol. 1. The surface features of Egypt, Their determining causes and relation to geological structure*. Egyptian survey Department, Cairo, 408 pp.
- Hume, WF (1965). *Geology of Egypt III*. Egypt Survey Department, 2:1-734, Cairo.
- Hunt, R, Haitjema, H, Krohelski, J, Feinstein, J (2003). Simulating groundwater-lake interactions, approaches and insights. *Ground Water*, 41(2): 227-237.
- IAH (2003). *World Hydrogeological Map*. IAH Commission on Mapping. International Association of Hydrogeologists, <http://www.iah.org>, last accessed: Mai.2007.
- Ibrahim, MM (1956). The origin of the depressions in the Libyan Desert. *Obs. Proc. Geol. Soc. Egypt*, 2 (1): 6-20.
- Idris, H, Nour, S (1990). Present Groundwater in Egypt and the Environmental Impacts. *Environ. Geol. Water Sci. Vol. 16(3)*: 171-177.
- Idris, H, Nour, S (1990). Present groundwater status in Egypt and the environmental impacts. *Environmental Geology*, 16(3): 171-177.
- Inoue, M, Simunek, J, Shiozawa, S, Hopmans, JW (2000). Estimation of aquifer parameters under transient and steady state. *Advances in Water Resources*, 23: 677-688.
- Isaaks, EH, Srivastava, RM (1989). *An Introduction to Applied Geostatistics*. Oxford University Press, New York, 561 pp.
- Issawi, B (1969). The geology of Kukur-Dungul area. *Geol. Surv. Egypt*. 46: 102 pp.
- Jas, C, Klitzch, E, Schandelmeier, H, Wycisk, P (1988). Geological map of NW Sudan and SW Egypt, NF 35 Jabal Uweinat, 1:1 000000.
- Journel, AG (1989). *Fundamentals of Geostatistics in Five Lessons*. American Geophysical Union, Washington D.C, Short course in geology, volume 8: 40 pp.
- Kehl, H, Bornkamm, X (1993). Landscape ecology and vegetation units of the Western Desert of Egypt. In Meissner, B, Wycisk, P (eds). *Geopotential ecology: analysis of a desert region*. *Catena Suppl.* 26: 155-178.
- Kheir, OM (1986). Hydrogeology of Dongola area, northern Sudan. *Berl. geowiss. Abh., (A)*, 74: 1-81.
- Khudeir, A (1983). *Geology of the ophiolite suite of El Rubshi area, Eastern Desert, Egypt*. PhD thesis, Assiut University.
- Kim, J, Sultan, M (2002). Assessment of long term hydrologic impacts of Lake Nasser and related irrigation projects in southwestern Egypt. *J. Hydrology*, 262: 68-83.
- Kleindienst, MR, Churcher, CS, McDonald, MA, Schwarcz, HP (1999). *Geography*,

- Geology, Geochronology and Geoarchaeology of the Dakhleh Oasis Region: An Inter Report. In Churcher, CS. and Mills, AJ (eds). Reports from the Survey of the Dakhleh Oasis 1977–1987, 1–54.
- Klitzsch, E (1979). Zur Geologie des Gilf Kebir Gebietes in der Ostsahara. *Clausth. Geol. Abh.* 30: 113-132.
- Klitzsch, E (1981). Lower Paleozoic rocks of Libya, Egypt and Sudan. In Holland, CH (ed.). *Lower Paleozoic of the Middle East, Eastern and Southern Africa, and Antarctica*. John Wiley & Sons, London, pp 131–163.
- Klitzsch, E (1983). Geological research in and around Nubia. *Episodes*, 3: 15-19.
- Klitzsch, E (1984). Northwestern Sudan and bordering areas; geological developments since Cambrian time. *Berl. Geowiss. Abh., (A)*, 50: 23-45.
- Klitzsch, E (1989). Zur Stratigraphie Nubiens. *Z. dt. geol. Ges.*, 140: 151-160.
- Klitzsch, E (1990). Palaeozoic. In Said, R. (ed). *Geology of Egypt*. Balkema, Rotterdam, pp 393-406.
- Klitzsch, E (1994). Geological exploration history of the Eastern Sahara. *Geol. Rundsc.*, 83: 475- 483.
- Klitzsch, E, List, F, Pöhlmann, G (1987). Geological Map of Egypt. Scale 1:500,000, 20 sheets. Techn Fachhochsch, Berlin.
- Klitzsch, E, Semtner, A (1993). Silurian paleogeography of Northeast Africa and Arabia: An updated interpretation. In Thorweihe, U, Schandelmeier, H (eds). *Geoscientific research in Northeast Africa*, Belkema, Rotterdam, pp 341-344.
- Klitzsch, E, Squyres, CH (1990). Paleozoic and Mesozoic geological history of northeast Africa based upon new interpretation of Nubian strata. *Am. Assoc. Petrol. Geol. Bull.*, 74: 1203-1211.
- Klitzsch, E, Wycisk, P (1987). Geology of the sedimentary basins of northern Sudan and bordering areas. *Berliner Geowiss. Abh., (A)*, 75: 97-136.
- Klitzsch, E, Wycisk, P (1999). Beckenentwicklung und Sedimentationsprozesse in Kratonalen Bereichen Nordost-Afrikas im Phanerozoikum. In Klitzsch, E, Thorweihe, U (eds). *Nordost-Afrika: Strukturen und Ressourcen*, John Wiley & Sons-VCH, Weinheim, pp 61-108.
- Knetsch, G, Yallouze, M (1955). Remarks on the origin of the Egyptian oases depressions. *Bull. Soc. Geograph. Egypt*, 28: 21-33.
- Krabbenhoft, D, Anderson, M (1986). Use of a numerical ground-water flow model for hypothesis testing. *Ground Water*, 24 (1): 49-55.
- Krige, DG (1951). A statistical Approach to some basic mine valuation problems on the Witwatersrand. *Jour. Chem. Metal. & Mining Soc. South Africa*, 52 (6): 119–139.
- Krige, DG (1952). A statistical analysis of some of the borehole values in the Orange Free State goldfield: *Jour. Chem. Metal. & Mining Soc. South Africa*. 53 (3): 47–64.

- Kroepelin, S (1990). Lower Wadi Howar. *Berl. Geowiss. Abh., (A)*, 120: 223-234.
- Kröpelin, S (1993b). Geomorphology, Landscape evolution and Palaeoclimatics of southeast Egypt. In Meissner, B and Wycisk, P (eds.). *Geopotential and ecology of the Western Desert, Egypt. Catena Supplement*, 26: 31-66. Cremlingen, Catena.
- Kröpelin, S (1999). Terrestrische Paläoklimatologie heute arider Gebiete: Resultate aus dem Unteren Wadi Howar (Südöstliche Sahara/NW-Sudan). In Klitzsch, E and Thorweihe, U (eds.). *Nordost-Afrika: Strukturen und Ressourcen*, John Wiley & Sons-VCH, Weinheim, pp 448-508.
- Kröpelin, S (2001). Inter-Hemispheric Correlation of Monsoon Controlled Climatic Change in Northeast Africa with Climate Evolution in Southwest Africa during the Past 20,000 years. *Geophysical Research Abstracts*, volume 3: 317-323.
- Kuniansky, EL, Danskin, WR (2003). Models gone bad - Common modeling problems and how to solve them. In Poeter et al. (eds). *MODFLOW and More 2003, Understanding through modeling*, Conference Proceedings, Colorado School of Mines, Golden, Colorado, pp 356-360.
- Laeven, MT (1991). Hydrogeological study of the Nile Delta and adjacent desert areas in Egypt with emphasis on hydrochemistry and isotope hydrology. MSc.Thesis, Free University, Amsterdam.
- Langguth, HR, Voigt, R (1980). *Hydrogeologische Methoden*. 1st ed. Springer Verlag, Berlin, 486 pp.
- Leake, SA, Claar, DV (1999). Procedures and computer programs for telescopic mesh refinement using MODFLOW. U.S. Geological Survey, Open-File Report 99-238, 53 pp.
- Lee, TC (1999). *Applied Mathematics in Hydrogeology*. CRC Press, New York, 382 pp.
- Li, H, Yail, Q (2000). A least squares penalty algorithm for inverse problems of steady state aquifer models. *Advances in Water Resources*, 23: 867-880.
- Mainguet, MM (1995). *L'Homme et la Secheresse*. Collection Geographie, Mason, Paris, 335 pp.
- Malys, S, Slater, JA (1994). Maintenance and Enhancement of the World Geodetic System 1984. *Proceedings of ION GPS-94*, Salt Lake City, Utah, vol. 34: 192-301.
- Mansour, HH (1973). Geological and sedimentological studies on the Dakhla Oasis area, Western Desert, Egypt. PhD Thesis, Assiut University, Egypt.
- Mansour, N, Klitzsch, E, Wycisk, P (1993). *Geological Map of Khartoum*. Scale 1:250 000. Techn. Fachhochsch., Berlin.
- Margat, J, Foster, S, Droubi, A (2006). Concept and importance of non-renewable resources. *IHP-V, Technical Documents in Hydrogeology*, 42: 13-24. UNESCO, Paris.
- Marquardt, DW (1963). An algorithm for least-squares estimation of non-linear parameters.

- Journal of the Society for Industrial and Applied Mathematics, 11 (2): 431-441.
- Maxey, GB (1964). Hydrostratigraphic units. *Journal of Hydrology*, 2:124-129.
- Maxwell, TA (1982). Sand Sheet and lag deposits in the southwestern desert: desert landforms of southwest Egypt. In El-Baz, F, Maxwell, TA (eds). *A basis for comparison with mars*, NASA Cr-3611: 157-173.
- McDonald, MG, Harbaugh, AW (1988). MODFLOW, A modular three dimensional finite difference groundwater flow model. USGS, Open file report 83-875, Chapter A1, 586 pp.
- Mehl, SM, Hill, C (2002). Development and evaluation of a local grid refinement method for block-centered finite difference groundwater models using shared nodes. *Advances in Water Resources* 25 (5):497-511.
- Meneisy, M (1990). Volcanicity. In Said, R (ed). *The Geology of Egypt*, Balkema, Rotterdam, pp 157-172.
- Meshref, WM (1990). Tectonic framework. In Said, R (ed). *The Geology of Egypt*, Balkema, Rotterdam, pp 113-155.
- Mildrexler, DJ, Zhao, M, Running, SW (2006). Where are the hottest spots on the earth? *EOS*, 87 (43): 462-463.
- Mitwally, M (1953). Physiographic features of the oases of the Libyan Desert. *Bull. Desert Inst.*, 2: 32-48, Cairo.
- Moore, JE (1979). Contributions of groundwater modeling to planning. *Journal of Hydrology*, 43: 121-128.
- Morgan, P (1990). Egypt in the framework of global tectonics. In Said, R (ed). *The Geology of Egypt*, Balkema, Rotterdam, pp 91-111.
- MPWWR (1999). Groundwater Development and Management Strategies for the New Valley. Ministry of Public Works and Water Resources Internal report, pp 11-22, Cairo.
- Murray, GW (1952). The artesian water of Egypt. *Surv. Dept., Ministry of Finance and Economy*, Paper No. 52, 20 pp.
- Myers, JC (1997). Geostatistical error management: Quantifying uncertainty for environmental sampling and mapping. Van Nostrand Reinhold, New York, 571 pp.
- NASA (2005). Shuttle Radar Topography Mission data sets. National Aeronautics and Space Administration, <http://www.jpl.nasa.gov/srtm>, last accessed, April 2007.
- NASA (2006). Visible Earth, a catalog of NASA images and animations of our home planet. National Aeronautics and Space Administration, <http://visibleearth.nasa.gov>, last accessed, April 2007.
- Neuman, SP (1997). Stochastic Approach to subsurface flow and transport: a view to the future. In Dagan and Neuman (eds.). *Subsurface flow and transport*. International hydrology series, UNESCO, Cambridge University press, pp 231–241.

- Neuman, SP, Witherspoon, PA (1969). Applicability of current theories of flow in leaky aquifers. *Water Resources Research*, 5: 817-829.
- Neumann, K (1989). Holocene vegetation of the Eastern Sahara: Charcoal from prehistoric sites. *The African Archaeological review*, 7: 97-116.
- Nicoll, KA (2001). Radiocarbon Chronologies for Prehistoric Human Occupation and Hydroclimatic Change in Egypt and Northern Sudan. *Geoarchaeology: An International Journal*, 16 (1): 47-64.
- Nour, S (1996). Groundwater potential for irrigation in the East-Oweinat area, Western Desert, Egypt. *Environmental Geology*, 27: 143-154.
- Olea, RA (1999). *Geostatistics for Engineers and Earth Scientists*. Kluwer Academic Publishers, Boston, 303 pp.
- Pachur, HJ (1999). Paläo-Environment und Drainagesysteme der Ostsahara im Spätpleistozän und Holozän, In Klitzsch, E and Thorweihe, U (eds.). *Nordost-Afrika: Strukturen und Ressourcen*, John Wiley & Sons -VCH verlag GmbH, Weinheim, pp 366-445.
- Pachur, HJ, Roepr, HS, Kroepelin, S, Goschin, M (1987). Late Quaternary hydrography of the Eastern Sahara. *Berliner Geowiss. Abh. (A)* 75(2): 331-384.
- Pallas, P (1980). Water Resources of the Socialist People's Libyan Arab Jamahiriya. In Salem, MJ, Busrewil, MT (eds). *The Geology of Libya*, Academic Press, London, vol. 2, pp 539-594.
- Pallas, P, Salem, O (2001). Water resources utilization and management of the Socialist People Arab Jamahiriya. IHP-V, *Technical Documents in Hydrogeology*, 42: 147-172. UNESCO, Paris.
- Pannatier, Y (1996). *VarioWin - Software for Spatial Data Analysis in 2D*. Springer Verlag, New York, 91 pp.
- Peaceman, DW (1978). Interpretation of Well-Block Pressures in Numerical Reservoir Simulation. *Society of Petroleum Engineers Journal* 18 (3):183-194.
- Poeter, E, Hill, M (1997). Inverse Models- A necessary next step in groundwater modeling, *Groundwater*, 35(2):250-260.
- Poulsen, TG (1994). An adoptable two dimensional numerical model for simulating movement of organic pollutants in unsaturated soils. Ms. Thesis, the University of Washington, Seattle, Washington.
- Prickett, T.A. 1967. Designing pumped well characteristics into electrical analog models. *Ground Water* 5 (4):38-46.
- Prickett, TA, Lonquist, CG (1971). Selected digital computer techniques for groundwater resources evaluation. *Illinois state water survey, Urbana Bulletin*, 55: 44 pp.
- Puri, S, Appelgren, B, Arnold, G, Aureli, A, Burchi, S, Margat, J, Pallas, P (2001). Internationally Shared (transboundary) Aquifer Resources Management. A Framework Document. UNESCO/IHP, IHP-VI, Non Serial Documents in

- Hydrology. Paris, France, 71 pp.
- Richter, A, Schanderlmeier, H (1990). Precambrian basement inliers of Western Desert geology, petrology and structural evolution. In Said, R (ed). The Geology of Egypt, Balkema, Rotterdam, pp185-200.
- RIGW (1988). Hydrogeological Map of Egypt, Scale 1:2,000,000. Research Institute for Ground Water, Cairo, Egypt.
- RIGW (1992). Hydrogeological map for the Nile Delta area, Scale 1: 500000. Research Institute for Ground Water, Cairo, Egypt.
- RIGW (1993). The Hydrogeological Map of Egypt. Scale 1:2,000,000. Research Institute for Ground Water, Cairo.
- RIGW (1999). A plan for the development and management of deep groundwater in the Oases. Internal strategy report, Research Institute for Ground Water, Cairo, pp 86.
- RIGW (2001). Southern Egypt development project. Research Institute for Ground Water, unpublished internal report, p 16.
- Robinson, CA, El-Baz, F, Al-Saud, TS, Jeon, SB (2006). Use of radar data to delineate palaeodrainage leading to the Kufra Oasis in the eastern Sahara. *Journal of African Earth Sciences*, 44 (2): 229-240.
- Sacks, L, Herman, J, Konikow, L, Vela, A (1992). Seasonal dynamics of groundwater-lake interactions at Donana National Park, Spain. *Journal of Hydrology*, 136: 123-154.
- Said, R (1961). Tectonic framework of Egypt and its influence on distribution of foraminifera. *Amer. Assoc. Petrol. Geol. Bull.*, 45: 198-218.
- Said, R (1962). *The Geology of Egypt*. Elsevier. Amsterdam, 377 pp.
- Said, R (1990). Geomorphology. In Said, R (Ed). *The geology of Egypt*. Balkema Rotterdam, pp 9-25.
- Salem, MJ, Belaid, MN (1991). *The Geology of Libya*. 3rd Symposium on Geology of Libya, Elsevier, Amsterdam, pp 1713-2096.
- Salem, O (1991). Drinking water demand vs Limitation of supply (1990-2025). Internal report (in Arabic),GWA, Tripoli, pp 16.
- Salem, O (1992). The Great Man-Made River Project: A Partial Solution to Libya's Future Water-Supply. *Water Resources Development*, 8 (4): 63-91.
- Salem, O, Pallas, P (2004). The Nubian Sandstone Aquifer System. In Appelgren, B (ed). *Managing Shared Aquifer Resources in Africa*. ISARM-AFRICA. UNESCO, IHP-VI, Series on Groundwater No. 8: 19-21.
- Sallam, O (2001). Groundwater sustainability for development. MSc. Thesis, Ain Shams University, Egypt.
- Sandford, KS (1935). Geological observations on the southwestern frontiers of the Anglo-Egyptian Sudan and the adjoining part of the southern Libyan Desert. *Q. Geol. Soc. London*, 80: 323-381.

- Schandelmeier, H, Klitzsch, E, Hendriks, F, Wycisk, P (1987a). Structural development of north-east Africa since Precambrian times. *Berliner Geowiss. Abh., (A)*, 71(1): 25-48.
- Schatzman, M (2002). *Numerical Analysis: A Mathematical Introduction*. Clarendon Press, Oxford, 516 pp.
- Seaber, R (1988). Hydrostratigraphic Units. In Back, W., Rosenshein, S., Seaber, R. (eds). *Hydrogeology, The Geology of North America*. Geol. Soc. America Vol. 0-2: 9-14.
- Seber, GAF, Wild, CJ (1989). *Nonlinear regression*. John Wiley & Sons, New York, 768 pp.
- Sefelnasr, A (2002). Hydrogeological studies on some areas on the new Valley governorate, Western Desert, Egypt. MSc thesis, Assiut University.
- Shata, A (1953). New light on the structural development of the Western Desert of Egypt. *Bulletin of Desert Institute*, 5: 63-77, Cairo.
- Shata, A, Knetsch, G, Degens, ET, Munnich, O, El-Shazli, M (1962). The geology, Origin and age of the ground water supplies in some desert areas of U. A. R. *Bull. Inst. Desert Egypt*, 2: 61-124.
- Shatta, A (1962). Remarks on the geomorphology, pedology and groundwater potentialities of the southern entrance of the New Valley. Part 1, The Lower Nuba Area, Egypt, UAR. *Bull. Soc. Geogr. Egypt*, 35: 273-299.
- Sigaev, VN (1959). The main tectonic features of Egypt. An explanatory note on the tectonic map of Egypt, scale 1: 200,000. *Geol. Surv. Cairo*, 39: 26 pp.
- Soltan, ME (1999). Evaluation of groundwater quality in Dakhla oasis (Egyptian Western Desert). *Environmental Monitoring and Assessment*, 57: 157-168.
- Sonntag, C (1984). Autochthonous groundwater in the confined Nubian Sandstone Aquifer. *Berliner Geowiss. Abh., (A)*, 50: 217-220.
- Sonntag, C (1986). A time dependent groundwater model for the Eastern Sahara. *Berliner Geowiss. Abh., (A)*, 72: 124-134.
- Sonntag, C (2001). Assessment methodologies: isotopes and noble gases in Saharan palaeowaters and change of groundwater flow pattern in the past. UNESCO/IHP, IHP-VI, Technical Documents in Hydrogeology, 42: 205-220. UNESCO, Paris.
- Sonntag, C, Christmann, D (1987). Groundwater evaporation from east Saharian depressions by measuring Deuterium and Oxygen-18 in soil moisture. *Berliner Geowiss. Abh., (A)*, 75(2): 385-396.
- Sophocleous, M (2002). Interactions between groundwater and surface water: the state of the science. *Hydrogeology Journal*, 10: 52-67.
- Sun, NZ (1994). *Inverse problems in groundwater modeling*. Volume 6, Kluwer Academic, Dordrecht, pp 337.
- Surfer® 8 User's Guide (2002). *Countouring and 3D surface mapping for scientists and*

- engineers. Golden Software Inc., Colorado, pp 640.
- Tamer, M, Sherif, M, Ahmed, S (1987). Inter-relationship between the High Dam Reservoir and the groundwater in its vicinity. *Asw. Sci. Tech. Bull.*, 8: 11-23.
- Tarantota, A (2005). Inverse problem theory and methods for model parameter estimation. Society for Industrial and Applied Mathematics, Philadelphia, 416 pp.
- Tawadros, E (2001). *Geology of Egypt and Libya*. Balkema, Rotterdam, 480 pp.
- Theis, CV (1935). The lowering of the piezometric surface and the rate and the discharge of well using groundwater storage. *Transactions, American Geophysical Union*. 16: 519-535.
- Thorweihe, U, Heinl M, (1999). Groundwater Resources of the Nubian Aquifer System. UNESCO, IHP V, Technical Documents in Hydrology, 42, 23 pp.
- Thorweihe, U, Heinl, M (1996). Groundwater Resources of the Nubian Aquifer System. Aquifer of major basins, non-renewable water resource, Sahara and Sahel Observatory, Paris, 20 pp.
- Thorweihe, U, Heinl, M (2002). Groundwater resources of the Nubian Aquifer System, NE-Africa. Modified synthesis submitted to: Observatoire du Sahara et du Sahel. OSS, Paris, 23 pp.
- Thorweihe, U, Schandelmeier, H (1993). Geoscientific Research in Northeast Africa. Proc. Int. Conf. Geosci. Research in Northeast Africa, Berlin, 17-19 June 1993. Balkema, Rotterdam, 776 pp.
- Thorweihe, U. & Heinl, M. (2000): Map Hydrogeology of the Nubian Aquifer System. Scale 1:2,500,000. Annex to Thorweihe and Heinl (1996), 23 pp.
- Todd, DK (1980). *Groundwater Hydrogeology*. John Wiley & Sons, New York, 535 pp.
- Townley, LR, Wilson, JL (1980). Description of and user's manual for a finite-element aquifer flow model AQUIFEM-1. Cambridge Massachusetts. Ralph M. Parson Laboratory Technology Adaption Program, Technical Report No. 252: 294 pp.
- UN (2003). Water for people, water for life; the United Nations World Water Development Report, U.N. Sales No. 92-3-103881-8, 36 pp. Barcelona, Spain: UNESCO/Bergahn Books.
- USGS (2000). United States Geological Survey Open File Report 97- 470A, ver. 2.0, <http://pubs.usgs.gov/of/1997/ofr-97-470/OF97-470A/>, last accessed: Mai 2007.
- USGS (2004). SRTM data, USGS Seamless Data Distribution System-Enhanced. United States Geological Survey, <http://srtm.usgs.gov>, last accessed: March 2007.
- USGS GEO-DATA (2004). Geologic Data and Hazards of the World. United States Geological Survey, Geological Division, Geological Data. Reston, USA, <http://geode.usgs.gov/>, last accessed: March 2007.
- Van Dam, JC, Wessel, J (1993). Transboundary river basin management and sustainable development. Technical Documents in Hydrology, Vol. 2, 354 pp, UNESCO, Paris.

- Verruijt, A (1982). *Theory of Groundwater Flow*. 2nd ed. Palgrave Macmillan Press LTD, Hong Kong, 152 pp.
- Waltham, T (2001). Pinnacles and barchans in the Egyptian Desert. *Geology Today*, 17 (3): 101-104.
- Ward, DS, Buss, DR, Mercer, JW, Hughes, SS (1987). Evaluation of a Groundwater Corrective Action at the Chem- Dyne Hazardous-Waste Site Using a Telescopic Mesh Refinement Modeling Approach. *Water Resources Research* 23 (4):603-617.
- White, F (1983). *The vegetation of Africa: a descriptive memoir to accompany the UNESCO/AETFAT/UNSO vegetation map of Africa*. UNESCO, Paris, 356 pp.
- WHO (1984). *Guidelines for drinking water quality, Vol. 1; Recommendations*. World Health Organization, Geneva, Switzerland, pp 8.
- Williams, M, Faure, H (1980). *The Sahara and the Nile*. Balkema, Rotterdam, pp 622.
- Wycisk, P (1987). Contributions to the subsurface geology of the Misaha Trough and the southern Dakhla basin (S. Egypt/N. Sudan). *Berliner Geowiss. Abh., (A)*, 75: 137-150.
- Wycisk, P (1987a). Contributions to the subsurface geology of the Misaha Trough and southern Dakhla Basin (S Egypt/N Sudan). *Berl. geowiss. Abh., (A)*, 75: 137-149.
- Wycisk, P (1987b). Sequential arrangement of Cratonic sedimentation since Silurian Time (NW Sudan/ SW Egypt). In Matheis, G, Schandelmeier, H (eds). *Current research in African earth sciences*, Balkema, Rotterdam, pp211-216.
- Wycisk, P (1990). Aspects of Cratonic sedimentation: Facies distribution of fluvial and shallow marine sequences in NW Sudan/SW Egypt since Silurian Time. *Jour. Afr. Earth Sci.*, 10(1/2): 215-228.
- Wycisk, P (1991). Stratigraphic update of the nonmarine Cretaceous form SW Egypt and NW Sudan. *Cret. Res.*, 12: 185-200.
- Wycisk, P (1993). Outline of the geology and mineral resources of the southern Dakhla Basin, southwest Egypt. In Meissner, B, Wycisk, P (eds). *Geopotential and Ecology: Analysis of a desert region*, Catena Supplement, 26: 67-89.
- Wycisk, P (1994). Correlation of the major late Jurassic- Early Tertiary low- and high stand cycles of SW Egypt and NW Sudan. *Geol. Rsch.* 83: 759-772.
- Wycisk, P, Klitzsch, E, Jas, C, Reynolds, O (1990). Intracratonic sequence development and structural control of Phanerozoic strata in Sudan. *Berl. geowiss. Abh., (A)*, 120: 45-86.
- Yan, YE, Becker, R, Sultan, M, Ballerstein, E (2003). Development of Tushka Lakes in the Southwestern Desert of Egypt. *Geological Society of America Annual Meeting*, Seattle, Washington, November 2-5, Paper 151-4.
- Yeh, GT (1981). On the computation of Darcian velocity and mass balance in the finite

- element modeling of groundwater flow. *Water Resources Research*, 17 (5): 1529–1534.
- Yeh, WW (1986). Review of parameter identification procedures in groundwater hydrology: The inverse problem. *Water Resources Research*, 22 (2): 95-108.
- Youssef, MS (1957). Upper Cretaceous rocks in Quseir area. *Bull. Desert. Inst. Egypt*, 7 (2): 35-53.
- Youssef, MS (1959). Relation between groundwater composition and geology of Dakhla Oasis. Report of Desert Institute, Cairo, UAR, 42 pp.
- Zahoran, MA, Willis, AJ (1992). *The Vegetation of Egypt*. Chapman and Hall, London, 444 pp.
- Zhou, G, Esaki, T, Mori, J (2003). GIS-based spatial and temporal prediction system development for regional land subsidence hazard mitigation. *Environmental Geology*, 44: 665-678.
- Zimmerman, DL, Zimmerman, MB (1991). A Comparison of Spatial Semivariogram Estimators and Corresponding Ordinary Kriging Predictors. *Technometrics*, 33(1): 77-91.

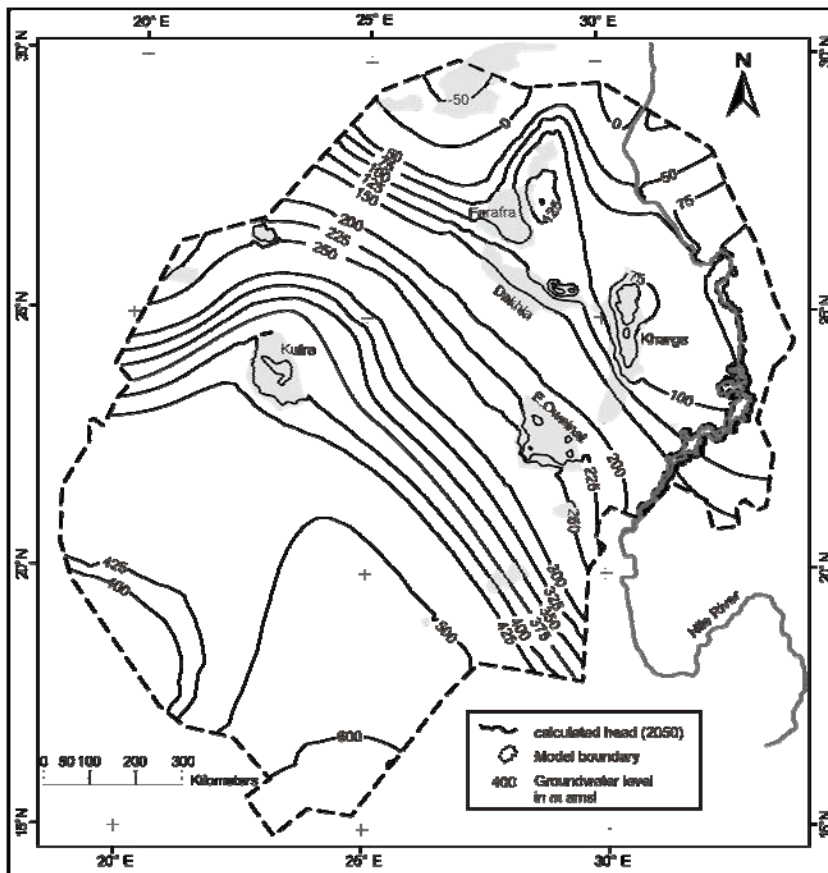
Appendix A.1. Data sources.

These sources include the institute of geological sciences at Martin Luther University Halle-Wittenberg, Germany. As since 1997, the work team at the institute has been working on the NSAS, developing groundwater flow models for the evaluation of its resources. These studies were a main guide and comparison reference for this work.

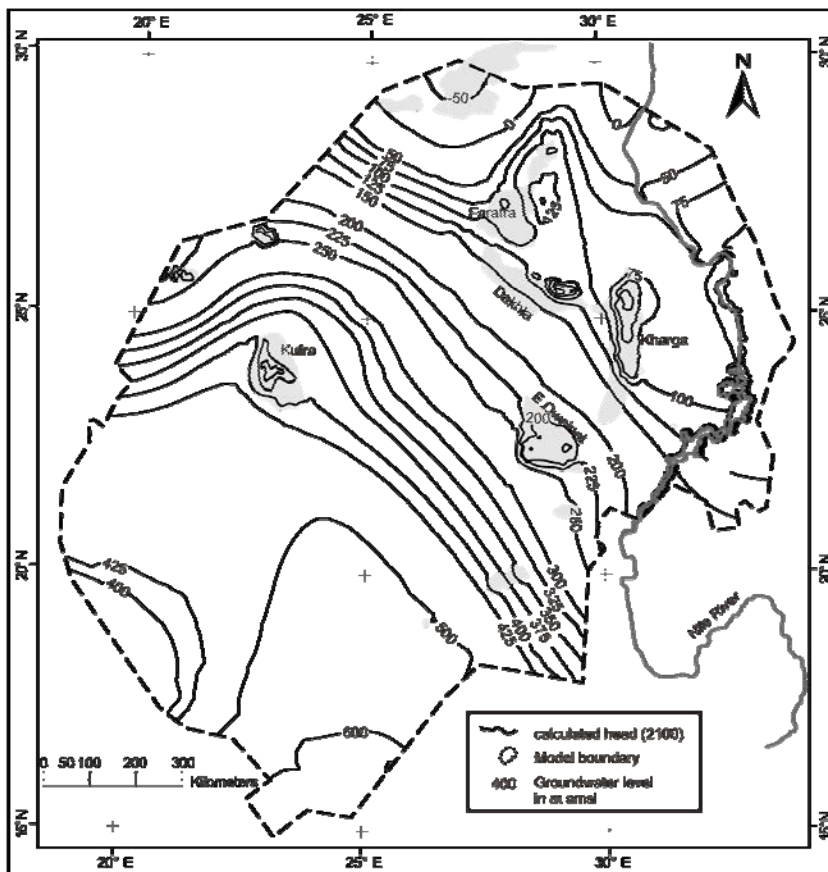
Groundwater and Development Center in the Kharga Oasis, Egypt, Branch of Academy of Scientific research and Technology in the Kharga oasis, Groundwater and Irrigation Center in the Dakhla Oasis, Egypt. They have provided the author with some well logs, observation records, well data, cross sections and the extraction rates of the Dakhla oasis.

The General Authority for Lake Nasser Development, the General Company for Research and Ground Water (REGWA), Cairo, the Tushka Project and the Kingdom Agriculture Development Company, Tushka, Egypt. From these authorities the author has got a lot of information on Nasser Lake, i.e. Fluctuations of the lake, history records of lake stage, and observation data around the lake.

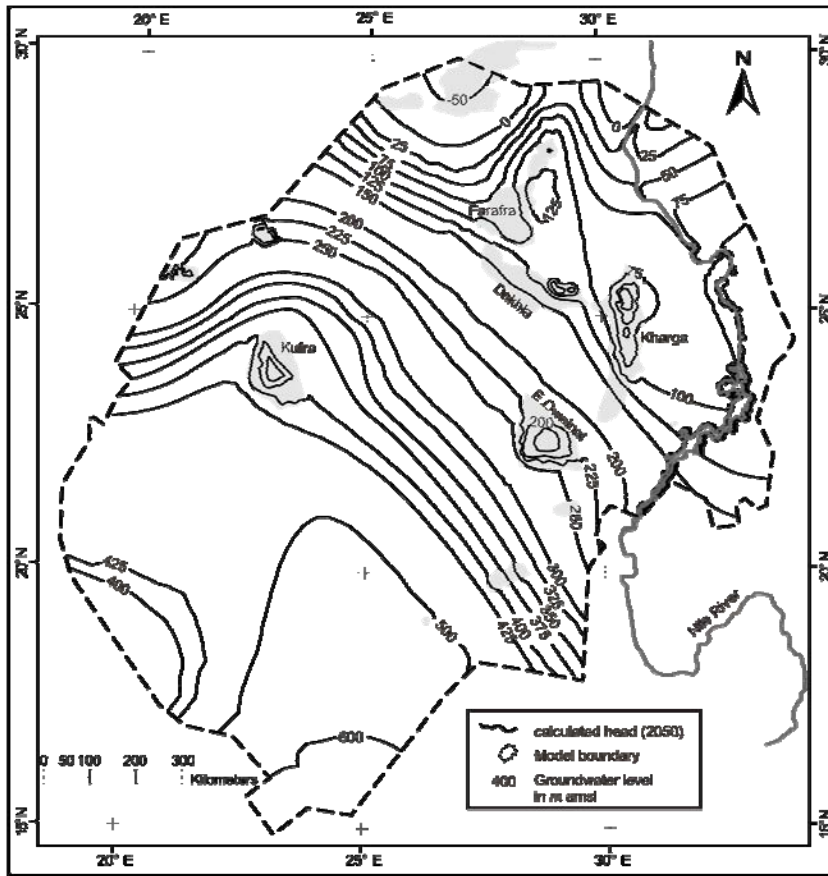
The published and internal technical and academic reports and literature, for example, the Research Institute for Groundwater (RIGW), Ministry of Public Works and Water Resources (MPWWR) in Egypt, the Groundwater Authority (GWA), the Great Man-Made River Authority (GMMRA) in Libya and the documents of CEDARE, UESCO and FAO. From these reports the author has got the necessary data for building the structure model of the regional NSAS, aquifer parameters, extraction rates, observation records and well data.



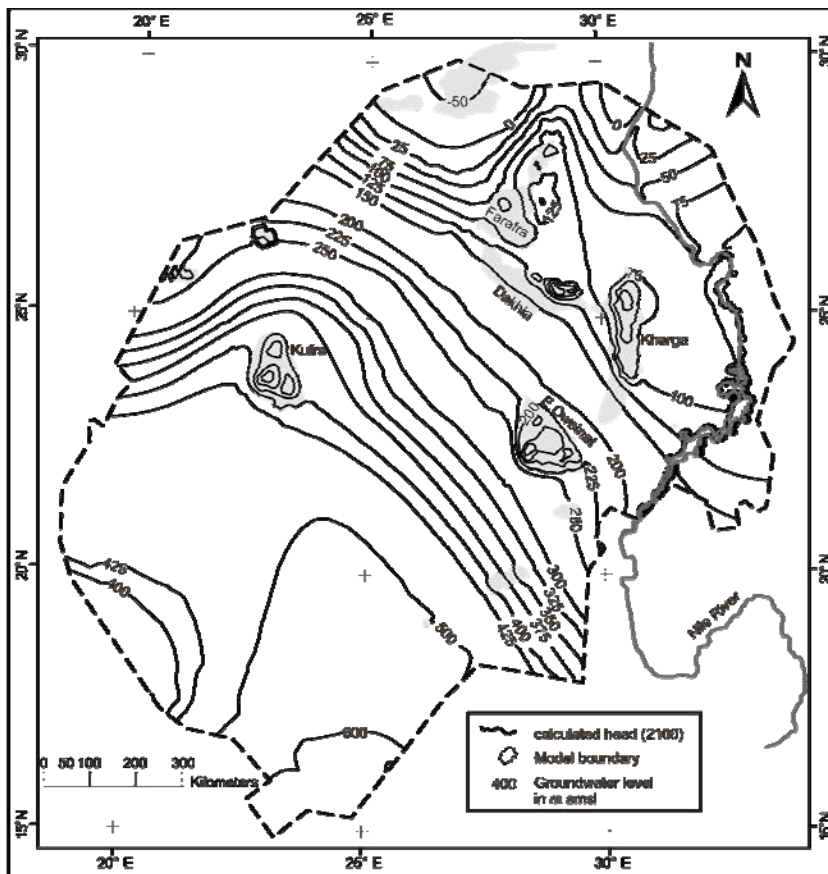
Appendix A.2. Simulated hydraulic head of the NSAS by year 2050 with the implementation of the extraction rates of scenario 2. Contour interval 25 m.



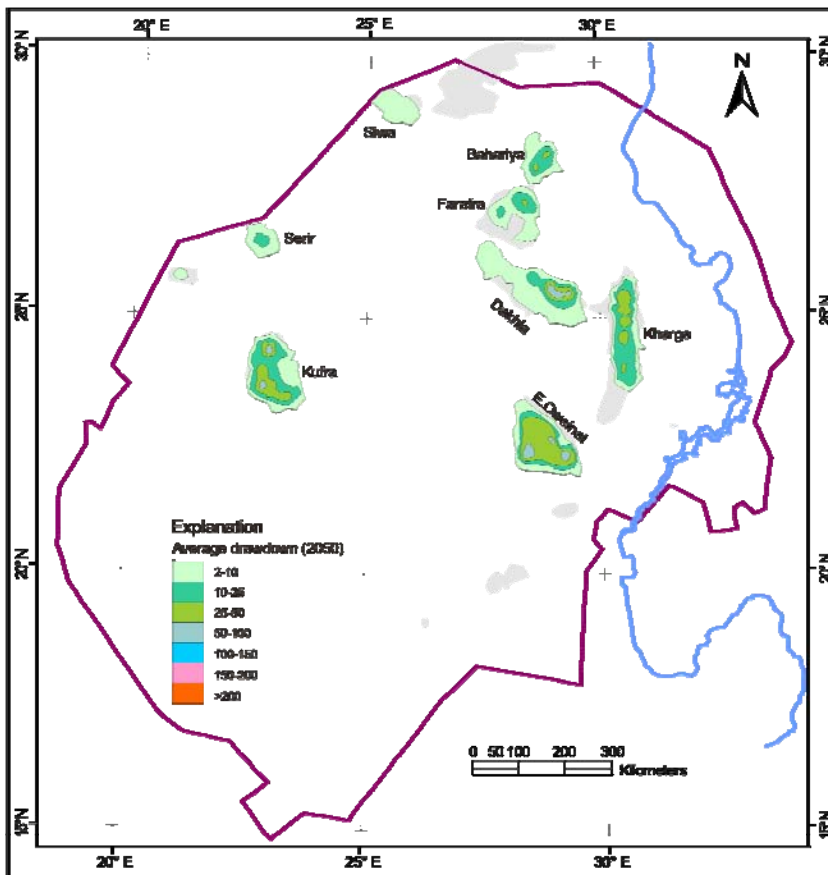
Appendix A.3. Simulated hydraulic head of the NSAS by year 2100 with the implementation of the extraction rates of scenario 2. Contour interval 25 m.



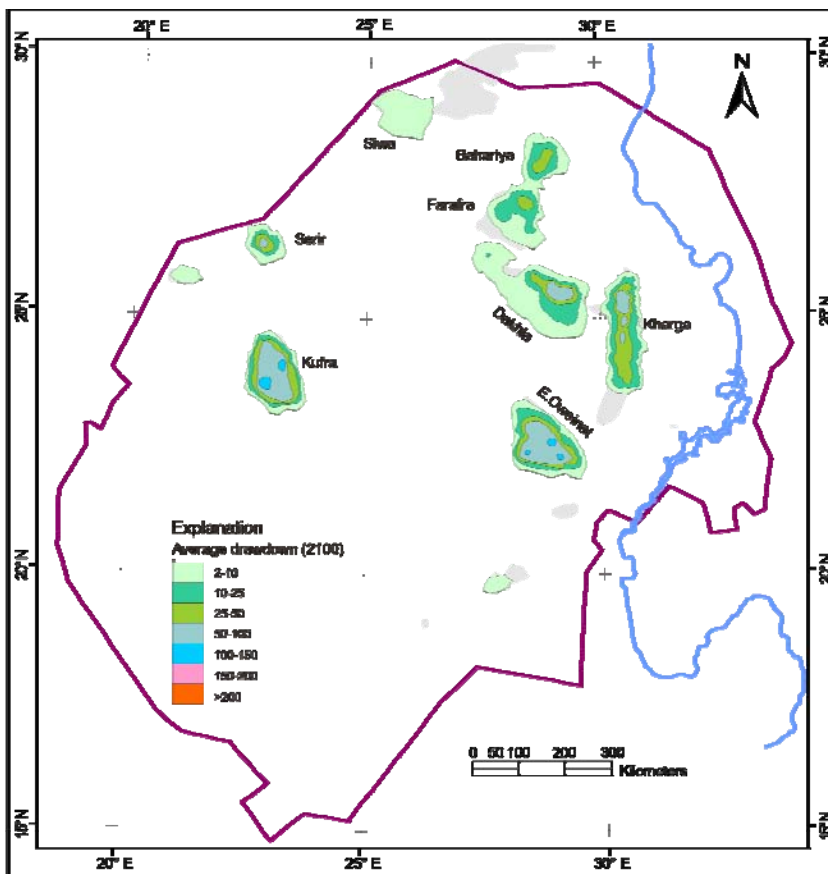
Appendix A.6. Simulated hydraulic head of the NSAS by year 2050 with the implementation of the extraction rates of scenario 3. Contour interval 25 m.



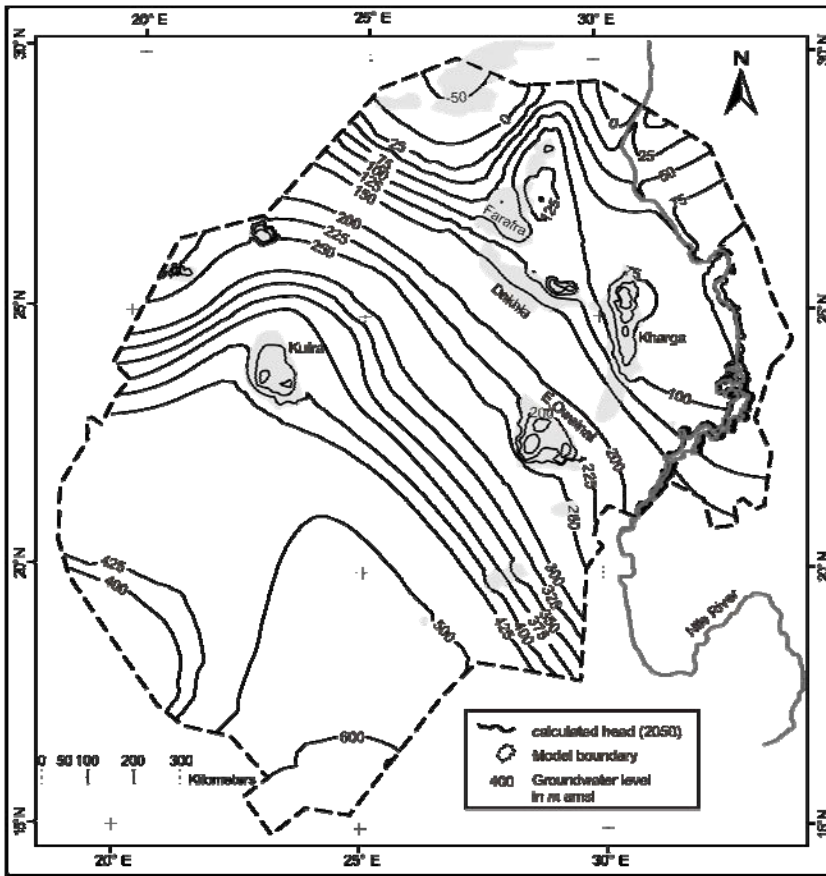
Appendix A.7. Simulated hydraulic head of the NSAS by year 2100 with the implementation of the extraction rates of scenario 3. Contour interval 25 m.



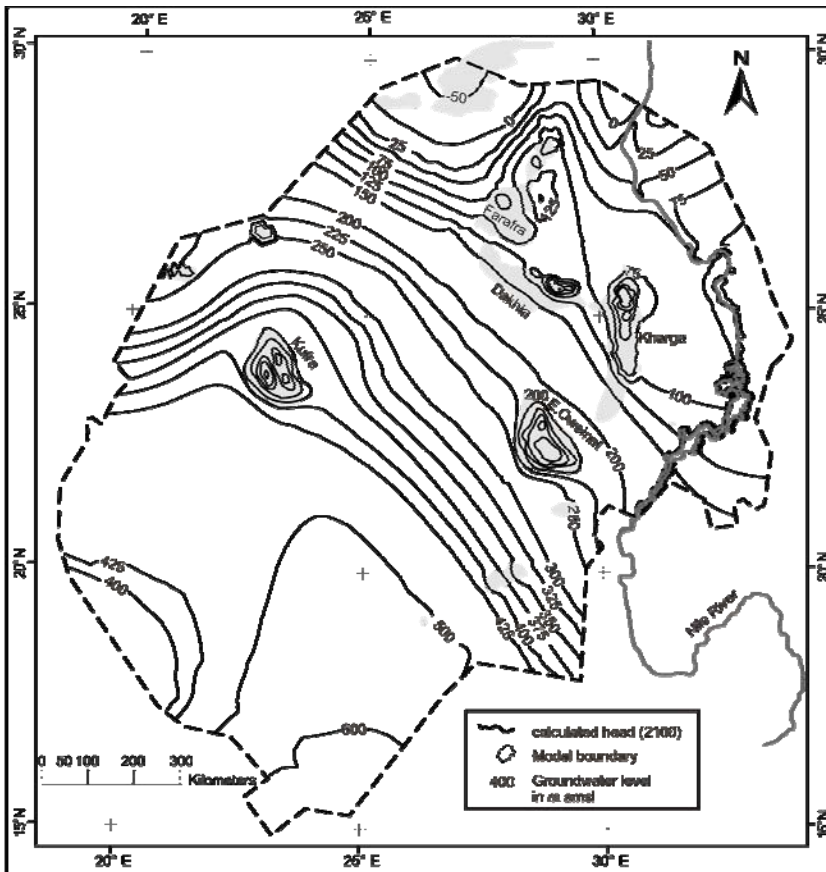
Appendix A.8. Resulting drawdown by year 2050 for the NSAS, suggesting the extraction rates of scenario 3 are constant until year 2100.



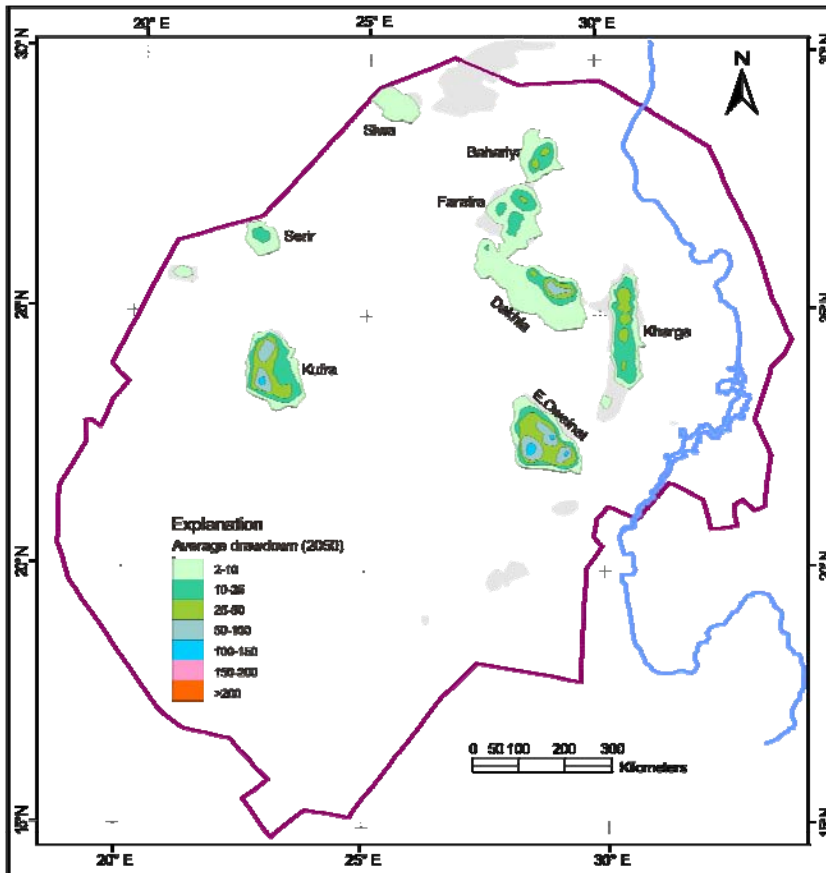
Appendix A.9. Resulting drawdown by year 2100 for the NSAS, suggesting the extraction rates of scenario 3 are constant until year 2100.



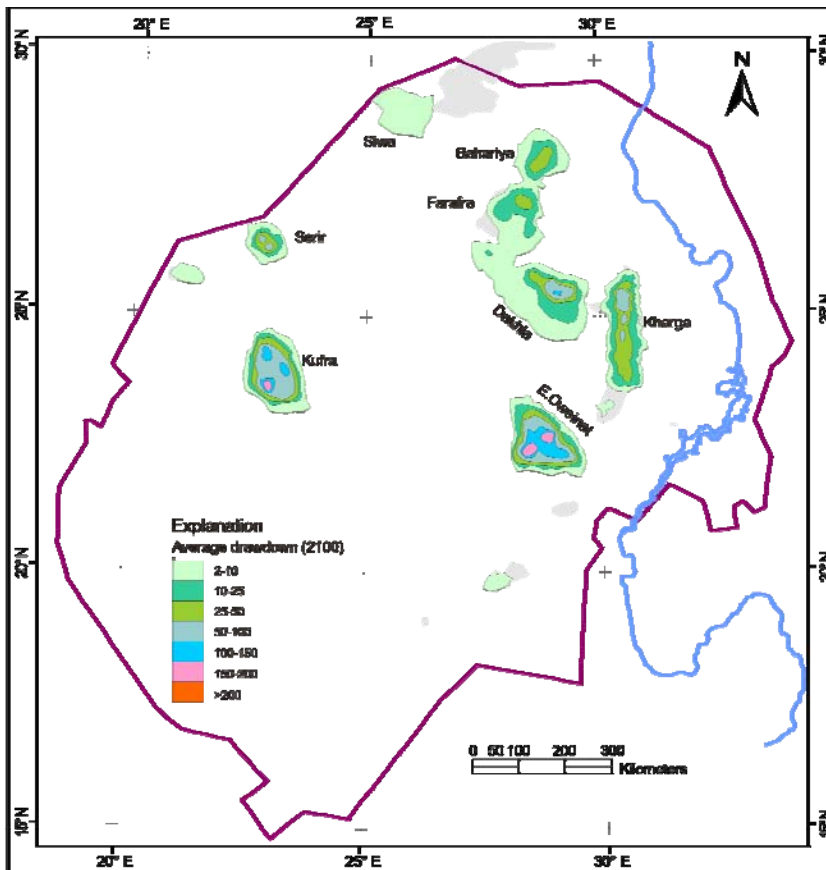
Appendix A.10. Simulated hydraulic head of the NSAS by year 2050 with the implementation of the extraction rates of scenario 4. Contour interval 25 m.



Appendix A.11. Simulated hydraulic head of the NSAS by year 2100 with the implementation of the extraction rates of scenario 4. Contour interval 25 m.

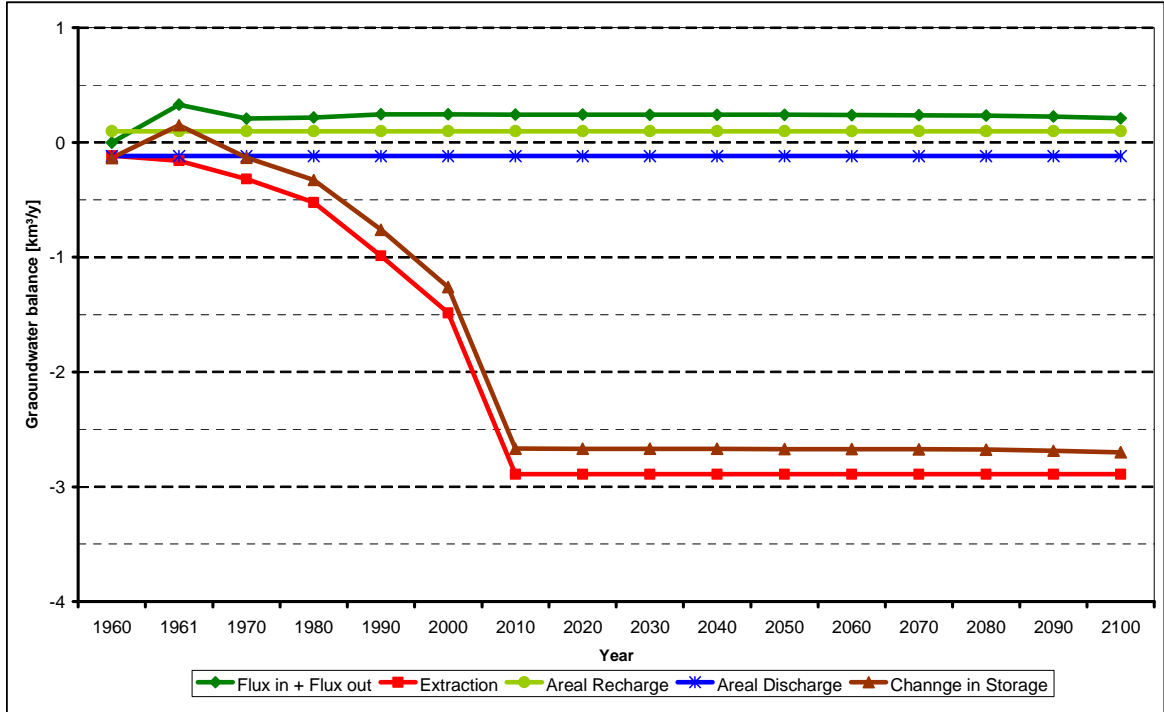


Appendix A.12. Resulting drawdown by year 2050 for the NSAS, suggesting the extraction rates of scenario 4 are constant until year 2100.

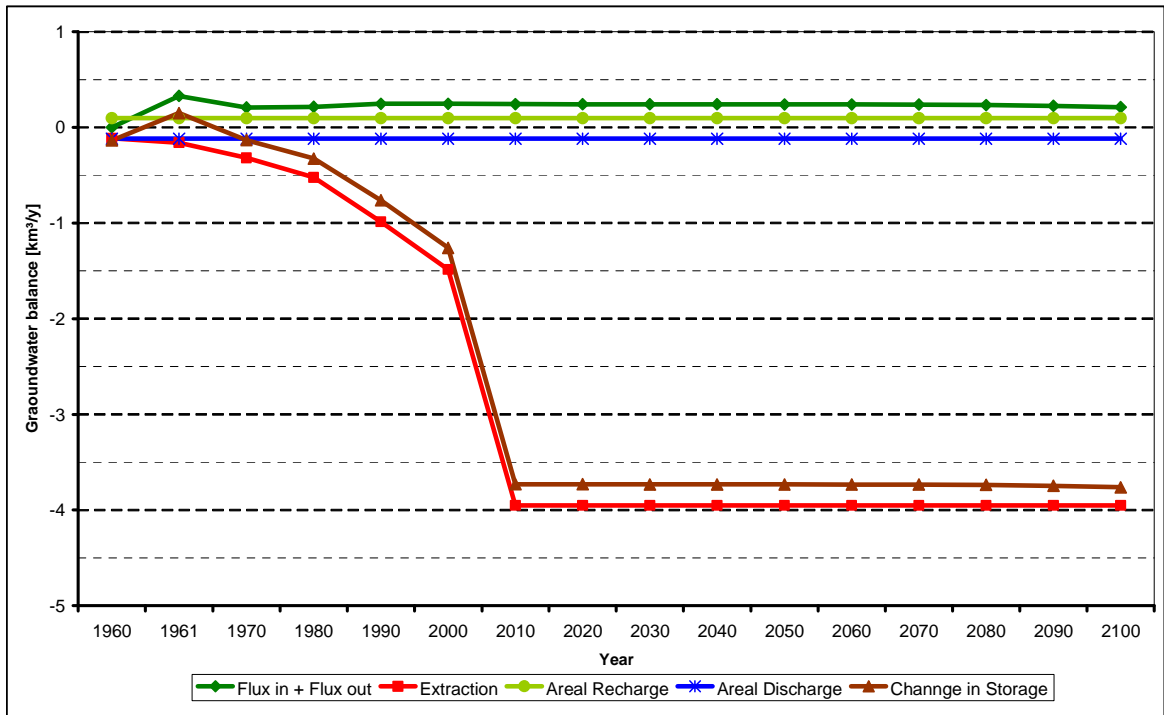


Appendix A.13. Resulting drawdown by year 2100 for the NSAS, suggesting the extraction rates of scenario 4 are constant until year 2100.

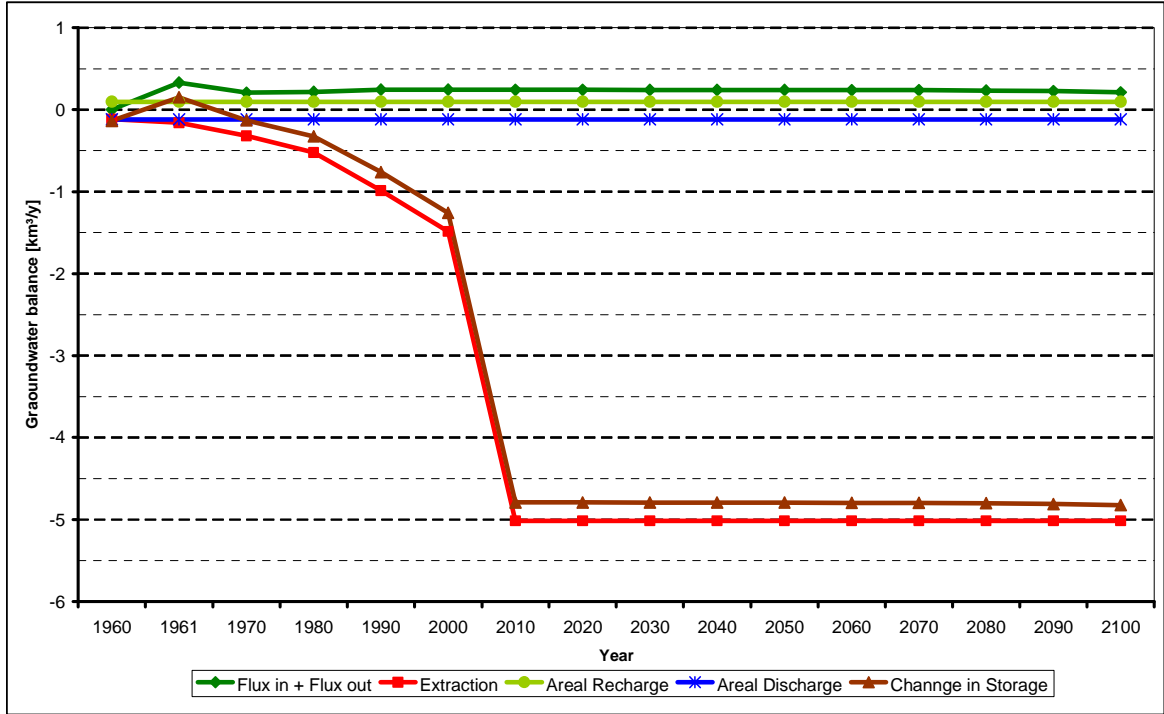
Appendix A.14. Groundwater balance for the NSAS for the period 1960-2100, scenario 2.



Appendix A.15. Groundwater balance for the NSAS for the period 1960-2100, scenario 3.



Appendix A.16. Groundwater balance for the NSAS for the period 1960-2100, scenario 4.



Appendix B.1. Extraction rates of the individual settlement areas of the Dakhla oasis from 1960 to 2005, values are given in m³/d.

Year	Area					
	Tenieda	Balat	Ismant	Maasara	SheikhWali	Mut
1960	23544.5	43155.8	8872.6	24625.1	3715.2	39893.0
1961	21996.1	40317.7	8289.1	23005.7	3470.9	37269.5
1962	22992.8	42144.7	8664.7	24048.2	3628.2	38958.4
1963	31344.1	57452.1	11811.8	32782.7	4946.0	53108.5
1964	36812.0	67474.5	13872.4	38501.6	5808.8	62373.1
1965	44213.3	81040.8	16661.5	46242.7	6976.7	74913.8
1966	42799.0	78448.4	16128.5	44763.4	6753.5	72517.4
1967	41273.2	75651.7	15553.6	43167.6	6512.7	69932.2
1968	43313.6	79391.6	16322.4	45301.6	6834.7	73389.2
1969	42924.7	78678.8	16175.9	44894.9	6773.3	72730.4
1970	44854.2	82215.4	16903.0	46912.9	7077.8	75999.6
1971	40689.1	74581.2	15333.4	42556.7	6420.6	68942.5
1972	38857.5	71223.8	14643.2	40641.0	6131.5	65838.9
1973	39272.7	71984.9	14799.7	41075.3	6197.1	66542.6
1974	40000.3	73318.5	15073.8	41836.2	6311.9	67775.3
1975	40350.0	73959.4	15205.6	42202.0	6367.1	68367.8
1976	40420.2	74088.2	15232.1	42275.5	6378.1	68486.9
1977	41675.7	76389.4	15705.2	43588.6	6576.2	70614.0
1978	41662.4	76365.1	15700.2	43574.7	6574.2	70591.5
1979	41464.5	76002.3	15625.6	43367.7	6542.9	70256.2
1980	45801.2	83951.4	17259.9	47903.5	7227.2	77604.3
1981	51115.0	93691.3	19262.4	53461.2	8065.7	86607.8
1982	58069.2	106437.9	21883.0	60734.5	9163.1	98390.7
1983	61414.2	112569.1	23143.6	64233.1	9690.9	104058.4
1984	65986.7	120950.4	24866.7	69015.5	10412.4	111806.0
1985	68058.2	124747.2	25647.3	71182.0	10739.3	115315.8
1986	72287.2	132498.8	27241.0	75605.1	11406.6	122481.3
1987	72891.2	120242.5	28991.6	72430.1	13673.0	96752.0
1988	72989.6	123673.0	26001.0	72496.1	9604.4	98529.5
1989	73512.4	134744.6	27702.7	76886.6	11600.0	124557.3
1990	74233.1	136065.6	27974.3	77640.4	11713.7	125778.5
1991	75130.6	123936.8	29882.3	74655.4	14093.0	99724.6
1992	77828.0	150465.0	24045.0	76859.0	8562.0	137549.0
1993	76395.3	140028.7	28789.1	79901.7	12054.9	129441.9
1994	80641.9	155094.8	25514.3	79648.7	9644.2	141855.9
1995	84339.6	162206.5	26684.2	83300.8	10086.4	148360.5
1996	83788.9	161147.3	26510.0	82756.9	10020.6	147391.7
1997	90476.3	174008.8	28625.8	89361.9	10820.4	159155.4
1998	84182.3	161903.8	26634.4	83145.4	10067.6	148083.7
1999	78675.0	151312.0	24892.0	77706.0	9409.0	138396.0
2000	72071.0	132102.5	27159.5	75379.0	11372.5	122115.0
2001	72241.0	119170.0	28733.0	71784.0	13551.0	95889.0
2002	67583.0	114512.0	24075.0	67126.0	8893.0	91231.0
2003	72695.0	112526.0	27293.0	74583.0	9246.0	110921.0
2004	63517.0	109837.0	29425.0	76305.0	10033.0	109587.0
2005	65467.0	112893.0	29427.0	73052.0	13336.0	105834.0

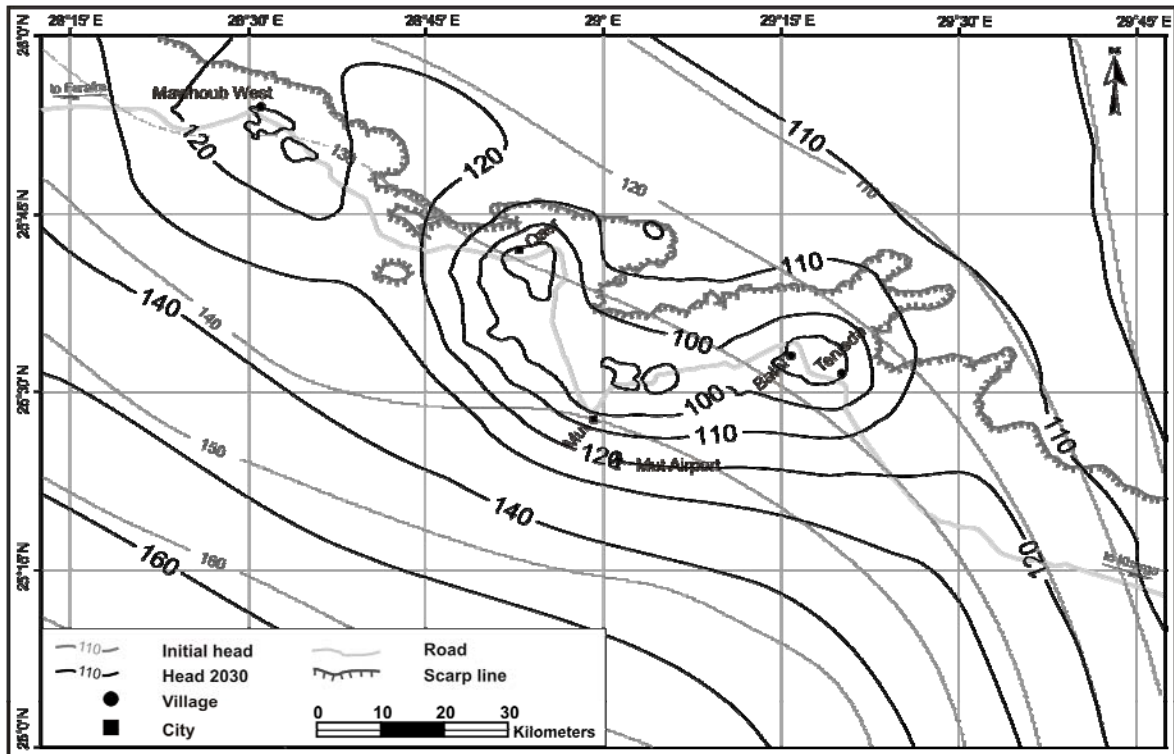
Appendix B.1. *continue*

Year	Area						
	Hindaw	Oweina	Rashda	Qalamon	Gedida	Moshiya	Bedkhulu
1960	13284.0	5605.9	13896.5	9392.8	15301.1	8569.7	11309.0
1961	12410.4	5237.2	12982.6	8775.1	14294.8	8006.2	10565.3
1962	12972.7	5474.6	13570.9	9172.8	14942.6	8369.0	11044.0
1963	17684.6	7463.0	18500.0	12504.4	20369.9	11408.7	15055.3
1964	20769.6	8764.9	21727.3	14685.8	23923.4	13398.9	17681.7
1965	24945.5	10527.1	26095.7	17638.5	28733.4	16092.8	21236.8
1966	24147.5	10190.4	25261.0	17074.2	27814.2	15578.0	20557.4
1967	23286.7	9827.1	24360.4	16465.5	26822.6	15022.7	19824.6
1968	24437.8	10312.9	25564.7	17279.5	28148.6	15765.3	20804.6
1969	24218.4	10220.3	25335.2	17124.4	27895.9	15623.8	20617.8
1970	25307.1	10679.7	26474.0	17894.1	29149.8	16326.1	21544.6
1971	22957.1	9688.0	24015.7	16232.5	26443.1	14810.1	19544.0
1972	21923.7	9251.9	22934.6	15501.8	25252.7	14143.4	18664.2
1973	22158.0	9350.8	23179.7	15667.5	25522.6	14294.5	18863.7
1974	22568.4	9524.0	23609.1	15957.7	25995.4	14559.3	19213.1
1975	22765.8	9607.3	23815.5	16097.2	26222.6	14686.6	19381.1
1976	22805.4	9624.0	23857.0	16125.2	26268.3	14712.2	19414.8
1977	23513.7	9922.9	24598.0	16626.1	27084.2	15169.2	20017.9
1978	23506.2	9919.8	24590.1	16620.8	27075.6	15164.3	20011.5
1979	23394.6	9872.6	24473.3	16541.8	26946.9	15092.3	19916.4
1980	25841.4	10905.2	27033.0	18271.9	29765.3	16670.8	21999.5
1981	28839.5	12170.4	30169.3	20391.8	33218.6	18604.9	24551.8
1982	32763.1	13826.2	34273.8	23166.1	37738.0	21136.1	27892.1
1983	34650.4	14622.6	36248.1	24500.6	39911.9	22353.6	29498.8
1984	37230.2	15711.3	38946.9	26324.7	42883.5	24017.9	31695.1
1985	38398.9	16204.6	40169.5	27151.1	44229.6	24771.9	32690.0
1986	40785.0	17211.5	42665.6	28838.3	46978.0	26311.2	34721.4
1987	42322.5	22518.9	44939.9	32946.9	46824.7	28476.0	34862.0
1988	40270.0	19072.8	43071.5	30234.6	45088.9	25449.1	32284.4
1989	41476.3	17503.2	43388.8	29327.0	47774.3	26757.2	35309.9
1990	41882.9	17674.8	43814.1	29614.6	48242.6	27019.5	35656.0
1991	43622.8	23210.7	46320.6	33959.1	48263.3	29350.9	35933.0
1992	43475.0	16155.0	43368.0	27603.0	45794.0	23662.0	36507.0
1993	43102.8	18189.6	45090.3	30477.1	49647.8	27806.5	36694.6
1994	45430.1	17427.1	45320.4	29161.3	47807.0	25121.7	38287.9
1995	47513.2	18226.1	47398.5	30498.4	49999.2	26273.6	40043.5
1996	47202.9	18107.1	47089.0	30299.3	49672.7	26102.1	39782.0
1997	50970.3	19552.3	50847.3	32717.5	53637.2	28185.4	42957.1
1998	47424.5	18192.1	47310.1	30441.5	49905.9	26224.6	39968.8
1999	44322.0	17002.0	44215.0	28450.0	46641.0	24509.0	37354.0
2000	40663.0	17160.0	42538.0	28752.0	46837.5	26232.5	34617.5
2001	41945.0	22318.0	44539.0	32653.0	46407.0	28222.0	34551.0
2002	37287.0	17660.0	39881.0	27995.0	41749.0	23564.0	29893.0
2003	48676.0	18979.0	44614.0	23802.0	40687.0	25384.0	29105.0
2004	37004.0	18980.0	40971.0	29054.0	47566.0	27956.0	31881.0
2005	37004.0	17318.0	40861.0	29054.0	47034.0	27956.0	31881.0

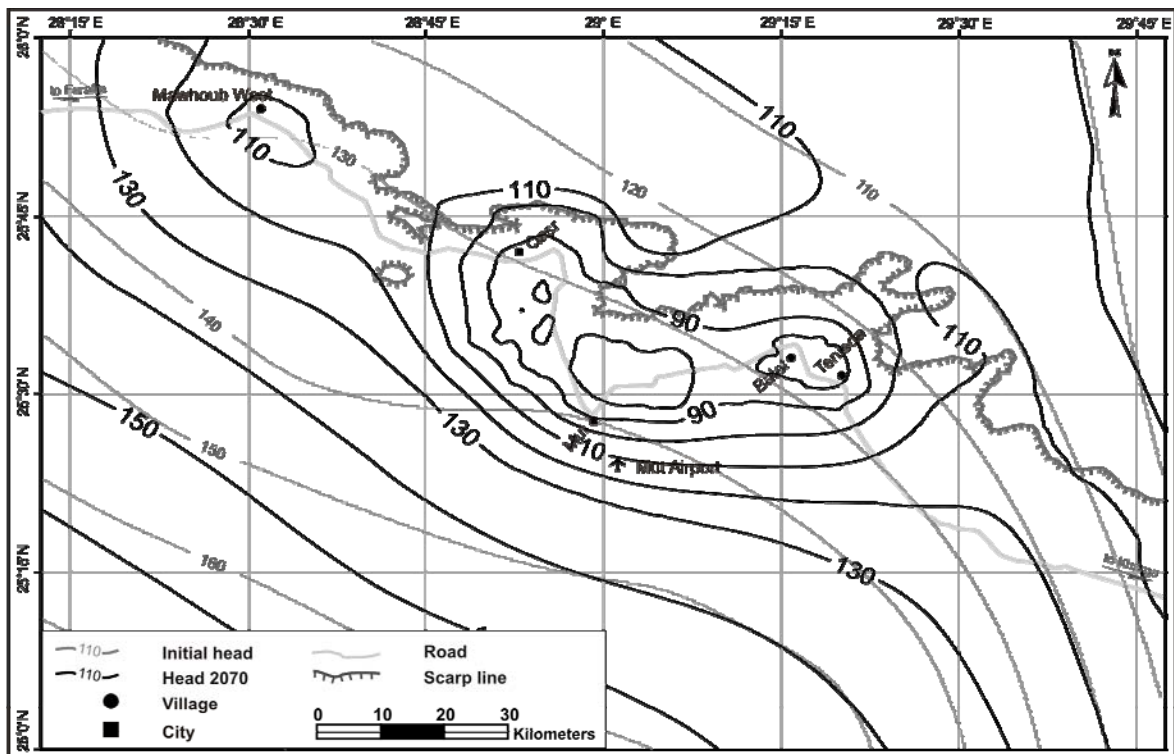
Appendix B.1. *continue*

Year	Area			
	Ezab Qasr	Qasr	Mawhoub	Mawhoub West
1960	13990.6	19150.6	10759.8	50562.9
1961	13070.5	17891.1	10052.2	47237.7
1962	13662.8	18701.9	10507.7	49378.2
1963	18625.3	25494.6	14324.3	67312.9
1964	21874.4	29942.1	16823.1	79055.5
1965	26272.4	35962.2	20205.5	94950.3
1966	25432.0	34811.8	19559.2	91913.0
1967	24525.4	33570.8	18861.9	88636.3
1968	25737.8	35230.3	19794.3	93018.0
1969	25506.7	34914.0	19616.6	92182.9
1970	26653.2	36483.4	20498.4	96326.5
1971	24178.3	33095.7	18595.0	87381.9
1972	23089.9	31605.8	17757.9	83448.3
1973	23336.6	31943.6	17947.7	84340.1
1974	23768.9	32535.4	18280.1	85902.5
1975	23976.7	32819.8	18440.0	86653.5
1976	24018.5	32876.9	18472.1	86804.4
1977	24764.5	33898.1	19045.8	89500.5
1978	24756.6	33887.3	19039.7	89472.0
1979	24639.0	33726.3	18949.3	89047.0
1980	27216.0	37253.7	20931.2	98360.4
1981	30373.6	41575.9	23359.6	109772.1
1982	34505.9	47232.2	26537.7	124706.4
1983	36493.5	49953.0	28066.3	131890.0
1984	39210.6	53672.2	30156.0	141709.8
1985	40441.5	55357.1	31102.6	146158.3
1986	42954.5	58796.9	33035.3	155240.3
1987	47362.5	56000.5	38430.8	148276.6
1988	45664.6	54910.4	36104.4	153679.7
1989	43682.5	59793.4	33595.2	157871.5
1990	44110.8	60379.6	33924.6	159419.3
1991	48817.6	57721.0	39611.5	152832.2
1992	41567.0	55431.0	34575.0	153129.0
1993	45395.6	62138.3	34912.7	164062.6
1994	43474.4	57685.0	36307.6	157825.4
1995	45467.8	60330.0	37972.4	165062.3
1996	45170.9	59936.1	37724.4	163984.4
1997	48776.1	64719.7	40735.3	177072.4
1998	45383.0	60217.5	37901.5	164754.3
1999	42414.0	56278.0	35422.0	153976.0
2000	42826.0	58621.0	32936.5	154776.0
2001	46940.0	55501.0	38088.0	146954.0
2002	42282.0	50843.0	33430.0	142296.0
2003	45518.0	51728.0	32388.0	99426.0
2004	43363.0	53999.0	30451.0	153976.0
2005	43238.0	60964.0	30451.0	155576.0

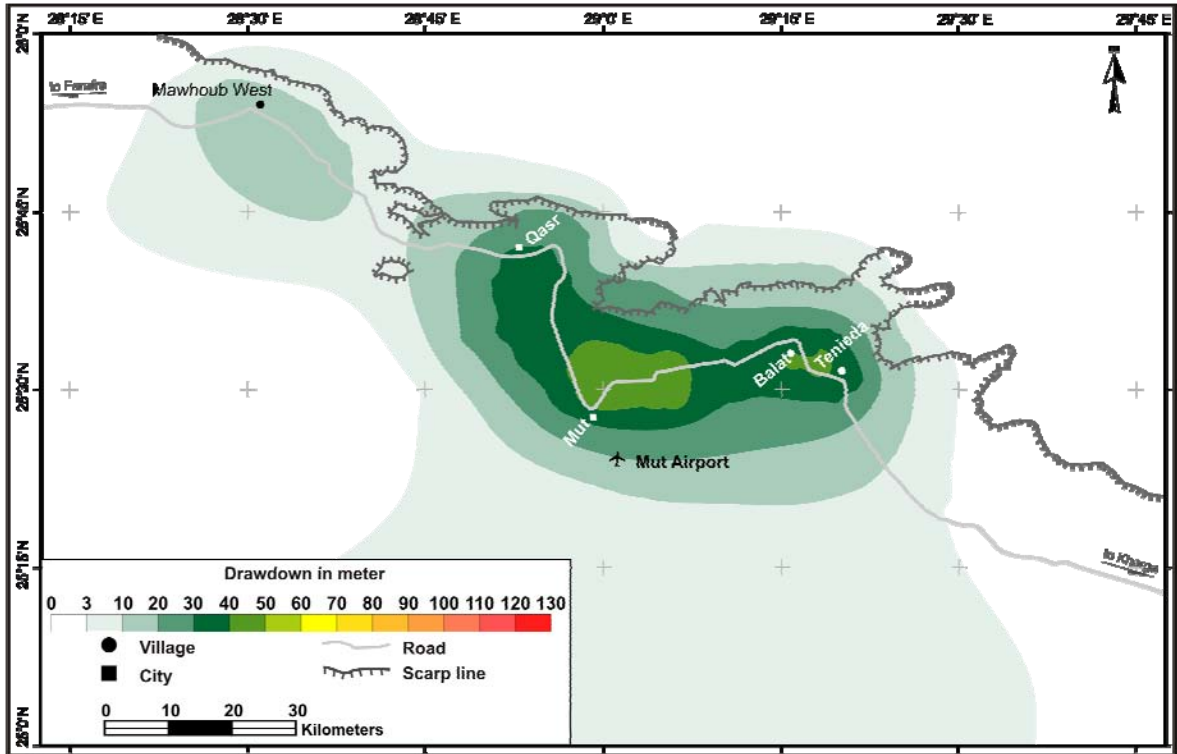
Appendix B.2. Simulated hydraulic head m (amsl) for the NSAS in the Dakhla oasis by 2030, assuming the actual extraction rates of 2005 are constant until 2100 (scenario 1).



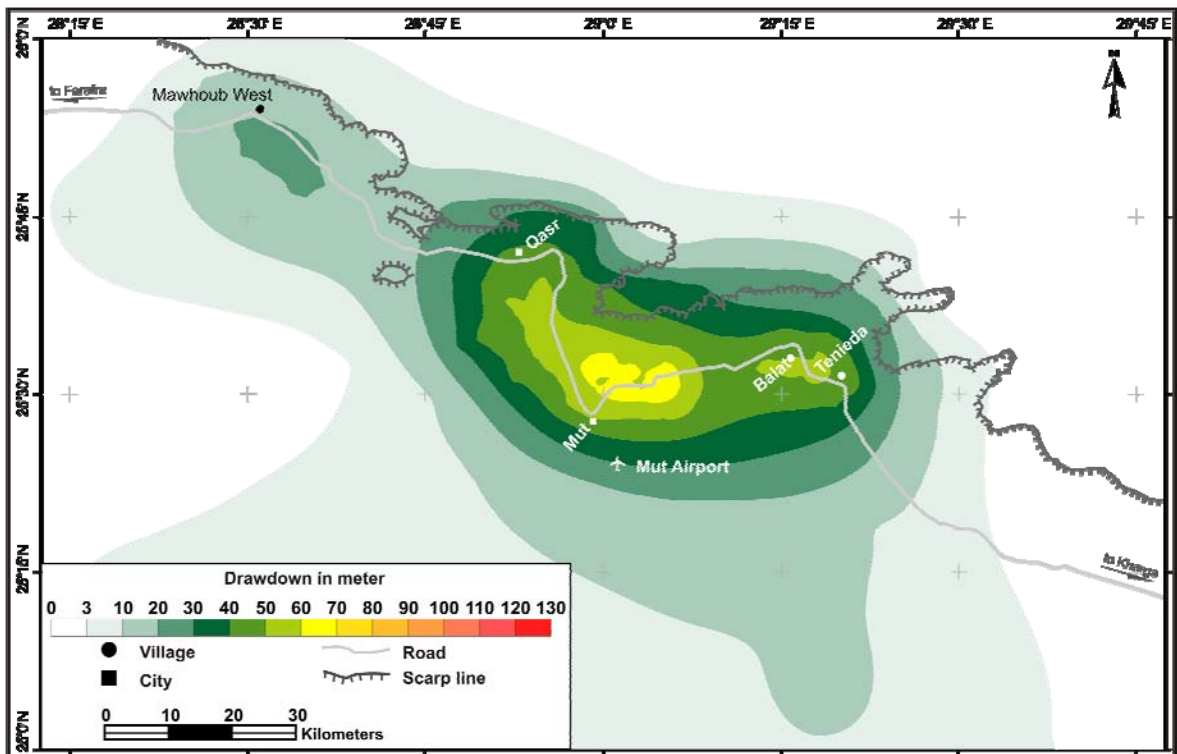
Appendix B.3. Simulated hydraulic head m (amsl) for the NSAS in the Dakhla oasis by 2070, assuming the actual extraction rates of 2005 are constant until 2100 (scenario 1).



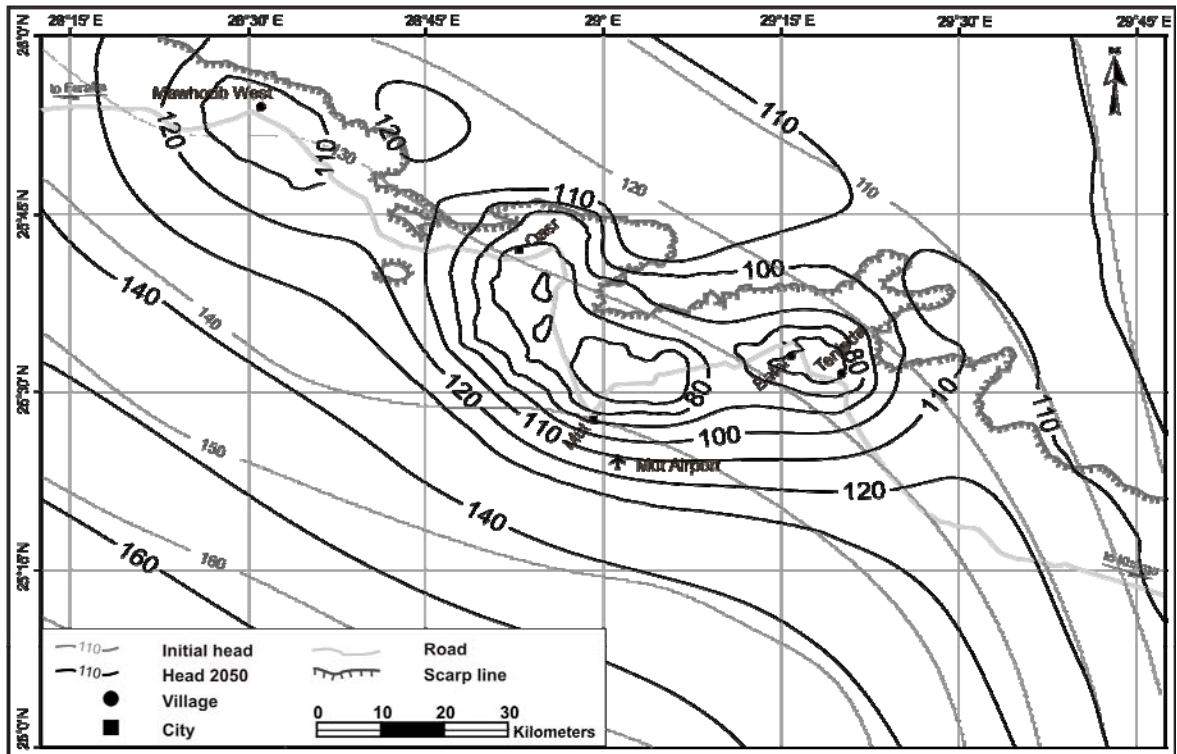
Appendix B.4. Simulated decline in hydraulic head (in meter) for the NSAS in the Dakhla oasis by 2030, assuming the actual extraction rates of 2005 are constant until 2100, (scenario 1).



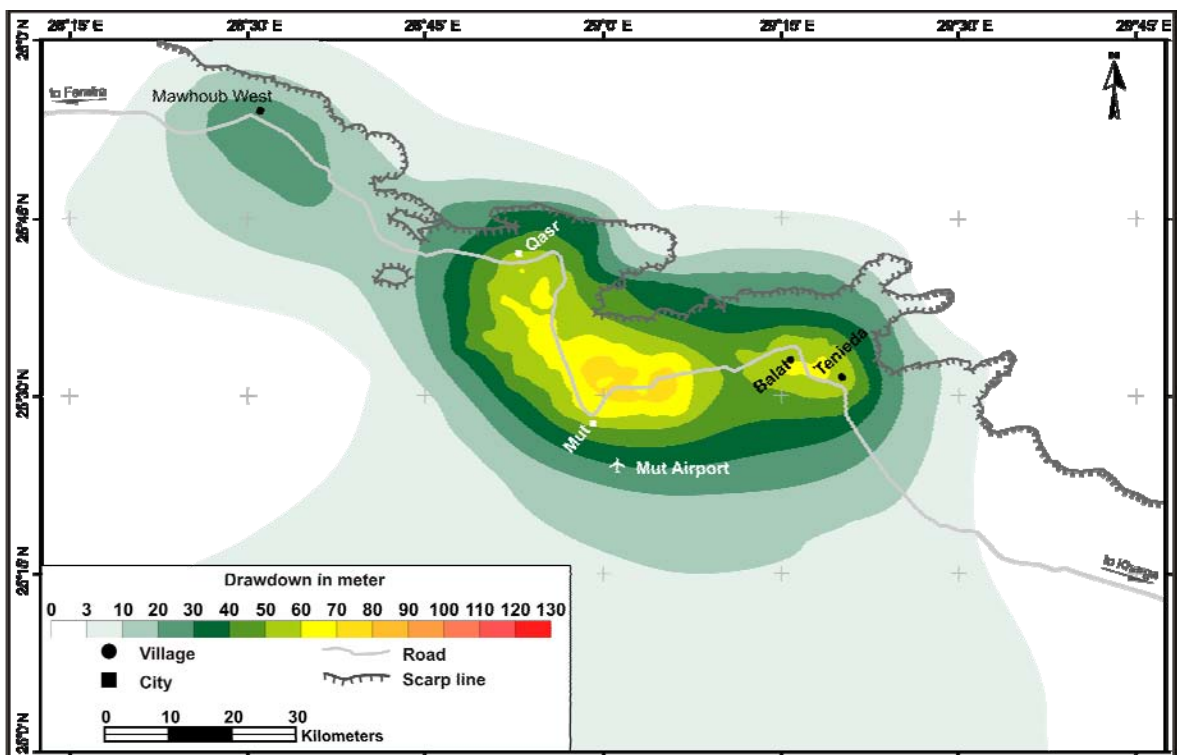
Appendix B.5. Simulated decline in hydraulic head (in meter) for the NSAS in the Dakhla oasis by 2070, assuming the actual extraction rates of 2005 are constant until 2100, (scenario 1).



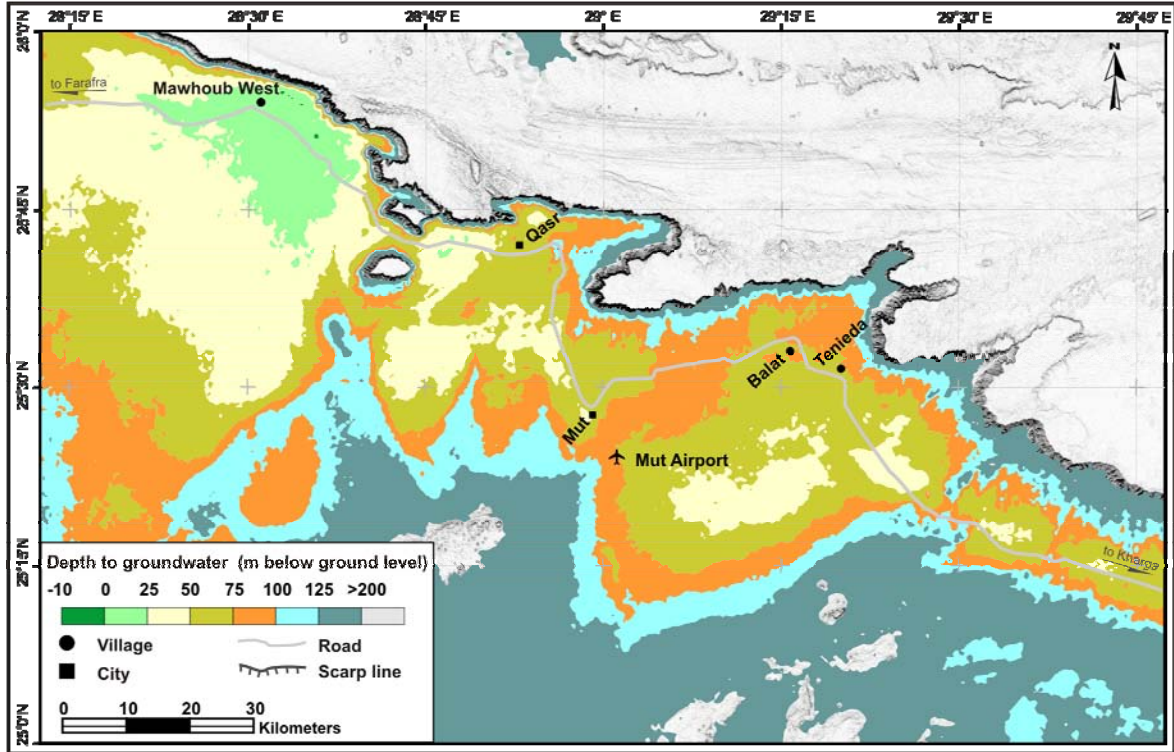
Appendix B.6. Simulated hydraulic head m (amsl) for the NSAS in the Dakhla oasis by 2050, assuming the extraction rates of scenario 2 are constant until 2100.



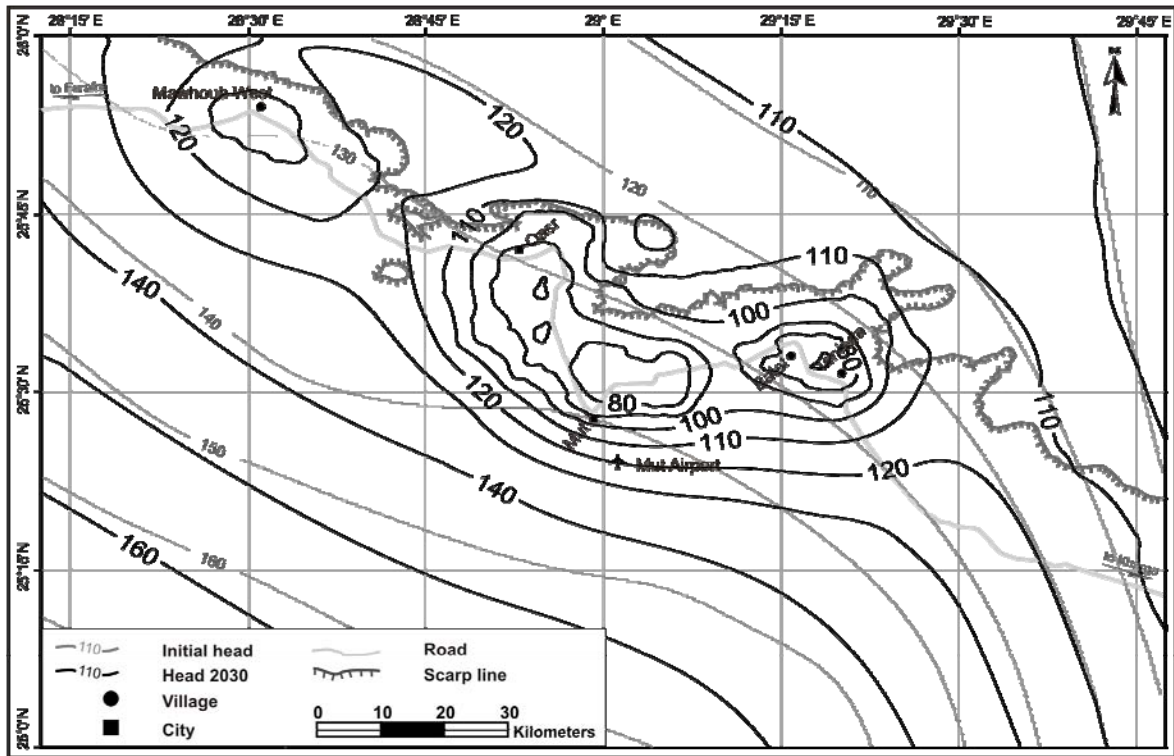
Appendix B.7. Simulated decline in hydraulic head (in meter) for the NSAS in the Dakhla oasis by 2050, assuming the extraction rates of scenario 2 are constant until 2100.



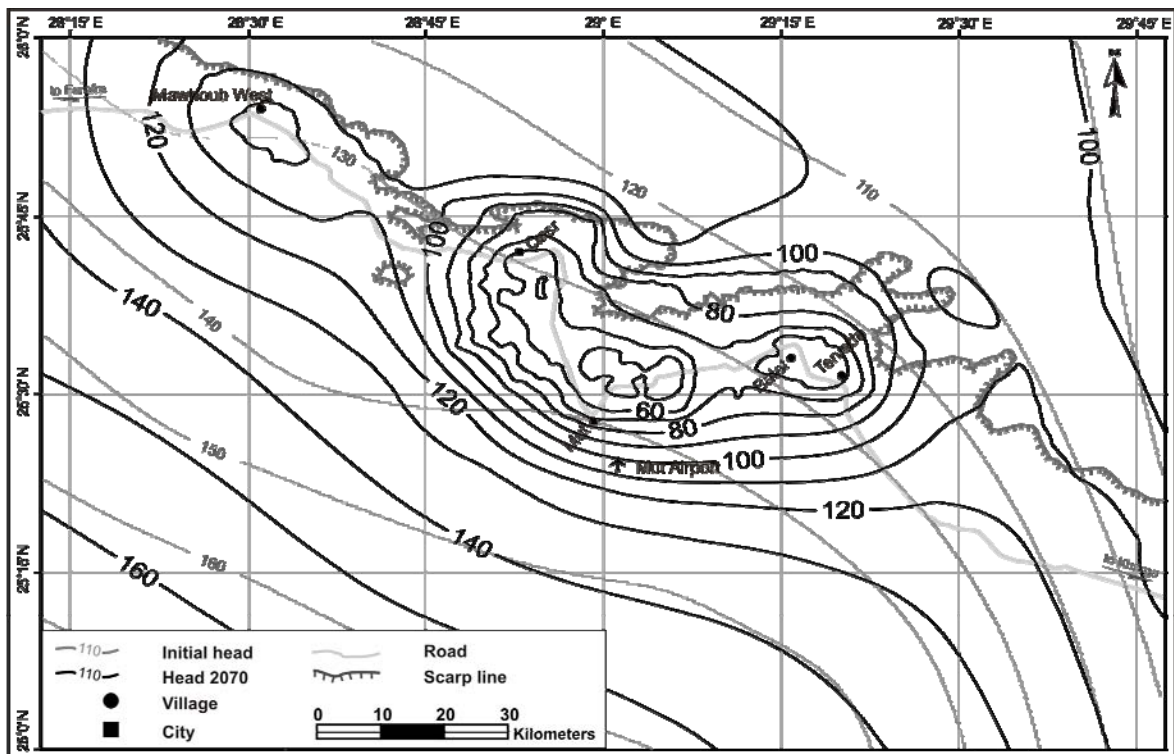
Appendix B.8. Calculated depth to groundwater (in meter below ground level) for the NSAS in the Dakhla oasis by 2100 assuming the extraction rates of scenario 2 are constant until 2100.



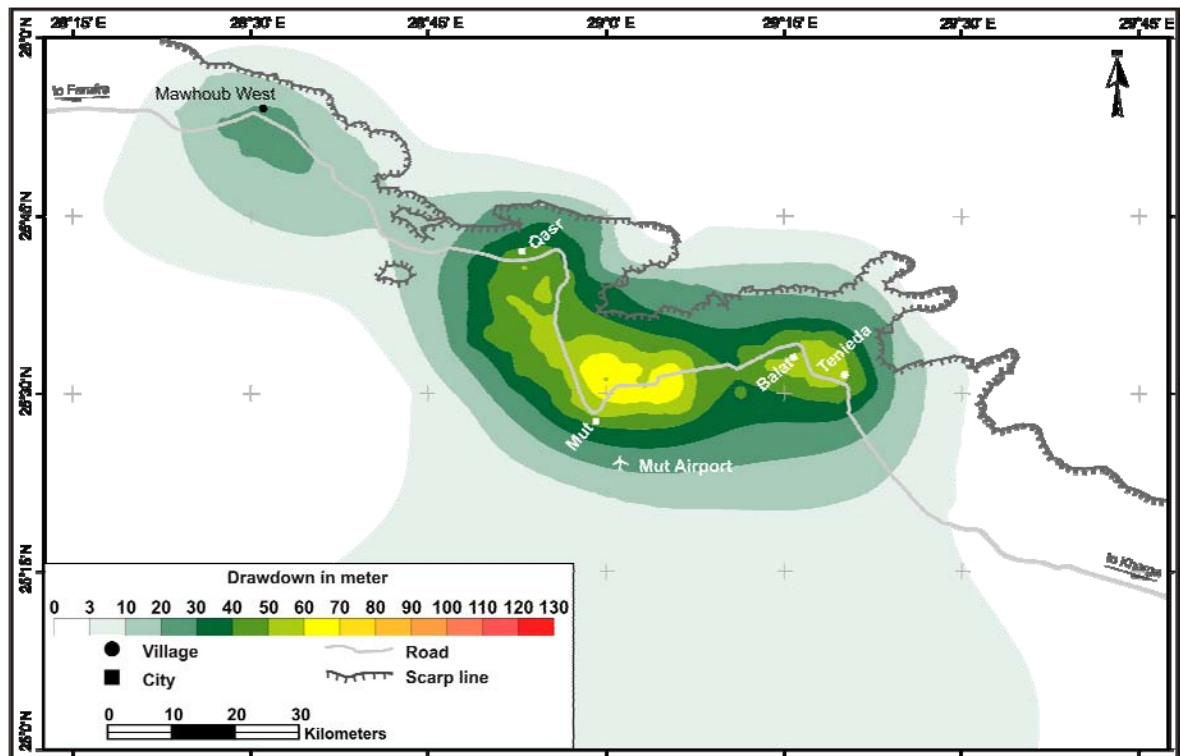
Appendix B.9. Simulated hydraulic head m (amsl) for the NSAS in the Dakhla oasis by 2030, assuming the extraction rates of scenario 3 are constant until 2100.



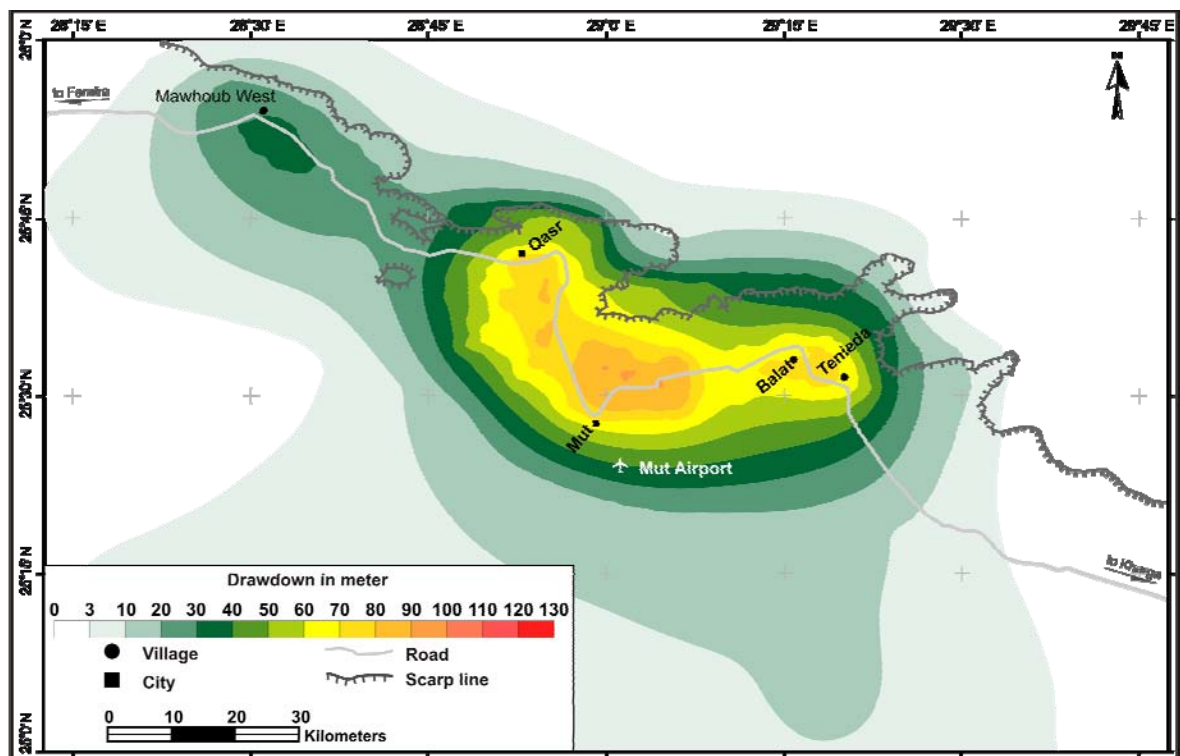
Appendix B.10. Simulated hydraulic head m (amsl) for the NSAS in the Dakhla oasis by 2070, assuming the extraction rates of scenario 3 are constant until 2100.



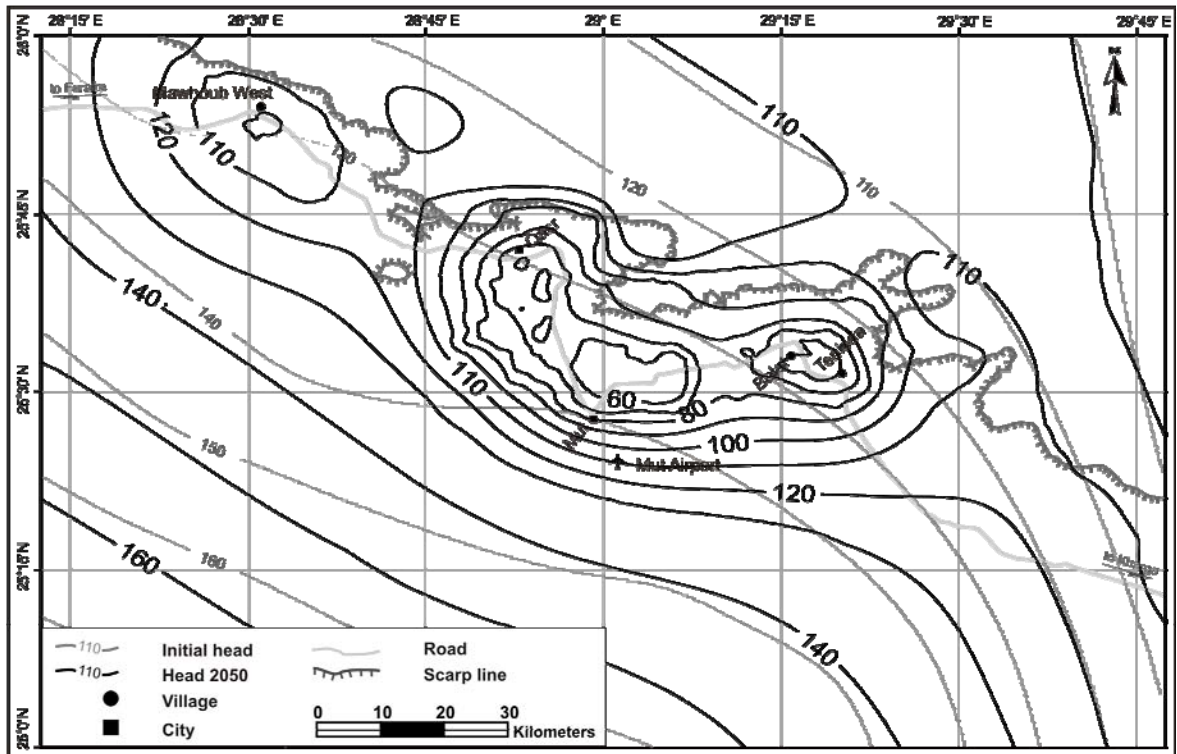
Appendix B.11. Simulated decline in hydraulic head (in meter) for the NSAS in the Dakhla oasis by 2030, assuming the extraction rates of scenario 3 are constant until 2100.



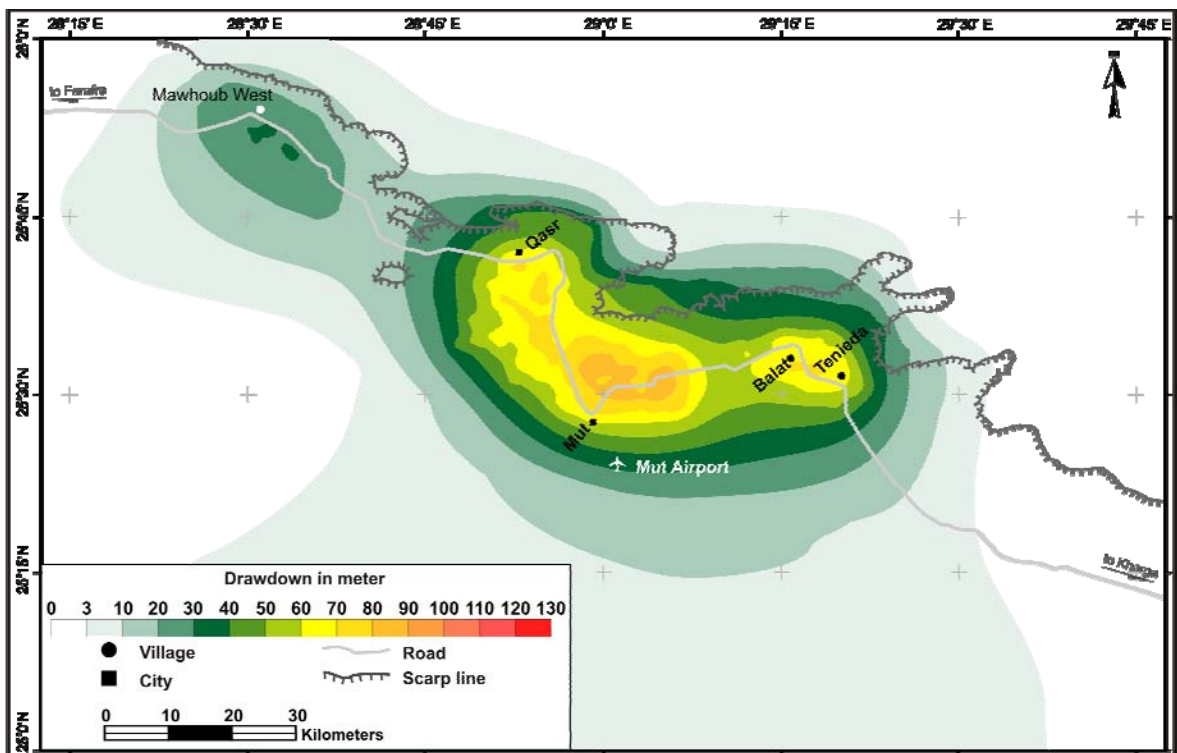
Appendix B.12. Simulated decline in hydraulic head (in meter) for the NSAS in the Dakhla oasis by 2070, assuming the extraction rates of scenario 3 are constant until 2100.



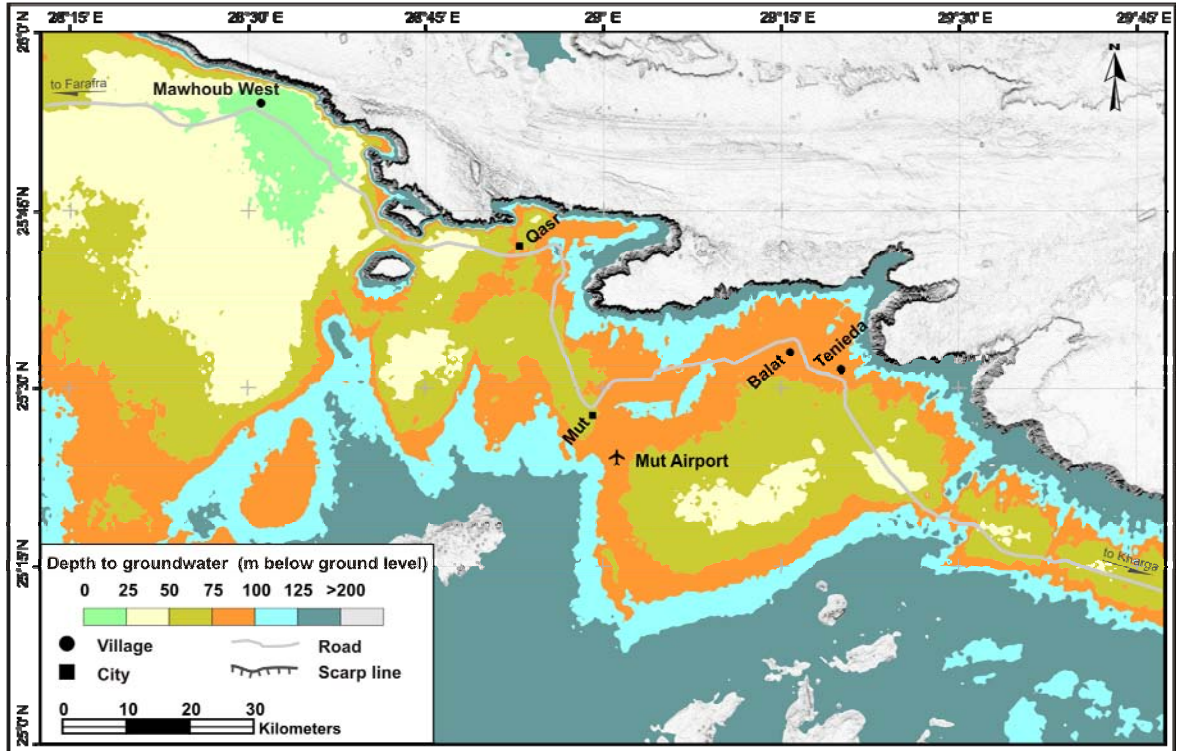
Appendix B.13. Simulated hydraulic head m (amsl) for the NSAS in the Dakhla oasis by 2050, assuming the extraction rates of scenario 4 are constant until 2100.



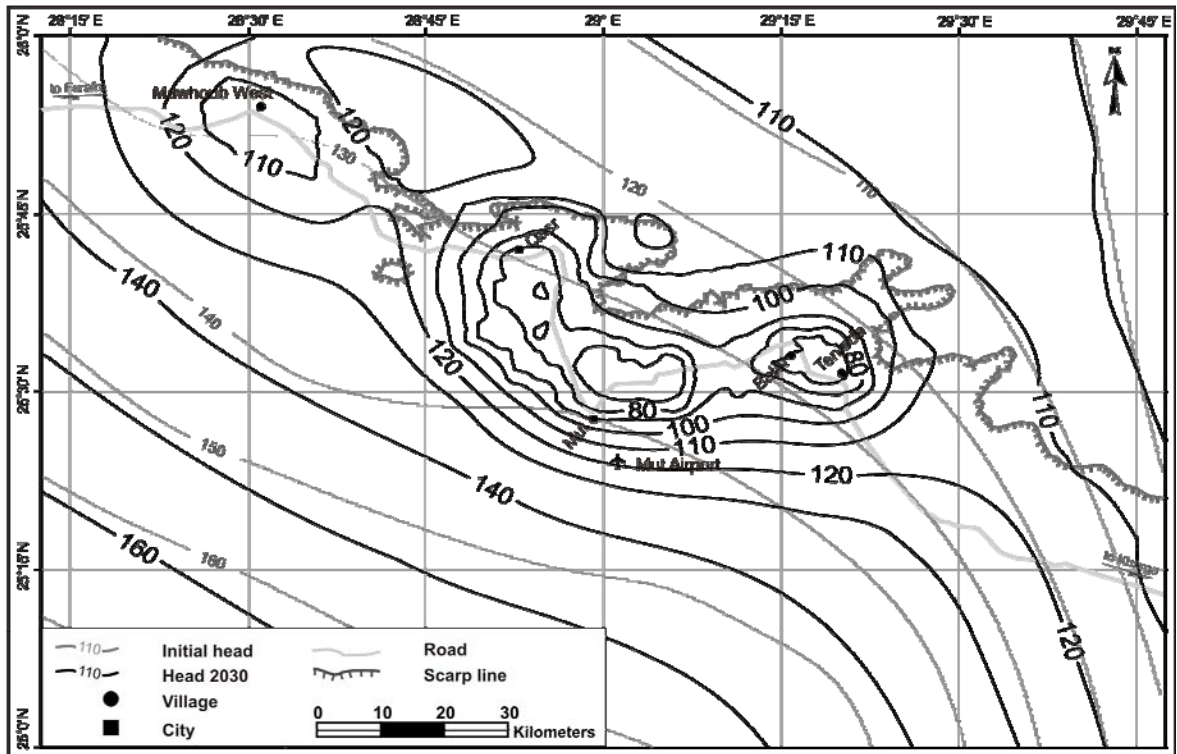
Appendix B.14. Simulated decline in hydraulic head (in meter) for the NSAS in the Dakhla oasis by year 2050, assuming the extraction rates of scenario 4 are constant until 2100.



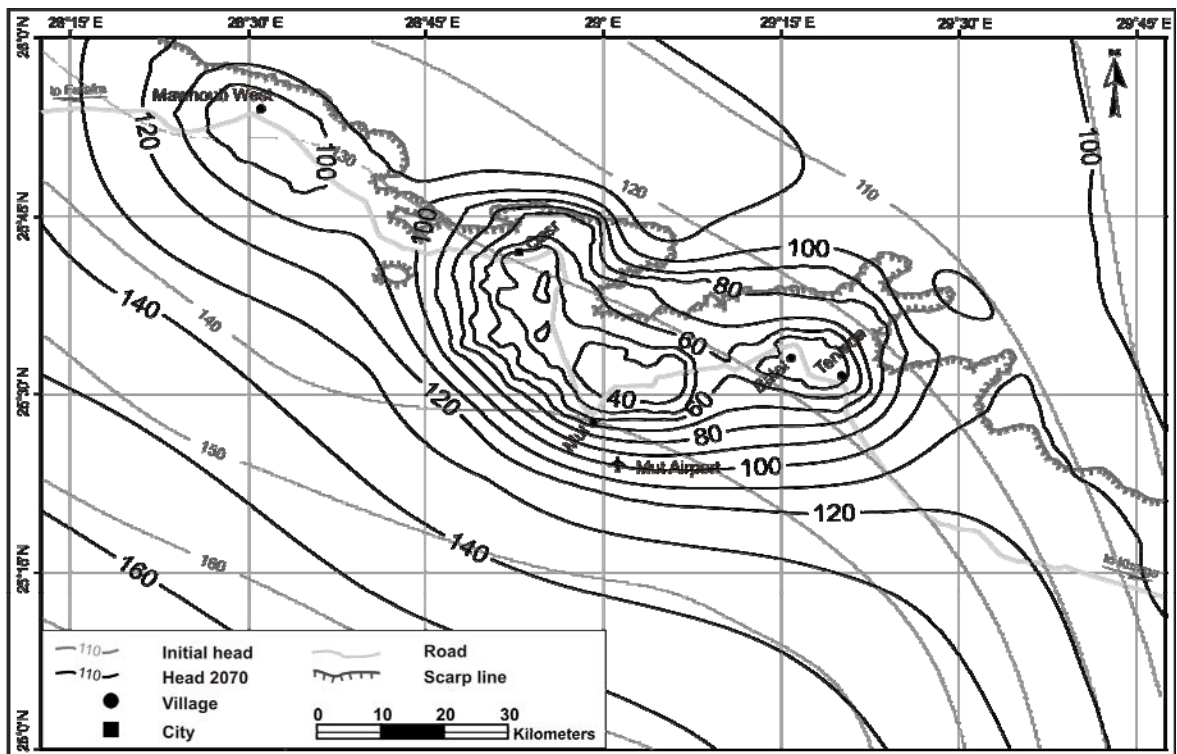
Appendix B.15. Calculated depth to groundwater (in meter below ground level) for the NSAS in the Dakhla oasis by 2100 assuming the extraction rates of scenario 4 are constant until 2100.



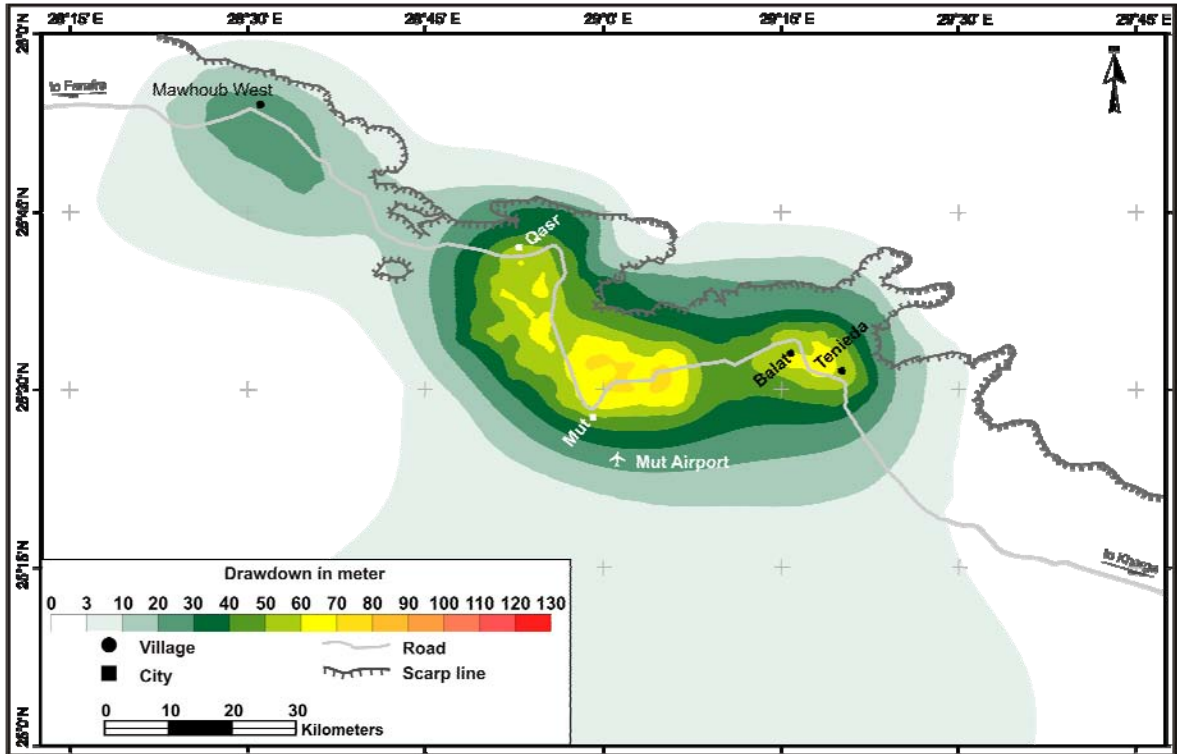
Appendix B.16. Simulated hydraulic head m (amsl) for the NSAS in the Dakhla oasis by 2030, assuming the planned extraction rates of scenario 5 are constant until 2100.



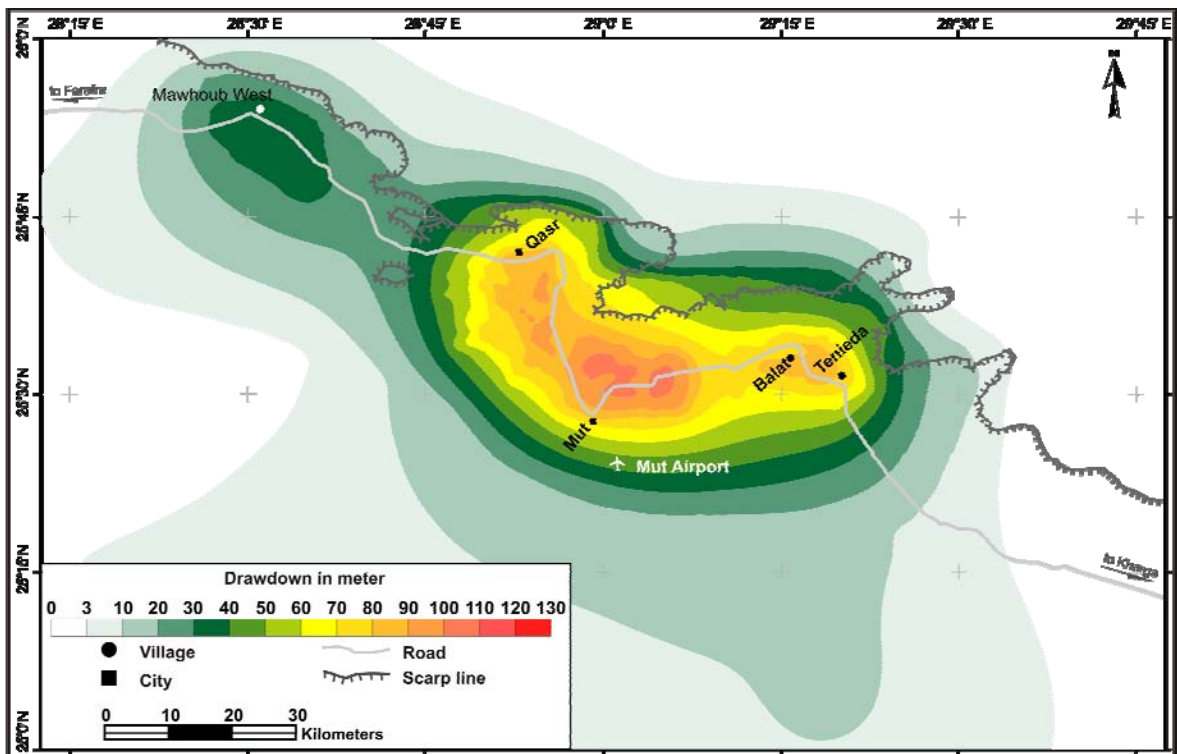
Appendix B.17. Simulated hydraulic head m (amsl) for the NSAS in the Dakhla oasis by 2070, assuming the planned extraction rates of scenario 5 are constant until 2100.



Appendix B.18. Simulated decline in hydraulic head (in meter) for the NSAS in the Dakhla oasis by 2030, assuming the planned extraction rates of scenario 5 are constant until 2100.



Appendix B.19. Simulated decline in hydraulic head (in meter) for the NSAS in the Dakhla oasis by 2070, assuming the planned extraction rates of scenario 5 are constant until 2100.



Statement of Original Authorship

I hereby state that this submission is my own work and to the best of my knowledge and belief, the thesis contains no material previously published or written by another person, nor material which to a substantial extent has been accepted to the award of any other degree in the Martin Luther University Halle-Wittenberg, or any other institution, excluding where due reference is made in this thesis. Any contribution made to the research by others, with whom I have worked at the Martin Luther University Halle-Wittenberg or elsewhere, is explicitly acknowledged in this thesis.

I also affirm that I have never submitted work for Doctor Degree or such at any other university or institution.

I give consent to this copy of my thesis, when deposited in the library of the Martin Luther University Halle-Wittenberg, being available for loan and photocopying in part or as a whole.

Signature:

Ahmed Sefelnasr

Date: 01/11/2007

Submitted for Review: 18/05/2007
Examiners' Reports received: September/2007
Oral Defense: 22/10/2007

CURRICULUM VITAE

Ahmed Sefelnasr

Lecturer assistant, Geology Department, Assiut University, Egypt
DAAD-Scholarship holder, Martin Luther University Halle-Wittenberg, Germany

Address

Present address

Ernst-Barlach-Ring 27
D-06124 Halle/Saale
Germany
Tel: +49 345 55 26137
Fax: +49 345 55 27177

Home country address

Geology Department, Faculty of Science
Assiut University, 71516 Assiut
Egypt
Tel: +2 088 241 2110
Fax: +2 088 231 2546

Email: ahmed.sefelnasr@geo.uni-halle.de

Personal Data

First Name: Ahmed
Family Name: Sefelnasr
Gender: Male
Born on: 4.11.1974
Born in: Elwady Elgadiid
Citizenship: Egypt

Professional activities

2004-2007	DAAD-scholarship holder for the award of the PhD in Hydrogeology, Martin Luther University Halle-Wittenberg, Germany.
2002-2003	InWent (CDG) Ltd., Mannheim, Germany. Training on Groundwater resources management and protection.
2002-present	Lecturer assistant of hydrogeology, Geology Department, Assiut University, Assiut, Egypt.
1996-2002	Demonstrator of hydrogeology, Geology Department, Assiut University, Assiut, Egypt.

Education

2002	MSc in Hydrogeology, Assiut University, Geology Department, Faculty of Science. Thesis: "Hydrogeological studies on some areas in the New Valley Governorate, Western Desert, Egypt."
1996	BSc in geology, Assiut University, Geology Department, Faculty of Science.
1992	Secondary school, Balat secondary School, Elwady Elgadiid, Egypt.
1989	Preparatory school, Tenieda Preparatory School, Elwady Elgadiid, Egypt.
1986	Primary school, Tenieda Primary School, Elwady Elgadiid, Egypt.

Halle/Saale,